UNIVERSITÉ DU BURUNDI
GRENIER DU SAVOIR DU BURUNDI
Dépôt institutionnel officiel
https://repository.ub.edu.bi

Impact of integrating an intelligent solar tracker associated with a battery management system to optimize photovoltaic efficiency in Burundi

Icoyitungiye, Olivier

2026-03
UB, Ecole doctorale
https://repository.ub.edu.bi/handle/123456789/2346

Document téléchargé depuis le **Grenier du Savoir du Burundi** — https://repository.ub.edu.bi

University of Burundi



Doctoral School

Research Center in Infrastructure, Environment and Technologies

Impact of integrating an intelligent solar tracker associated with a battery management system to optimize photovoltaic efficiency in Burundi

By

ICOYITUNGIYE Olivier

PhD thesis presented and defended in order to obtain a degree of Doctor in Electrical Engineering (Dr. PhD)

Specialization: Renewable energy and embedded technology

Supervisor: Pr. Eng. BUKURU Denis, Higher Institute of Education (ENS) of Burundi

Co-Supervisor: Pr. PRITPAL Singh, Villanova University, USA

Bujumbura, March 2026

Composition of the jury members

1.	Pr NDIKUMAGENGE Jérémie	University of Burundi	: **President**
2.	Dr Col. NIYONGABO Prime	University of Burundi	: **Secretary**
3.	Pr. Eng. BUKURU Denis	Higher Institute of Education (ENS) of Burundi	**: Supervisor**
4.	Pr. PRITPAL Singh	Villanova University, USA	**: Co-supervisor**
5.	Pr. Eng. NIYONZIMA Jean Bosco	University of Burundi	: **member**
6.	Dr Eng. NTAWUHORAKOMEYE Noel	Higher Institute of Education (ENS) of Burundi	**: Member**

Dedication

I dedicate this work to my family and my parents.

To the pillars of my education and a constant source of motivation.

To my family and loved ones, for their love, unwavering support and prayers.

To all those who, in one way or another, contributed to the success of this work.

ICOYITUNGIYE Olivier

Acknowledgements

I give thanks to God for the strength, wisdom and perseverance He has granted me throughout this doctoral journey, which have enabled me to complete this work.

I would like to express to our thesis supervisor Pr. Eng. BUKURU Denis and Pr. PRITPAL Singh, for the time they devoted to its scientific supervision, the approach of their guidance, the relevance of their advice and their constant support throughout this work. Their availability and scientific rigor were decisive in the conduct and completion of this work. I would like to express my sincere thanks to Pr. Eng. NIYONZIMA Jean Bosco and Dr Eng. NTAWUHORAKOMEYE Noël for the honor they have bestowed upon me by agreeing to support this work, as well as for their constructive observations, which have contributed to the scientific improvement of the work.

I would also like to thank the institutions, organizations and technical bodies that provided scientific and technical support for this work, in particular by providing the data, resources essential to its completion.

Finally, I would like to express my gratitude to my family for their constant moral support, patience and sacrifices throughout my doctoral studies.

To all those who contributed, directly or indirectly, to the completion of this work and who could not be mentioned explicitly, I express my deep appreciation.

Publications and International Conferences

Publications

1. Olivier, I., Denis, B., Singh, P., Bosco, N.J., and Noel, N. (2025) Determining the Ideal Solar Panel Tilt Angle and the Energy Generated in the Various Burundian Provinces. *Journal of Power and Energy Engineering, 13, 11–35.*
   HTTPS://DOI.ORG/10.4236/JPEE.2025.135002
2. Olivier, I., Denis, B., Singh, P., Bosco, N.J., and Noel, N. (2025) Creation of an Algorithm Based on a Mechanism for Controlling Lead Acid Battery Charge and Discharge to Maximize Burundi's Solar Energy Production. *Journal of Power and Energy Engineering, 13, 107-126. HTTPS://DOI.ORG/10.4236/JPEE.2025.136007*
3. Olivier, I., Noel, N., Denis, B., Singh, P., and Bosco, N.J. (2025). Intelligent Solar Tracker Developed to Increase Burundi's Photovoltaic Production. *Journal of Power and Energy Engineering, 13, 41-60.*
   HTTPS://DOI.ORG/10.4236/JPEE.2025.1310004

International Conferences

1. International Conference on Renewable Energy in Burundi at IES LA MERCED, Valladolid, Spain, Erasmus+ 2023-1-ESO1-KA171-HED-00012839.
2. Exhibition of a prototype device that manages battery charging and discharging to optimize photovoltaic systems., Regional conference (4th edition), Higher Institute of Education (ENS) of Burundi, 30 to 31 December 2024
3. Presentation of a published article, « Determining the Ideal Solar Panel Tilt Angle and the Energy Generated in the Various Burundian Provinces », Regional conference (5th edition), Higher Institute of Education (ENS) of Burundi 23 to 24 December 2025

Acronym, abbreviations and symbols

PID	: Proportional Integrated Derivate
USB	: Universal Serial Bus
DC	: Direct Current
IGEBU	: Geographic Institute of Burundi
MW	: Mega Watt
GWp	: Giga Watt peak
TWp	: Teta Watt peak
kWh	:Kilo Watt hour
I	: Intensity
V	: Voltage
Vmpp	: Voltage at maximum power point
SOC	: State of Charge
SOC	: State of Health
SOCmin	: State of Charge minimum
SOC max	: State of Charge maximum
MPPT	: Maximum power point tracking
EIS	: Electrochemical Impedance spectroscopy
PV	: Photovoltaic
BMS	: Battery management system
RUL	: Remain useful life
DoD	: Depth of discharge
LDR	: Light dependent resistor
GlobHor	: Global horizontal irradiation
FT	: Transposition factor
GlobHor_opt	: Global horizontal irradiation for optimum angle
PR	: Performance ratio
MATLAB	: Matrix laboratory
OLS	: Ordinary least squares
dPv	: Solar power variation
dV	: Voltage variation
dI	: Current variation
Ipv	: Current of solar panel
Vpv	: Voltage of solar panel

Ppv	: Power of solar panel
VMPPT	: Voltage at maximum power point tracking
Inc	: Incrementation
HC	: Hill climbing
FCO	: Open circuit voltage
SFCC	: Short circuit current fraction
I MPP	: Current at maximum power point
DMPP	: duty cycle at maximum power point
GWO	: Grey wolf optimization
FLC	: fuzzy logic controller
PMPPT	: Power at MPPT
RTC	: Real time clock
CAD	: computer aided-design
IDE	: Integrated Development Environment
PWM	: Pulse width modulation
E_avial	: Energy available
Lopt	: Los at optimum
βopt	: Optimum angle
MOSFET	: Metal oxide semi-conductor
AI	: Artificial intelligence
Voc	: Voltage open circuit

List of figure

Figure1.1:Diagram of the Earth's movement around the Sun 5
Figure1.2: Global solar radiation schema 7
Figure1.3: I-V characteristic curve of a PV module for five different irradiation values and a constant temperature 7
Figure1.4: Variation in the P-V characteristic curve of a PV module for five different irradiation values and a constant temperature 8
Figure1.5: I-V characteristic curve of a PV module for five different temperature values and constant irradiation 8
Figure1.6: Variation in the P-V characteristic curve of a PV module for four different temperature values and constant irradiation 9
Figure1.7: Choosing the orientation of the solar panel based on the hemisphere of the site..... 9
Figure1.8: Distribution of electrical energy generated in Burundi. 17
Figure1.9: Distribution of solar energy generated in different provInces of Burundi. 18
Figure1.10: Solar radiation at various IGEBU sites in 2012 19
Figure1.11: Solar radiation at various IGEBU sites in 2017 ……..……22
Figure2.1: Tilt of solar panels using PVSyst software 26
Figure2.2: Direction in which the solar panels are facing at all Burundian sites. 27
Figure2.3 **:** Diagram of a boost converter 30
Figure2.4: MPPT search using the conductance increment method 31
Figure2.5: Conductance Increment control algorithm : 32
Figure2 6: Social hierarchy of grey wolves 35
Figure2.7: Diagram of the P&O MPPT control algorithm 38
Figure2 8: Graphical representation of a classical set and a fuzzy set 39
Figure2 9: Main structure of a fuzzy logic controller 39
Figure2.10 : Architecture of the system for the P&O algorithm integrated integrated with fuzzy logic..... 42
Figure2.11: Diagram of the fuzzy set functions of the first input of the FL controller 43
Figure2.12: Diagram of the fuzzy set functions of the second input of the FL controller..... 43
Figure2.13: Diagram of fuzzy set functions for the output of the FL controller 43
Figure2.14: 3D curve of relationships between the inputs and the fuzzy output..... 44
Figure 2. 15: Algorithm for the two-axis solar tracker designed 46
Figure2. 16: Block diagram of single-axis solar tracker 47
Figure2.17: Diagram showing the structure of the two-axis solar tracking system configuration 49

Figure2.18: Control mechanism for a battery charge/discharge monitoring system with temperature regulation. 50
Figure2.19:Schematic model of the mechanism of a battery charging and discharging monitoring system with temperature regulation. 50
Figure2.20: Equivalent circuit of a solar cell 51
Figure2.21 : Technical aspects of LDR voltage reading 53
Figure2.23: Arrangement of the LDR detectors 55
Figure2.24: Block diagram showing a voltage dividing bridge..... 59
Figure 2.25: Architecture of multi-inverters under centralized management..... 61
Figure3.1: Design diagram of a photovoltaic system regulated by the Incremental MPPT and conductance algorithm 62
Figure3.2: Variation curve of power output using Inc MPPT algorithm..... 62
Figure3.3 : Design diagram a photovoltaic system regulated by the P&O MPPT algorithm regulated coupled with a fuzzy logic regulator. 63
Figure3.4: Variation curve of irradiance, current and voltage using the MPPT algorithm. 63
Figure3.5 : Power produced using the P&O MPPT algorithm and fuzzy logic processor. 64
Figure3.6: Photovoltaic area performance index. 68
Figure3.7: Variations in the optimal horizontal global radiance (a) in the center of Burundi, (b) in south of Burundi, (c) in north of Burundi , (d) in east of Burundi and (d) in west of Burundi 76
Figure3.8 : Photovoltaic solar panel has a 30° slant. 77
Figure3.9: Photovoltaic solar panel has a 14° slant. 77
Figure3.10: Curve showing power distribution in December,21/2023..... 78
Figure3.11: Curve showing power distribution in December, 28/2023..... 78
Figure3.12: Path of the sun in Burundi schema 79
Figure3.13: Controlling the solar tracker at an angle desired 80
Figure3.14: Displaying how the solar panel is tracked at the desired angle 80
Figure3.15: Design diagram of the single-axis tracker 81
Figure3.16: Panel rotation (a) for detection of panel rotation from East to West at 11:00 AM and (b) for detection of panel rotation from East to West at 11:12 AM 82
Figure3.17: Control circuit of the dual-axis solar tracker 82
Figure3.18: Servo motor 1 rotating directly from East to West and servo motor 2 in stop position..... 83
Figure3.19: Showing of the behavior of the developed algorithm 84
Figure3.20: (a) View from above of the three-dimensional design of the two-axis solar tracker structure et (b) The basic design of a dual-axis solar tracker. 85

Figure3.21: (a): (a) Internal diagram of the servomotor design; (b): Sectional representation of the internal design of the servomotor, (c) Schematic diagram of the general design of the servomotor. 86
Figure3.22: Experimental prototype of the dual-axis solar tracker 87
Figure3.23: Diagram displaying the results on the serial monitor. 87
Figure3.24: Diagram of experimental results of dual axis tracker solar (a) for 7/29/2025, (b) for date 8/22/2025 and (c) for date 8/25/2025. 89
Figure3.25: Diagram of experimental results of dual axis tracker solar (a) for 8/23/2025, (b) for date 8/26/2025 90
Figure3.26: MATLAB block diagram for modelling a lead-acid battery. 92
Figure3.27: Battery discharge 92
Figure3.28: Battery completely charged indicator 93
Figure3.29: design of the battery storage management system with temperature regulator ... 94
Figure3.30: Curves showing the state of charge and discharge of batteries with temperature monitoring. 94
Figure3.31: Built algorithm's design schematic for the battery charging and discharging system with temperature control. 96
Figure3.32: Battery 1 charging diagram when all batteries are discharged 97
Figure3.33: Battery 2 charging diagram when battery 1 is charged 98
Figure3.34: Case where battery 1 is discharged and battery 2 is fully charged 98
Figure3.35: Battery 1 with SOC of 85% and battery 2 fully charged 99
Figure3.36 : Battery 1 fully charged, Battery 2 fully charged, DC LOAD Activate charging and FAN_CONTROL1 when the temperature is over 25°C. 100
Figure3.37: Impact of temperature on resistance 101
Figure3.38: Impact of varying temperatures on battery voltage 101
Figure3.39: Impact of varying temperatures on the battery capacity 102
Figure3.40: Impact of battery discharging current on battery voltage. 102
Figure3.41: Diagram showing variation in the number of cycles of a lead-acid battery as a function of DoD 103
Figure3.42: Indicator for charging of battery 1 104
Figure3.43: Indicator for charging of battery 2 104
Figure3.44 : Displays results via the serial monitor. 105
Figure3.45: Plx_DAQ system recorded the following temperature and humidity variation curves on 11/07/2024. 105
Figure3.46: Design diagram of a solar tracker system equipped with a battery charge and discharge management system 106

Figure3.47: (a) and (b): Variation curve of the solar tracker for different desired angles with variation curve of the battery state of charge for different SOC values and temperatures 108
Figure3.48: Design Schematic diagram of a two-axis solar tracker with a battery charging and discharging management system. 110
Figure3.49: Diagram showing battery1 charging and dual-axis solar tracker control with display 110
Figure3.50: Case of charging battery 2 if battery 1 is charged and servomotor 2 is in the stop position. 111
Figure3.51: Situation where all batteries are fully charged and the North LDR sensor's voltage is greater than the South LDR sensor's voltage 112
Figure3.52: Servomotor rotation in the indirect direction and detection of high temperature 113
Figure3.53: Battery 1 charging scenario when battery 2 is charged and the servomotors are in the stop position 114
Figure3.54: Case where all batteries are charged with a time detection of 4:24 PM 114
Figure3.55: Behavior of the algorithm developed at 6:30 PM 115
Figure3.56 :Experimental assembly of a solar tracker with a battery charging and discharging management system 116
Figure3.57: Battery 1 charging indicator 116
Figure3.58: Battery 2 charging indicator 117
Figure3.59: DC Load charging indicator 117
Figure3.60 Using the serial monitor to display the results at 9:00 AM 118
Figure3.61 Using the serial monitor to display the results at 9:12:00 AM 119

List of table

Table1.1: Monthly solar radiation data expressed in kWh/m²/day 18
Table1.2: Monthly solar radiation data expressed in kWh/m²/day 19
Table2.1: Annual meteorological data and geographical coordinates for each of the sites studied 23
Table2.2: Monthly global horizontal irradiance for the optimum tilt angle 24
Table3.1:The annual optimum tilt angle for a solar panel in 36 sites of Burundi. 65
Table3.2:Table of the impact of solar panel tilt angles on energy production at the Marangara location 66
Table3.3:The major results for a solar panel with a tilt angle of 30°. 67
Table3.4:The major results for a solar panel with a tilt angle of 13°.. 67
Table3.5: Table summarizing the model coefficients for determining R. 69
Table3.6: Table showing non-standardised and ..... standardised coefficients…….……69
Table3.7: Table of model's correlation coefficient R and coefficient of determination R^2…….……..…70
Table3.8:This table displays both standardized and non-standardized coefficients…….……..…70
Table3.9: Verification results of the models created using the geographic coordinates and meteorological information from ……...……71
Table3.10: Table showing the optimum annual tilt and the amount of energy produced using the generated models in all sites……..…….…..71
Table3.11: Comparison table of values obtained with pvsyst and the models developed…..……..……..……72

Abstract

This work is part of efforts to optimize photovoltaic systems in Burundi, a country located in the equatorial zone and characterized by highly variable solar radiation due to cloud cover, humidity, and the inability to fully charge batteries during periods of low radiation on rainy period. Most photovoltaic installations are fixed, which leads to significant energy losses since the sun's rays are rarely perpendicular to the surface of the solar panel throughout the day. This work aims to develop an intelligent solar tracker capable of automatically orienting solar panels according to the position of the sun and irradiation conditions, while integrating an intelligent battery charge and discharge management system to optimize the use of the energy produced. The device is based on an active orientation approach using two photo resistor light sensors arranged in a cross configuration, generating control signals for a servomotor that provides azimuth movement. At the same time, the date and time read by a DS3231 Real Time Clock module are used to control a second servomotor for East-West orientation, ensuring greater accuracy even in variable irradiation conditions. The control and command element is an Arduino UNO microcontroller. The first step in the work is to analyze the optimal tilt of fixed solar panels in Burundi based on meteorological data from PVGIS 5.2 for the year 2020. Using linear regression modeling via the R method in SPSS, the optimal tilt angle for fixed solar panels varies between 13° and 15.8°, offering an energy gain of around 20% compared to the uniform 30° tilt commonly used on house roofs. The work combines a hybrid MPPT algorithm combining Perturb & Observer (P&O) and fuzzy logic controller. Next, a battery charge and discharge management mechanism algorithm was implemented on an Arduino UNO microcontroller, which also controls the internal temperature measured by a DHT11 sensor. The work Includes modeling, mechanical design, and complete programming of the system using MATLAB 2020a, Proteus 8.13, Arduino IDE1.8.13, and SolidWorks 2023 software. The simulations carried out confirmed the consistency and reliability of the experimental results. The performance obtained shows significant energy gains of 29% to 41% Increase in production for the single-axis solar tracker and 42% to 50% for the dual-axis tracker, compared to a fixed solar panel. We observed a 67% energy gain in servomotor consumption. The device developed represents a major technological advance for autonomous, robust, and high-performance solar installations.

Keywords : Solar tracking system, battery storage control system, optimization of solar energy

Table of contents

Dedication ……ii
Acknowledgements.....iii
Publications and international conferences.....iv
Acronym, abbreviations and symbols.....v
List of figure v
List of table.. xi
Abstract……xii
Table of contents.....xiii
General introduction 1
Chapter 1: Literature review 5
1.1. Introduction 5
1.2. Solar resource.....5
1.3. Photovoltaic solar energy 6
1.4 Types of solar panels and efficiency.....6
1.5. Solar radiation 6
1.6. Optimization of fixed solar panel photovoltaic systems 7
1.6.1. Solar irradiation 7
1.6.2. Ambient temperature 8
1.6.3. Orientation and angle of Inclination of the panels 9
1.6.4. Shadows and obstacles 10
1.6.5. Dust and dirt 10
1.6.6. Degradation of PV modules 10
1.6.7. Types of regulators 10
1.7. The tracking system for the sun.....12
1.7.1. Solar tracker integration technologies 12
1.7.2. Types of solar tracker systems.....13
1.7.3. Solar tracker control techniques 14
1.8. Energy storage and battery management in photovoltaic systems.....14
1.8.1 Energy storage 14
1.8.2. Critical parameters to monitor in batteries 14
1.8.3 Role of artificial intelligence in PV systems 14
1.8.4. Charge and discharge management of lead-acid batteries in PV systems.....15
1.8.5 Battery management system integration technologies 15
1.9. Smart integrated photovoltaic systems 16

1.10.Energy access situation……..16
1.11. Solar potential in Burundi 18
1.12. Local constraints and factors affecting PV systems..... 20
Chapter 2: Methodology and materials used 22
2.1 Documentary study..... 22
2.2. Meteorological data and geographical coordinates in the different provinces of Burundi 22
2.3Method for optimizing a fixed solar panel PV system 24
2.3.2. Method for optimization a fixed solar panel PV system by integration of an MPPT controller..... 29
2.4. Method for designing an intelligent solar tracking system equipped with a battery management system..... 44
2.4.1. Design of an intelligent solar tracking system..... 44
2.4.2 Mechanism for the control of the charge/discharge of lead acid batteries..... 49
2.5 Setup of the intelligent solar tracking mechanism coupled with a battery charging and discharging monitoring system 51
2.6. Materials 51
2.6.1. Solar panel 51
2.6.2 MPPT charge regulator..... 52
2.6.3 Light Dependent Resistor sensor..... 52
2.6.4. Real Time Clock 3231 53
2.6.5. Arduino..... 54
2.6.6. The servomotor component..... 54
2.6.7 Anemometer 54
2.6.8 A switching apparatus 55
2.6.9 DHT11 Temperature sensor 55
2.6.10 Battery 55
2.6.11 Technique of multi-inverters under centralized management 58
2.7. Software used..... 59
2.7.1. The PVsyst software..... 59
2.7.2.The MATLAB sotware..... 59
2.7.3.Proteus professional software..... 59
2.7.5.SolidWorks software 59
2.8. Methodological limitations..... 60
Chapter 3.Presentation and interpretation of results obtained using simulation and experimentation tools 61

3.1. Introduction 61
3.2. Results of the impact of a fixed solar panel tilted at an optimal tilt angle regulated by a regulator MPPT 61
3.2.1 Design and simulation of MPPT controller 62
3.2.2. A perfect solar array tilt angle 64
3.2.2.1 Determination of the optimum angle using pvsyst software 64
3.2.3 Photovoltaic system efficiency 73
3.2.4. Experimental Results 76
3.3. Results obtained for the design and simulation of the intelligent solar tracker 79
3.3.1 Simulation results for the sun's trajectory 79
3.3.2 The solar tracker's mechanical design and modelling 85
3.3.3 Experimental results 86
3.4 Outcomes for the creation of a battery charge and discharge control system to maximize energy storage batteries 91
3.4.1. Design and simulation of the battery charge and discharge management mechanism 91
3.4.2. Analysis of the effect of temperature on various battery parameters 100
3.4.3 Predictive battery life cycle management 103
3.4.4.Experimental Results 103
3.5.The solar tracker's design with a battery charge and discharge control system. 106
3.6.Experimental prototype 116
Chapter 4 Discussion of results obtained 121
4.1.Introduction 121
4.2.Discussion of results on the impact of a fixed solar panel tilted at an optimal angle regulated by an MPPT controller 121
4.3.Discussion of results obtained for the intelligent solar tracker 123
4.4.Discussion of results obtained for a mechanism for managing the charging and discharging of energy storage batteries. 125
General conclusion 129
References 135
APPENDICES 148

General introduction

Humans have long understood the value of exploiting sources of electrical energy to provide the electricity needed for all income-generating activities around the world. Electricity is a strong enable of development, as it has a positive social impact on the development of individuals and countries worldwide. Before the 20th century, humans began to exploit the world's finite resources such as fossil fuels (oil, gas, coal, etc.). Following climate change due to the greenhouse effect, various oil crises, and multiple economic crises, research on electrical energy has turned to renewable resources. One of the oldest renewable energy resources is solar energy. The photovoltaic effect was initially noticed in 1839 by French physicist Edmond Becquerel, who noted that when exposed to light, some materials generate tiny amounts of electrical current [1]. The energy that comes to us from the sun is the result of a nuclear fusion process that is infinitely more energetic than the nuclear fission used in the nuclear power plants. It is energy that we must capture, harness using solar panels, convert and store in batteries. Access to reliable, sustainable, and affordable electrical energy is now a strategic global issue, particularly in developing countries where population growth, urbanization, and economic needs are putting Increasing pressure on existing electrical infrastructure. In Burundi, this problem is all the more acute as the country still has a low electrification rate, an interconnected grid characterized by insufficient production, and a heavy dependence on hydropower sources that are vulnerable to climatic variations.

Like many other countries around the world, Burundi exploits solar energy, which is stored using rechargeable batteries. Of the photovoltaic parks that have already been installed, only two are grid-connected systems without batteries. The others are photovoltaic systems with energy storage in lead-acid batteries. Since Gaston Planté first developed a rechargeable lead-acid battery in 1859, batteries have transformed the way energy is stored [2]. However, during the day, the Earth rotate on its axes causes a change in the sun's rays, while a photovoltaic generator exposed to the sun remains fixed in position, thus losing a considerable amount of available energy. We also note that battery ageing and temperature influence battery charging [3]. Our research has also revealed that, depending on the season, as long as the sun is shining, big batteries can be fully charged. Nevertheless, charging every battery during the wet season is challenging.

In recent scientific literature, numerous studies highlight the importance of optimal tilt angles for fixed panels, the efficiency of modern MPPT (maximum power tracking) algorithms, the benefits of smart solar trackers, and the challenges associated with battery management. However, very few studies simultaneously integrate these elements into a comprehensive system adapted to a country's climatic and economic realities. However, the combination of

these approaches to geometric optimization, electronic optimization, embedded intelligence, and energy management is an essential lever for significantly improving the performance of local photovoltaic systems.

The hypotheses presented in this work are as follows: the latitude impacts the ideal tilt angle for a solar array, the ideal tilt angle of the solar panel influences how much solar energy is captured; the combination of the MPPT algorithm Increases precision and stability, particularly in conditions of fluctuating irradiation, a mechanism for repositioning the solar panel perpendicular to the sun's rays provides an energy gain compared to a fixed solar panel, a battery charge/discharge management mechanism manages the solar energy produced and optimizes battery longevity. The combined integration of intelligent MPPT, solar tracking, and advanced battery management produces a photovoltaic system that is overall more efficient than a traditional photovoltaic system with fixed solar panel. Despite significant solar potential, the actual yield of installations remains relatively low. Several factors limit the energy efficiency of currently deployed photovoltaic systems: Solar panels mounted in a fixed position lose energy because the sun's rays are not perpendicular to them during the day, there is also an energy loss related to the optimal tilt angle of fixed solar panels, rapid changes in irradiation due to local climatic conditions disrupt the stability of the MPPT of the solar panels. Traditional MPPT algorithms, such as Perturb & Observer (P&O), have limitations in fluctuating conditions and reduce the system's ability to correctly detect the highest power point. The lack of integration between solar trackers, smart MPPT, and battery management limits the overall performance of existing PV (photovoltaic) systems. The loss of energy consumed by the servomotors of existing solar trackers and the loss of unused energy when the battery is full result in inefficient photovoltaic systems. The influence of temperature on battery aging also contributes to energy loss.

Many questions arise in the context of optimizing the efficiency of photovoltaic systems worldwide, and particularly in Burundi: The first question concerns the possibility of recovering the energy lost when the sun's rays are not perpendicular to the solar panels by means of an intelligent mechanism that allows the solar panel to pivot in order to track the sun's rays. The second question concerns the possibility of saving the energy consumed by the servomotors for a solar tracker system. The third question relates to the possibility of recovering energy lost when the battery is charged while the sun is still shining, using an intelligent mechanism that manages the battery's state of charge. The fourth question concerns the possibility of charging battery groups one by one using a battery charge and discharge management mechanism as part of optimizing photovoltaic efficiency. The last question concerns the possibility of controlling the battery temperature using an intelligent mechanism to manage battery aging. This work, undertaken as part of research into optimizing photovoltaic

efficiency, has as its main objective the design, development, modeling, and validation of an intelligent photovoltaic system integrating both a single-axis and dual-axis solar tracker, a hybrid P&O type MPPT controller combined with a fuzzy logic controller, and an advanced battery charge and discharge management mechanism. The aim is to optimize solar energy capture, improve the energy efficiency of the solar panel, extend battery life, and Increase system reliability under variable conditions.

To achieve this objective, a methodology was developed to study and analyze the effect of the solar panel's tilt angle on photovoltaic efficiency; a model in mathematics was determined to calculate the solar panel's ideal angle of tilt; a model in mathematics was determined to calculate the amount of energy generated by a solar panel; the development of an improved MPPT algorithm in response to recent climate change; the design and implementation of an improved algorithm for controlling the pivoting of the solar tracker, which will solve the problems of energy loss from fixed panels and reduce energy consumption; the creation and use of a program based on a charging/discharging mechanism for two battery groups in a solar system; a study of a system for reducing the energy consumption of the solar tracker in comparison with other studies already carried out; and a study and analysis of the economic gains of the solar tracker in comparison with fixed solar panels in Burundi, as Burundi has great untapped solar potential despite the country's electricity shortage. Burundi is located in sub-Saharan Africa, where solar tracker systems are not integrated despite the region's solar potential.

The scope of the work is organized into four chapters. The first chapter, entitled **"Literature Review''**, presents a review of the literature on solar energy. It establishes the theoretical and conceptual foundations necessary for understanding the issue and justifying the methods used. It allow us identify the factors needed to optimize a photovoltaic power plant with fixed solar arrays as well as holes in current research on this topic. It summarizes recent work on solar tracking systems. The chapter explores battery charge and discharge management strategies used in recent literature. This chapter sets the stage for the methodology. It highlights the limitations of existing solutions, scientific gaps, and justifies the need for methodological contributions.

The second chapter, entitled **"Methodology and methods used,"** is devoted to presenting the methodology, methods, and materials. It translates the findings of the first chapter into a structured scientific and technical approach. It forms the technical backbone of the research project and directly addresses the issues highlighted in Chapter 1. The limitations identified in previous studies justify the development of specific models adapted to the Burundian context. The chapter draws directly on the gaps identified in the literature on solar panel system optimization to propose models for optimizing photovoltaic efficiency. It presents

the ethics and limitations of the solar tracking system equipped with a battery management system. The second chapter transforms the gaps identified in Chapter 1 into concrete scientific solutions in the form of algorithms, models, devices, and strategies.

The third chapter, entitled "**Presentation and interpretation of results obtained using simulation and experimentation tools,"** is dedicated to presenting the simulation results and experimental results by method. The third chapter provides the transition between methodological design and scientific validation. Data analysis is studied. It experimentally and experimentally verifies the models developed in the methodology. It shows the effectiveness of each methodological modification and confirms the relevance of the models developed for the conditions in Burundi. This chapter concludes the coherence of the work: it interprets the results of Chapter 3 in light of the knowledge in Chapter 1 and evaluates the validity of the models in Chapter 2 in a real-world context. It thus completes the scientific cycle: Problem → Method → Results → Interpretation → Innovation. This chapter provides scientific proof that the models and algorithms developed actually work. It serves as a transition to the overall discussion.

The fourth chapter, entitled **"Discussion of the results obtained**," is devoted to discussing the results by method and the main results of the solar tracker equipped with a battery management system. A comparison of the literature with the results obtained and the main contributions of our research will be addressed. It brings together the major contributions from chapters 2 and 3 and shows the overall consistency of the designed system, its impact on solar energy optimization in Burundi, and its technical, economic, and social benefits. It puts into perspective the performance of the integrated solar tracker, the operation of the battery management system, the contributions of the smart MPPT, the relevance of the optimal angle of inclination and the fixed solar panel, and the contribution of the mathematical models developed. It also allows us to discuss the limitations, propose research perspectives, and formulate practical suggestions for Burundi.

Finally, the work will conclude with a general conclusion on the results obtained, while showing the impact of the research, future work, and the limitations of this work.

Chapter 1: Literature review

1.1. Introduction

This chapter is devoted to describing the literature review on photovoltaic efficiency optimization. We will present global solar energy consumption and consumption in the study region, as well as a description of solar energy conversion. This section will review the literature on studies of photovoltaic yield optimization for fixed solar panels, solar tracking systems, and lead-acid battery charge and discharge management systems. We will highlight gaps in research compared to other existing studies.

1.2. Solar resource

The solar resource is a set of data describing the evolution of available solar radiation over a given period. The sun is a virtually unlimited source of energy, able to supply several thousand times our global energy consumption. This is why humans have long sought to harness this significant energy source, which is distributed across the entire planet, and have succeeded in doing so through the use of photovoltaic cells. The Earth's movement around the sun takes place in a plane called the elliptic plane. The axis of the poles, around which the Earth rotates, is not perpendicular to the plane of the elliptic. The Earth's center of gravity describes an ellipse with the sun at one of its foci (see Figure 1.1).

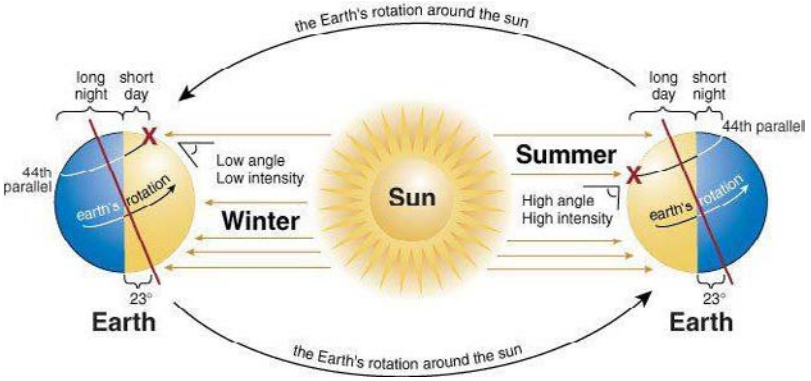


Figure1.1: Diagram of the Earth's movement around the Sun [4]

The two distinct movements of the Earth are [5]:

- The first is its rotation around its axis in 24 hours. In this case, the Earth rotates around the sun at an angle of 360° in 24 hours, i.e. a rotation of 15° per hour. In this case, the position of the sun during the day and its angle relative to North (azimuth) Increases by 15° every hour.
- The second is the Earth's revolution around the sun in 365 days, 5 hours, 48 minutes and 40 seconds ≈365.25 days. This movement occurs in a trigonometric direction and causes the cycle of the seasons.

1.3. Photovoltaic solar energy

The direct exploitation of solar energy involves two distinct technologies. One is solar thermal energy, which relies on the use of flat-plate collectors, and the other is solar photovoltaic energy, which relies on the use of solar cells. For this work, the research focuses on solar photovoltaics. In remote areas and mountainous regions of the world, where transporting electricity via power lines is sometimes costly or extremely unlikely, solar energy is a reliable source of power. Today, solar energy is widely used in smart grid systems, electric cars and building-integrated solar systems. Photovoltaic solar energy relies on the ability of certain semiconductor materials to convert sunlight into electricity through the photovoltaic effect. Photovoltaic modules are composed of several cells connected in series or in parallel in order to obtain voltages and currents adapted to requirements. The direct current (DC) produced can be stored in batteries or converted into alternating current (AC) via an inverter.

1.4 Types of solar panels and efficiency

There are several types of cells depending on the microscopic structure of the silicon [6, 7]:

- monocrystalline silicon: this crystal silicon is the type that most closely resembles the theoretical model described below. However, it is also the most difficult to obtain.
- polycrystalline silicon: this is obtained by casting Si crystals, which makes its structure heterogeneous. Its efficiency is lower than that of monocrystalline silicon
- amorphous or thin-film silicon: amorphous silicon is arranged in a thin layer on a substrate, most often glass or a synthetic material.

Crystalline silicon (monocrystalline or polycrystalline) is the most widely used material due to its abundance, stability and acceptable efficiency (between 18% and 22% in practice). In fact, it is mainly found in the form of silicon dioxide (SiO2), which is the main component of sand. However, to be usable in electronics, Si must be pure. Other technologies are emerging, such as thin-film cells, multi-junction cells and the very promising perovskite cells.

The choice of panel type depends on the installation context (available space, budget, and climate).

1.5. Solar radiation

The energy received by a surface depends on various factors such as the season, altitude, weather conditions, terrain, pollution, surface orientation, etc. The solar radiation relevant to photovoltaics is electromagnetic radiation (ultraviolet, visible and infrared radiation). At ground level, there are several components [8]:

- direct radiation: is received directly from the sun, without diffusion by the atmosphere. It is the difference between global radiation and diffuse radiation.

- diffuse radiation: is due to the absorption and scattering of light by the atmosphere and its reflection by clouds and aerosols. When the sky is overcast, it corresponds to the total energy received at ground level.
- reflected solar radiation (albedo) : is the radiation that is reflected by the ground or by objects on its surface. This albedo can be significant when the ground is particularly reflective (water, snow, etc.).
- global radiation: is the total solar radiation from the sun that reaches a horizontal surface on planet Earth. This therefore includes the vertical component of direct solar radiation as well as diffuse solar radiation. Figure 1.2 illustrates this.

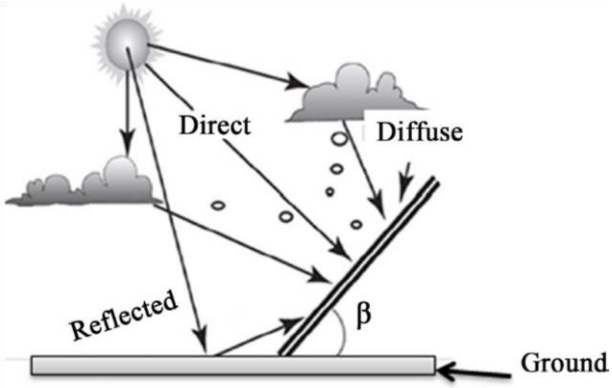


Figure1.2: Global solar radiation schema [8]

1.6. Optimization of fixed solar panel photovoltaic systems

The actual optimization of fixed solar panel photovoltaic systems depends on many environmental and technical factors.

1.6.1. Solar irradiation

The intensity and quality of the solar radiation received by a PV module directly influences its energy production. The more intense the sunlight, the higher the energy production. Irradiation is more stable in equatorial regions, but it is often disrupted by cloud cover [9]. Figure 1.3 illustrates the characteristic I-V curve of a PV module for five different variations in solar radiation and for a constant temperature (25 degrees Celsius).

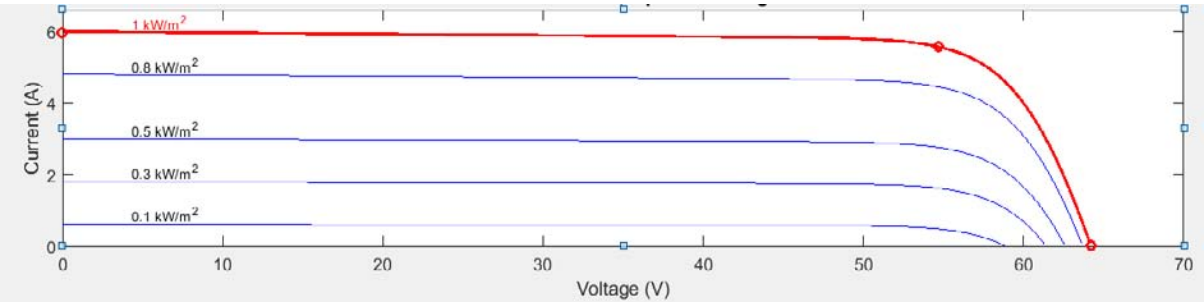


Figure1.3: I-V characteristic curve of a PV module for five different irradiation values and a constant temperature

We observe that the output current of the solar panel depends on the variation in current solar irradiation intensity. The higher the irradiation, the greater the current. However, the voltage will remain almost constant and will not very much, even though solar irradiation Increases or decreases. A variation in solar irradiation at a constant temperature has an effect on MPPT. Figure 1.4 shows the variation in the P-V (Power-Voltage) curve of a PV (photovoltaic) module as a function of 5 different solar irradiation values and at a constant temperature (25 degrees Celsius).

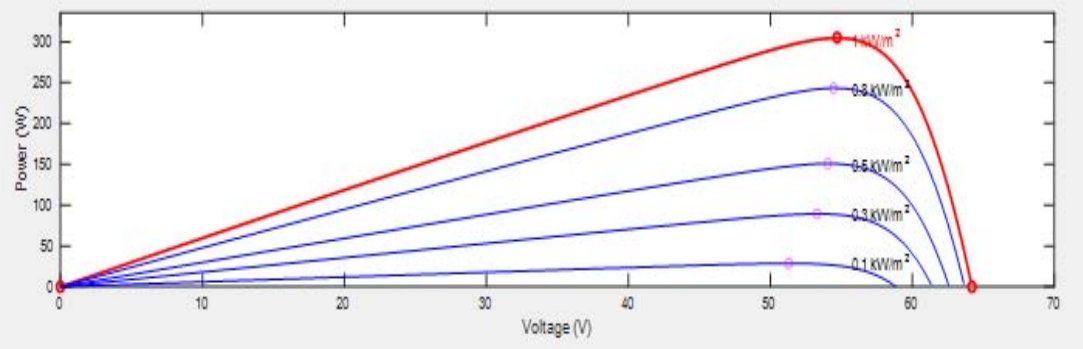


Figure 1.4: Variation in the P-V characteristic curve of a PV module for five different irradiation values and a constant temperature

1.6.2. Ambient temperature

In equatorial climates, high ambient temperatures cause PV modules to get very hot. This overheating reduces the efficiency of the cells and accelerates their ageing, which fixed systems cannot correct by adjusting their orientation to minimize direct sunlight at critical times. Above 25°C, cell performance generally decreases. The temperature coefficient is a critical parameter to consider in tropical regions. The performance of photovoltaic cells decreases as the temperature rises [10]. Figure 1.5 shows the I-V curve characteristic of the PV module for five different temperature values and for constant irradiation (1000 W/m²).

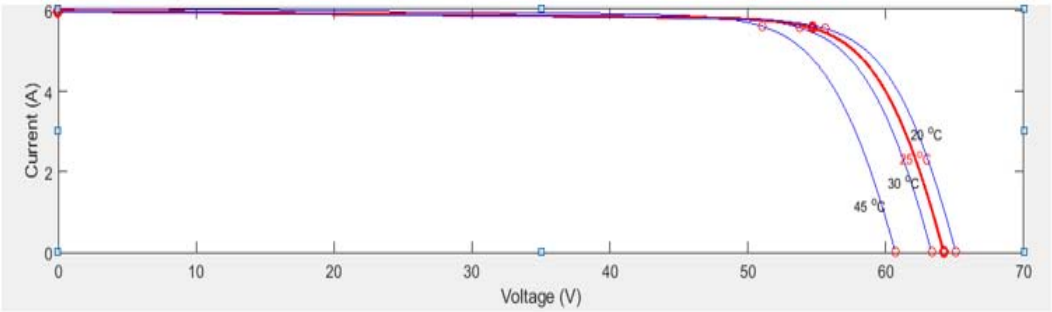


Figure 1.5: I-V characteristic curve of a PV module for five different temperature values and constant irradiation

The exposed solar panel is also subject to temperature. High temperatures reduce the voltage and power of the solar panel. Figure 1.6 shows the variation in the P-V characteristic of a PV module for four different temperature values and constant irradiation (1000 W/m²).

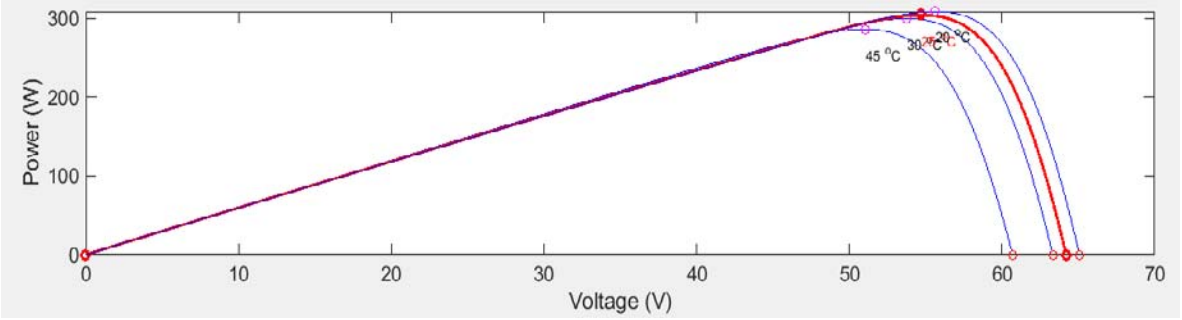


Figure 1.6: Variation in the P-V characteristic curve of a PV module for four different temperature values and constant irradiation

1.6.3. Orientation and angle of Inclination of the panels

1.6.3.1 Optimization of photovoltaic efficiency based on the solar panel's positioning

The modules must be oriented due South for sites in the northern hemisphere and due North for sites in the Southern hemisphere. The use of a compass is strongly recommended to avoid any approximation that could lead to a loss of power due to incorrect orientation. In order for solar panels to produce maximum energy, the sun's rays must be perpendicular to them and they must be oriented according to the hemisphere [11]. Figure 1.7 illustrates the choice of panel orientation according to the hemisphere.

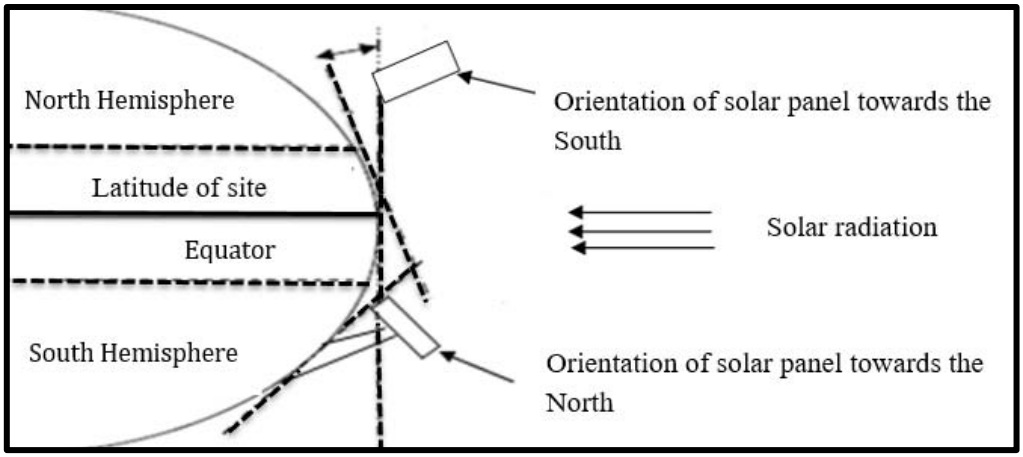


Figure 1.7: Choosing the solar panel's orientation based on the hemisphere of the site

1.6.3.2 Optimizing photovoltaic efficiency through the optimal angle of inclination of the solar panel.

The tilt of the fixed solar panels directly influences the quantity of energy produced. Several studies show that the optimal tilt angle of fixed solar panels has an effect on the energy captured. Several authors have previously studied ways to maximize solar energy production from photovoltaic systems by optimizing the orientation of the tilt angle of the solar panels in different regions. [12]- [14] demonstrate that the tilt angle is near to the latitude of locations in Saudi Arabia, China, and the United States. According to a report [15], a photovoltaic cell in

Basra (latitude 30°30') should have an annual tilt angle of 28°. According to [16], the ideal yearly tilt angle for the majority of Palestinian cities is roughly 29°, which enables an energy Increase of about 10% when compared to a solar panel set horizontally. In order to determine the ideal tilt angle for any Indian city based on its latitude, [17] suggested a mathematical method.

According to [18], 31° is the ideal tilt angle for all Iraqi locations, Including Baghdad (latitude 33°20'), Diyala (33°14'), and Tikrit (34°35'). [According to [19], Sukkur, in northern Pakistan, has an ideal tilt angle of 29.5°. According to [20]'s research, the ideal yearly tilt angles for specific Nigerian locations are 20.50°, 20.50°, 21.50°, 20.20°, 21.30°, and 22.40°. According to [21], the tilt angle is 40° since the latitude of the MOSTAGANEM site in Algeria is 36°; if the latitude is smaller than 10°, the tilt angle is 10°.

1.6.4. Shadows and obstacles

The presence of shadows (trees, buildings) significantly reduces energy production. A single partially shaded module can affect an entire solar field connected in series. The equatorial climate is characterized by dense vegetation and frequent cloud cover. These factors cause temporary shading that significantly affects the output of a fixed system, unlike a mobile system, which can partially compensate for these losses.

1.6.5. Dust and dirt

The accumulation of dirt reduces the transparency of the glazing and therefore the amount of light reaching the cells. In humid tropical climates, the combination of dust, humidity and organic matter (moss, fungi) makes cleaning solar panels more difficult, especially for fixed systems installed at height.

1.6.6. Degradation of PV modules

The efficiency of solar panels decreases over time as the photovoltaic modules degrade. Degradation can be linked to the deterioration of the glass, wear and tear on the solar cells, overvoltage between the frames and the solar cells, etc. In our work, taking into account the climatic changes that affect the energy efficiency of fixed solar panels, we will evaluate the optimization of photovoltaic efficiency by adjusting the irradiation, orientation and angle of Inclination of the panel.

1.6.7. Types of regulators

1.6.7.1. Pulse width modulation (PWM) regulator

A PWM regulator connects the solar panel to the battery via a switch (often a MOSFET) that performs voltage chopping (pulse width modulation). When the battery needs to be charged, the controller ‘pulls’ the panel to the battery voltage level (or close to it) using pulses, so the panel does not necessarily operate at its maximum power point (Vmpp).

For PWM controllers, the duty cycle varies according to the energy to be supplied to the battery in order to achieve a constant voltage charge. In a direct application, the output voltage of the panels is reduced to the nominal voltage of the batteries [22].

1.6.7.2. MPPT regulator

An MPPT controller incorporates a DC-DC converter (e.g. buck, boost or buck-boost) and an algorithm that adjusts the input voltage/current so that the panel operates at the maximum power point (MPP) of its I-V / P-V curve. The converter adapts the voltage to maximize P = V.I, and recovers the excess energy at a voltage that is useful for the battery. It contains a microprocessor and a static converter that allows all the energy to be drawn from the photovoltaic module despite variations in the output of these generators. The idea is to introduce an intermediate stage between the PV module and the battery, which will consist of a DC-DC converter [22]. In this work, taking into account its efficiency, we chose the MPPT regulator.

1.6.7.3 Recent work on MPPT technologies

Several MPPT studies have been proposed to resolve the significant problems of conventional MPPT methods, taking into account the climate changes of recent years. [23] provides a summary of state-of-the-art MPPT algorithms, accompanied by a critical analysis, in order to improve the choice of the most suitable algorithm for a specific application. Finally, this review article aims to provide a relevant reference for research trends in Pertuber and Observer (P&O) MPPT algorithms. According to their findings of [24], artificial intelligence provide quick and effective tracking speed and have a tracking efficiency of almost 99% when compared to the other strategies studied. A study was conducted by [25] on solar energy systems using technology for maximum power point tracking, compared to fixed disturbance steps and a fixed multiplier, the proposed method allows for faster convergence of disturbances, maintaining fast tracking in 9 steps with a duty cycle of 4% in steady state and up to 99.98% in steady state. [26] implements a new intelligently optimized adaptive model reference controller using a number of MPPT techniques for photovoltaic systems . A comparative study was conducted between the MPPT techniques. [27]- [31] demonstrates an improved maximum power point tracking technique using Pertuber and Observer for solar photovoltaic. Results clearly demonstrate the effectiveness of the improved algorithm and for [31] the P&O strategy outperformed the other approaches. [32] creates a hybrid model. A fuzzy logic controller serves as its foundation. In his studies, he does this. Although these hybrid approaches are more efficient than traditional ones, their design is more intricate.

1.7. Tracking system for the sun

The rise of renewable energies, particularly solar photovoltaic energy, represents a strategic response to global energy and climate challenges. In equatorial regions such as Burundi, where sunshine is abundant but irregular, the optimization of photovoltaic (PV) systems is crucial to ensuring stable and efficient energy production. During the day, the earth rotates on its axes, while a photovoltaic generator is fixed in position, thus losing a considerable amount of energy that could otherwise be available. This is because the sun's rays do not remain perpendicular to the surface of the solar panel. For a panel tilted at an optimal angle and correctly oriented in the hemisphere, the energy supplied by the photovoltaic modules is only at its maximum at noon [33]. This shows that the principle of solar panel optimization requires the flat surface on which the photovoltaic cells are mounted to be perpendicular to the sun's rays for maximum efficiency.

Optimizing photovoltaic energy production is a crucial issue for developing countries, particularly Burundi, where rural electrification remains limited. They promote energy independence for isolated communities, reduce dependence on the national grid and stimulate sustainable local development. One technical means of improving the efficiency of photovoltaic panels is the use of solar tracking systems, which maximize solar radiation capture by following the sun's trajectory. This section presents a summary of existing work on solar trackers, focusing on solar tracking technologies and their applicability to the Burundian context.

1.7.1. Solar tracker integration technologies

The idea of tracking the sun to maximize energy capture is not new, but the control techniques and strategies used differ from one designer to another. The first solar tracking systems date back to the 1960s, mainly in the fields of astronomy and space communications, where heliostats (devices that orient a mirror towards the sun) were already in use. In 1975, McFee introduced the first automatic solar tracking systems in which an algorithm was developed to calculate the total power received and the flux density distribution in a central receiver solar energy system [33]. In 1983, a solar tracking system consisting of a two-axis equatorial mount and a microprocessor was developed by Al-Naima and Yaghobian. This technique was based on the astronomical coordinates of the sun [34]. However, simulations of single-axis tracking systems are less accurate, with 2% and 1% of the bifacial gain measured in Denmark [35].

Studies of [36]-[39] revealed significant differences between tracking performance and that of fixed systems (8% versus 85%), depending on numerous factors such as weather, tracking type, location and the application itself. [37] shows also that single-axis tracking systems are less efficient than dual-axis solar trackers. It has been revealed by studies [40]-[45]

that an improvement of more than 15% to 40% in energy yield is generally offered by solar tracking systems compared to fixed photovoltaic panels in the United States, China, Ouargla, Vietnam, Colombia and Malaysia. Studies [46]-[50] demonstrate the gains of the dual-axis solar tracker compared to the fixed panel, a 40% of gain in Turkey, a 22% to 56% of gain in Romania, a 24.7% of gain in Trabzon, and a 60.64% of gain in Algeria. [51] shows the gain of a dual-axis solar tracking system with heliostats in Saudi Arabia. The results of [52]- [55] show also the gain of the solar tracker compared to an optimally oriented static solar panel. In an equatorial area, employing a dual-axis solar tracker can boost solar energy capture by 31.8% to 37.0%, according to [56].

1.7.2. Types of solar tracker systems

Solar tracker systems are classified according to the number of axes of rotation, the tracking technology used and their application. This classification makes it possible to identify the systems best suited to different geographical, technical and economic contexts.

The literature distinguishes between two categories of solar trackers based on their operating principle [57]:

- single-axis tracker: Single-axis solar tracking allows rotation around a single axis, usually horizontal (East-West). This type of tracking adjusts the tilt of the panels according to the apparent movement of the sun during the day, but does not adapt to seasonal variations in solar height. It is widely used in ground-mounted solar farms.
- dual-axis tracker: Dual-axis tracking allows movement on two axes: one horizontal (azimuth) and one vertical (elevation), allowing the panel to be optimally oriented towards the sun at all times. It compensates for both daily and seasonal variations in the sun's position. It is used in systems where maximum yield is a priority.

Solar tracker systems are also classified according to their mode of operation.

The operation of a solar tracker system is based on the detection of the sun's rays in relation to the Earth's movement around the sun and the implementation of an intelligent mechanism that orients the panels. The literature distinguishes between three modes of operation for solar trackers [58]:

- active tracker: Active solar trackers use the principle of light detection with light sensors (photo resistors) that follow the sun's path, seeking to optimize the angle of incidence of solar radiation on their surface.
- passive tracker: Operates without electronic components, using thermal expansion of fluids or gases to cause mechanical tilting.
- Semi-passive or hybrid tracker: Combines both approaches to optimize consumption and accuracy.

1.7.3. Solar tracker control techniques

Several approaches are used to orient solar panels:

- tracking based on LDR (Light Dependent Resistors) sensors: photo resistors detect light intensity and adjust the motors to balance exposure. This method is simple and inexpensive but sensitive to local shadows.
- algorithmic tracking based on time and date: algorithms such as Spencer or Solar Position Algorithm (SPA) precisely calculate the sun's position at any given moment [59].

1.8. Energy storage and battery management in photovoltaic systems

1.8.1. Energy storage

Energy storage is essential in stand-alone or hybrid photovoltaic systems to ensure the availability of electricity when there is no sun (at night or in cloudy weather). Several battery technologies are used [60]. The literature distinguishes between several types of batteries, namely:

- lead-acid batteries, which have a limited lifespan (3–5 years) and are sensitive to deep discharges.
- lithium-ion (Li-ion) batteries, which can withstand deep discharges and have a longer lifespan (8–15 years), but are more expensive.
- liFePO4 batteries: a sub-family of lithium batteries, very thermally stable, with an excellent compromise between safety, lifespan and performance.

The choice of technology depends on the budget, the desired lifespan, the thermal environment and the charging cycles.

1.8.2. Critical parameters to monitor in batteries

To preserve the longevity and safety of batteries, several parameters must be monitored:

- SOC (State of Charge): percentage of remaining capacity,
- SOH (State of Health): ageing indicator
- voltage, current, temperature: to be monitored to avoid overcharging/overheating
- number of cycles: directly related to useful lifespan.

Poor management of these parameters can lead to a drastic reduction in performance and even a risk of fire in the case of lithium batteries.

1.8.3 Role of artificial intelligence in PV systems

The integration of artificial intelligence (AI) into photovoltaic systems enables autonomous decision-making based on real-time data. Machine learning algorithms optimize panel orientation and stored energy management, and anticipate weather conditions.

1.8.4. Charge and discharge management of lead-acid batteries in PV systems

A BMS (Battery Management System) is a set of sensors, algorithms and electronics that allows you to:

- protect the battery from overcharging, excessive discharge and overheating,
- balance the cells to avoid internal imbalances,
- accurately estimate SOC and SOH,
- communicate with other system components (microcontroller, solar charger).

Effective lead-acid battery management relies on precise control of charge and discharge thresholds, avoiding overcharging or deep discharge. Microcontrollers (such as Arduino or Raspberry Pi) and control algorithms (PID, fuzzy logic) enable predictive energy management. Due to the simultaneous global challenges of the depletion and future of fossil energy resources, solar energy is regarded as the primary energy source in the framework of sustainable development. Batteries are needed for storage in order to capture solar energy. Batteries have revolutionized energy storage since Gaston Planté created the first rechargeable lead-acid battery in 1859 [2].

1.8.5 Battery management system integration technologies

Numerous studies have shown that integrating a BMS into photovoltaic systems significantly improves overall system efficiency, battery life, and storage safety and stability. Various studies on battery charging and discharging systems have been conducted by several authors. [62, 63] provide a Li-ion battery or lead-acid state of charge indicator based on fuzzy logic. This is used to assess the batteries' level of charge. An overview of next-generation BMS is presented in [64, 65]. [61, 66]- [68], the BMS is an operating system that monitors, manages, and optimizes the operation of one or more battery modules in an energy storage system. Heat is produced inside a battery during the charge/discharge cycle, according to [69]. The state of research on lead-acid solar batteries and its regeneration is shown in [70]–[73]. Lead-acid solar batteries are recyclable and have a lifespan of seven to fifteen years. Studies of [74] - [76] show approach for estimating the state of health (SOH) and remaining life (RUL) of lead-acid batteries. In terms of comments/shortcomings and suggestions, [76] are among those most directly applicable to a specialized BMS for lead-acid batteries (with EIS monitoring and active balancing). [77] discusses cycle vs. cost optimization, whereby BMS must balance energy gains with constraints such as battery degradation, wear and tear, and control costs. [78] propose a battery management unit (BMS) integrated into a multi-port DC/DC converter for an autonomous PV system.

[79] develop a control strategy coupled with SOC estimation using a neural network in a PV-battery system to extend battery life by avoiding overcharging or deep discharge. [80] have compiled a state-of-the-art review of intelligent BMS systems for $LiFePO_4$ batteries in Asian micro-grids. [81, 82] show that even in hybrid systems, BMS strategies for the lead-acid portion are important for protecting the service life of these batteries.

1.9. Smart integrated photovoltaic systems

Integrating a photovoltaic system with a solar tracker and a battery management system (BMS) creates an autonomous, smart and optimized energy solution. The typical architecture Includes:

- solar panels (energy sources),
- solar tracker (optimization of received irradiance),
- charge controller (often with MPPT),
- battery with BMS (energy storage and management),
- microcontroller or embedded control unit (overall control,
- inverter (if the load is AC).

This type of integration is essential in rural areas that are not connected to the grid, as is the case in many regions of Burundi.

In the field of embedded systems, microcontrollers such as Arduino, ESP32 or Raspberry Pi are frequently used to:

- controlling the positioning of the panels (solar tracking),
- reading sensors (voltage, current, brightness, temperature),
- monitoring charging and discharging via the BMS,
- implementing energy optimization algorithms,
- enabling a user interface or remote communication (Bluetooth, Wi-Fi, Internet of Thing).

This approach is particularly suited to low-resource contexts such as rural areas in Burundi.

1.10. Energy access situation

Global energy consumption has continued to rise due to rapid population growth, particularly in developing countries and newly industrialized countries. By the end of 2022, global installed solar energy capacity exceeded 1,000 GWpand 2 TWp by the end of 2024 [83,84]. In 2020, Germany had installed about 67 GWp of total photovoltaic electricity [85]. The Netherlands had installed about 14 gigawatts (GW) of peak capacity installed by 2021[86]. Photovoltaics is the fastest growing source of electricity generation from renewable energies and is a pillar of the EU's energy transition [87]. In Algeria, solar energy is expected to account

for more than 37% of national electricity production by 2030 [88]. Today, 1.1 billion people worldwide do not have access to electricity; 600 million of them are in sub-Saharan Africa [89]. Burundi is one of the East Africa, in 2023-2024; the rate of access to electricity is estimated at around 11.6% of the population and plans to Increase this rate to 70% by 2030 through the national 'COMPACT National' plan [90,91].

The data from Burundi's Ministry of Water, Energy and Mines shows that the country's three main sources of electrical energy are hydroelectric power, thermal energy and solar energy, with a combined output of 188.969 MW. Figure 1.8 shows how electrical energy is distributed in Burundi

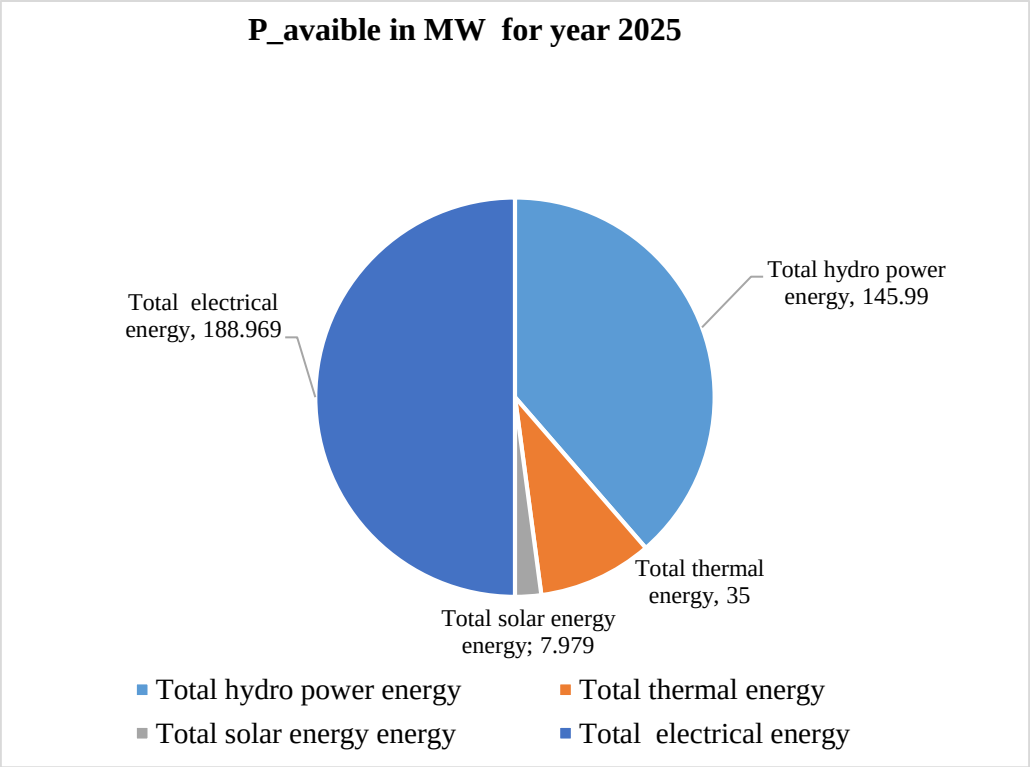


Figure 1.8: Graph showing the distribution of electrical energy generated in Burundi in 2025.

Despite this investment, installed solar capacity remains very low (a few megawatts) compared to the country's needs [89]. Figure 1.9 shows the available solar energy capacity recorded by the Ministry of Energy and Mines in the different province of Burundi for year 2025.

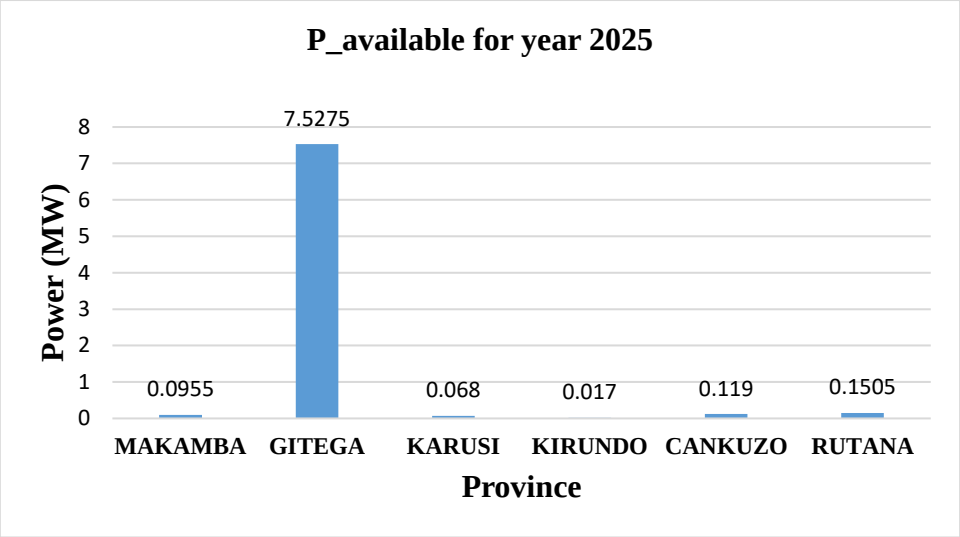


Figure 1.9: Distribution of solar energy generated in different provinces of Burundi.

Data collected by the Ministry of Water, Energy and Mines show that GITEGA is the only province where a 7.5275 MW photovoltaic field has been installed. This situation highlights the urgency and relevance of a project on decentralized and optimized solar energy electrification, especially in rural areas that are not connected to the grid.

1.11. Solar potential in Burundi

Burundi enjoys a good level of solar radiation, making it favorable for the development of photovoltaic systems. Table 1.1 shows the solar radiation data collected at IGEBU for the year 2012.

Table1.1: Monthly solar radiation data expressed in kWh/m²/day

Site	Jan	Feb	Mar	Apr	Ma	Jun	Jul	Aug	Sep	Oct	Nov	Dec
Gisozi	225	231	229	224	201	217	291	208	208	170	98	174
Cankuzo	206	175	207	160	217	233	266	254	225	198	150	159
Nyamuswaga	128	106	104	84	87	127	196	187	143	105	72	80
Bujumbura	123	161	177	104	182	224	256	222	199	181	138	153
Imbo (sems)	215	191	202	164	193	259	268	262	218	203	151	106
Gitega	199	169	215	134	188	233	284	253	216	201	133	150
Kinyinya	184	125	203	135	146	126	213	239	214	177	167	121
Kirundo	210	164	175	110	133	186	231	217	180	159	136	152
Makamba	142	79	82	74	113	170	311	234	194	141	74	69
Muriza	148	106	194	62	85	106	220	218	201	175	78	67
Nyanza lac	71	138	74.2	161.6	90.0	27.8	0.0	43.5	52.1	68.4	281.1	147.3
Ruvyironza	161	123	137	131	150	190	241	209	149	163	117	86
Ruyigi	146	152	195	111	175	148	224	224	198	131	124	105
Mpota (tora)	172	159	186	119	155	213	258	245	210	84	137	124
Mparambo	180	140	185	134	181	217	234	216	182	161	133	76

Where Jan is January, Feb is February, Mar is March, Apr is April, Jun is June, Jul is July, Aug is August, Sep is September, Oct is October, Nov is November and Dec is December. This abundant solar resource is a major asset for a tracking project with storage management, as it maximizes daily and seasonal electricity production. Figure 1.10 shows the daily solar irradiation collected at the various IGEBU sites in 2012.

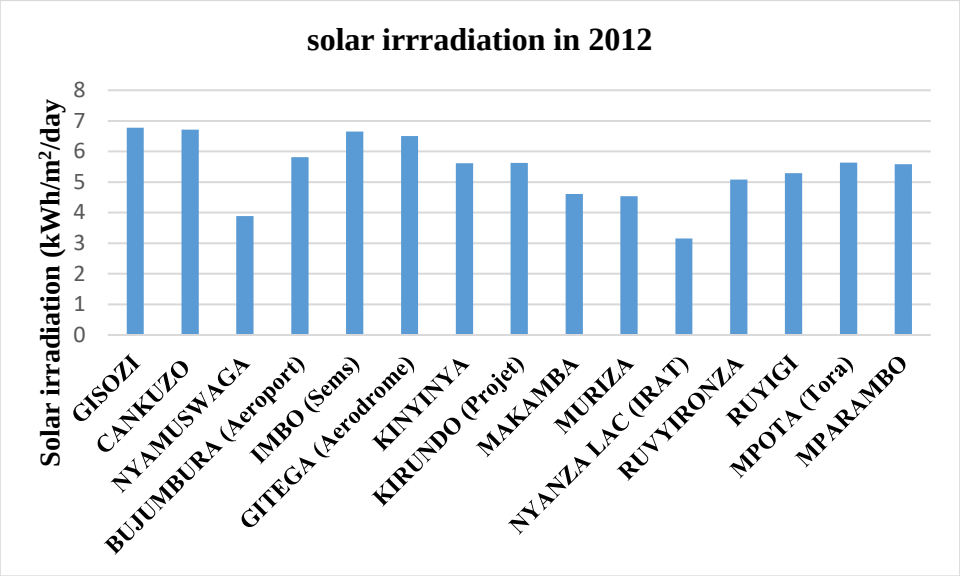


Figure 1.10: Solar radiation at various IGEBU sites in 2012

It can be seen that the average sunshine duration was 5.431 kWh/m²/day for 2012. Table 1.2 shows the solar radiation data collected at IGEBU for 2017.

Table1.2: Monthly solar radiation data expressed in kWh/m²/day

Site	Jan	Feb	Mar	Apr	May	Jun	Jul	Aug	Sep	Oct	Nov	Dec
Gisozi	169	142	159	144	181	264	245	192	189	146	152	171
Cankuzo	198	174	261	203	282	270	324	322	268	210	190	220
Nyamuswaga	128	92	84	89	167	158	198	203	161	133	96	95
Bujumbura	120	75	82	60	129	247	227	139	135	98	83	87
Imbo (sems)	122	96	97	59	128	183	201	137	125	101	83	85
Gitega	99	80	103	106	156	261	233	164	147	121	85	90
Kinyinya	195	169	217	158	220	256	318	302	262	243	168	182
Kirundo	169	116	158	147	154	266	251	179	166	186	139	177
Makamba	98	67	101	95	138	162	236	140	153	147	106	66
Muriza	122	75	88	62	98	165	163	121	95	85	69	102
Nyanza lac	145	97	130	160	246	290	268	229	229	155	77	108
Ruvyironza	92	99	130	120	121	183	238	235	175	128	80	78
Ruyigi	70	53	97	87	99	181	179	185	176	147	80	90
Mpota (tora)	67	42	161	162	95	178	140	66	198	111	41	47
Mparambo	77	60	169	177	98	213	264	112	175	103	72	87

Figure 1.11 shows the daily solar radiation collected at various IGEBU sites in 2017.

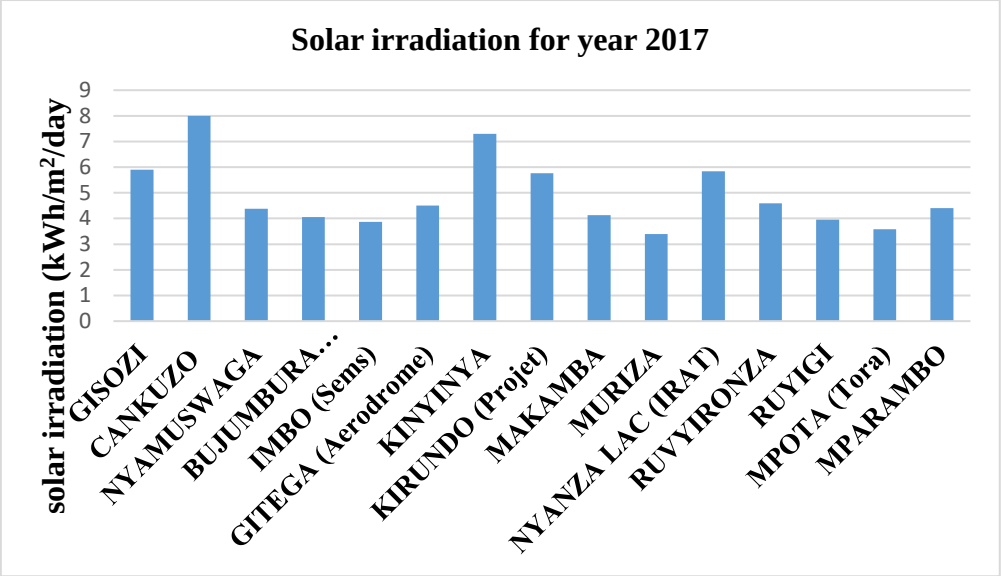


Figure 1.11: Solar radiation at various IGEBU sites in 2017

It can be seen that the average daily sunshine is 4.91066667kWh/m²/day for 2017, and we note a decrease in sunshine for 2017 compared to previous years. Due to problems with the equipment used to collect sunlight data, which is currently not working, IGEBU currently only has data for 2017.

1.12. Local constraints and factors affecting PV systems

When installing photovoltaic systems with trackers equipped with a battery management system in Burundi, several constraints must be taken into account:

- Climate variability: rainy seasons can reduce the available irradiation for several consecutive days, which requires a more robust battery sizing strategy.
- Altitude and topography: mountainous areas of Burundi may benefit from better sunshine (less cloud cover), but also from a colder climate, which can affect performance (frost or condensation effects).
- Cost and availability of components: specialized components (trackers, MPPT controllers, battery management systems) can be expensive to import and difficult to maintain locally.
- Maintenance and durability: in remote areas, systems must be designed to be robust, dust-resistant, and easy to repair by local technicians.
- Financing and social acceptability: Due to low purchasing power in rural areas, adapted financing models (pay-as-you-go, solar leasing, microcredit) are often necessary.
- Logistical infrastructure: Transport, access to difficult sites, security, etc., can have a significant impact on the overall cost of installation.

Conclusion

The literature review established the scientific and technological foundations for this research by highlighting the determining factors of photovoltaic efficiency and the approaches developed to optimize them. It showed that solar irradiation, the Inclination and orientation of the panels are essential parameters influencing the amount of energy captured. Furthermore, analysis of recent studies revealed significant advances in the integration of MPPT controllers and solar trackers, while highlighting the limitations of existing systems, particularly their lack of adaptation to the specific climatic and energy conditions of countries such as Burundi. We have shown the lack of data on sunshine and that the data available at IGEBU is from 2017.
The review also highlighted the central role of battery charge and discharge management systems in the reliability and sustainability of solar installations. Finally, an examination of the global and national energy context confirmed the relevance of a local approach to photovoltaic optimization adapted to the geographical and socio-economic realities of Burundi. Chapter 1 therefore concludes with the need to design an integrated system combining solar tracking, MPPT regulation and intelligent battery management, which will serve as a methodological framework for the development presented in Chapter 2.

Chapter 2: Methodology and materials used

This chapter describes the methodological approach adopted for the implementation and design of an intelligent solar tracker system, accompanied by a lead-acid battery system. It presents a literature review of existing solar research to highlight our contribution, a study of an optimized fixed solar panel photovoltaic system, an analysis of Burundi's sunshine data, the design of the solar tracking system, the design of the battery management system, mechanical modelling using CAD tools, a comparative study between fixed solar systems and solar tracking systems, predictive energy management, and the ethical and methodological limitations. In this chapter, we also present the materials used and the technological choices made to achieve the objectives of optimizing the efficiency of solar energy capture in the Burundian context. The methodology adopted in this work is based on an experimental approach involving the design, construction, testing and evaluation of a functional prototype. The process was structured in several successive stages, each aimed at meeting a specific objective.

2.1 Documentary study

A thorough review of the scientific and technical literature and current standards was carried out in the previous chapter to understand the concepts of solar energy, the principles and recent technologies of solar trackers, the characteristics of photovoltaic systems, and current technologies and research on battery charge and discharge management systems. The literature review enabled us to highlight the scientific and technological gaps that this research aims to achieve. The scientific and technological gaps identified enable us to present and describe the scientific and technical approaches to be taken in the work on optimizing photovoltaic efficiency.

2.2. Meteorological data and geographical coordinates in the different provinces of Burundi

In the work, we used satellite data for the year 2020 that is available. Meteorological and geographical data for the year 2020 are obtained using PVGIS v5.2 software at various sites in Burundi. Table 2.1 shows daily meteorological data and geographical coordinates for each site studied. Daily data was created using PVSYST software, from monthly data that was obtained using PVGIS v5.2 software. Table 2.2 shows monthly global horizontal irradiance data obtained using PVGIS v5.2 for the optimum angle of the site.

Table 2. 1 : Annual meteorological data and geographical coordinates for each of the sites studied for year 2020[8].

Province	SITE	Latitude	Longitude	Altitude	GlobHor	Temperature
		(°S)	(°E)	(m)	kWh/m2	(°C)
Bujumbura mairie	Kinama	-3.3250	29.3990	1797.000	4.910	22.10
	Mutanga sud	-3.3800	29.3910	900.000	4.750	22.10
Bujumbura	Mubimbi	-3.2950	29.4960	1764.000	4.610	22.10
	Kabezi	-3.5350	29.3450	805.000	4.660	22.10
Bubanza	Mpanda	-6.4610	31.5160	1293.000	5.570	22.10
	Musigati	-3.0670	29.4600	1399.000	4.780	22.10
Bururi	Mugamba	-3.6650	29.5870	2114.000	4.620	22.10
	Vyanda	-4.1040	29.6060	1841.000	5.020	22.10
Cibitoke	Mugina	-2.7940	29.9560	1545.000	5.070	22.10
	Buganda	-2.9750	29.2020	869.000	4.940	22.10
Cankuzo	Kigamba	-3.0370	30.5220	1648.000	5.360	22.10
	Cendajuru	-3.3130	30.6010	1293.000	5.410	22.10
Gitega	Nyarusange	-3.5680	29.6770	1775.000	4.910	22.10
	Buraza	-3.4780	29.9040	1736.000	4.790	22.10
Karusi	Gitaramuka	-2.9810	30.1730	1704.000	5.190	22.10
	Shombo	-3.2780	30.0500	1739.000	4.960	22.10
Kayanza	Muhanga	-2.9710	28.7260	1703.000	4.710	22.10
	Butaganzwa	-3.0840	29.7300	1756.000	4.840	22.10
Kirundo	Bugabira	-2.4330	30.0300	1469.000	5.380	22.10
	Vumbi	-2.6950	30.0800	1679.000	5.150	22.10
Makamba	Kayogoro	-4.1180	29.9500	1397.000	5.170	22.10
	Nyanza lac	-4.3380	29.6100	806.000	5.360	22.10
Muramvya	Mbuye	-2.1540	29.8400	1550.000	5.040	22.10
	Kiganda	-3.3450	29.6900	1930.000	4.390	22.10
Muyinga	Giteranyi	-2.4760	30.4700	1634.000	5.310	22.10
	Mwakiro	-3.0900	30.3100	1531.000	5.260	22.10
Mwaro	Ndava	-3.3780	29.7800	1987.000	4.860	22.10
	Bisoro	-3.6360	29.7100	1849.000	4.340	22.10
Ngozi	Marangara	-2.7310	29.9600	1400.000	5.110	22.10
	Tangara	-2.9140	30.0600	1719.000	5.190	22.10
Rumonge	Muhuta	-3.5700	29.4400	2084.000	4.630	22.10
	BURAMBI	-3.8140	29.5400	1791.000	4.750	22.10
Rutana	Musongati	-3.7270	30.0900	1738.000	5.240	22.10
	Bukemba	-4.0070	30.6200	1272.000	5.510	22.10
Ruyigi	Butezi	-2.3490	30.5500	1430.000	5.280	22.10
	Kinyinya	-3.6570	30.3400	1291.000	5.330	22.10

Table 2.2: Monthly global horizontal irradiance for the optimum tilt angle for year 2020.

Site	Jan	Feb	Mar	Apr	May	Jun	Jul	Aug	Sept	Octo	Nov	Dec
Nyarusange	145	151	152	140	161	135	137	161	157	153	145	153
Buraza	145	151	152	140	161	135	137	161	157	153	145	138
Musigati	145	151	152	140	161	135	137	161	157	153	145	137
Mpanda	145	151	152	140	161	135	137	161	157	153	145	134
Mubimbi	145	151	152	140	161	135	137	161	157	153	145	129
Kabezi	145	151	152	140	161	135	137	161	157	153	145	127
Mugamba	145	151	152	[2]	161	135	137	161	157	153	145	128
Vyanda	145	151	152	140	161	135	137	161	157	153	145	135
Mugina	145	151	152	140	161	135	137	161	157	153	145	161
Buganda	145	151	152	140	161	135	137	161	157	153	145	140
Kigamba	145	151	152	140	161	135	137	161	157	153	145	162
Cendajuru	145	151	152	140	161	135	137	161	157	153	145	162
Gitaramuka	145	151	152	140	161	135	137	161	157	153	145	160
Shombo	145	151	152	140	161	135	137	161	157	153	145	150
Kabarore	145	151	152	140	161	135	137	161	157	153	145	167
Bugabira	145	151	152	140	161	135	137	161	157	153	145	161
Vumbi	145	151	152	140	161	135	137	161	157	153	145	150
kayogoro	145	151	152	140	161	135	137	161	157	153	145	141
Nyanza	145	151	152	140	161	135	137	161	157	153	145	142
Mbuye	145	151	152	140	161	135	137	161	157	153	145	159
Kiganda	145	151	152	140	161	135	137	161	157	153	145	134
Giteranyi	145	151	152	140	161	135	137	161	157	153	145	167
Mwakiro	145	151	152	140	161	135	137	161	157	153	145	162
Ndava	145	151	152	140	161	135	137	161	157	153	145	143
Bisoro	145	151	152	140	161	135	137	161	157	153	145	128
Marangara	145	151	152	140	161	135	137	161	157	153	145	160
Tangara	145	151	152	140	161	135	137	161	157	153	145	161
Kinama	145	151	152	140	161	135	137	161	157	153	145	129
Muhuta	145	151	152	140	161	135	137	161	157	153	145	126
MutangáSud	145	151	152	140	161	135	137	161	157	153	145	129
Burambi	145	151	152	140	161	135	137	161	157	153	145	130
Musongati	145	151	152	140	161	135	137	161	157	153	145	136
Bukemba	145	151	152	140	161	135	137	161	157	153	145	153
Butezi	145	151	152	140	161	135	137	161	157	153	145	166
Kinyinya	145	151	152	140	161	135	137	161	157	153	145	158

2.3. Method for optimizing a fixed solar panel PV system

This section outline our contribution to the fixed panel PV system optimization methods. Our effort focusses on integrating a sun tracker with a battery management system to maximize the efficiency of a photovoltaic system in the equatorial region. The method first determines the ideal angle of Inclination of the fixed solar panel and its impact on the solar energy captured in order to precisely evaluate the energy gains of the solar tracker in comparison to a fixed panel solar system. Additionally, the technique incorporates an enhanced

MPPT regulator for an angle-optimized solar system, taking into consideration recent climate changes that also impact the efficiency of the solar panel. The ideal angle, solar panel tilt, and solar irradiation all have a significant impact on a photovoltaic system's efficiency.

2.3.1. Finding the ideal tilt angle for fixed solar panels and his impact on the amount of electricity that is available

This work aims to evaluate the energy gain of an intelligent solar tracking system compared to a fixed solar panel system. To conduct this study properly, the method consists first of determining the optimal angle of Inclination for the fixed solar panel. The optimum tilt angle of a fixed solar panel maximizes the amount of solar energy captured by aligning the panel as closely as possible with the apparent trajectory of the sun. In Burundi, precise knowledge of this angle is essential to maximize photovoltaic energy production, particularly in a context where access to electricity remains limited in rural areas. The optimal tilt angle is the angle between the solar panel and the horizontal plane that allows for maximum annual or seasonal solar radiation capture.

Let us proceed with our methodological approach to determining the optimal angle for fixed solar panels in Burundi. To determine the optimal tilt angle for solar panels in Burundi, we will use two methods. The first involves using pvsyst7.4 software and the second involves developing a mathematical model using the R technique in SPSS software. A comparison of the results of these two methods is necessary to validate the models developed. [8] describe the method for determining the optimal tilt angle of solar panels at different sites in Burundi. For the first method, the technique is based on the use of monthly meteorological data available until 2020, as well as geographical coordinates obtained using PVGIS5.2 software. To obtain this data, enter the name of each site under study. Data about solar radiation can be found in the PVGIS (Photovoltaic Geographic Information System) program of the European Union. Africa and Europe are the sources of this data. The Joint Research Centre (JRC) is responsible for its preparation. This makes it possible for us to get meteorological information. Additionally, it allows us to get geographic coordinate information [92]. The municipality in the province with the lowest or highest latitude determines the study location. In the first approach, pvsyst software is used to determine the ideal angle of Inclination of the fixed solar panel based on data collected with PVGIS software. Based on optimization with regard to the annual irradiance and meteorological yields, the PVsyst program uses the following parameters to establish the ideal annual angle of Inclination of the fixed solar panel [8]:

- the yearly Transposition Factor (FT), is a key parameter in photovoltaic solar energy. It is used to convert the solar radiation received on a horizontal surface into the radiation received on an Inclined surface, such as that of a solar panel. It allows you

to estimate how much energy a tilted solar panel receives compared to a horizontal surface. which is the ratio of Incident irradiance on the plane to Global Horizontal Irradiation (GlobHor), i.e. this is what you benefit from by tilting the collector plane. A favorable transposition factor is equivalent to a ratio of 1 or greater;

- losses with respect to optimum (Lopt) that we have decided are insignificant;
- Global on collector plane (GlobHor_opt) corresponds to the total solar energy received on the inclined surface of a solar panel, whether photovoltaic or thermal. We express it as a percentage.

It includes three components:

- Direct irradiation: solar radiation coming directly from the sun.
- Diffuse irradiation: radiation coming from the sky, scattered by the atmosphere.
- Reflected irradiation: radiation reflected by the ground or surroundings (albedo).

Performance ratio (PR) : Performance ratio (PR) of a solar panel, which is a key indicator that measures the actual efficiency of a photovoltaic system, taking into account losses (thermal, electrical, shading, dust, inverter efficiency, etc.).

The PR expresses the ratio between the energy actually produced by the system and the theoretical energy it produced under ideal conditions[93].

$$PR = \frac{Y_F}{Y_R} \tag{2.1}$$

Where: Y_F (system efficiency factor) is the ratio between the energy supplied to the system (alternating current) and the installed power, and Y_R (reference yield) defines the source, location and direction of solar radiation.

A percentage is used to indicate the PR . In general, the normal efficiency ratio falls between 70% and 80%. The configuration procedure for calculating the solar panel's tilt angle of Inclination using PVSyst software should be illustrated in Figure 2.1.

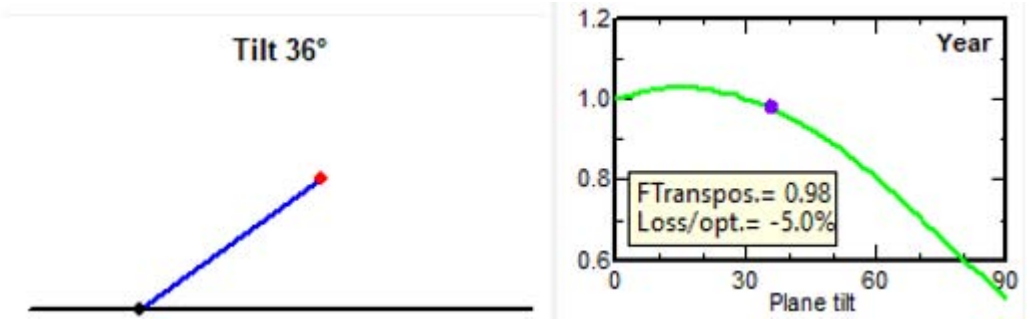


Figure2.1: Tilt of solar panels using PVSyst software[8]

This part will use MATLAB2020a program for the design and simulation as a program. We used information gathered from Burundi's Ministry of Energy and Mines report for 2023. The

following elements must be used in order to calculate the fixed panel's ideal annual tilt angle with pvsyst [8]:

- Two Sun POWER-SPR-305E-WTH-D silicon-monocrystalline solar panels with nominal power of 305W, voltage Voc=64.2V, voltage Vmpp=57.4V, current Isc=5.96A, current Impp=5.58A, surface area of 1.631, weight of 18.6 kg, and temperature with a temperature coefficient Voc of -0.27%/°C and a temperature coefficient Isc of 0.066%/°C.
- A DC-DC MPPT 1000W 48V/14A universal charge controller
- Turbo Energy's 48V 2.4kw lithium-ion battery with a 54V cut-off voltage, a 40.5V discharge voltage, and a 52Ah rated capacity.

We maked a solar powered device with some specific physical characteristics in the experimentation phase:

- Sunder brand solar panel S10-18p with maximum power of 10Wp, voltage Voc=21.24V, voltage Vmpp=18V, short-circuit current Isc=0.62A, current Impp=0.56A, temperature= 25°C.

The direction in which the solar panel is installed depends on the hemisphere, with the aim of optimizing the quantity of solar radiation captured. If the site where the solar panels are to be installed is in the northern hemisphere, the technique consists of orienting the solar panel towards the Southern hemisphere, and vice versa.

Figure 2.2 show the orientation technique of the fixed solar panel using Archicad software in all sites of Burundi.



Figure2.2: The direction in which the solar panels are facing at all Burundian sites.

Burundi is located in the Southern hemisphere, between meridians 29^0 00'-$30^0$25 East and parallels 2 ^{0}20^0 -4^{0}25' South, at an altitude of 1,614 m and covering an area of 27,834 km^2 [94]. For our study, the solar panel is oriented towards the northern hemisphere..

Let's provide a secondary approach for creating models that use SPSS software to calculate the ideal annual tilt angle and the fixed solar panel's generated electricity. [8] describes the second method, which uses simple or multiple linear regression to find a mathematical model that helps us determine the optimum tilt angle of the solar panel using SPSS software.

Linear regression:

The statistical approach for modelling the correlation between a dependent variable (Y) and one or more independent variables (X) known as linear regression. Its purpose is to predict or explain measurable phenomena, i.e. the dependent variable Y based on the independent variables X. The simple linear regression equation is given by the expression [95]:

$$Y = \beta_0 + \beta_1 X + \varepsilon \quad (2.2)$$

Where: Y is the dependent variable, X is the independent variable; β_0 is the Intercept (ordinate at the origin); β_1 is the regression coefficient (slope); ε is the random error or residual. Linear regression is based on the ordinary least squares (OLS) method, which estimates the coefficients β0 and β1 by minimizing the sum of the squares of the differences between the observed values Yi and the estimated (predicted) values. For multiple linear regression, there are several independent variables M, x^2, $_{Xk}$. The multiple linear regression model is given by equation 2.3[95]:

$$Y = \beta_0 + \beta_1 X_1 + \beta_k X_k + \varepsilon \quad (2.3)$$

Each coefficient βj measures the average effect of Xj on Y, all other things being equal. The model can be represented by equation 2.4[95]:

$$Y = X\beta + \varepsilon \quad (2.4)$$

Where X is the matrix of k potential explanatory variables, β is the vector of regression coefficients, and ε is the vector of residuals. These residuals are independent realizations of reduced normal variables. Linear regression allows several factors influencing Y to be taken into account. Linear regression is a powerful tool for analyzing and predicting relationships between quantitative variables. The correlation coefficient R and the coefficient of determination R^2 are used to assess the quality of the model fit.

The correlation coefficient R measures the strength and direction of the overall linear relationship between Y and the explanatory variables two v. (-1 R < 1).

- If R is negative, there is no linear correlation,
- If R is close to O, the correlation is weak,
- If R is close to 1, the correlation is strong

The coefficient of determination R^Z measures the proportion of the total variance of Y explained by the model. (O < R^2 < l). R^2 is the square of R in multiple linear regression [95].

$$R^2 = 1 - SSR / SST \quad (2.5)$$

$SSR = \sum_{i=1}^{n} (y_i - y_i)^2$, this is called the sum of residuals

$SST = \sum_{i=1}^{n} (y_i - \overline{y_i})^2$, it is called the sum of squares total

An R^2 value close to unity indicates a good fit between the theoretical residual standard deviation and the mean square deviation. An R^2value close to zero or negative indicates that the model has no predictive power and that, consequently, the regression established is of no interest for prediction.

- If R^2=O, the model explains nothing.
- If R^2=1, the model explains all the variance in Y.
- If R^2=O.8, this means that 80% of the variance is influenced by the explanatory variables.

The adjusted R^Z is an adjusted version of R^2 that takes into account the number of explanatory variables. The coefficient B Indicates the Influence of each variable on Y. If B is positive, this indicates a positive influence on the variable, and if B is negative, this indicates a negative influence on the variable [95].

[8] Establish a model for figuring out the ideal yearly angle of Inclination of a solar panel using the R technique in the SPSS software package, which is based on a basic linear regression model. This allow us to determine how much electricity a solar panel can produce anywhere in Burundi. We can create a model to determine the energy captured by a fixed solar panel tilted at an ideal yearly angle at any location in Burundi using the R approach in the program based on the multiple linear regression model. Analysis of variance testing utilizing simple or multiple linear regression analysis is the foundation for the results analysis used to test the hypothesis of the work. Using SPSS software to analyze quantitative variables to find two coefficients, R and R^2, that belong to the interval [-1, l] and a P value less than 0.05 is the method utilized to analyze the results and test our hypotheses.

2.3.2. Method for optimization a fixed solar panel PV system by integration of an MPPT controller

Considering changing the environment, the efficiency of permanent solar arrays tilted at an ideal angle is also impacted by changes in solar radiation in recent years, the technique also involves introducing an MPPT regulator to improve energy efficiency. When the solar panel is connected directly to the load, it does not operate at maximum power point (MPPT) unless the load is correctly matched to the photovoltaic system, but this match will not last due to varying climatic conditions. The MPPT controller's operating principle is based on the maximum power point tracking (MPPT) technique, while integrating adaptation by the DC-DC step-up chopper converter between the photovoltaic generator and its load to maximize the power produced by the solar panel.

In this subsection, we will present the DC-DC converter that plays the role of adaptation in the controller under study, and then we will describe the different methods of maximum

power point tracking and the classification of the different MPPT methods and algorithms. A choice of MPPT algorithm to be integrated to improve the efficiency of the existing maximum power tracking will be made.

2.3.2.1 Modelling of the DC-DC converter in photovoltaic systems

Choppers are DC-DC converters used to control power in DC circuits with high flexibility and efficiency. DC-DC converters called choppers are often used in PV systems to adapt a continuous source from the PV panel to a load that requires a constant DC voltage.
In this work, we chose a boost DC-DC converter because the photovoltaic generator provides a low voltage and requires adaptation of the nominal load voltage. A step-up converter is best suited to this type of conversion because it has a simple structure and a higher voltage gain than others for a given duty cycle [96]. Figure 2.3 illustrates the model diagram of a DC-DC boost converter.

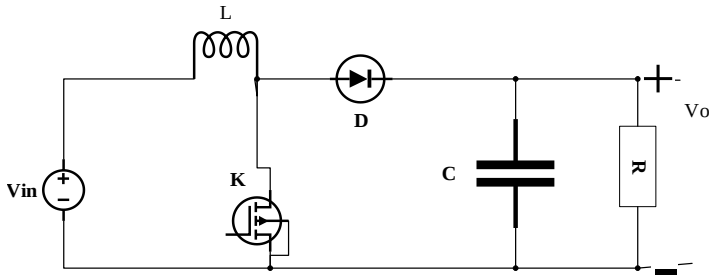


Figure2.3 : Diagram of a boost converter [96]

Where Vin is the input DC voltage, D is the diode, L is the Inductance, C is the capacitance, K is the field effect transistor, R is a resistor, and Vo is the high output voltage.
The voltage transfer gain for a DC-DC boost converter is given by the equation [96]:

$$V_0 = \frac{1}{1-D} V_{in} \tag{2.6}$$

2.3.2.2. Maximum power point tracking (MPPT) methods

Several MPPT control methods exist for finding the maximum power point. The literature describes two categories of MPPT algorithms, namely conventional algorithms and unconventional algorithms. [97, 98]. For conventional algorithms, the first is **the Perturbation and Observation (P&O) Algorithm.** The perturbation and observation (P&O) algorithm is generally the most widely used in MPPT algorithm control for PV panels [99]. It has a simple structure, low cost, easy implementation, few parameters, the possibility of introducing improvements, and can achieve high efficiency. In its configuration, this algorithm requires the voltage and current values of the solar panel as input. The algorithm outputs a duty cycle.

The second is the **increment and conductance algorithm.** The increment and conductance (IC) algorithm is a conventional MPPT method that requires two probes to measure the operating voltage V and current I of the PV module. For this technique, the system is at maximum power point if the derivative of the output power P (dP) with respect to the

derivative of the PV module voltage V(dV) is equal to zero. In this case, the MPPT system acts on the duty cycle to start controlling the panels at their maximum power. The duty cycle is given by equation 2.17 [100]:

$$D = \frac{dP_{PV}}{dV_{PV}} \tag{2.17}$$

The expression for the variation in the duty cycle is:

$$D = \frac{dI_{PV}}{dV_{PV}} \tag{2.18}$$

Figure 2.4 shows the following three conditions for positioning the maximum power point:

- If $\frac{dP_{PV}}{d_{PV}} > 0$, the target operating point lies to the left of the MPPT.
- If $\frac{dP_{PV}}{d_{PV}} = 0$, the target operating point is on the MPPT;
- If $\frac{dP_{PV}}{d_{PV}} < 0$, the operating is to the right of the MPPT

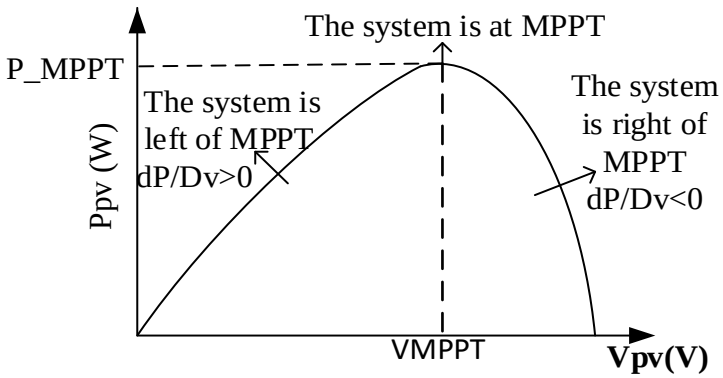


Figure2.4: MPPT search using the conductance increment method [100]:

The maximum power can then be tracked by making comparisons at each moment of the conductance value $\frac{I_{pv}}{Vpv}$ with that of the conductance Increment as $\frac{dI_{pv}}{dV_{pv}}$ illustrated in Figure 2.5, which shows the conductance Increment algorithm.

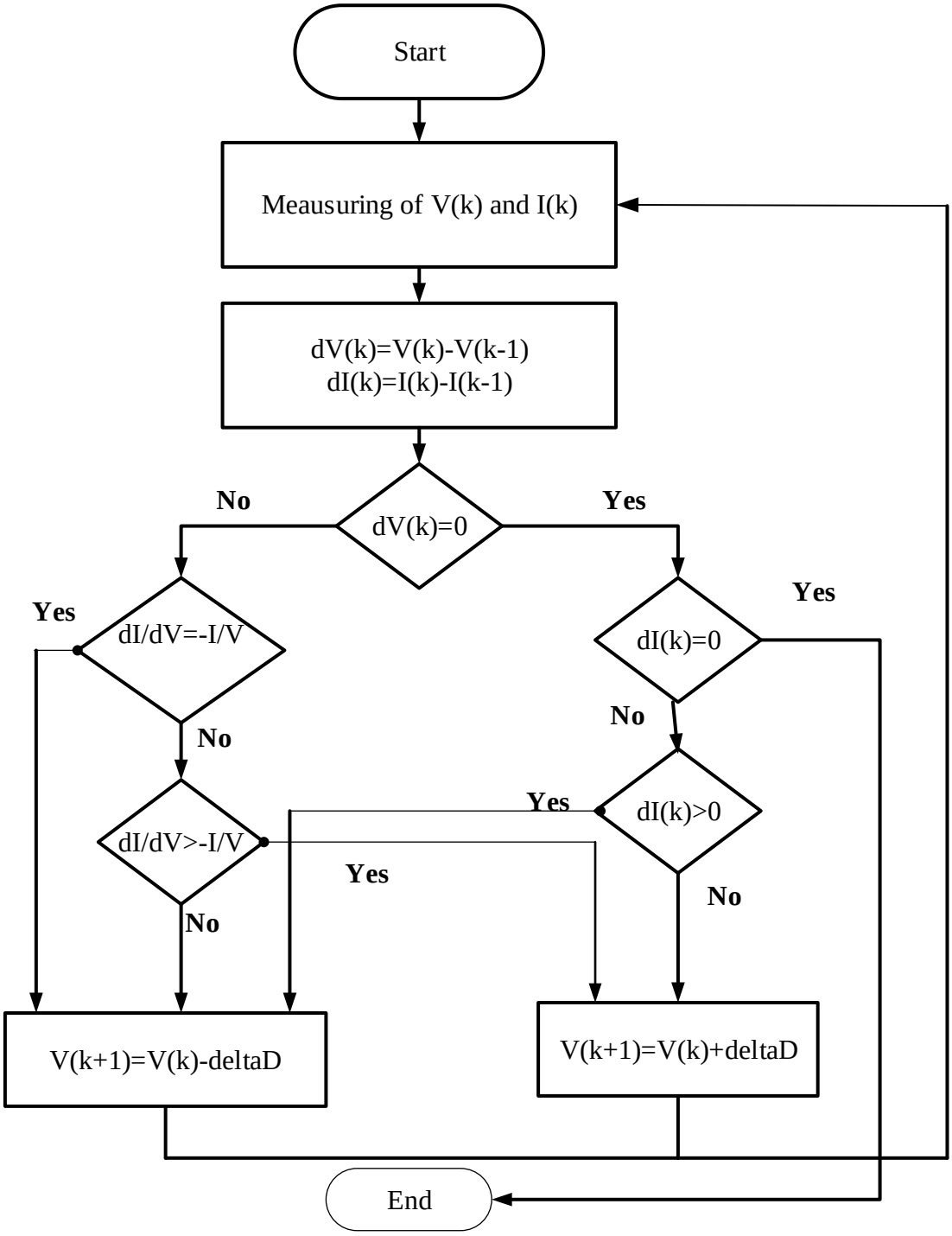


Figure2.5: Conductance Increment control algorithm [100]:

Here, V(k) corresponds to the reference voltage and forces the duty cycle photovoltaic to operate at this value. If we are at MPPT, then the voltage V(k) corresponds to the optimal voltage Vopt. Once MPPT is reached, the operating point can be maintained at this position until a variation in dl is detected. This indicates a change in climatic conditions, and therefore a new MPPT to be sought. To do this, the algorithm Increments or decrements the value of V(k) until PPM is reached. The Increment and Conductance algorithm in a photovoltaic system has limitations such as [101] :

- computational complexity: Inc is based on the differential calculation of instantaneous conductance (I/V) and Incremental conductance (ΔI/ΔV). This

requires frequent measurements and higher processing capacity than other algorithms such as Perturb & Observe (P&O), which can be challenging for microcontrollers with limited resources.

- Noise sensitivity: the calculation of numerical derivatives makes INC sensitive to disturbances and noise in current and voltage signals, which can lead to errors in detecting the maximum power point, especially in unstable environments.

The third **is the conventional algorithm is the Hill Climbing (HC) Algorithm.** The Hill Climbing algorithm is a classic method for tracking the maximum power point (MPPT) in photovoltaic systems. It adjusts the duty cycle of the DC-DC converter by making small variations and observing the effect on the output power. If the power Increases, the algorithm continues in the same direction; otherwise, it reverses the direction of the variation. This method seeks to "climb the hill" of the power-voltage curve to the peak, corresponding to the MPP. HC is conceptually similar to the Perturb and Observe (P&O) method, but is applied directly to the PWM control signal, which can simplify control in some cases [102]. The Hill Climbing algorithm has limitations such as: Oscillations around the MP, like other perturbation-type algorithms, Hill Climbing tends to oscillate around the optimum point, resulting in energy losses.

The fourth conventional is **the Fractional Open-Circuit Voltage (FCO) algorithm** for MPPT. The Fractional Open-Circuit Voltage (FCO) algorithm is a simple and widely used method for maximum power point tracking (MPPT) in photovoltaic systems. The voltage error is then used to adjust the duty cycle of the converter. The reference voltage is obtained from the known linear relationship between Vmpp and Vco of a PV module [103]:

$$V_{mpp} = K_V.V_{CO} \tag{2.19}$$

where kv is a constant depending on the type of solar panel and environmental conditions, generally between 0.73 and 0.80.

The Open Circuit Voltage Fraction (FCO) algorithm has limitations such as [104,105]:

- periodic measurement of open-circuit voltage: To determine VOC, the PV generator must be temporarily disconnected from the load, thereby interrupting energy production at each measurement. This Introduces recurring energy loss and disrupts the continuity of the power supply.
- non-universal approximation of the ki factor: The ki constant is highly dependent on the characteristics of the photovoltaic module, Irradiation and ambient temperature. An Incorrect estimation of k can lead to inaccurate maximum power point tracking.

- low accuracy in variable environmental conditions: Under conditions of rapid changes in sunlight or temperature, the relationship between VOC and VMPP becomes less reliable, reducing the robustness of the algorithm.
- lack of real-time tracking: Unlike dynamic algorithms such as P&O or INC, FCO does not continuously track MPP, which can lead to efficiency losses during rapid changes in the environment.
- unsuitable for continuous production systems: The need for temporary disconnection makes the algorithm unsuitable for grid-connected PV systems or critical loads requiring uninterrupted power supply.

The fifth is the **Short-Circuit Current Fraction (FCC) Algorithm for MPPT.** The FCC algorithm exploits the linear correlation through the short-circuit current Isc and the maximum power point current Impp. The relationship is expressed by the equation [106]:

$$I_{mpp} = K_i I_{CC} \quad (2.20)$$

Where ki is a current factor dependent on the behaviors of the PV cell and varies between 0.85 and 0.92.

The limitations of the Short-Circuit Current Fraction (SCCF) algorithm are [104, 107]:

- need to measure periodically ISC: Measuring short-circuit current requires the voltage to be set to zero, i.e. the panels to be temporarily short-circuited. This causes a temporary interruption in energy production, resulting in energy losses.
- low accuracy in variable environments: The value of k varies according to solar irradiance, temperature, panel condition and the technology used. This algorithm is therefore less reliable under changing conditions, which are particularly common in tropical or cloudy conditions.
- static approach: The FCC algorithm does not dynamically adjust the system operating point system operating point, unlike more adaptive techniques such as Perturb & Observe (P&O) or Incremental Conductance (INC).
- overall efficiency loss: The differences between ISC and IMPP Increase with ageing of panels, partial shading, or internal defects, thereby reducing the efficiency of MPPT tracking.

For the unconventional algorithm MPPT, the first is **The Grey Wolf Optimization (GWO) algorithm.** Grey wolves typically have four packs: Alpha, Beta, Delta, and Omega. The Grey Wolf Optimization algorithm is a swarm-based algorithm that draws inspiration from the social intelligence of grey wolf leadership and hunting tactics. Power and dominance are determined by a shared social order within each pack of grey wolves (see Figure 2.6). According to the grey wolf's hierarchical approach, the alpha, or strongest wolf,

is in charge of the pack's hunting, migrating, and feeding activities. The strongest wolf in the beta pack takes the lead when there isn't an alpha wolf in the group. Figure 2.6 illustrates how alpha and beta are more powerful and dominant than the other two packs, delta and omega. The GWO algorithm is mainly motivated by this societal intelligence. An additional source of motivation is the grey wolfs approach to hunting. When hunting their prey, grey wolves follow a set of effective steps: encircle and attack [108, 109]. This allows them to hunt large prey



Figure2 6: Social hierarchy of grey wolves [109].

To implement GWO-based MPPT, the duty cycle d is defined as a grey wolf. Therefore, the equation can be modified as follows[108]:

$$d_1(k+1) = d_1(k) - AD \tag{2.21}$$

Thus, the fitness function of the GWO algorithm is formulated as:

$$P(d_i^{k+1}) f P(d_i^k) \tag{2.22}$$

Where: P is the power; d is the duty cycle; i is the number of current grey wolves; k is the number of iterations.

The limitations of the Grey Wolf Optimizer (GWO) algorithm in a photovoltaic system are [109,110] :

- slow convergence time: GWO may require several iterations to converge to an optimal solution, especially in environments with fluctuating solar radiation. This can cause a delay in DMPP tracking, impacting the overall performance of the system.
- high computational load: Compared to conventional algorithms (P&O, INC), GWO requires more calculations, which can overload the low-power embedded microcontrollers typical of stand-alone PV systems.
- not always suitable for real-time systems: GWO is a stochastic algorithm, and therefore non-deterministic, which limits its predictability and responsiveness for real-time PV systems requiring quick decisions.

The second is **the Fuzzy logic algorithm.** Fuzzy logic, developed by Lofti Zadeh in 1965, is an extension of Boolean logic based on his mathematical theory of fuzzy sets, a generalization of set theory. This involves introducing the notion of degree into condition verification, thereby enabling a condition to exist in a state other than true or false, fuzzy logic provides considerable flexibility to the reasoning that uses it, making it possible to take into account inaccuracies and uncertainties [111]. FLC adapts effectively to rapid variations in irradiation and temperature. Unlike other algorithms, fuzzy logic does not require exact modeling of the PV system, making it simple to implement. It allows for more stable convergence towards the maximum power point with fewer oscillations compared to classical methods such as P&O or INC. Fuzzy logic is very effective at handling the Imprecision and uncertainty of measured signals (current, voltage), improving the robustness of the system.

Fuzzy logic has certain limitations, such as [112]:

- empirical design dependent on expertise: the definition of fuzzy rules and membership functions is often based on experience, which makes the design subjective and non-generalizable.
- complexity of adjustment: choosing the number of rules, variables and the form of membership functions can become complex and time-consuming, especially for systems with multiple inputs.
- less effective in extreme conditions: in extremely fluctuating or noisy conditions, FLC may lose performance compared to intelligent optimization methods (e.g. PSO, GWO).
- dependence on the microcontroller: its implementation requires more computing resources than simple methods such as P&O, which may limit its use in low-power embedded systems.

2.3.2.2. Choice of improved MPPT control

The MPPT is a crucial strategy for maximizing solar power's efficiency, regarding the climate changes of recent years. As a result, numerous MPPT methods have been developed and many variants of each method have been proposed to overcome various problems. These methods vary in terms of their complexity, the number of sensors required, their digital or analogue implementation, their convergence speed, their tracking capacity and their cost-effectiveness. When searching for the MPPT, it is not easy to decide which approach to use. Selection criteria Include:

- efficiency: the efficiency of maximum power point tracking is linked to the accuracy of MPPT tracking in a minimum amount of time. Some MPPT algorithms oscillate around the MPPT
- financial cost: the financial requirements of an MPPT algorithm depend on the characteristics of the MPPT tracking system, the complexity of the programming, the cost of materials, etc.
- ease of implementation: some methods are more complex to implement, while others are easy to implement.
- application

Based on the shortcomings of conventional algorithms and the unconventional algorithms already presented, in our research project, for conventional algorithms, we chose the Perturbation and Observation (P&O) algorithm, which performs better. For unconventional algorithms, we chose the fuzzy logic algorithm, which performs better than the other algorithms. The principle of this algorithm is to perturb the Vpv voltage while acting on the duty cycle D Under the effect of this perturbation, we obtain the current power supplied by the panel, denoted P(k), which is then compared to the previous power P (k-l) [99]. Figure 2.7 shows the perturbation and observation (P&O) algorithm.

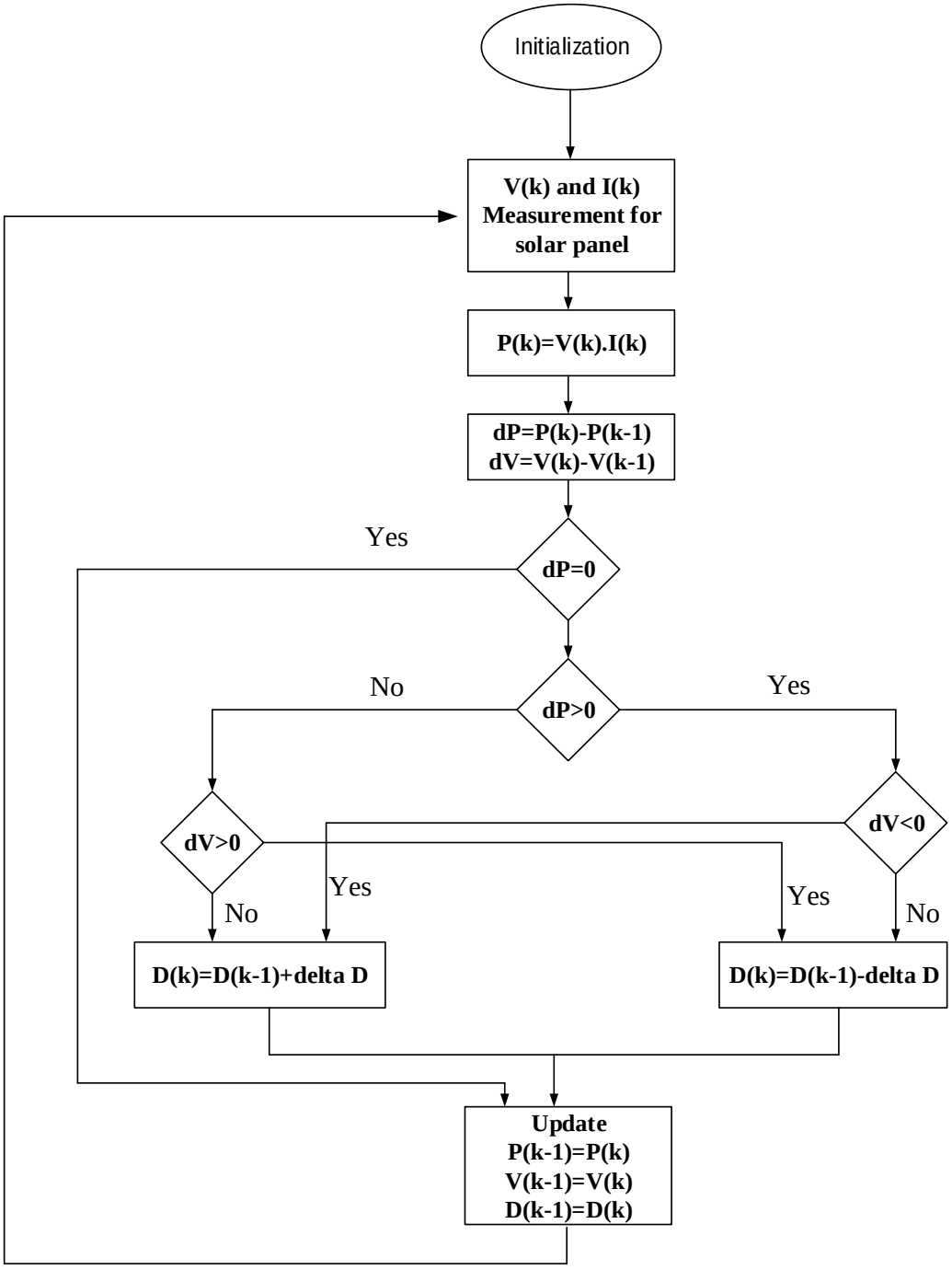


Figure2.7: Diagram of the P&O MPPT control algorithm [8]

As Burundi is located in a region subject to climatic and seasonal variation, it is necessary to make a contribution that takes into account the variability of solar radiation. In our work, considering the variation in radiation that affects solar panel efficiency, we will control this variation in solar radiation using a fuzzy logic controller.

Fuzzy logic is based on the concept of a 'fuzzy set', which is a generalization of the classical set [111]. In accordance with common usage in the literature, we will use the terms fuzzy subsets and fuzzy sets interchangeably. Classical sets are also known as clear sets, as opposed to fuzzy sets, and similarly, classical logic is also called Boolean or binary(see Figure2.8).

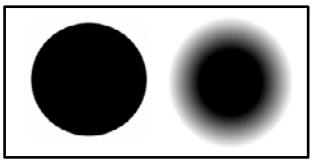


Figure2 8: Graphical representation of a classical set and a fuzzy set [111]

Figure 2.9 shows the main structure of a fuzzy logic controller.

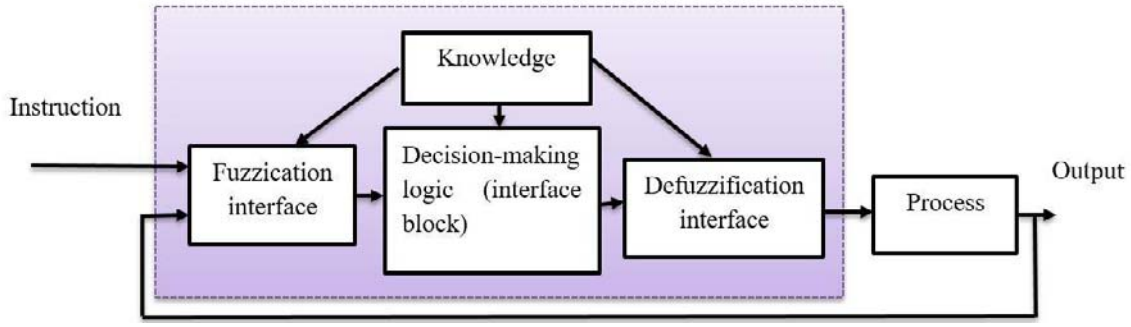


Figure2 9: Main structure of a fuzzy logic controller

The main structure of a fuzzy logic controller can be explained as follows:

- the fuzzification interface transforms inputs into linguistic variables that the inference block can then use to designate and follow rules.
- the knowledge base contains IF-THEN rules. These rules generally include fuzzy logic quantifications made by an expert in order to achieve optimal control.
- the inference engine optimally mimics expert decision-making by understanding information and applying it, always with the aim of optimally controlling input factors.
- the defuzzification interface transforms the results of the inference block into usable digital inputs usable digital inputs that will be inputs to the system (process).

a) The fuzzification

Fuzzification is the initial step in fuzzy logic systems that converts a precise (crisp) numerical value Into a degree of membership in a fuzzy set. This operation is essential for enabling fuzzy Inference and approximate reasoning in various control and decision-making systems. Fuzzification consists of associating each input value with one or more degrees of membership in fuzzy sets. A fuzzy set A on the inverse of discourse X is characterized by a membership function. A value is said to be crisp, and its fuzzification produces a vector of degrees of membership. To perform fuzzification, the variables and linguistic terms to be used must first be defined.

In this work, solar irradiation (Ir) is considered the linguistic variable that indicates the amount of sunlight projected onto the panel. Solar irradiation can be described in general linguistic terms as too high, high, medium, low, too low, and can serve as a decomposition set for the linguistic variable solar irradiation. The individual characteristics of this decomposition are labelled as linguistic terms and represent a portion of the total irradiation values. Next, in order to translate the Input data, which is numerical, into fuzzy linguistic terms, membership functions will be applied [111].

b) The membership function

The membership function is a central concept in fuzzy logic. Unlike classical logic, where an element either belongs or does not belong to a set (binary values O or 1), in fuzzy logic, an element can partially belong to a set with a degree of membership between O and l. The different possible shapes are as follows: Gaussian, triangular, trapezoidal, and generalized bell-shaped and sigmoidal. Of these, the triangular shape is the most commonly used, and the degree of the membership function is generally in the range [0 ,1].

- triangular membership function**:** Because it is easy to calculate, this approach is the most straightforward and widely used. It is defined by three parameters, a, b and where b is the apex of the triangle (maximum membership value);
- trapezoidal function**:** The trapezoidal function is a generalization of the triangular function, with a plateau at the apex defined by four parameters a, b, c and d. It allows you to define an interval where membership is complete.
- gaussian function: the Gaussian function is used to model continuous and natural data. It is defined by:

c) The fuzzy rules

Fuzzy rules are used to manage the output of a system that incorporates a fuzzy logic controller. The main objective of fuzzy systems is to create a theoretical basis for establishing hypotheses and logical associations between imprecise reference terms. In fuzzy logic technology systems, this is called approximate reasoning.

Fuzzy rules are at the heart of fuzzy logic, enabling the modelling of approximate reasoning and the handling of uncertainty in complex systems. They are often expressed in the form "IF. ..THEN. “linking fuzzy conditions to fuzzy conclusions. These rules can be developed manually, with the help of experts, or automatically, using machine learning methods. The fuzzy logic control process starts with a set of input data from any number of sensors (voltage, current, irradiation, temperature); this data is then fed into the control system. Simultaneously, the values of these input variables undergo a modification called fuzzification, which transforms discrete values into a wide range of values. The fuzzy inputs are then measured

against a set of production rules, and the selected rules generate the outputs. Finally, the output data is defuzzified by control commands.

d) The defuzzification

Defuzzification is a crucial step in fuzzy logic (FL) systems, used to convert a fuzzy set into a crisp value that can be used for decision-making or control. This operation is essential for interpreting the fuzzy outputs generated by inference rules and transforming them into concrete actions. Defuzzification techniques can be classified into two main categories:

1. maximum-based methods: These methods select a crisp value corresponding to the maximum of the membership function. They are particularly suitable for fuzzy inference systems.
2. area-based methods: These methods calculate a crisp value based on the area under the membership function curve, providing continuity that makes them suitable for fuzzy controllers.

The contribution we make to the optimization of fixed solar panels is based on the combination of the MPPT P&O algorithm with fuzzy logic, which takes consideration how the environment impact fixed photovoltaic panels tilted at a perfect angle. The goal is to Increase MPPT's effectiveness with regard to achieve optimal power output and reliable operating load, which are important characteristics for consumers and investors if they are to be attracted to the Installation of photovoltaic systems.

2.3.2.4. P&O algorithm combined with a fuzzy logic controller configuration is used for MPPT.

Our contribution concentrates on integrating an MPPT P&O algorithm with a fuzzy logic controller after outlining the several methods that have already been developed and their drawbacks. Every input/output variable in a fuzzy logic controller configuration needs to be defined as a component of the control surface. Linguistic levels can be used to describe this in fuzzy set notation. Membership functions are created by dividing each input and output variable into linguistic values and dividing each universe of discourse into neighboring intervals. PL (positive large), MeP (medium positive), Pl (small positive), Ze (zero), Nl (negative little), MeN (Negative Medium), and NL (Large Negative) are the definitions of the variables. The output duty cycle is determined by defuzzification using the centroid approach. We contribute to the MPPT technique by fusing fuzzy logic with the P&O MPPT algorithm. According to equations (2.29) and (2.30), the technique employs fuzzy logic to regulate the variance in solar irradiation in relation to the variation in solar panel voltage and current.

$$\Delta Irr = Irr - \frac{dIrr}{dt} \tag{2.29}$$

$$dE = \frac{V}{I} - \frac{\frac{dV}{dt}}{\frac{dI}{dt}} \quad (2.30)$$

where Irr is solar irradiation, V is voltage, I is solar panel output current, dV/dt is the change in solar panel voltage, dl/dt is the change in current during the day, and dlrr is the change m solar irradiation. The output of the FL dE controller is the variable duty cycle step. The values of dE were obtained after a simulation of the solar system.

The system setup for the P&O algorithm integrated with fuzzy logic is shown Figure 2.10.

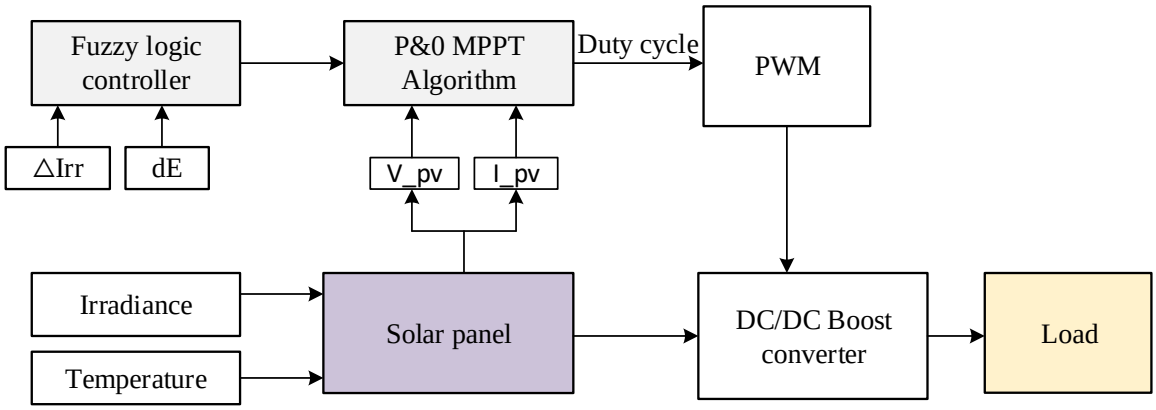


Figure2.10 : Architecture of the system for the P&O algorithm integrated integrated with fuzzy logic

Three changing environmental events have been taken into consideration when configuring the fuzzy logic controller:

- condition 1: To guarantee that the system rapidly achieves the maximum power point in the event of a considerable variation in solar radiation, the increment value must be quite big. In this instance, the voltage/current ratio difference, or dE, will fluctuate and eventually approach zero.
- Condition 2: When solar radiation varies on average, the Increment value must be neither too big to surpass the maximum power point nor too tiny to necessitate multiple iterations for the system to do so.
- Condition 3: In the event of a little fluctuation in solar radiation, the quantity will first Increase before declining until it reaches zero.

  When dE is 0 or negative, this will occur.

Figures 2.11 and 2.12 define the fuzzy sets for each input and output variable. For the fuzzy controller's input and output variables, the fuzzy subsets Nl (Negative Little), MeN (Negative Medium), NL (Negative Large), Ze (Zero), Sl (Positive Little), MeP (Positive Medium), and PL (Positive Large) were selected. We were able to ascertain the operational ranges of the dE fluctuations by recording the voltage and current output values in the solar

panel. To adjust to significant or slight changes in the inputs, the fuzzy controller's output is represented by a duty cycle Increase that ranges from zero to ten.

Figure 2.11 shows the trapezoidal and triangular shapes that were adopted for the membership functions.

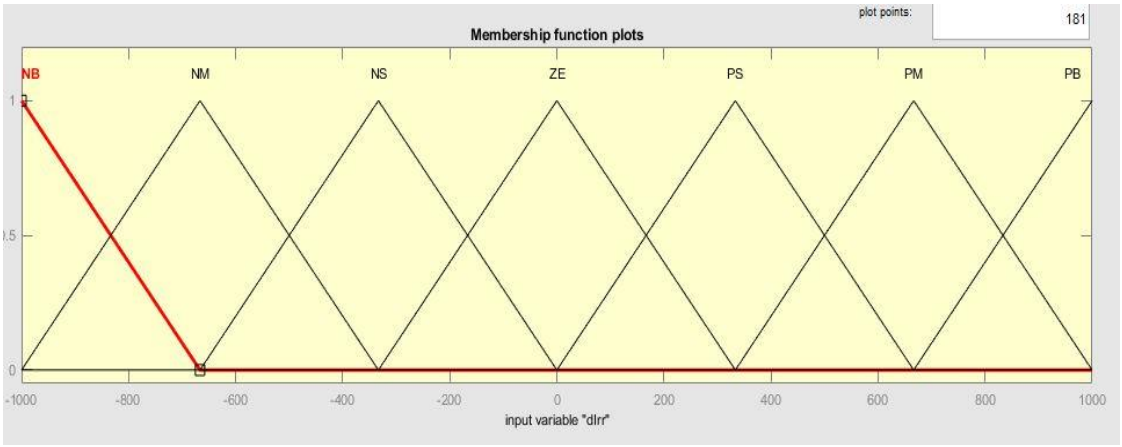


Figure2.11: Diagram of the fuzzy set functions of the first input of the FL controller

Here we see the view of technique for configuration of first input variables on solar radiation variation with a fuzzy logic controller.

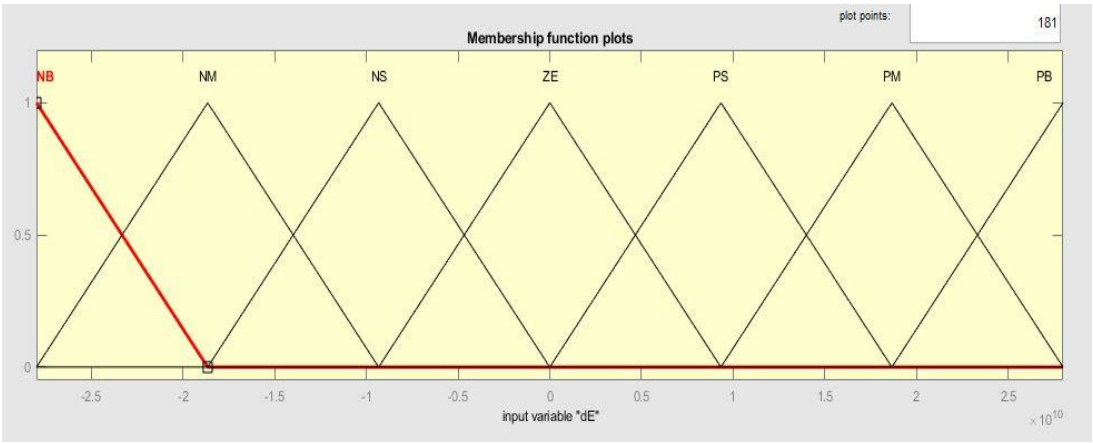


Figure2.12: Diagram of the fuzzy set functions of the second input of the FL controller

Here we see the view of technique for configuration of second input variables dE. Figure2 13 shows the diagram of fuzzy set functions for the output of the FL controller.

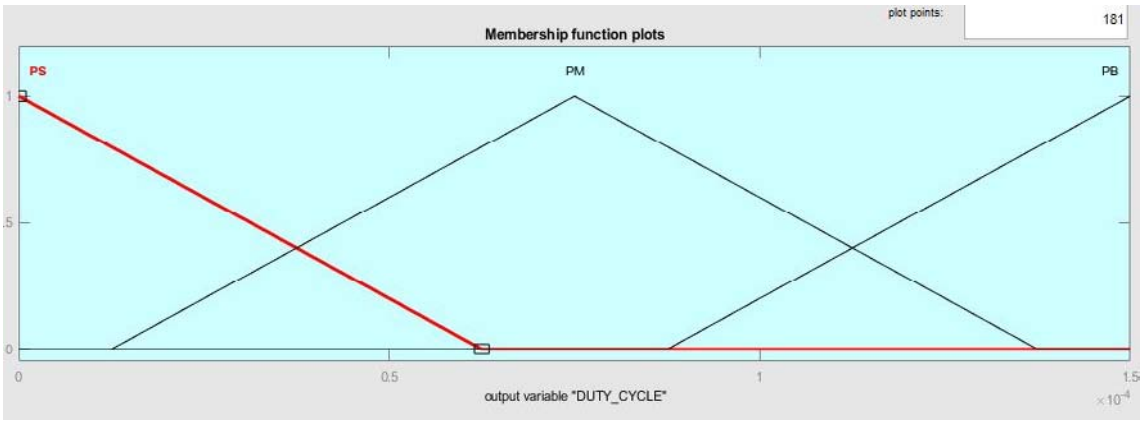


Figure2.13: Diagram of fuzzy set functions for the output of the FL controller

Here we see the view of technique for setting output variables of duty cycle. Figure2 14 shows the 3D curve of relationships between the inputs and the fuzzy output.

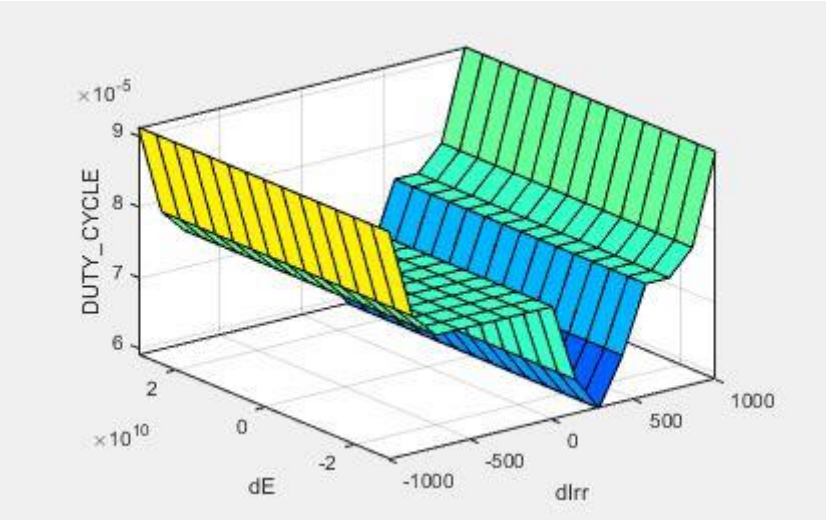


Figure2.14: 3D curve of relationships between the inputs and the fuzzy output.

Table 2.3 shows the rules for the fuzzy controller's membership functions using the three changing environmental

Table 2.3: Rules for the fuzzy controller's membership functions

dIrr **De**	**NL**	**MeN**	**Nl**	**Ze**	**Pl**	**MeP**	**PL**
NL	MeP	MeP	MeP	MeP	MeP	MeP	MeP
MeN	MeP	MeP	MeP	MeP	MeP	MeP	MeP
Nl	MeP	MeP	MeP	MP	MeP	MeP	MeP
Ze	MeP	MeP	MeP	MeP	MeP	MeP	MeP
PL	MeP	PL	PL	MeP	PL	PL	MeP
MeP	PL	MeP	PL	MeP	PL	MeP	MeP
PL	PL	PL	PL	MeP	MeP	PL	PL

2.4. Method for designing an intelligent solar tracking system equipped with a battery management system

2.4.1. Design of an intelligent solar tracking system

There are a number of solar tracker approaches such as dual-axis and single-axis solar trackers [113].There are two main techniques for solar tracking system. The first technique is known as the astronomical, as the position is directly dependent on the pre-programmed solar path. The other method is known as active, permanent or servo-controlled, as the algorithms used are based on light sensors, photo resistors. Both single-axis and two-axis solar tracking

systems are used in our investigation. We create a solar tracking algorithm that works in equatorial region.

In order to rotate the solar panel from east to west and vice versa (single axis), a solar tracker control algorithm based on a Real Time Clock RTC3231 module is developed. In order to rotate the solar panel from north to south, east to west and vice versa (dual-axis), a solar tracker control algorithm based on a light-dependent resistor (LDR) sensor and on a Real Time Clock is developed. MATLAB 2020a, Proteus 8.10.SP3, SolidWorks2023 and Arduino IDE1.8.13 are software used to create the control circuit , design, mechanical design ,3D modelling, and simulation of the solar tracker. Finding the ideal angle of inclination for a fixed solar panel is the first step in the process of comparing the energy gains of the solar tracker and we used this model's formula developed by [8].

$$\beta = 0,939\,\lambda + 11,079 \tag{2.31}$$

Where, β is the optimum tilt angle and λ is the latitude.

2.4.1.1 One-axis solar tracker's management mechanism

Several algorithms have been developed in recent years. Today, tracking techniques rely on rapid information processing and control via conventional electronic systems or embedded electronics. Based on the general principle of orienting the solar panel in an East-West direction. The technique involves using the DS3231 sensor, which is a Real Time Clock (RTC) based on a temperature-compensated crystal oscillator, which allows the exact time to be maintained even in the event of a power failure. The DS3231 provides the exact date and time in exact format, day, month and year. Figure 2.15 show the control for the single-axis solar tracker designed

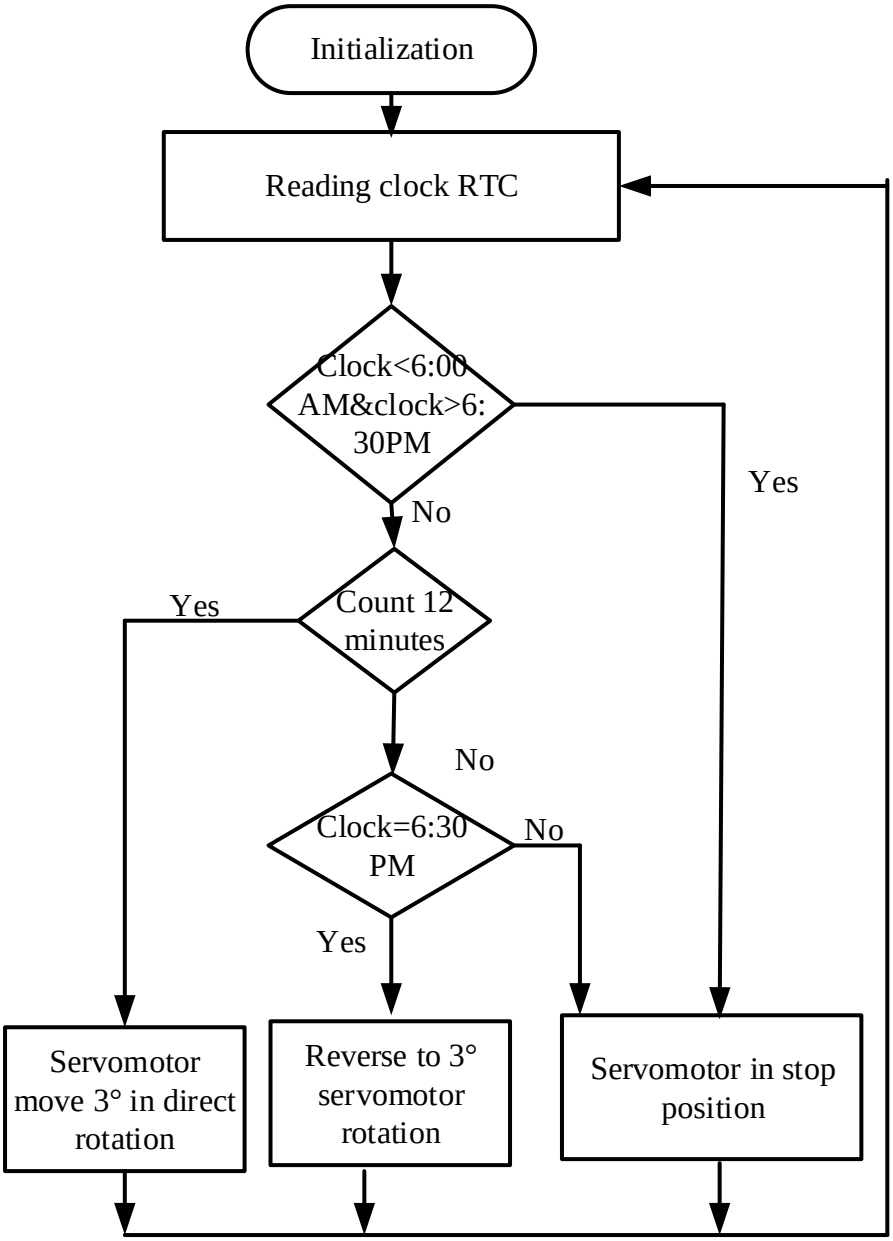


Figure 2.15: Algorithm for the two-axis solar tracker designed

The microcontroller receives information from the DS3231 via the PC module to retrieve the current time, date, month and year. Through a program, the DS3231 generates interruptions (alarms) every 12 minutes corresponding to a 3° change in the position of the sun. The microcontroller receives this information and sends pulses to the servomotor to

adjust the position of the solar panel at an angle of 3°. **Figure 2.16** illustrates block diagram of single-axis solar tracker.

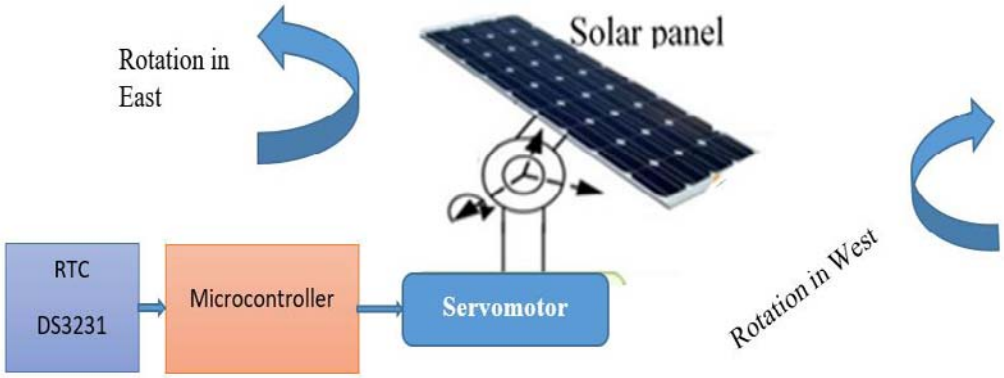


Figure2.16: Block diagram of single-axis solar tracker

2.4.1.2 Control algorithm for the dual solar tracker

We are utilizing a dual solar tracker to guarantee full tracking of the sun's east-west and north-south motions in order to appropriately manage the position of the solar panel. The process involves creating a control algorithm for the tracker utilizing two LDR light sensors and a Real Time Clock RTC3231 while moving the solar panel from East to West or from West to East. Figure 2.17 shows one-axis solar tracker's management mechanism

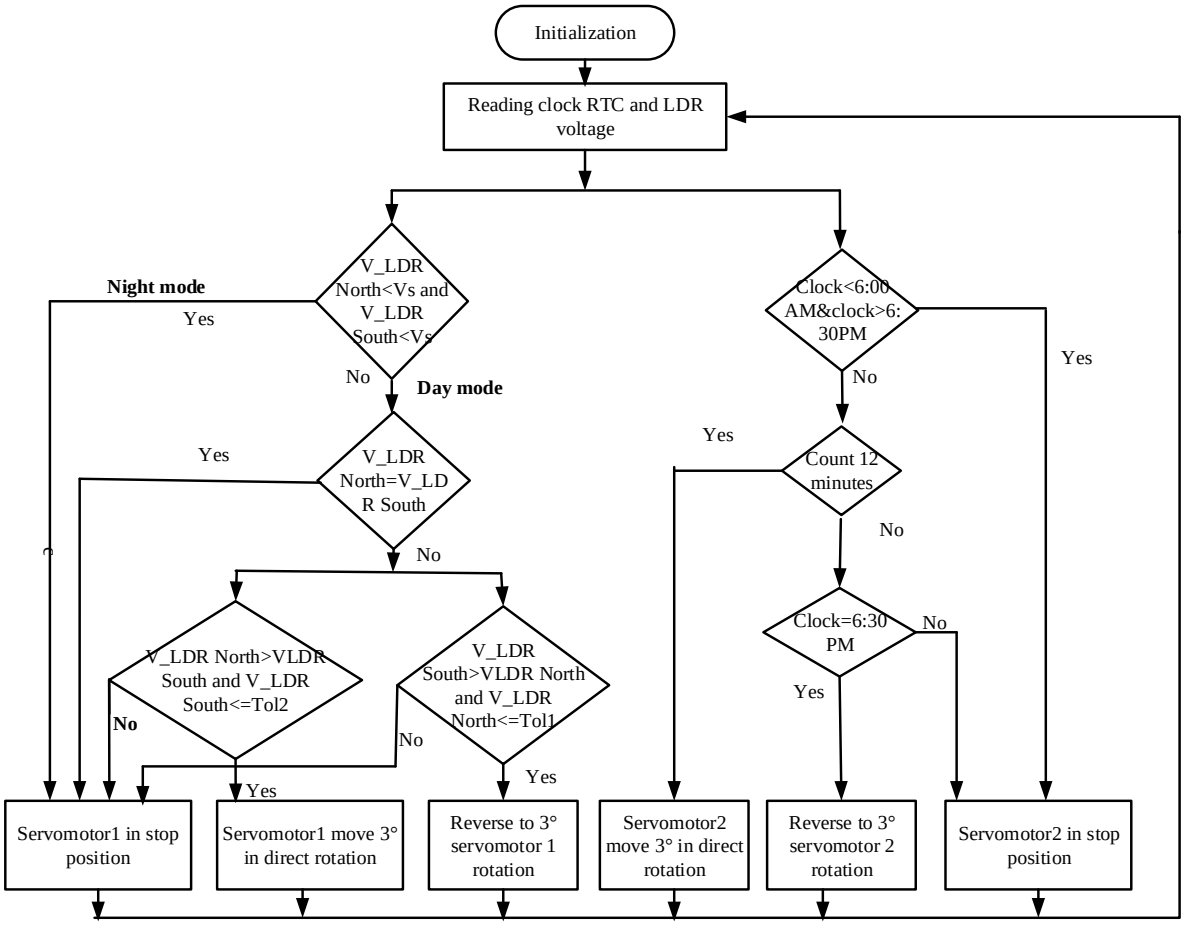


Figure2.17: Control algorithm of two-axis solar tracker

In the event that the solar panel is moved from north to south or from south to north. In our research:

- V LDR South is attributed to the voltage of the light sensor situated in the West
- V LDR North refers to the voltage of the light sensor in the east.
- Vs designation is used to denote the light sensor threshold voltage. Tol2 is the voltage differential of the West and East light sensors.
- Tol1 indicates the difference in voltage between the east and west light sensors.

To adjust the solar array from the east to the west, the approach involves of using a DS3231 Real Time Clock and the operating principle of a single-axis tracker. Next, we add two LDR photo resistor sensors that will emit control signals for moving the solar panel from North to South and vice versa. The method relies on the variation in incident light intensity between two photo resistive light sensors (LDRs) mounted on the solar panel and separated by an opaque wall. In this algorithm, we must first differentiate between day mode and night mode via the voltages of the two LDR light sensors. If the voltage delivered by the LDR sensor is lower than Vs (sensor threshold voltage expressed in V), no change is made to the position of the panel, and the system is in stop mode. If the North V LDR voltage is higher than South V LDR, this means that the light sensor located to the South is more exposed to sunlight while the other sensor is shaded. The servomotor outputs are activated by the Arduino UNO microcontroller and the panel turns towards the light source in the West until V LDR West is equal to V LDR South.

The same reasoning applies in the opposite case. Overall, we can distinguish between the following four cases:

- V LDR North < vs & V LDR South < vs: Night mode, system on standby.
- V LDR North > V LDR South: Day mode, PV panel rotates towards the North.
- V LDR North < V LDR South: Day mode, PV panel rotated towards the South.
- V LDR North = V LDR South: Motor stop condition, the panel is in an optimal position.

Each difference in illumination is subject to a tolerance to avoid repositioning the panel every time there is a small difference. Figure 2.18 shows Block diagram of solar tracker single axis

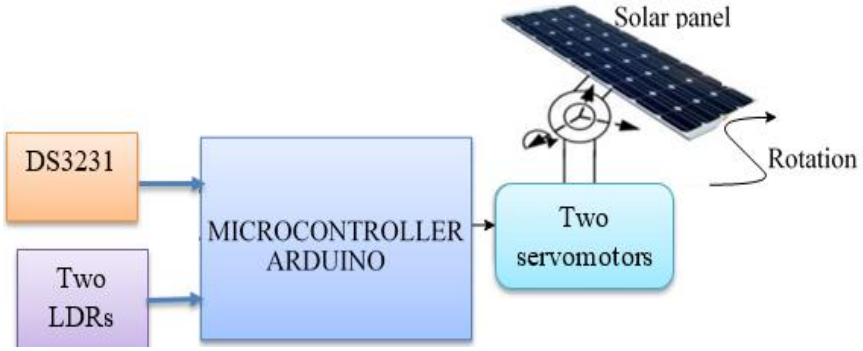


Figure2.18: Diagram showing the structure of the two-axis solar tracking system configuration

2.4.2 Mechanism for the control of the charge/discharge of lead acid batteries.

In this section, we devised a strategy for the tasks and materials required to establish a battery charge and discharge control system. The strategy entails creating an algorithm to control the temperature and charge/discharge status of two sets of batteries in a cascade. The method entails dividing all batteries acquired through the photovoltaic system modelling approach into two categories. "Battery 1" (Bat1) is the label for the first group, while "Battery 2" (Bat2) is the label for the second. We used a fan for air conditioning and the DHTII temperature sensor to keep an eye on the temperature. In order to ensure a 15-year service life, the battery must be kept at a working temperature between 20°C and 25°C. This is because a temperature of 25°C is regarded as high [28]. The Arduino UNO serves as the control and command component, and the algorithm is written using the Arduino1.8.13 software. The regulator and management circuit of the system was designed using Proteus Professional v8.0 SP3 software. The process also involves developing an algorithm using MATLAB 2020a software and making a comparison with the results obtained using Arduino IDE and Proteus Professional 8 software.

The algorithm works as follows:

- the first step is to initialize the input variables and then read the values of these variables.
- secondly, the technique consists of charging the first group of batteries In after ensuring that $V_{BAT1} \leq V_{MIN}$ and $V_{BAT2} \leq V_{MIN}$. This indicates that all batteries are discharged.
- test whether all batteries are fully charged, $VBAT_1 \geq V_{MAX}$ and $V_{BAT2} \geq V_{MAX}$, a switch is activated via a relay to charge other DC loads

Test whether the voltage of one of the battery groups is higher than the other to activate the charging of the group whose voltage is lower than or equal to $V_{MIN.}$ If all batteries are discharged, $VBAT1 <= V_{MIN}$ et $VBAT2 <= V_{MIN}$, our prototype returns the system's energy to

charge battery1first, so battery1 must be charged as a priority. When battery1 is charged, our prototype switches the charge to battery2. Figure 2.19 illustrates the functional diagram of the system under study.

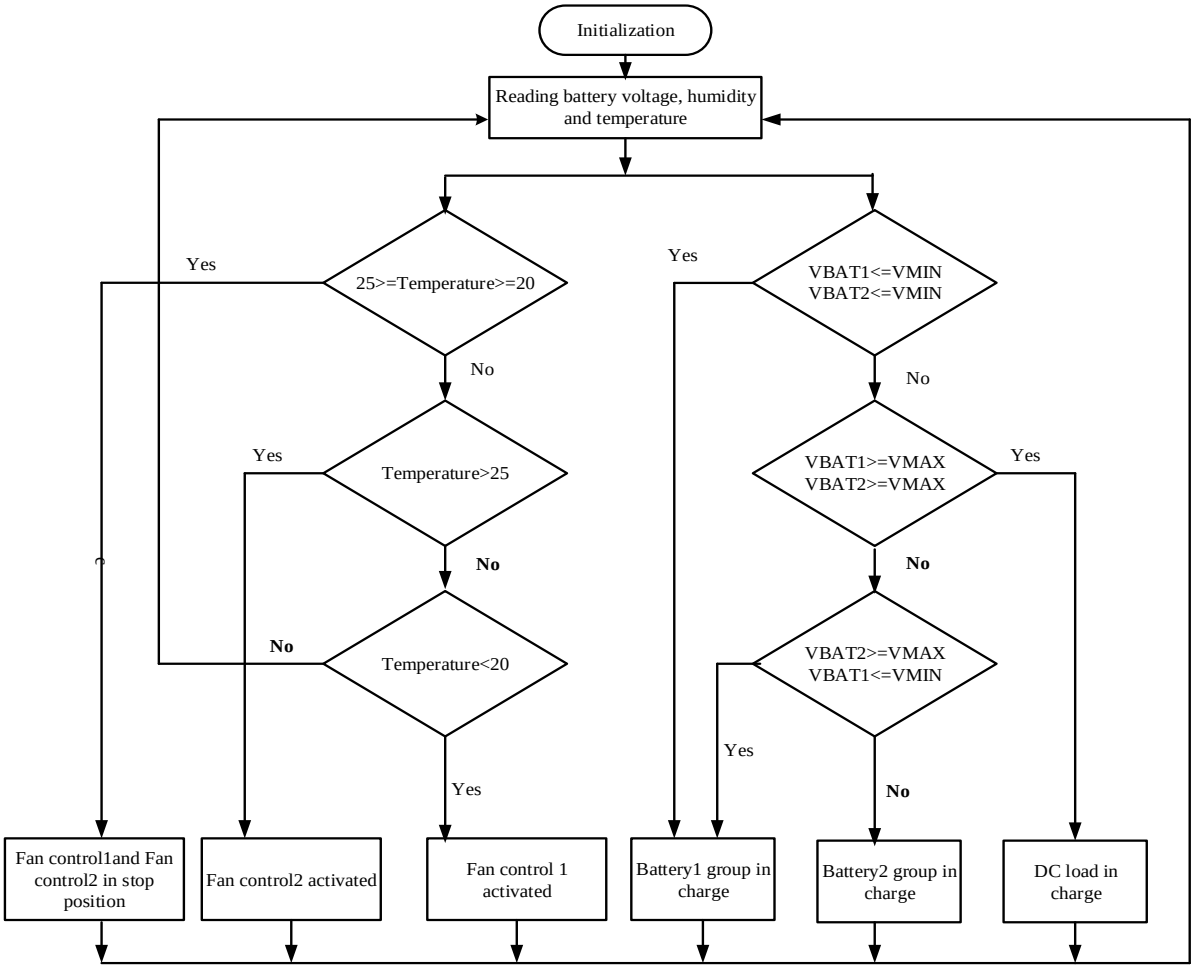


Figure2.19: Control mechanism for a battery charge/discharge monitoring system with temperature regulation.

Figure 2.20 shows a block diagram of a battery charging and discharging monitoring system with temperature regulation.

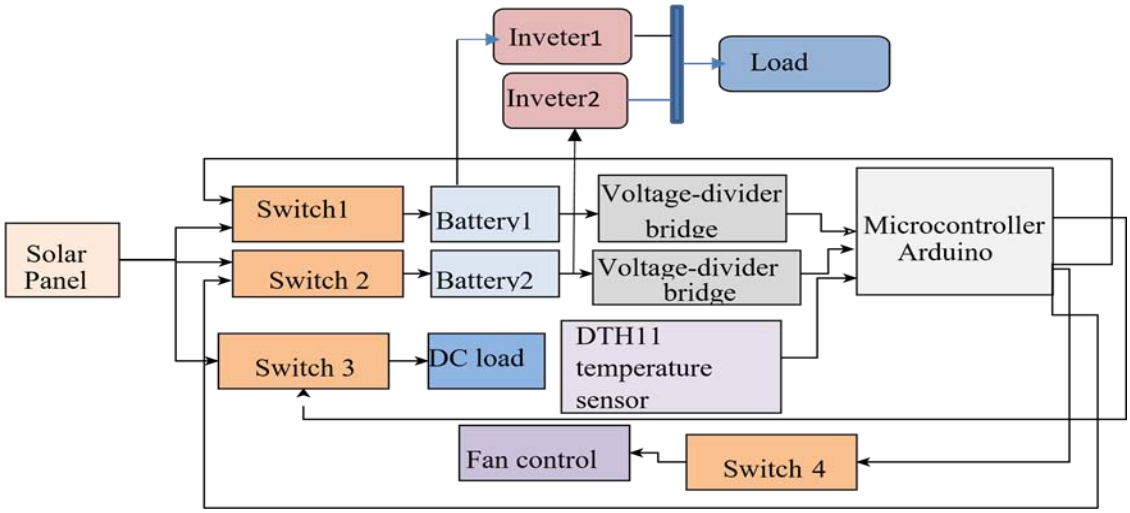


Figure2.20: Schematic model of the mechanism of a battery charging and discharging monitoring system with temperature regulation.

2.5. Setup of the intelligent solar tracking mechanism coupled with BMS

The setup of the solar tracking mechanism combined with the battery charging and discharging monitoring mechanism is make with the combination of the two diagrams below, Diagram showing the structure of the solar tracking system configuration (**Figure2.18)** and the Schematic model of the mechanism of a battery charging and discharging monitoring system with temperature regulation (**Figure2.20).**

2.6. Materials used for a setup of an intelligent solar tracking mechanism associated with BMS

2.6.1. Solar panel

Indicated otherwise, a free electron-hole pair moves through a semiconductor when it is exposed to sunlight. The hole travels to the P side and the electron to the N side as a result of the electric field. Holes exhibit a variety of behaviors similar to those of particles with an electron-like positive charge. The electrical cell's positive and negative terminals can be used to measure the voltage. At null current, the cell's maximum voltage is approximately 0.6 V. The open-circuit voltage is the name given to this voltage. The short-circuit current (I_{SC}) is the highest current generated [114]. A photovoltaic cell remains the basic element of any photovoltaic generator, regardless of the considerable power required. The equivalent diagram of the solar cell is shown in Figure2.21, which consists of an ideal current source connected in parallel with a diode and two resistors to account for internal losses.

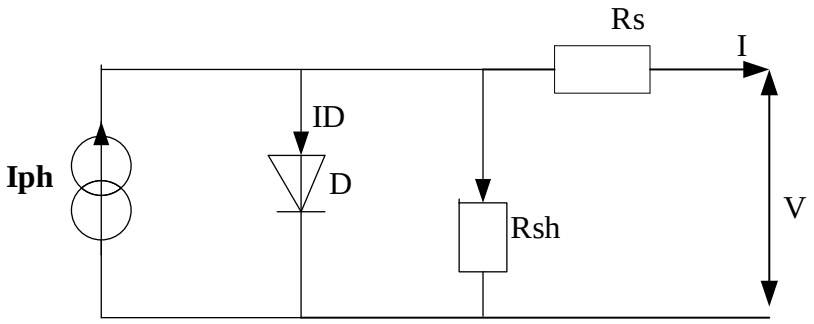


Figure2.1: Equivalent circuit of a solar cell [11].

R series (RS) represents the series resistance that takes into account the ohmic losses of the metallization material and the metal/semiconductor contact, R shunt (Rsh) represents a parallel resistance (or leakage resistance) resulting from parasitic currents between the top and bottom of the cell, particularly at the edges, and within the material due to irregularities or impurities. To predict its performance, it is crucial to know its mathematical model.

According to Figure 2.22, the current generated by the photovoltaic cell I is given by [11]:

$$I = I_{ph} - I_D - I_{RSH} \quad (2.32)$$

Where:

I_{Rsh} : the electric current passing through Rsh .

$$R_{SH} = \frac{V - R_S I}{R_{SH}} \tag{2.33}$$

I_D: the electric current passing through the diode is given by:

$$I_D = I_S\left[\exp\left[q\frac{V + R_S I}{AKT}\right] - 1\right] \tag{2.34}$$

Where

I : the current supplied by a cell (Amperes)

I ph : the photocurrent (Amperes)

ID : the diode current (Amps)

Is : the saturation current of the diod (Amps)

V : the voltage across the cell terminals (Volts)

q : the charge of an electron (q=l .602.10-^{19}), k: Boltzmann's constant, 1.38* 10^{-23} J/K

T : the effective temperature of the cell in Kelvin (^{0}K)

A : The non-ideality factor of the junction (1< A>3)

Rsh : The shunt resistance characterizing the junction leakage currents

Rs : The series resistance representing the various resistances of the contacts and connections.

2.6.2 MPPT charge regulator

The battery is shielded from excessive charging and draining by the MPPT charge regulator. A three-step charging procedure (rapid charge, absorption or boost, and maintenance) keeps lead-acid batteries from being overcharged. Using MPPT technologies, it maximizes the solar energy generated by a stationary solar panel in reaction to climatic change. The Victron Blue Solar MPPT 75/10A-12V charge controller was utilized in the fixed solar panel optimization case study. For the photovoltaic tracker system case research study, we employed a mini 1.2 Wp solar panel with a 6 V voltage, which could be moved using a little MG996R servo motor. An MPPT regulator was not used in the test prototype for the fixed solar panel or the photovoltaic tracker system.

2.6.3 Light Dependent Resistor sensor

A variable resistor component used to gauge light intensity is the light-dependent resistor (LDR). With order to regulate the servomotors and move the solar panel with respect to the sun's rays, it transmits the light intensity value as an electrical signal to the microcontroller. Semiconductors, a material sensitive to light, are used to make LDRs. The amount of light that strikes the LDR's surface determines its sensitivity and influences the output signal that the

LDR sends to the microcontroller. How to measure the light sensor's voltage is shown in Figure 2.22.

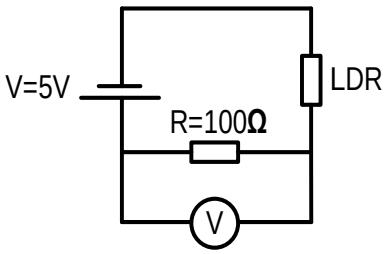


Figure2.22 : Technical aspects of LDR voltage reading [8]

The voltage across the LDR is obtained by the mesh law.

$$U_{-LDR} = V - U_R \quad (2.35)$$

Figure 2.23 illustrates the layout of the LDR sensors. Here, “ε is what angle does the solar eclipse occur at" ε a" it is a result of the wall's elevation, H, and the spacing "d" between it and the collector; "c," is the threshold angle or the limit of the solar eclipse.

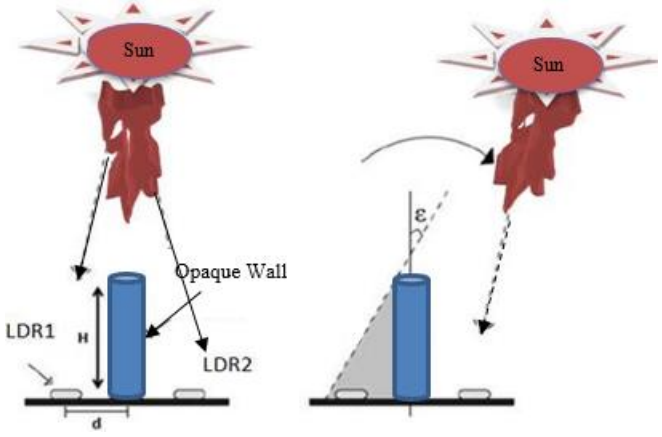


Figure 2.23: Arrangement of the LDR detectors [8]

The LRD sensor was chosen because it is inexpensive and effective for solar tracking.

2.6.4. Real Time Clock 3231

The current time and date are recorded via the real-time clock (RTC). It is commonly used in computers, laptops, mobile phones, embedded application devices, etc. In many embedded systems, it is necessary to add a timestamp when recording data, i.e. sensor values, GPS coordinates, etc. It has to be appropriately configured to monitor the sun's trajectory. The main functions of the Real Time Clock are:

- generate the date and time in 24-hour or 12-hour format
- generate the day, month and year
- Generate programmable alarms
- PC interface to communicate with a microcontroller (Arduino, ESP32, etc.).

The Real Time Clock 3231 was chosen because RTC3231 has many advantages:

- high precession for precise hourly movements

- low energy consumption
- allows movements to be planned without a light sensor
- easy to interface via pc with ARDUINO, ESP32 or Raspberry Pi

2.6.5. Arduino microcontroller

A type of microcontroller is an information-processing component to which internal components have been added to facilitate interaction with the outside world, eliminating the need for external components. Using the Arduino board, we can develop programs and interface circuits, as well as create algorithms to manage switches and sensory devices. In our research work, we chose the Arduino UNO microcontroller. Arduino UNO was chosen for its simplicity, availability and ease of programming.

2.6.6. Servomotor component

A servomotor is a linear or rotary drive that provides fast and accurate position adjustment for closed-loop management applications. The difference between the desired and actual positions determines the motor's speed. To create more precise control signals in digital control applications, a microcontroller generates PWM pulses in terms of duty cycles. The servomotor's electrical equation is as follows [115]:

$$u(t) = k\omega(t) + Ri(t) + L\frac{di(t)}{dt} \tag{2.36}$$

Where i(t) is the armature current (in A), L is the armature winding's inductance (in H), R is the resistance in ohms, k is the servomotor's constant constriction, and is the angular velocity (in rad/sec).

The following formula's equation of motion is utilized to compute the solar array's rotational angle [115]:

$$J\frac{d\omega t}{dt} = T - T_r - f\omega(t) \tag{2.37}$$

Where: T is the torque supplied by the rotor (m N.m), and Tr is the torque due to resistive forces (In N.m), "f.ω(t)" is the viscous friction coefficient, J is the solar panel's moment of inertia in kg m². In this work, we used the MG996R servomotor: The servomotor was chosen because it allows for precise positioning.

2.6.7 Anemometer

Anemometers are instruments that track wind speed in true time at the installation location. The solar tracking regulator receives this data (usually through a microcontroller). Rather than directly contributing to energy optimization, the anemometer in our study of the solar tracking system serves a crucial function in safety and protection during heavy winds.

2.6.8 A switching apparatus

In this work, we employed a relay. A relay is a preconditioned actuator composed of at least one electric magnet, a movable rod supporting the movable contact, a fixed contact, and a return spring for the movable contact. By supplying power to the coil from an electrical source, an electrical interface is closed when its pivoting part is adjusted.

2.6.9 DHT11 Temperature sensor

A microcontroller may process an object's humidity and provide an analogue voltage output. The DHT11 sensor is a module that measures temperature. It is more responsive than other types of sensors since it can immediately determine an object's temperature and relative humidity. Additionally, it is difficult to tamper with the collected data.

2.6.10 Battery charge and discharge monitoring system

An apparatus used for keeping electrical energy generated by photovoltaic solar power plants. Unlike in the home electrical network, the current that enters or exits the battery must be direct current (DC) rather than alternating current (AC).

2.6.10.1 Battery Modelling

For solar energy production systems, batteries made from lead acid are the recommended type of storage. Lead-acid batteries are mainly used in solar systems to store and supply electricity. The stored chemical energy can be converted into electrical energy and vice versa. Lead-acid batteries were chosen because they are still the most widely used in Burundi due to their relatively low cost. Equation 2.38 describe the electrochemical reactions [116]:

$$Pb0_2 + 2H_2S0_4 + Pb \xrightarrow{\text{discharge}} \xleftarrow[\text{charge}]{} 2P_bS0_4 + 2H_20 \quad (2.38)$$

The operation of the battery's voltage is presented by equation 2.39 [116].

$$V = V_{0C} \pm IR \quad (2.39)$$

Where V_{oc} is the open-circuit voltage, I is the battery current, and R is the internal resistance of the battery.

The charging and discharging models for a lead-acid battery are given by equations (2.40) and (2.41) [117].

$$V_{bat} = V_0 - Ri - Rpol_1(i + 1^*) + Exp(t) \quad (2.40)$$

$$V_{bat} = V_0 - Ri - Rpol_2(i^*) - Rpol_1 i + Exp(t) \quad (2.41)$$

Where: Vbat is the battery voltage (V), VO is the constant battery voltage (V), K is the polarization constant (V/Ah), C=battery capacity (Ah), it is the actual battery charge (Ah), A is the amplitude of the exponential zone (V), b is the Inverse of the time constant of the exponential zone (Ah-I), R is the internal resistance (Q), Rpoll is the polarization resistance

when i>O, Rp012 is the polarization resistance when i<O, i is the battery current and i* is the filtered current.

The battery current i and the filtered current i* are equal 2 The polarization resistance in discharge mode is given by equation (2.42) [117].

$$Rpol = K\frac{C}{C - it} \tag{2.42}$$

The resistance to polarization in load mode is given by equation (2.43) [117]:

$$Rpol = K\frac{C}{it - 0.1C} \tag{2.43}$$

The relationship between the voltage and the exponential growth of a lead-acid battery is given by the equation (2.44) [117]:

$$Exp(t) = B|i(t)| - (-Exp(t) + Au(t)) \tag{2.44}$$

Where u(t) is the charge or discharge mode, Exp(t) is the exponential voltage (V), and A is the battery current. The initial value of Exp(t), u(t)=l in charge mode or u(t)=O in discharge mode, determines the exponential voltage. The real battery charge is 0 (it=O) when the battery is fully charged. The battery voltage starts to decrease in this situation. The battery is still being overloaded by the charge (it<O). The reduction in polarization resistance is what causes the voltage to drop. The polarization resistance is infinite when it=O (battery fully charged).

2.6.10.2 Battery state of charge monitoring

The state of charge (SOC) indicates the charge level of a battery, expressed as a percentage. The BMS controls this cell rebalancing through installed instrumentation and a predetermined strategy (algorithm) implemented in the BMS. This control can range from a simple temperature measurement to review the strategy of the auxiliary equipment to be used, as is the case for VRLA batteries, to heating or cooling the battery through active thermal control (active radiator, heater, thermostat, etc.). Several methods are used to estimate the state of charge (SOC) of a battery. These techniques are as follows [118, 119]:

1. Coulomb counting method
2. Voltage recovery method
3. The impedance approach

In various literature, several mathematical estimating techniques are categorized based on their methodology.

2.6.10.3 Voltage divider bridge component

The Arduino microcontroller operates at a voltage of approximately 5 V. In this situation, a voltage rectifier bridge is required to adapt the battery pack voltage for the microcontroller's input. Figure 2.24 shows a block diagram showing a voltage dividing bridge.

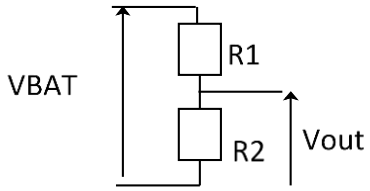


Figure 2.24: Block diagram showing a voltage dividing bridge[8]

The voltage divider law is applied, and the result is:

$$V_{out} = \frac{R_1}{R_1 + R_2} VBAT \tag{2.52}$$

In our case, VBAT =14V, R_1 =33KΩ and R_2 =57KΩ.

$$Vout = \frac{33}{33 + 57}.14V = 5V \tag{2.53}$$

VMIN equal to 11.2V is the result of reducing the battery to a SOC of 80% of the original capacity. The conversion of V_{MIN} to binary corresponds to 818.4.

$$Vout = \frac{R_1}{R_1 + R_2} VBAT \tag{2.52}$$

2.6.10.4 Batteries' declining health

The conditions in which a battery is used have a direct impact on how old it gets. The quantity of charge-discharge cycles is the primary determinant. The battery needs to be kept at a level of charge higher than 50% for ten to fifteen years. The method used in this study keeps the battery's state of charge at 80% to prevent it from ageing. The following three variables affect how quickly lead-acid batteries age [120]:

- The first factor, which is present in all battery applications, is cycle life and resilience to high temperatures.
- The consequences of undercharging and sulphation, which are unique to solar applications, constitute the second consideration.
- Catastrophic reasons, which are frequently avoidable, include manufacturing flaws, under sizing, overuse, intense freezing, etc.

In addition to overheating and causing corrosion, distortion, and erosion of the plates, high overloads can cause Pb particles to agglomerate, which reduces porosity. The connection between the battery's depth of drain and its level of charge is [121]:

$$SOC_{Min} = (1 - DoD) SOC_{Max} \tag{2.54}$$

DoD : Represents the depth of discharge. In our study, the maximum depth of discharge DoD_{Max} is set at 70%.

There are several types of lead-acid batteries, namely:

- BGELI: GEL VRLA SOLAR flat plate battery;

- BGEL2: Flat plate battery, GEL VRLA SOLAR Block type,
- BGEL3: GEL VRLA A600 SOLAR tubular plate battery;
- BSI: OPzS stationary flat plate battery;
- BS2: OPzS Solar-Cells stationary tubular plate battery;
- BS3: OPzS Solar-Blocks stationary flat plate battery

The mathematical models for calculating the ageing of these types of batteries are given by the following equations [121]:

$$N_{C(DoD)} = 12850e^{-(9.738.DoD)} + 3210e^{-(1.429.DoD)} \quad (2.55)$$

$$N_{C(DoD)} = 13820e^{-(7.426.DoD)} + 3763e^{-(1.139.DoD)} \quad (2.56)$$

$$N_{C(DoD)} = 14690e^{-(5.8276.DoD)} + 4391e^{-(1.021.DoD)} \quad (2.57)$$

$$N_{c(DoD)} = 11250e^{-(8.087.DoD)} + 2863e^{-(1.17.DoD)} \quad (2.58)$$

$$N_{C(DoD)} = 24090e^{-(9.346.DoD)} + 6085e^{-(1.319.DoD)} \quad (2.59)$$

$$N_{C(DoD)} = 14850e^{-(7.98.DoD)} + 3766e^{-(1.158.DoD)} \quad (2.60)$$

Où Nc est le nombre maximum de cycles de la batterie. Le vieillissement est défini à partir de la caractéristique du cycle de vie de la batterie

2.6.11 Technique of multi-inverters under centralized management

By using only the required number of inverters, this kind of architecture offers significant flexibility in maintenance and administration of the installation's usage time. Additionally, depending on the amount of sunlight, this control guarantees that the inverters are operating at their maximum power.

Figure2.25 illustrates the architecture of centrally managed multi-inverters.

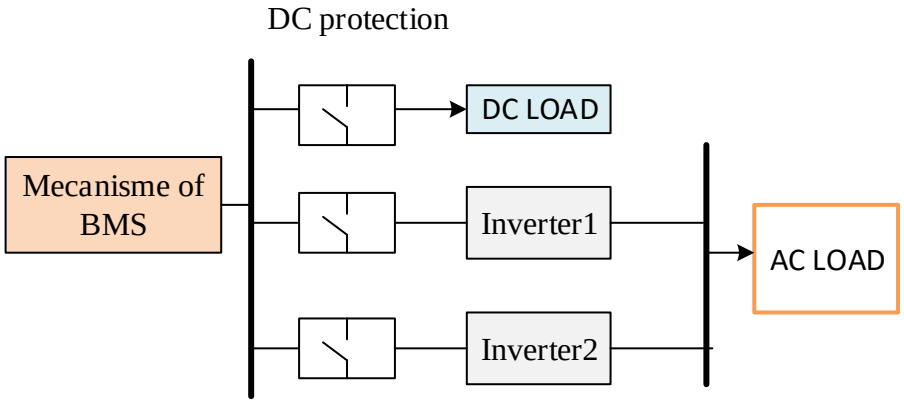


Figure 2.25: Architecture of multi-inverters under centralized management

2.7. Software used for designing and modeling an intelligent solar tracking mechanism associated with BMS

2.7.1. PVsyst software

PVsyst software is a professional computer tool dedicated to the design, simulation and analysis of photovoltaic systems. It can be used to study different types of solar installations: grid-connected, off-grid, pumping and even direct current networks (e.g. public transport). It was developed by Michel Andre Mermoud and Michel Villoz [93].

2.7.2. MATLAB software

In contrast to more complex languages like C and C++, MATLAB (Matrix Laboratory) is a matrix calculating application with a "simple" syntax. Because it makes it possible to solve complicated numerical problems faster, it is used in engineering and scientific computations [94].

2.7.3. Proteus professional software

Proteus Professional is a comprehensive tool for schematic design, digital simulation and microcontroller co-simulation with analogue circuits, demonstrating its effectiveness in teaching and research in electronic circuits [122].

2.7.4. Arduino IDE software

The development of embedded systems has become more widespread thanks to the introduction of accessible hardware and software platforms such as Arduino. The Arduino Integrated Development Environment (IDE) is an open-source development environment designed for programming Arduino and compatible boards. This tool is recognized for its simplicity, portability and educational role in learning programming and electronics. The IDE is based on the C/C++ language and uses the avr-gcc compiler (for AVR microcontrollers such as the ATmega328P). It includes: a text editor for writing programs called sketches, a compiler that translates the code into machine language, and a program loader (bootloader) that transfers the binary to the microcontroller via a USB connection [123]

2.7.5. SolidWorks software

Several academic applications demonstrate that SOLIDWORKS is now essential for parametric modelling and mechanical analysis, whether for optimizing machine design, automating the generation of technical drawings, or preparing 3D (tree dimension) models prior to equipment simulation**[124]**.

2.8. Methodological limitations

- Technological limitations: The studied model is generally verified through simulation and on an operating prototype, but it may not reflect all real-world conditions, such as dust, rain, strong winds and corrosion.
- Financial limitations: The research does not always consider the true cost of the entire system, including import duties, taxes and maintenance.
- Energy restriction: Energy efficiency is the sole focus of the study, with storage, distribution and network losses not considered.
- It is assumed that during charge and discharge cycles, internal resistance remains constant and does not change with the amount of current.
- The model's parameters are determined by its discharge properties and are expected to be consistent with those of the model;
- The battery is unaffected by changes in current intensity(no Peukert effect);
- The experimental approach may be limited by locally available resources;
- The behavior of the system may differ under real conditions over a long period of time.

Conclusion

This chapter translated the findings from the literature into a rigorous and integrated methodological approach. The mathematical models developed to ascertain the best possible tilt angle made it possible to adapt solar radiation capture to the geographical conditions of Burundi. The optimization algorithm based on the combination of the P&0 MPPT regulator and the fuzzy logic controller represents a significant contribution to the stability and accuracy of MPPT, even under rapid variations in irradiation. The development of control algorithms for both single-axis and dual-axis solar trackers, as well as the implementation of an intelligent battery charge and discharge management mechanism, have resulted in a complete architecture for the system under study. Predictive modelling of battery life cycles has added a forward-looking dimension to the research by integrating sustainability into the energy optimization process. In conclusion, this chapter has laid the scientific and technical foundations for the smart photovoltaic system, defining the methods and tools needed for its design, simulation, validation and testing, which will be discussed in the next chapter.

Chapter 3 Presentation and interpretation of results obtained using simulation and experimentation tools

3.1. Introduction

This chapter presents the design, simulation and experimental results for each method of optimizing photovoltaic efficiency. A summary of the results is been examined for each method. Our work is based on the integration of a solar tracker equipped with a battery management system to optimize photovoltaic efficiency. We first show and summarize the results of optimizing the photovoltaic efficiency of a fixed solar panel photovoltaic system controlled by an MPPT regulator and tilted at an optimal angle. The outcomes of the MPPT regulator in comparison to a non-MPPT regulator is summarized and examined. We next provide the outcomes of the models created, one for figuring out the ideal solar panel Inclination angle and the other for figuring out the energy that is accessible. These findings serve as the foundation for researching Burundi's solar tracker's advantages over a fixed solar panel photovoltaic system. The outcomes of the design and simulation of an intelligent solar tracker is presented after the results of maximizing the photovoltaic efficiency of a stationary solar panel system. The findings of the intelligent solar tracker and its advantages over a fixed solar panel is examined. The creation of an algorithm based on a battery charge and discharge management mechanism for optimizing photovoltaic efficiency is presented as we wrap up. The outcomes of efficient lead-acid battery management, which is predicated on exact control of charge and discharge thresholds to prevent overcharging or deep drain, is examined. We look at a battery life prediction analysis.

3.2. Results of the impact of a fixed solar panel tilted at an optimal tilt angle regulated by a regulator MPPT

The efficiency of producing power from fixed-angle solar systems is impacted by the recent rapid climate change. In order to help optimize fixed solar panels, we developed and simulated a photovoltaic system controlled by an MPPT controller based on the MPPT P&O algorithm in conjunction with a fuzzy logic controller in this part. A comparative analysis of the results of a PV system with a P&O MPPT controller, a PV system with a conductance Increment MPPT controller, and a PV system with a non-MPPT (PWM) controller is presented to show the impact of integrating an MPPT controller. The design of the developed algorithm is in line with our objective of dynamically improving the efficiency of electricity generation in the field of photovoltaic systems.

3.2.1 Design and simulation of MPPT controller

Let us evaluate the Increment and conductance MPPT algorithm to show its shortcomings compared to the P&O MPPT algorithm. We used a Sun POWER-SPR-305E-WTH-D solar array (with specific physical characteristics shown in section 2.3.1), a boost converter; L2=1.93mH,two capacitors C=220mF ; L2=1.79.10^{-3}; 10e-6; time of control Ts=5.10^{-5};a load with a voltage of 220V, nominal frequency of 50Hz,active power of 610W; voltage measurement and a current measurement. Figure 3.1 illustrates the design diagram of a photovoltaic system regulated by the Increment and conductance MPPT algorithm. After performing the simulation, Figure 3.2 illustrates the power variation curve using the Incremental MPPT and conductance algorithm.

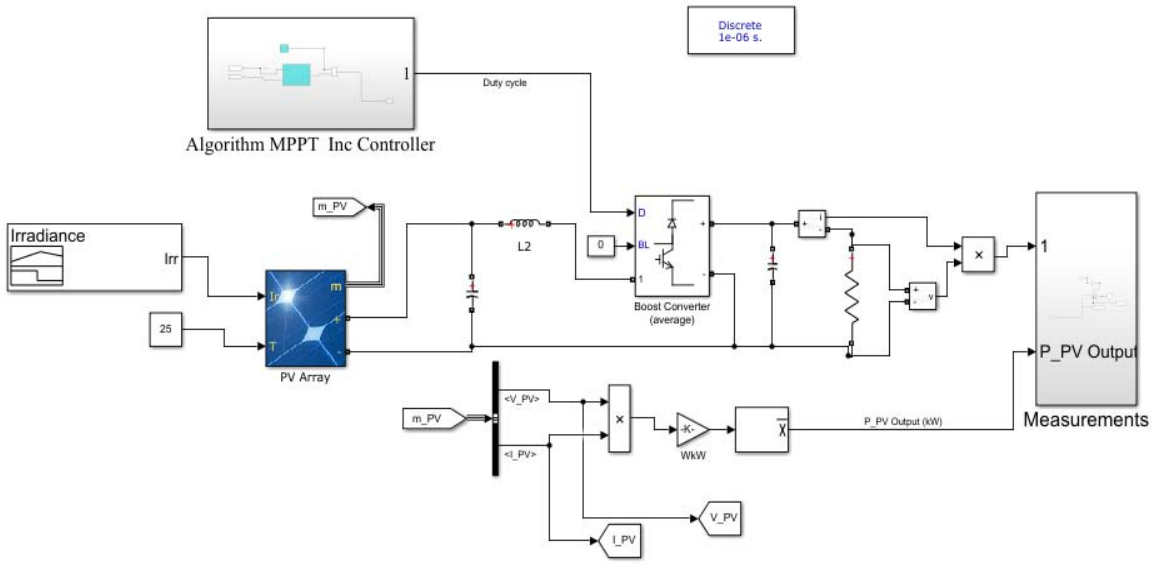


Figure3.1: Design diagram of a photovoltaic system regulated by the Incremental MPPT and conductance algorithm

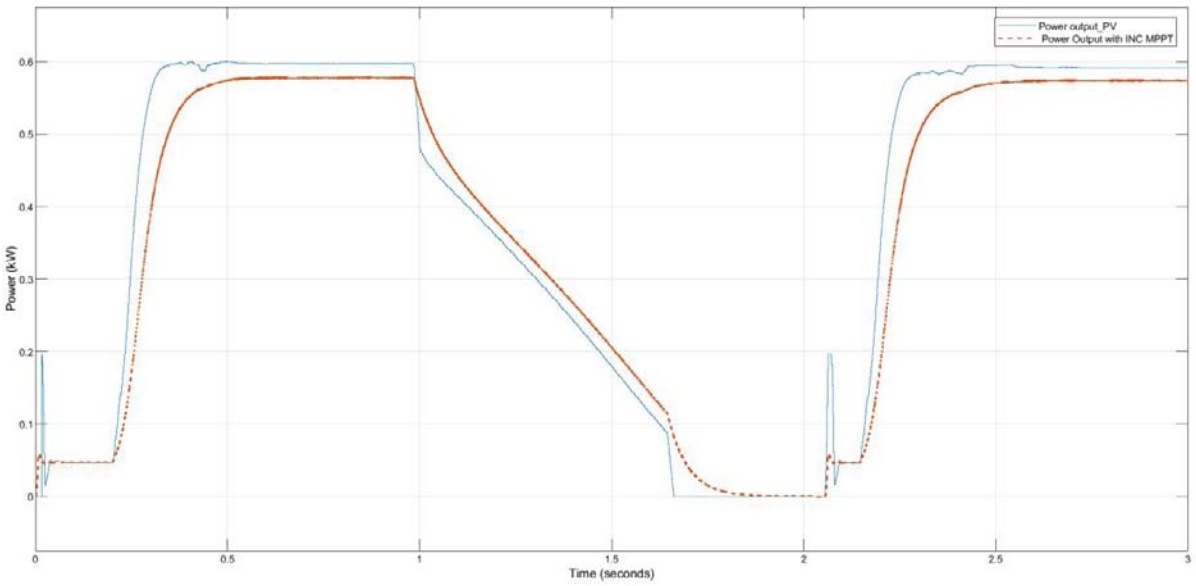


Figure3.2: Variation curve of power output using Inc MPPT algorithm

Analysis of the results of the power output variation curve shows a significant delay in tracking the reference power. We also note that the power obtained by the regulator is lower than the panel's power output. We used a Sun POWER-SPR-305E-WTH-D solar array (with specific physical characteristics shown in section 2.3.1);a boost converter; L=1.93mH,C=220mF ; a load with a voltage of 220V, nominal frequency of 50Hz,active power of 610W; voltage measurement and a current measurement. Figure 3.3 illustrates the design diagram of a solar-powered photovoltaic system supervised by the Perturber and Observer MPPT algorithm coupled with a fuzzy logic and his results as shown in Figure 3.4.

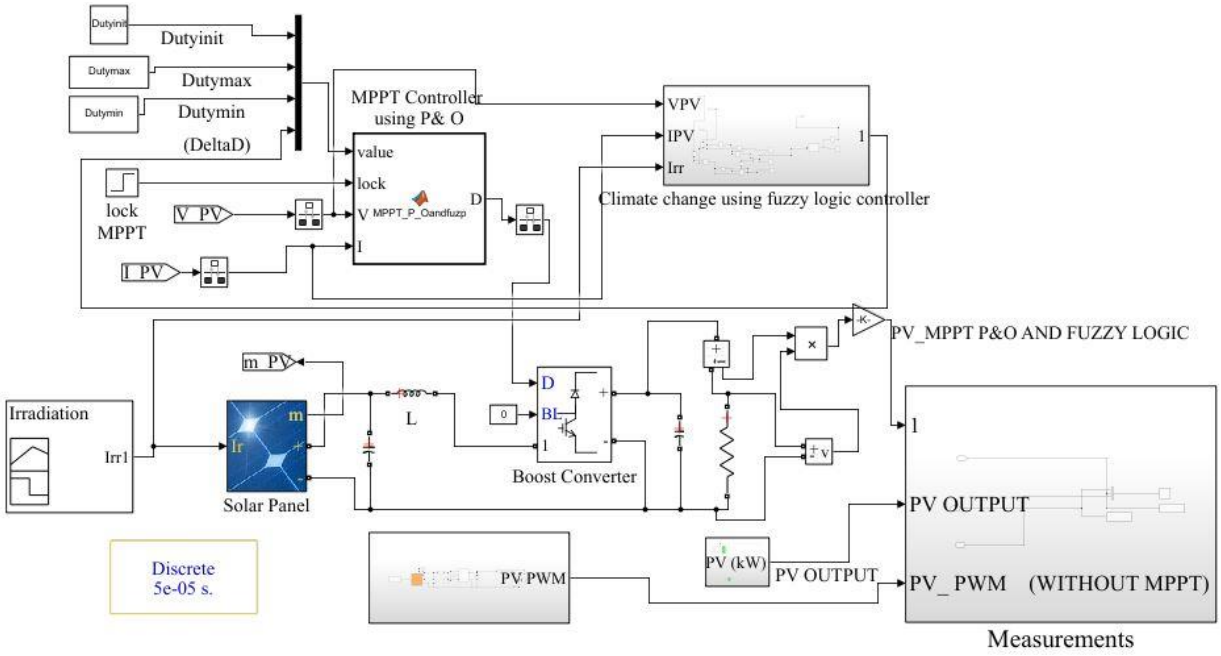


Figure3.3 : Design diagram a photovoltaic system regulated by the P&O MPPT algorithm regulated coupled with a fuzzy logic regulator.

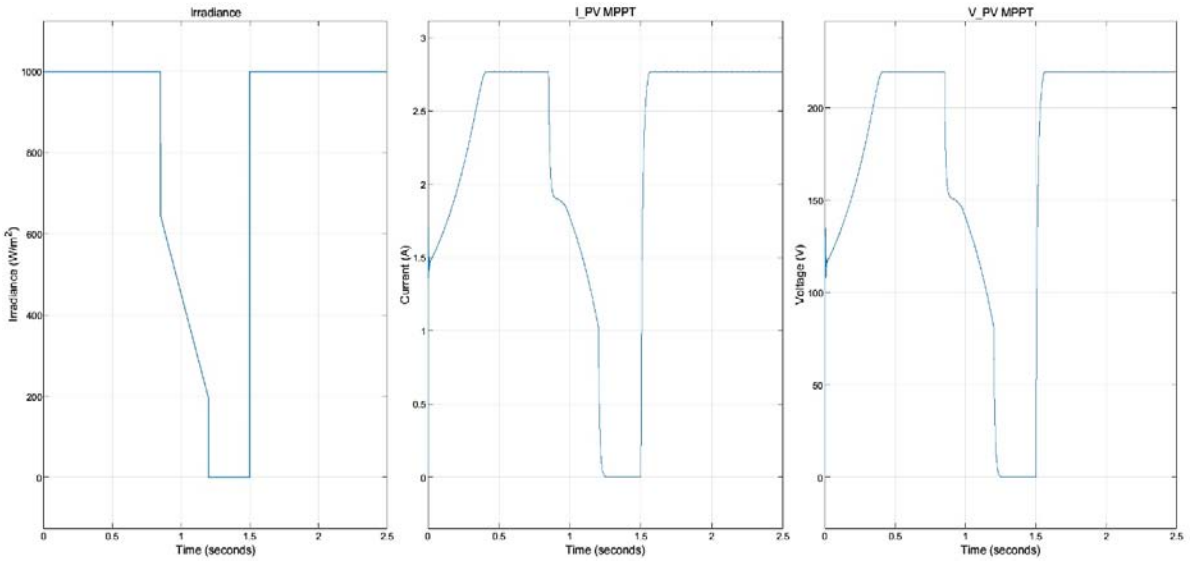


Figure3.4: Variation curve of irradiance, current and voltage using the MPPT algorithm.

The outcomes of the simulation demonstrate that changes in irradiance are correlated with changes in current and voltage. Figure 3.5 shows how much power a fixed solar panel with a fuzzy logic process controller and the P&O MPPT algorithm produces in comparison to a solar panel without MPPT in a step size of simulation of 3seconde.

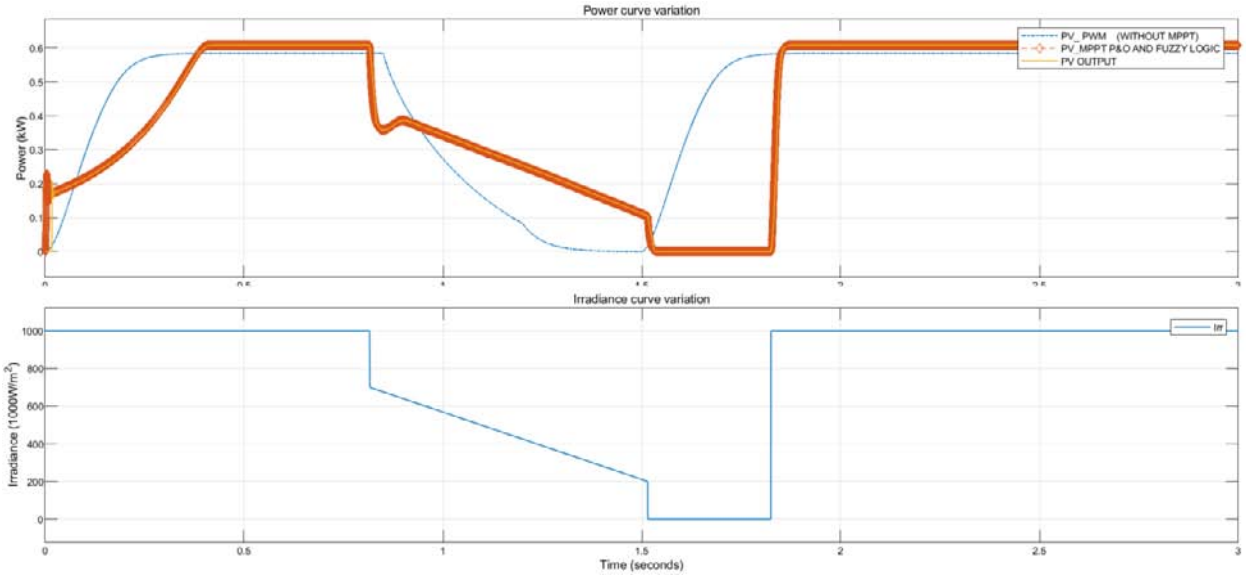


Figure3.5 : Power produced using the P&O MPPT algorithm and fuzzy logic processor.

Analysis of the power variation curve results shows that this technique, based on the developed algorithm, achieves MPPT in 0 seconds (see power variation curve in Figure3.5 in the range [0, 0.5]) and provides good tracking of the reference power. Based on the power variation curves produced by the two types of controllers, we find that the use of the MPPT controller maximizes the power produced compared to the use of the PWM controller. We also note that the tracking delay of P&0 MPPT has been eliminated. The simulation results show that the P&O MPPT algorithm associated with fuzzy logic controller performs better than the increment and conductance MPPT algorithm. This validates our choice of the P&O algorithm for conventional methods. We confirm the improved MPPT tracking efficiency of the developed algorithm and the speed at which the system responds to changes in irradiance.

3.2.2. Perfect solar array tilt angle

3.2.2.1 Determination of the optimum angle using pvsyst software

The simulation findings that show the ideal solar panel tilt angle for various Burundian locations are presented in this section. The amount of energy generated by solar panels is significantly improved by their tilt angle. We start by displaying the outcomes of utilizing PVSYST 7.4 software to find the ideal annual tilt angle based on the first method. Three factors are used to establish the fixed solar panel's ideal tilt angle:

- the annual transposition factor (FT),
- annual losses relative to the optimum (Lopt) expressed as a percentage
- global radiation on the collector plane (GlobHor_opt) expressed in kWh/m^2.

Residential roof inclinations range from 45° to 12°, according to the literature. Since different designers in Burundi have different Inclination angles for their roofs, in this work, we decided to place the solar panel at a 30° average angle of inclination for residential rooftops (we choose an angle for the roofs between 45° and 12°). Considering simulation findings given by below factors for in the range angle of 30° and a perfect annual angle of tilt of the solar array βopt in degrees, we can evaluate the influence of the perfect angle of tilt of the solar panel on the amount of power available (E_Avail). The values acquired for the ideal yearly tilt angle of the fixed solar panel for 36 locations in Burundi using the pvsyst program are displayed in Table 3.1. We selected two locations in every province: the location with the highest latitude and the location with the lowest latitude.

Table3.1 : Annual optimum tilt angle for a solar panel in 36 sites of Burundi.

			For 30˚ angle				**For optimal yearly tilt angle**					
Province	Site	Latitude	FT	Lopt	Glob Hor	E_Avail	FT	Lopt	Glob Horopt	β_{opt}	E_Avail	RP
		˚S	%	%	kWh/m^2	kWh	%	%	kWh/m^2	˚	kWh	%
Bujumbura-mairie	Kinama	−3.325	0.950	5.000	4.50	853.0	1.0	0.00	4.760	**14.0**	906.50	78.10
	Mutanga sud	−3.380	0.960	4.700	4.440	843.0	1.0	0.00	4.650	**15.0**	884.0	74.0
Bujumbura	Mubimbi	−3.295	0.960	4.700	4.450	840.0	1.0	0.00	4.670	**14.0**	890.0	73.80
	Kabezi	−3.535	0.960	4.600	4.480	853.0	1.0	0.00	4.690	**15.0**	903.0	73.50
Bubanza	Musigati	−3.067	0.950	5.000	4.560	873.0	1.0	0.00	4.80	**14.0**	930.0	78.0
	Mpanda	−5.181	0.980	3.600	5.400	1040.0	1.0	0.00	5.670	**15.7**	1084.0	75.10
Bururi	Mugamba	−3.665	0.960	4.500	4.440	845.0	1.0	0.00	4.640	**15.0**	893.0	74.30
	Vyanda	−4.104	0.970	4.400	4.840	928.0	1.0	0.00	5,050	**15.0**	968.0	74.10
Cibitoke	Mugina	−2.794	0.950	5.500	4.790	896.0	1.0	0.00	5.070	**13.0**	962.0	74.10
	Buganda	−2.9750	0.950	5.000	4.710	892.0	1.0	0.00	4.960	**14.0**	949.0	75.40
Gitega	Nyarusange	−3.5680	0.95	5.300	4.650	870.0	1.0	0.00	4.910	**15.0**	933.0	76.50
	Buraza	−3.7480	0.960	4.700	4.590	868.0	1.0	0.00	4.80	**15.0**	919.0	78.0
Karusi	Gitaramuka	−2.9810	0.950	5.300	4.920	928.0	1.0	0.00	5.190	**14.0**	989.0	78.0
	Shombo	−3.2780	0.950	5.200	4.700	886.0	1.0	0.00	4.960	**15.0**	944.0	75.50
Kayanza	Muhanga	−2.9710	0.950	5.200	4.470	831.0	1.0	0.00	4.710	**14.0**	892.0	73.50
	Butaganzwa	−3.0840	0.950	5.000	4.610	870.0	1.0	0.00	4.860	**14.0**	924.0	77.20

Kirundo	Bugabira	−2.4330	0.950	5.100	5.120	953.0	1.0	0.00	5.390	**13.0**	1014.0	75.10
	Vumbi	−2.6950	0.960	4.700	4.940	921.0	1.0	0.00	5.190	**13.0**	978.0	77.40
Muyinga	Giteranyi	−2.4760	0.950	5.400	5.010	933.0	1.0	0.00	5.30	**13.0**	996.0	76.40
	Mwakiro	−3.0900	0.950	5.400	4.970	929.0	1.0	0.00	5.260	**14.0**	992.0	77.0
Ngozi	Tangara	−2.9140	0.950	5.300	4.920	924.0	1.0	0.00	5.190	**14.0**	986.0	77.60
	Marangara	−2.7310	0.940	5.500	4.820	906.0	1.0	0.00	5.10	**13.0**	965.0	79.30
Makamba	Kayogoro	−4.1180	0.960	4.600	4.970	924.0	1.0	0.00	5.200	**15.0**	976.0	77.20
	Nyanza lac	−4.3380	0.960	4.500	5.170	965.0	1.0	0.00	5.400	**15.0**	1018.0	74.80
Muramvya	Mbuye	−2.1540	0.940	6.40	4.710	896.0	1.0	0.00	5.040	**12.0**	958.0	74.70
	Kiganda	−3.3450	0.960	4.800	4.190	796.0	1.0	0.00	4.410	**14.0**	844.0	75.50
Mwaro	Ndava	−3.3780	0,960	4.900	4.640	877.0	1.0	0.00	4.870	**14.0**	930.0	76.90
	Bisoro	−3.6360	0.960	4.600	4.440	833.0	1.0	0.00	4.640	**15.0**	880.0	74.20
Rumonge	Muhuta	−3.5700	0.960	4.400	4.460	839.0	1.0	0.00	4.660	**15.0**	885.0	74.0
	Burambi	−3.8140	0.960	4.500	4.580	863.0	1.0	0.00	4.780	**15.0**	910.0	77.0
Rutana	Musongati	−3.7270	0.970	4.200	5.090	953.0	1.0	0.00	5.300	**15.0**	1002.0	75.20
	Bukemba	−4.0070	0.970	4.400	5.330	998.0	1.0	0.00	5.560	**15.0**	1050.0	76.60
Ruyigi	Butezi	−2.3490	0.950	5.400	4.990	930.0	1.0	0.00	5.270	**13.0**	995.0	76.90
	Kinyinya	−3.6570	0.950	5.400	5.040	940.0	1.0	0.00	5.330	**15.0**	1003.0	76.0
Cankuzo	Kigamba	−3.0370	0.950	5.300	5.070	950.0	1.0	0.00	5.350	**14.0**	1013.0	75.50
	Cendajuru	−3.3130	0.950	5.200	5.130	964.0	1.0	0.00	5.400	**14.0**	1026.0	74.60

The ideal yearly tilt angle of the fixed solar panel in the 36 Burundian sites under study ranges from 12˚ to 15.7˚, based on the outcomes of the simulation. Based on the outcomes of the simulation, losses compared to the optimal range from 4.2% to 5.5% for a solar panel tilt angle of 30˚, while there is no loss relative to the optimum for a stationary solar panel slanted at the ideal annual angle. According to the same studies, the transposition factor fluctuates between 0.94% and 0.98% for a solar panel tilt angle of 30˚, whereas it is 1% for a stationary solar panel slanted at an ideal yearly angle. We see a low transposition factor of less than 1 when compared to the values for a solar panel slanted at a 30° angle. In comparison to the values found for the solar panel tilted at an ideal annual angle, the simulation results likewise demonstrate reduced overall radiation on the collector plane for the solar panel slanted at a 30° Inclination. As for the values of the energy produced (E_Avail), we note that a solar panel tilted at the optimal annual angle produces much more than one tilted at an angle of 30°. The simulation results also show a performance ratio (PR) for all sites between 73.5% and 79.3%.

Let's also assess how the solar panels' tilt angle affects the amount of energy collected at one of the locations under investigation. The impact of solar panel tilt angles on energy output at the Marangara location is displayed in Table 3.2.

Table3.2 : Table of the impact of solar panel tilt angles on energy production at the Marangara location

Site	Latitude	GlobHor	Angle	E_Avail
	(˚S)	(kWh/m^2/day)	(˚)	(kWh/yr)
Marangara	−2.7310	5.100	13.0	965.0
Marangara	−2.7310	5.060	18.0	953.0
Marangara	−2.7310	4.940	25.0	926.0
Marangara	−2.7310	4.820	30.0	900.0
Marangara	−2.7310	4.670	35.0	868.0
Marangara	−2.7310	4.300	45.0	791.0
Marangara	−2.7310	4.080	50.0	750.0

Again, we remark that the energy generated by the solar panel's ideal tilt angle is substantial in comparison to the other angles. The main findings and outcomes for a solar panel tilt angle of 30° and an ideal tilt angle of 13° at the Marangara location are shown in Tables 3.3 and 3.4.

Table3.3: Major results for a solar panel with a tilt angle of 30°.

	GlobHor	GEff	E_Avail	EUnused	E_Miss	E_User	E_Load	SolFrac
	kWh/m^2	kWh/m^2	kWh	kWh	kWh	kWh	kWh	Ratio
Year	1863.40	1668.40	900.330	22.330	46.920	845.140	892.060	0.9470

Table3. 4: Major results for a solar panel with a tilt angle of 13°..

	GlobHor	GEff	E_Avail	EUnused	E_Miss	E_User	E_Load	SolFrac
	kWh/m^2	kWh/m^2	kWh	kWh	kWh	kWh	kWh	Ratio
Year	1863.40	1791.20	964.610	34.4700	0.00	892.060	892.060	1.00

Where E_Load is the energy for the load, GEff is the effective global energy, SolFrac is the solar fraction, Eunused is the unused energy, E_User is the energy supplied for use, E_Miss is the missing energy, and GlobHor is the global horizontal irradiation.

For a solar panel tilted at an angle of 13°, the results obtained indicate that the energy demand (load) is 892.06 kWh/year, the energy supplied to users is 892.06 kWh/year, with an annual production (E_Avail) of 964.61 kWh/year. We can see that the energy supplied to users corresponds to the energy demand. For a solar panel tilted at an angle of 30°, we have an energy demand (load) of 892.06 kWh/year, energy produced of 900.33 kWh/year and energy supplied to users of 845.14 kWh. We note that the energy supplied to users is lower than the energy demand (892.06 kWh/year), which differs from the results obtained for a panel tilted at an optimal angle. Figure 3.6 shows the monthly and yearly values of the performance ratio obtained for the Marangara site.

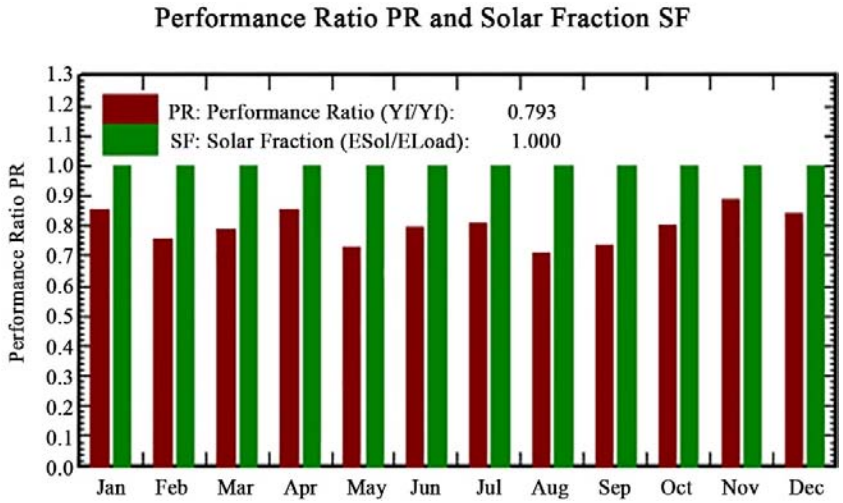


Figure3.6: Photovoltaic area performance index.

Burundi benefits from a substantial yield on the photovoltaic system, as seen by the data obtained (Table 3.1), which reveal a PR that varies between 73.5% and 79.3% at the various sites evaluated. Figure 8 displays a Performance Ratio of 79.3% for the Marangara site. According to a loss diagram, this indicates that approximately 21.7% of the energy emitted during the observation period could not be used because of losses from unused battery energy (2.98%), solar panel collecting losses (10.35%), and system losses (7.37%).

3.2.2.2 Developed an optimal tilt angle model, developed an absorbed energy model of solar panels and analyzed the results

The project's initial contribution, which is based on the creation of a model for figuring out the fixed solar panel's ideal tilt angle and a model for figuring out the solar energy captured, has been presented in this part. We created a model to calculate the ideal annual tilt angle of the solar panel and a model to calculate the annual energy available for a fixed solar panel tilted at an ideal angle at any location at a latitude below 10° using the R method of the SPSS software, which is based on the linear regression model. We examined whether the models' input parameters enable us to determine an output value that matches the values discovered by the pvsyt. To confirm and validate our theory that the ideal tilt angle of the solar panel varies according to latitude, let's use SPSS software to examine the simulation results for the Marangara site described in Table 3.2. We used the angle and the site's latitude as the model's input parameters. One dependent variable is the angle parameter. The model's correlation coefficient and coefficient of determination (R^2) are described in detail in Table 3.5.

Table3 5: Table summarizing the model coefficients for determining R.

Model	R	R-two	R-two adjusted	Standard error of the estimate
1	0.825[a]	0.681	0.672	0.4918

a. Predictors: (Constant), latitude.

We find a correlation coefficient R value of 0.825 and a coefficient of determination R^2 value of 0.681 based on the outcomes of the basic linear regression model. The statistical analysis shows that there is a statistical association, with an average percentage of 68.1%, between the latitude and the tilt angle of the fixed solar panel based on the correlation coefficient value. The P value (sig) and the standardized and unstandardized coefficients are shown in Table 3.6.

Table3 6: Table showing non-standardised and standardised coefficients.

Coefficients[a]						
Model		**Non-standardized coefficients**		**Standardized coefficients**	**T**	**Sig.**
		B	**Standard error**	**Beta**		
1	(Constante)	11.079	0.380		29.150	0.000
	Latitude (˚S)	0.939	0.110	0.825	8.522	0.000

a. Dependent variable: Angle.

Our hypothesis that there is a statistically significant association between the solar panel's angle of Inclination and latitude is supported by the simulation results shown in this table, which show a P value of less than 0.05. The following equation is the mathematical model that was produced, which expresses the ideal yearly angle of Inclination of the solar panel for each of the sites examined:

$$\beta = 0.939\lambda + 11.079 \qquad (3.1)$$

where β is optimum yearly tilt of Inclination (in ˚); where λ is latitude of the site (in ˚S).

It is simple to get the ideal annual angle of Inclination for the fixed solar panel for each location in Burundi by entering the site's latitude coordinates into the created mathematical model. To verify the impact of the ideal tilt angle of the solar panel on the available energy, let's examine the simulation results shown in Table 3.2 using SPSS software based on the R approach in multiple linear regression. The input parameters in this instance Include available energy, global horizontal irradiation, and the ideal yearly angle. The dependent variable is available energy. The model's correlation coefficient R and coefficient of determination R^2 are outlined in Table 3.7.

Table3.7: Table of model's correlation coefficient R and coefficient of determination R^2.

Model	R	R-two	R-two adjusted	Standard error of the estimate
1	1.000[a]	1.000	1.000	1.130

a. Predictors: (Constant), Angle, GlobHr.

We identify a correlation coefficient R equal to 1 and a coefficient of determination R^2 equal to 1 based on the simulation results produced by this multiple linear regression model. The tilt angle of the solar panels and the worldwide horizontal irradiance have a statistical impact on the available energy with a high percentage of 100%, according to statistical study of these coefficients. The P (sig) value and the standardized and unstandardized coefficients are shown in Table 3.8.

Table 3.8: Table displays both standardized and non-standardized coefficients.

Model	Non-standardized coefficients		Standardized coefficients	T	Sig.
	B	Standard error	Beta		
(Constante)	64.583	32.014		2.017	0.114
GlobHor (kWh/m^2)	178.893	5.738	0.851	31.174	0.000
Angle (˚)	−0.913	0.164	−0.152	−5.550	0.005

a. Dependent variable: E_avail.

The results show that there is a statistically significant association between the variables (Inclination angle and global horizontal radiation) and accessible energy, with P values for GlobHor and Angle values being less than 0.05. We find a weak negative connection of 15.2% for the tilt angle of solar panels on available energy and a large positive correlation of 85.1% for global horizontal radiation by examining the values of B and Beta. The following equation is the mathematical model created to determine available energy:

$$E_Avail = \left(-0.913\,\beta + 178.893\,GlobHr + 64.583\right).\frac{P_C}{610} \qquad (3.2)$$

Where β is the angle expressed in degrees (°) and Pc is the power of the solar panel expressed in watts.

We determine the annual energy available for any solar panel power at each site by entering the value of the site's total horizontal irradiation and the ideal annual angle of Inclination of the solar panel. The verifications of the models created using the geographic coordinates and meteorological information from Table 3.1 are shown in Table 3.9.

Table 3.9: Verification results of the models created using the geographic coordinates and meteorological information from Table 3.1

Site	Latitude	GlobHor for 30°	GlobHoropt	Optimum tilt	E_Avail for 30°	E_Avail for optimum tilt
	°S	kWh/m²	kWh/m²	(°)	(kWh/yr)	(kWh/yr)
Kinama	-3.3250	4.50	4.760	14.20	856.630	903.140
Mubimbi	3.2950	4.450	4.670	14.170	833.000	887.070
Gitaramuka	-2.9810	4.920	5.190	13.880	917.650	980.360
Nyarusange	-3.5680	4.650	4.910	14.420	869.530	929.780
Mpanda	-5.1810	5.400	5.670	15.80	1003.200	1064.40
Mbuye	-2.1540	4.710	5.040	13.0	879.700	954.300

The models created validate every site examined, although we have only displayed the verification for a few sites in Table3. 9. We see that, for the two distinct tilt angles of the fixed solar panel, the simulation results produced with pvsyst software in Table 3.1 closely match the findings obtained by the created models. Using the models created for the sites under study, Table 3-10 displays the values for the ideal angle of inclination of the solar panel and the energy available.

Table3.10: Table showing the optimum annual tilt and the amount of energy produced using the generated models in all sites.

Province	Site	Latitude	β_{opt}	E_Avail
		˚S	˚	kWh
Bujumbura Mairie	Kinama	3.325	**14.2**	**903.1**
	Mutanga Sud	3.38	**14.3**	**883.4**
Bujumbura	Mubimbi	3.295	**14.2**	**887.1**
	Kabezi	3.535	**14.4**	**890.4**
Bubanza	Musigati	3.067	**14.0**	**910.5**
	Mpanda	5.181	**15.9**	**1064.3**
Bururi	Mugamba	3.665	**14.5**	**881.4**
	Vyanda	4.104	**14.9**	**954.4**
Cibitoke	Mugina	2.794	**13.7**	**959.1**
	Buganda	2.975	**13.9**	**939.2**
Gitega	Nyarusange	3.568	**14.4**	**929.8**
	Buraza	3.748	**14.6**	**909.9**
Karusi	Gitaramuka	2.981	**13.9**	**980.4**
	Shombo	3.278	**14.2**	**939.0**
Kayanza	Muhanga	2.971	**13.9**	**894.5**
	Butaganzwa	3.084	**14.0**	**921.2**
Kirundo	Bugabira	2.433	**13.4**	**1016.6**

	Vumbi	2.695	**13.6**	**980.6**
Muyinga	Giteranyi	2.476	**13.4**	**1000.5**
	Mwakiro	3.09	**14.0**	**992.8**
Ngozi	Tangara	2.914	**13.8**	**980.4**
	Marangara	2.731	**13.6**	**964.5**
Makamba	Kayogoro	4.118	**14.9**	**981.2**
	Nyanza Lac	4.338	**15.2**	**1016.8**
Muramvya	Mbuye	2.154	**13.1**	**954.2**
	Kiganda	3.345	**14.2**	**840.5**
Mwaro	Ndava	3.378	**14.3**	**922.8**
	Bisoro	3.636	**14.5**	**881.4**
Rumonge	Muhuta	3.57	**14.4**	**885.0**
	Burambi	3.814	**14.7**	**906.3**
Rutana	Musongati	3.727	**14.6**	**999.4**
	Bukemba	4.007	**14.8**	**1045.7**
Ruyigi	Butezi	2.349	**13.3**	**995.2**
	Kinyinya	3.657	**14.5**	**1004.8**
Cankuzo	Kigamba	3.037	**13.9**	**1008.9**
	Cendajuru	3.313	**14.2**	**1017.6**

Based on the results obtained by the model developed, we note that the optimal annual angle of Inclination for fixed solar panels in Burundi varies between 13° and 15.9°. Table 3.11 shows a comparison of the results obtained by the software and the results of the models developed.

Table3.11: Comparison table of values obtained with pvsyst and the models developed

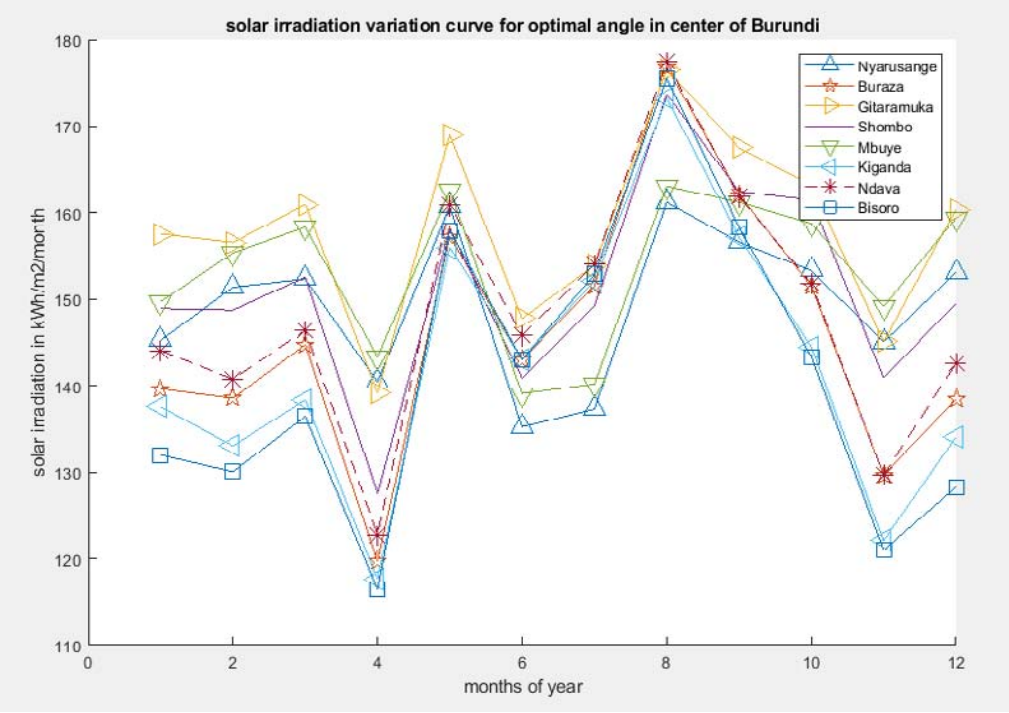
		Resultats using pvsyst			Resultats using the model	
Province	Site	Latitude	β_{opt}	E_Avail	β_{opt}	E_Avail
		˚S	˚	kWh	˚	KWh
Bujumbura Mairie	Kinama	3.325	14	906.5	14.2	903.1
	Mutanga Sud	3.38	15	884	14.3	883.4
Bujumbura	Mubimbi	3.295	14	890	14.2	887.1
	Kabezi	3.535	15	903	14.4	890.4
Bubanza	Musigati	3.067	14	930	14.0	910.5
	Mpanda	5.181	15.7	1084	15.9	1064.3
Bururi	Mugamba	3.665	15	893	14.5	881.4
	Vyanda	4.104	15	968	14.9	954.4
Cibitoke	Mugina	2.794	13	962	13.7	959.1
	Buganda	2.975	14	949	13.9	939.2
Gitega	Nyarusange	3.568	15	933	14.4	929.8
	Buraza	3.748	15	919	14.6	909.9
Karusi	Gitaramuka	2.981	14	989	13.9	980.4
	Shombo	3.278	15	944	14.2	939.0

Kayanza	Muhanga	2.971	14	892	13.9	894.5
	Butaganzwa	3.084	14	924	14.0	921.2
Kirundo	Bugabira	2.433	13	1014	13.4	1016.6
	Vumbi	2.695	13	978	13.6	980.6
Muyinga	Giteranyi	2.476	13	996	13.4	1000.5
	Mwakiro	3.09	14	992	14.0	992.8
Ngozi	Tangara	2.914	14	986	13.8	980.4
	Marangara	2.731	13	965	13.6	964.5
Makamba	Kayogoro	4.118	15	976	14.9	981.2
	Nyanza Lac	4.338	15	1018	15.2	1016.8
Muramvya	Mbuye	2.154	12	958	13.1	954.2
	Kiganda	3.345	14	844	14.2	840.5
Mwaro	Ndava	3.378	14	930	14.3	922.8
	Bisoro	3.636	15	880	14.5	881.4
Rumonge	Muhuta	3.57	15	885	14.4	885.0
	Burambi	3.814	15	910	14.7	906.3
Rutana	Musongati	3.727	15	1002	14.6	999.4
	Bukemba	4.007	15	1050	14.8	1045.7
Ruyigi	Butezi	2.349	13	995	13.3	995.2
	Kinyinya	3.657	15	1003	14.5	1004.8
Cankuzo	Kigamba	3.037	14	1013	13.9	1008.9
	Cendajuru	3.313	14	1026	14.2	1017.6

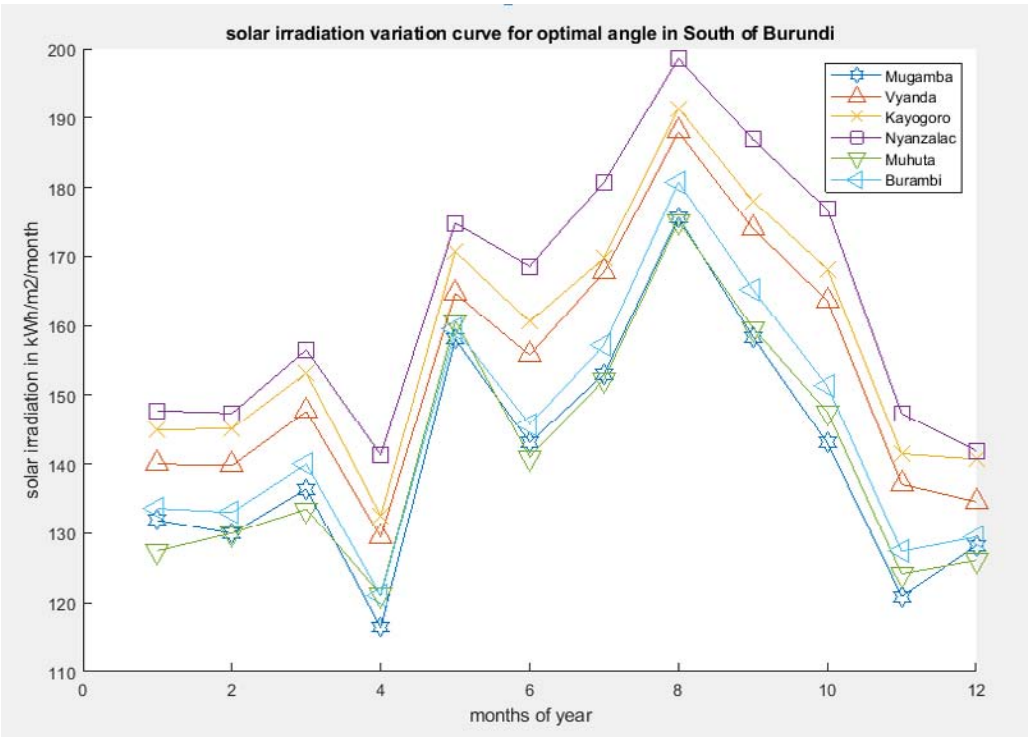
We see that the outcomes produced by the models are comparable to the simulation outcomes produced by the pvsyst software, which validates the models created.

3.2.3 Photovoltaic system efficiency

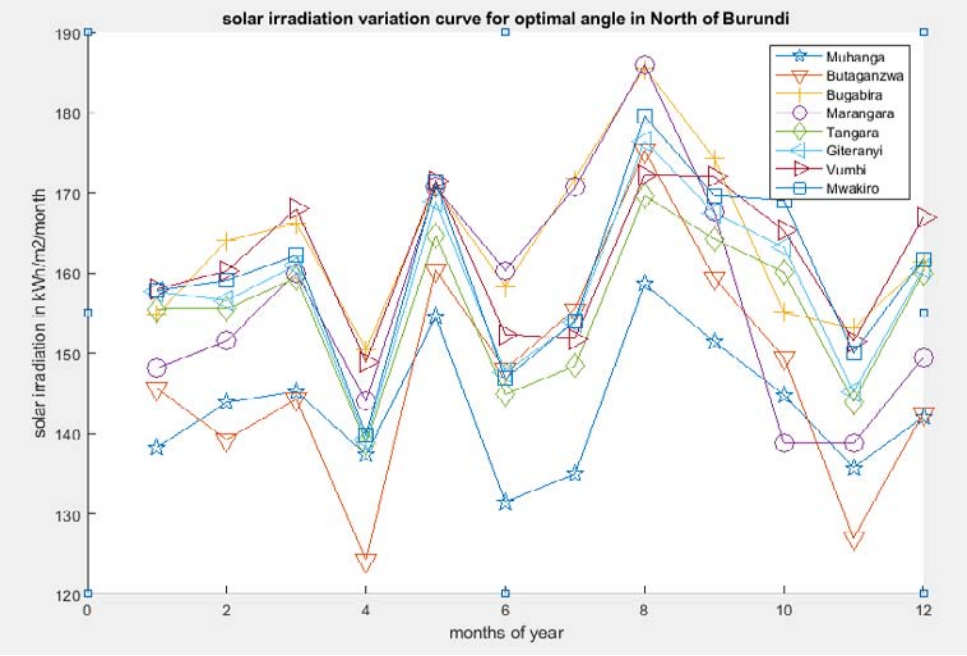
In this chapter, we have shown the solar energy production in Burundi's various provinces. The literature shows that Burundi is a country with rich solar potential. Based on the geographical data in Table 1 obtained using PVGIS software, Figure 3.7 the graph that depicts the change in overall horizontal irradiation for the optimal angle at the sites under study.


solar irradiation variation curve for optimal angle in center of Burundi
solar irradiation in kWh/m2/month
months of year
Nyarusange
Buraza
Gitaramuka
Shombo
Mbuye
Kiganda
Ndava
Bisoro

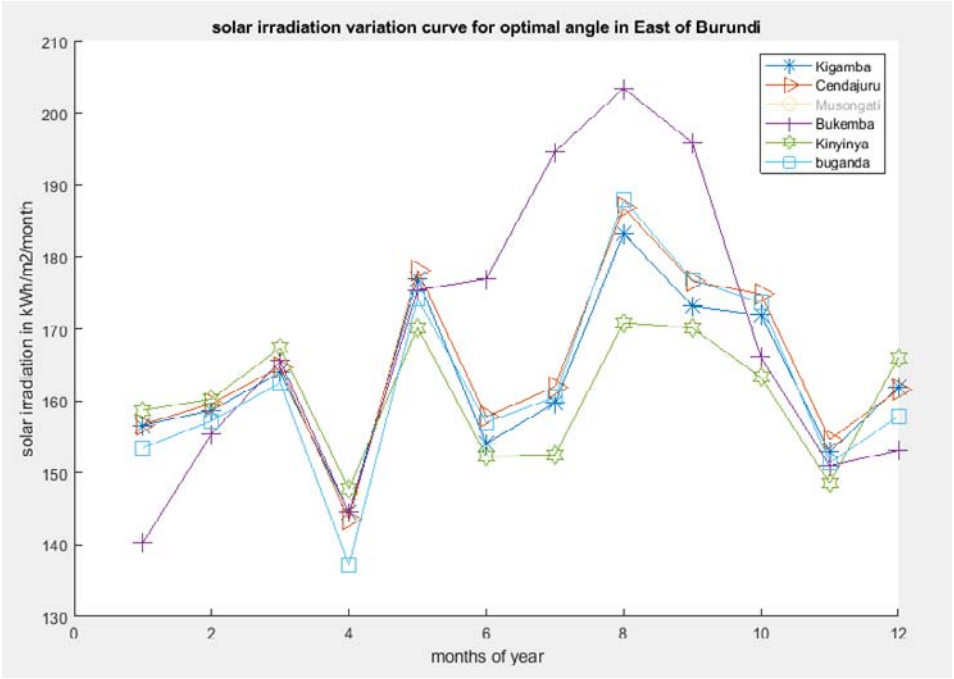
(a)


solar irradiation variation curve for optimal angle in South of Burundi
solar irradiation in kWh/m2/month
months of year
Mugamba
Vyanda
Kayogoro
Nyanzalac
Muhuta
Burambi

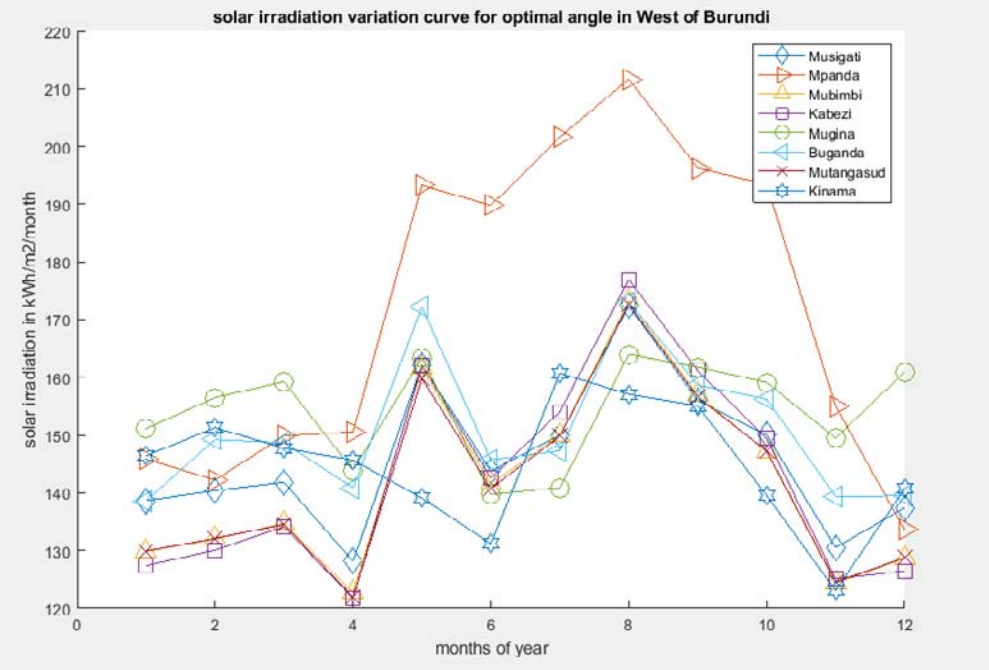
(b)


solar irradiation variation curve for optimal angle in North of Burundi
Muhanga
Butaganzwa
Bugabira
Marangara
Tangara
Giteranyi
Vumbi
Mwakiro
solar irradiation in kWh/m2/morth
months of year

(c)


solar irradiation variation curve for optimal angle in East of Burundi
Kigamba
Cendajuru
Musongati
Bukemba
Kinyinya
buganda
solar irradiation in kWh/m2/month
months of year

(d)



(e)

Figure3.7: Variations in the optimal horizontal global radiance (a) in the center of Burundi, (b) in south of Burundi, (c) in north of Burundi , (d) in east of Burundi and (d) in west of Burundi.

According to the simulation results obtained using MATLAB software, analysis of the variation curves indicates that all provinces of Burundi have high solar energy potential throughout the year. We note that the Mpanda sites in Bubanza province, the Marangara site in Ngozi province, the Bukemba site in Rutana province and the Nyanza-Lac site in Makamba province have high solar energy yields compared to other sites during the period between May and September. This analysis of curve variation shows the regions where national or international solar energy investors can invest as a priority. Data from the Ministry of Energy and Mines has shown us that the province of Gitega (in the center of the country) is heavily exploited for solar energy (94.34% of national solar production), even though it is not among the provinces mentioned above. This shows a significant loss of untapped solar energy in Burundi. This analysis shows that the center of the country is not rich in solar resources compared to the four cardinal points of the country. The Mpanda site would also be a site to be exploited first because it is close to high-voltage power transmission lines. Hybridization in this area is possible without the need for additional power lines.

3.2.4. Experimental Results

The experimental outcomes of two 10Wp solar panels with two Victron BlueSolar MPPT 75/10A-12V charge controllers is assessed in this section. At the Nyakabiga location, whose

geographic coordinates match those of Kinama, one of the panels was slanted at an angle of 30˚ and the other at an ideal angle of 14˚ (Table 3.1). When compared to PWM charge controllers, the Victron MPPT controller is an Incredibly quick MPPT controller that Increases solar production. **Figure 3.8** and **Figure 3.9** show the experimental setup diagram.



Figure3.8 : Photovoltaic solar panel has a 30° slant.



Figure3.9: Photovoltaic solar panel has a 14° slant.

We recorded the experimental results for the dates 21/12/2023 and 28/12/2023. Figure 3.10 and Figure 3.11 Present the curves of the obtained experimental results.

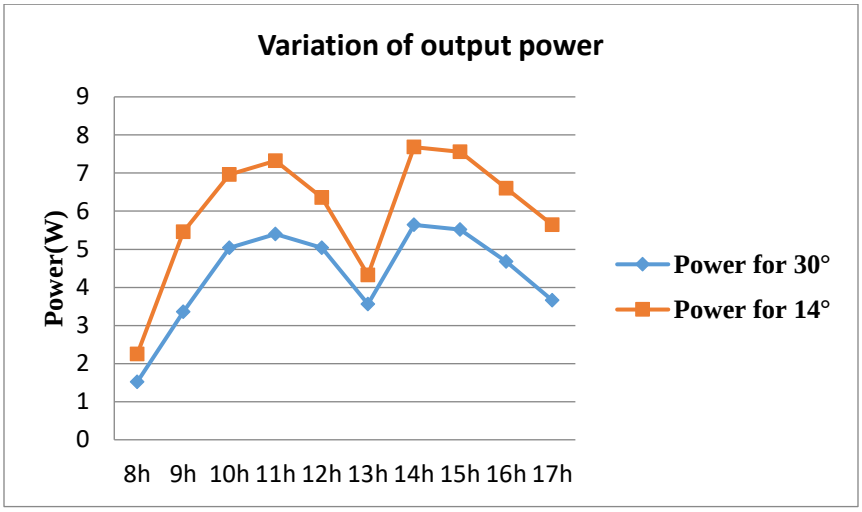


Figure3.10: Curve showing power distribution in December,21/2023

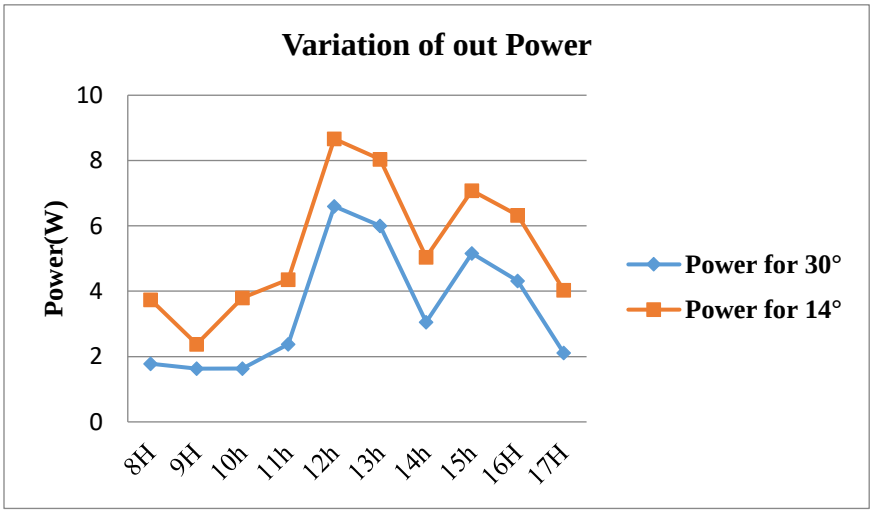


Figure3.11: Curve showing power distribution in December, 28/2023

Based on the variation curves, we note that between 9 A.M. and 11 A.M. and between 2 P.M. and 5 P.M. on 21/ 12/2023, there was a difference of approximately 2W in power between a solar panel tilted at an angle of 14˚ relative to the tilt of the solar panel on a house roof at an angle of 30˚. We also observe the same difference in power output for the power variation curves obtained on 28/12/2023 from 10:00 to 17:00, representing a gain of 20%. On 21/12/2023 at 1:00 P.M. and on 28/12/2023 at 2:00 P.M., we noticed a significant drop for both setups, with a power difference of approximately 0.7 W. This shows that there is a decrease in solar radiation when the sky is cloudy.

3.3. Results obtained for the design and simulation of the intelligent solar tracker

The build, computation, and simulated outcomes of an intelligent solar tracker are shown in this section. We also showcase the prototypes' experimental outcomes. To confirm and validate the generated algorithm, an analysis of the simulation and experimental data is conducted. The benefits of the basic solar tracker and the solar tracker in comparison to a stationary solar panel Inclined at the ideal angle is be assessed. Together with an experimental realization, a design and simulation utilizing MATLAB, SolidWorks, Proteus Professional, and the Arduino IDE software is completed. To demonstrate our contribution to previous research, the findings is addressed in reference to other studies.

3.3.1 Simulation results for the sun's trajectory

In order to accurately track the sun's rays in relation to the Earth's movement around the sun, we need to calculate the sun's trajectory in Burundi country using sunEarthtools software. **Figure 3.12** shows the sun's trajectory in Burundi Gitega province.

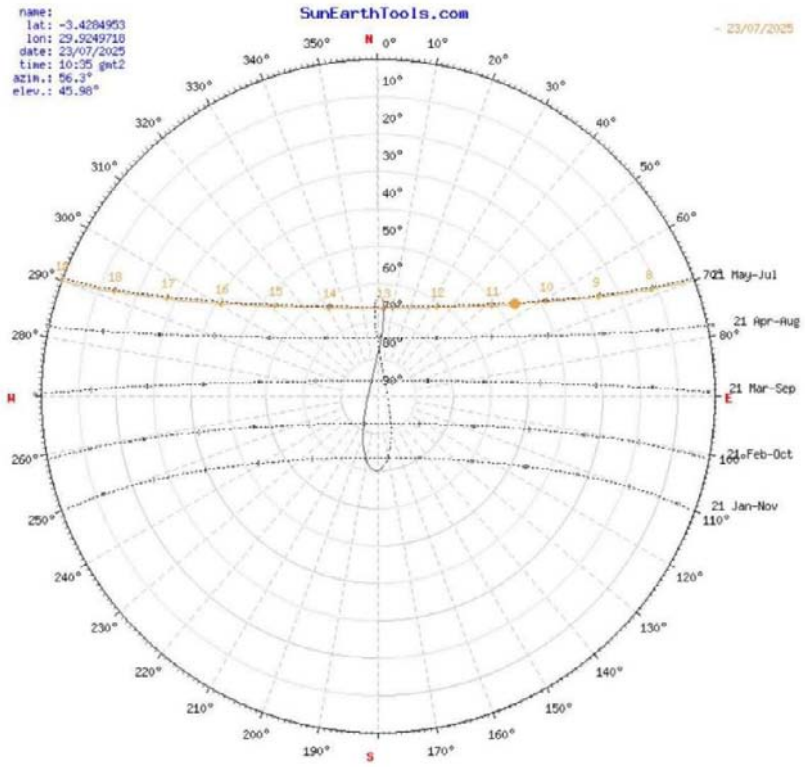


Figure3.12: Path of the sun in Burundi schema

We observe that the sun moves from east to west in April, August, March, September, February, and October.

3.3.2 Design and simulation of the intelligent solar tracker

Using equations 2.36 and 2.37 for the servomotor assembly and solar panel movement, we design and model the solar tracker system using MATLAB software. **Figure 3.13** shows controlling the solar tracker at an angle desired in MATLAB software

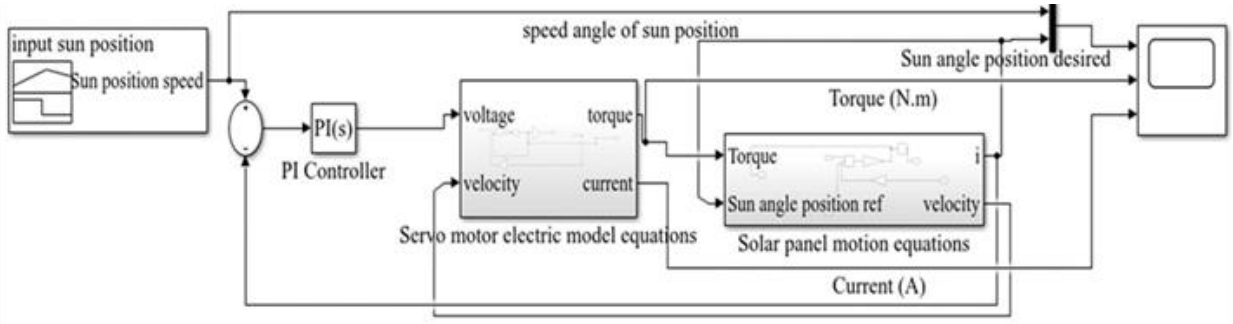


Figure3.13: Controlling the solar tracker at an angle desired

To identify the angles at which the solar panel may be positioned in accordance with the required angle, let's test three reference angles for moving the solar panel simultaneously: the 3°, 15°, and -3° angles. Additionally, we assess how they affect the power consumption of the servomotor. For Kg=1500; Kf=0.0700;R=15; L=1.0000e-05;J=4.6;Kd=5;Kt=0.0700; **Figure 3.14** shows the simulation results for repositioning the solar panel at a reference angle.

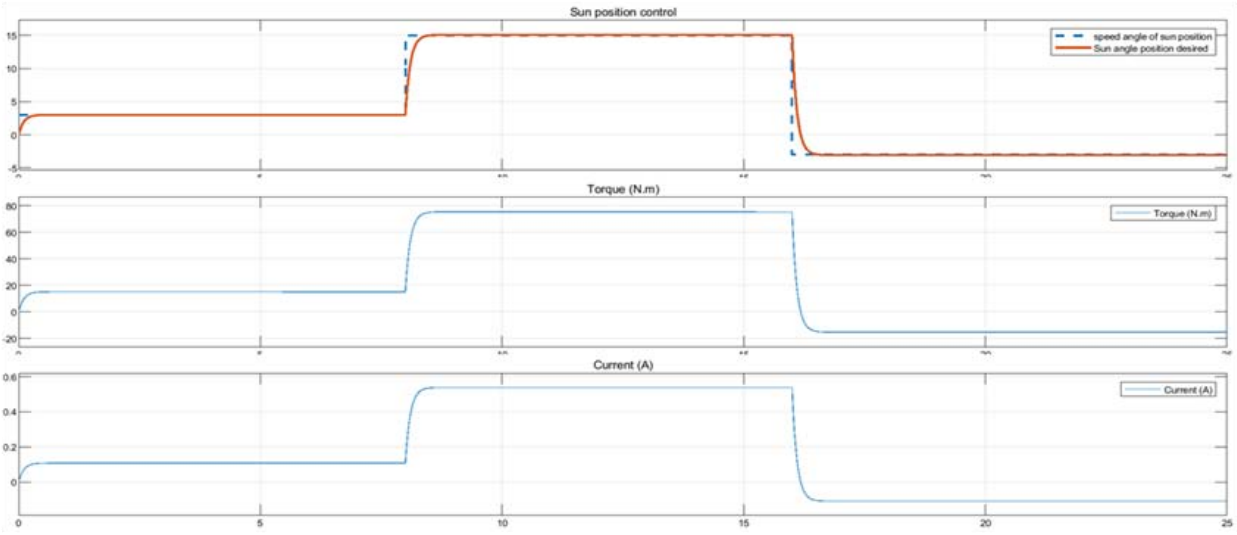


Figure3.14: Displaying how the solar panel is tracked at the desired angle

The servomotor rotates through an angle of 3° for an input value of a positive angle of 3° in the interval [0,8], repositioning the panel at an angle of 3° in the direction of the servomotor's rotation, according to an analysis of the variation curves of the simulation results produced. We find that the servomotor rotates by an angle of 3° for an input value of a negative angle of -3° in the interval [16,24], which causes the solar panel to pivot by an angle of -3°. The energy savings

in terms of battery capacity powering the servomotors for our proposed algorithm are demonstrated by the observation that an Increase in the angle of rotation results in an Increase in the electrical current and torque values. Let us evaluate the developed algorithm for the single-axis solar tracker by designing and simulating the solar tracker using the professional Proteus software. The developed algorithm is programmed using Arduino IDE software. The hexadecimal file with the .hex extension is uploaded to the designed control circuit. The design diagram of the single-axis solar tracker Includes a power supply, a servomotor, an RTC3231 real-time clock, an Arduino UNO board, and a display screen, as shown in **Figure 3.15**.

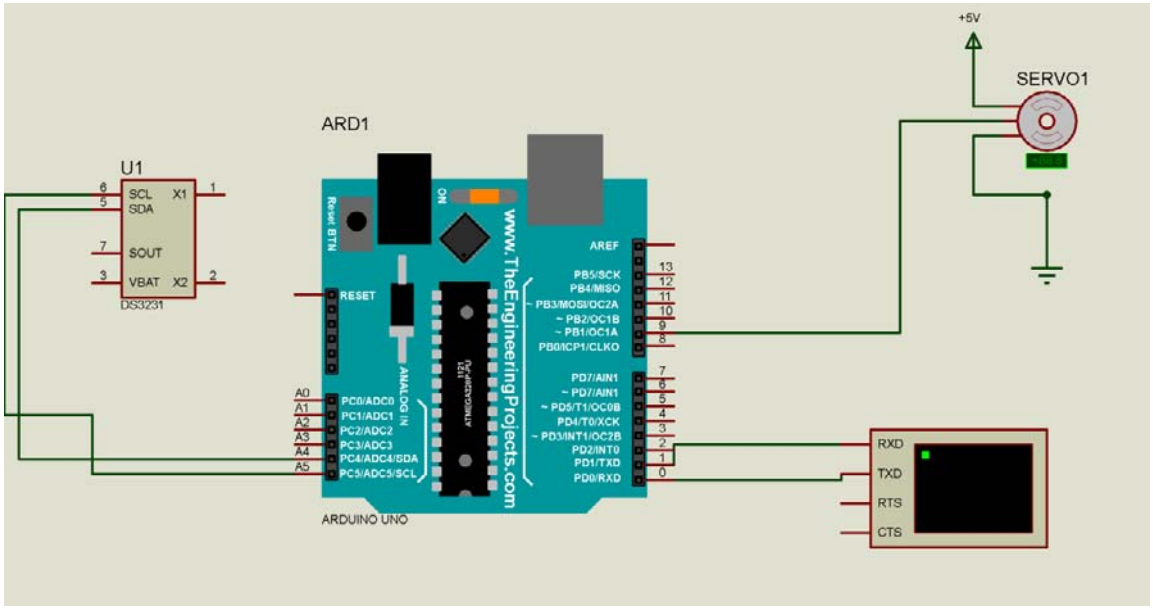
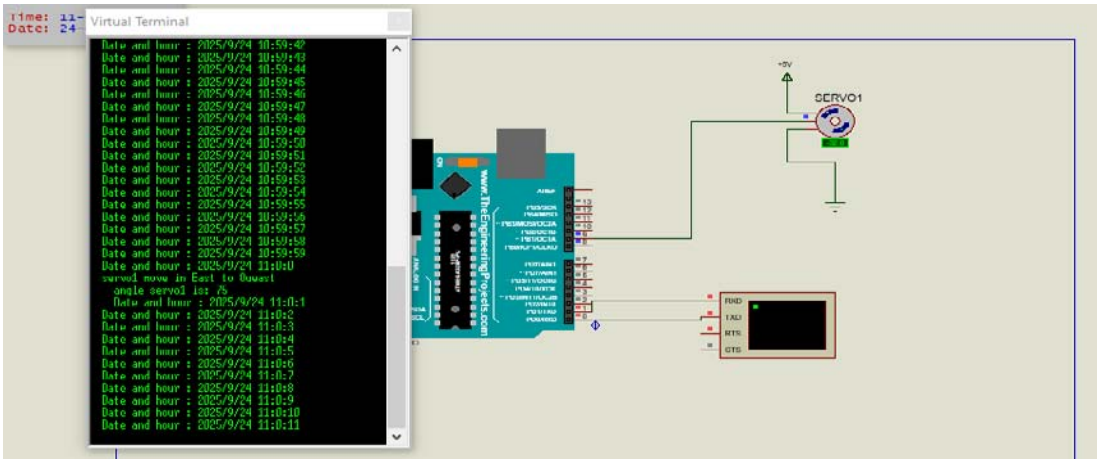
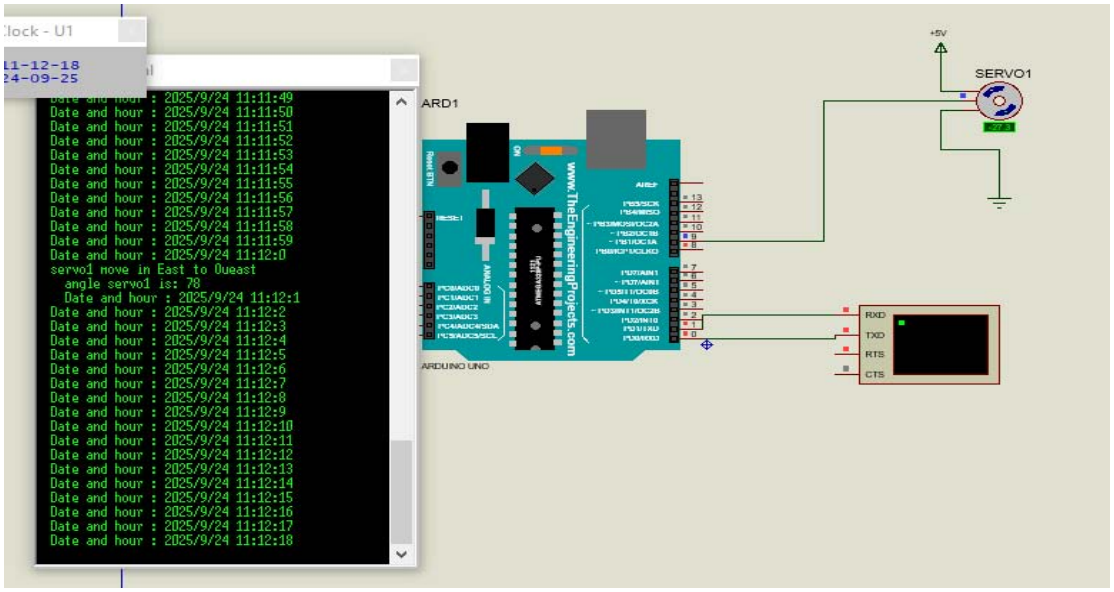


Figure3.15: Design diagram of the single-axis tracker

After simulation, Figure 3.16 (a) and Figure 3.16(b) show the simulation results obtained for detecting the rotation of the panel from East to West.



(a)



(b)

Figure3.16: Panel rotation (a) for detection of panel rotation from East to West at 11:00 AM and (b) for detection of panel rotation from East to West at 11:12 AM

We observe that the panel is moved every 12 minutes based on the simulation results and the display messages. The Arduino UNO microcontroller detects the time at 11:00 and uses port 9 to instruct the servomotor to rotate by 3°. As seen in Figure 3.17, the dual-axis solar tracker's design diagram consists of a power supply, a servomotor, an RTC3231 real-time clock, an Arduino UNO board, two LDR light sensors, and a screen.

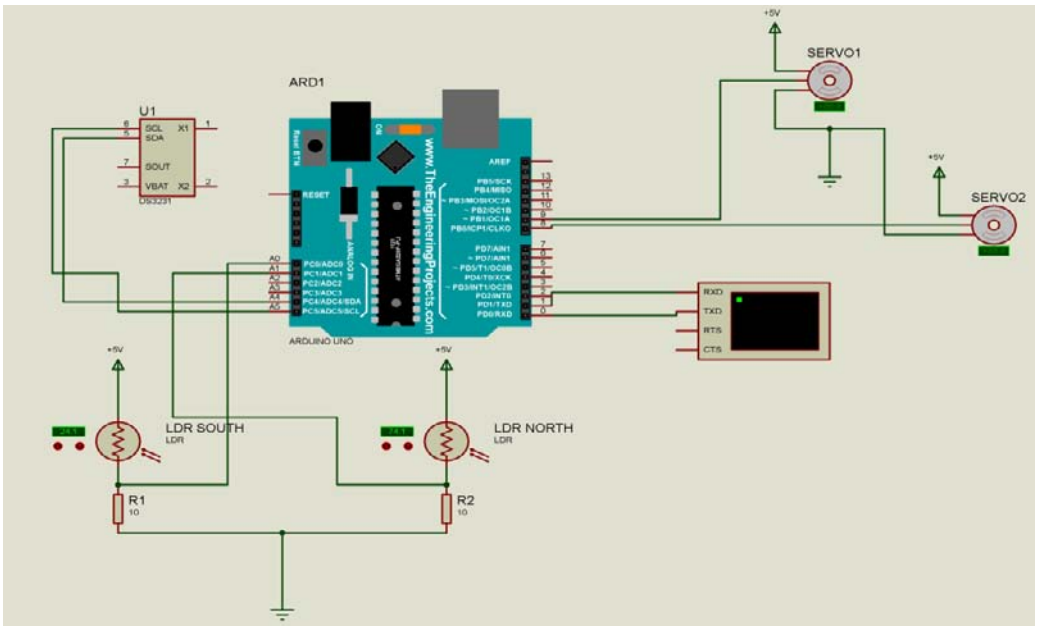


Figure3.17: The control circuit of the dual-axis solar tracker

The proposed algorithm states that the solar tracker shifts the solar panel's location every 12 minutes between 6 a.m. and 6 p.m. We conducted a one-hour simulation test, which involved one position change every minute from 12 p.m. to 2 p.m., because this simulation can run all day. We didn't want to wait from 6 a.m. to 6:30 p.m. for the simulation, so we only took one minute. Figure 3.18 displays the simulation's outcomes.

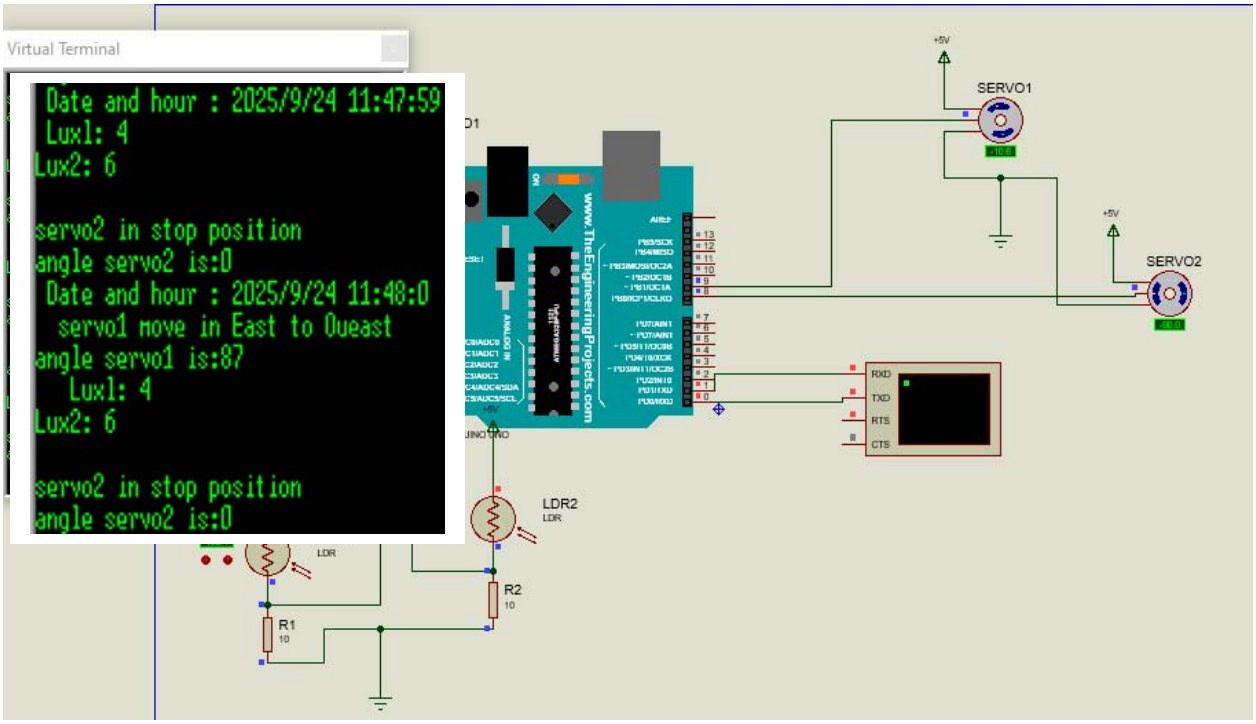


Figure3.18: Servo motor 1 rotating directly from East to West and servo motor 2 in stop position

The messages that come from the built algorithm are shown in Figure 3.19, this displays the angle at which the solar module rotates by 3° each minute along with duration and light sensor readings for each step.

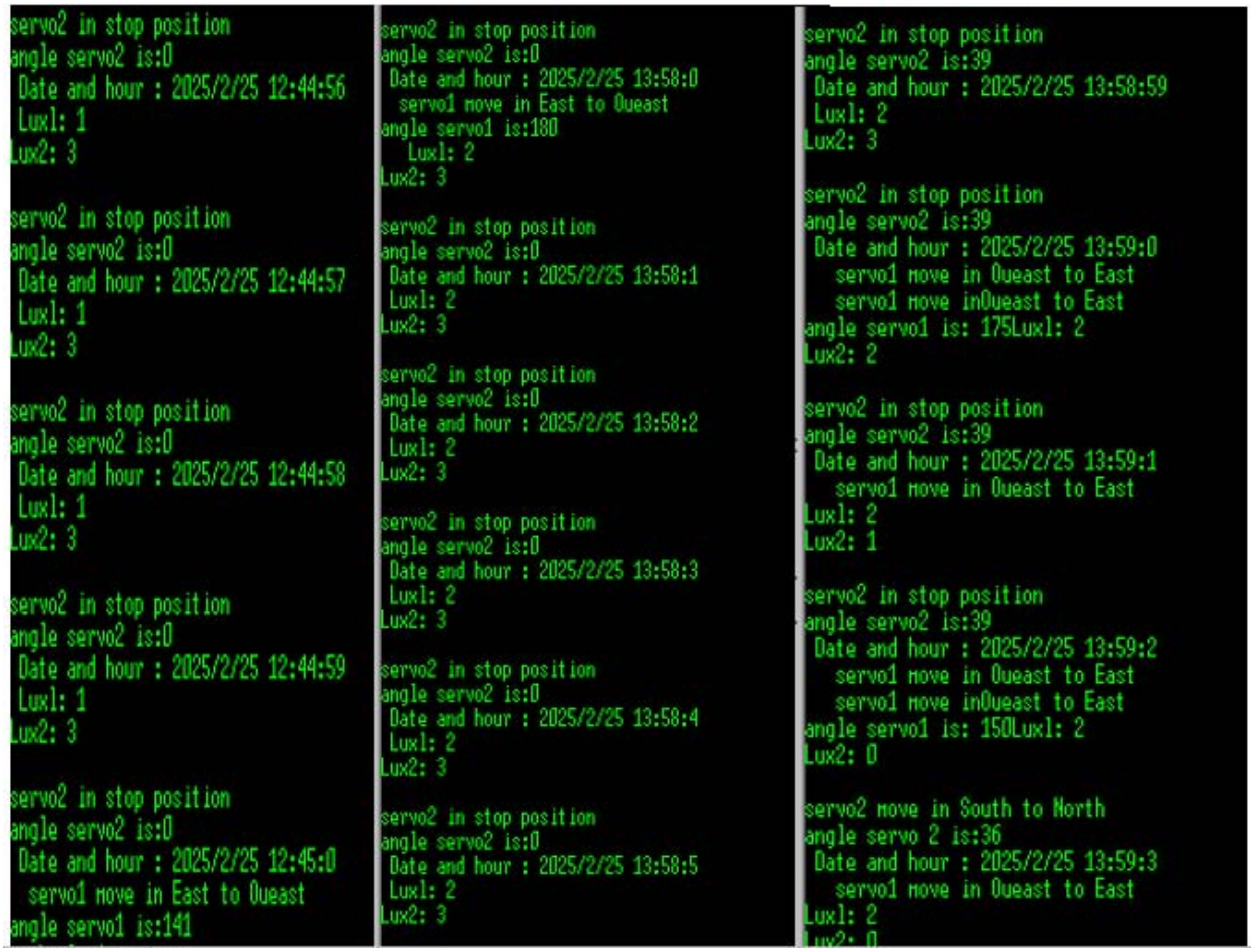


Figure3.19: Showing of the behavior of the developed algorithm

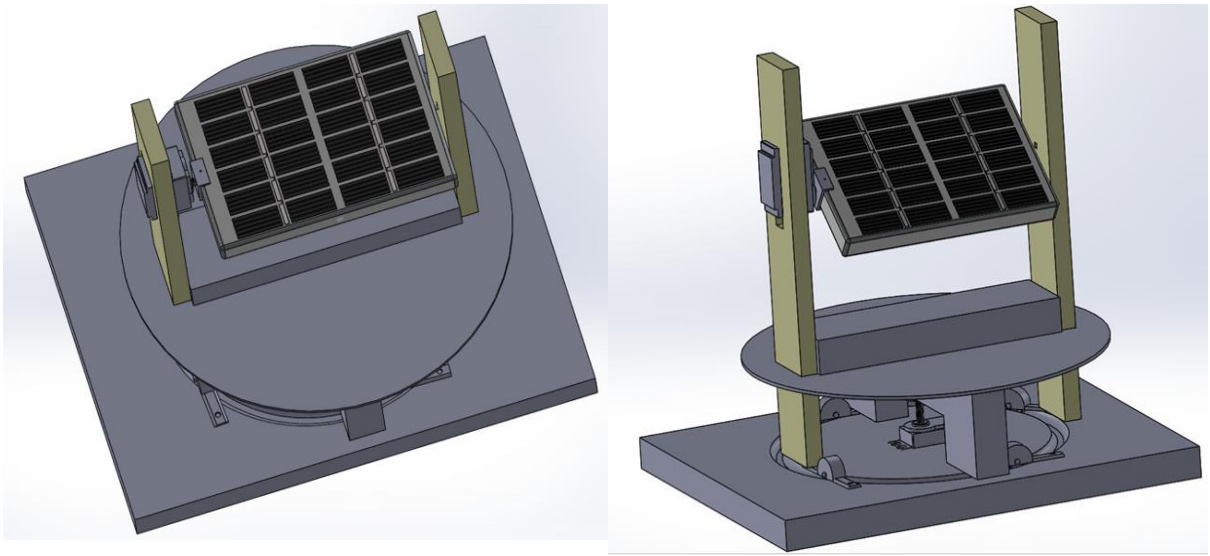
The outcomes of the simulation in this initial example show that the Arduino microcontroller gets an impulse from the Real Time Clock RTC 3231 until 12:58 P.M., based on the information provided by the sensor, one minute after 12 noon (which actually equates to 6 A.M.). Every twelve minutes, the computer signals servomotor 1 via pin 9 to elevate the solar panel to a 3° angle from east to west. Servomotor 1 spins 180°, or 60 repositioning of the solar panel, at 12:58 PM (which is actually 6 PM), and then stops. The RTC3231 real-time clock transmits a signal to the Arduino microcontroller at 12:59 PM, which is actually 6:30 PM. The Arduino microcontroller then instructs servomotor 1 to rotate the solar panel from West to East to its starting position in the morning. Otherwise, servomotor 1 stays stationary.

In the following case, servomotor 2 uses information from the two light sensors (LDR) to shift the solar array from north to south, is controlled by the variations in illumination between

sensors LDR1 and LDR2. If the electrical voltage of one light sensor greater than that of the other, with a tolerance, the Arduino microcontroller get an analogue signal from the LDR sensor via its analogue inputs A0 and A1. If the voltage of the South light sensor is greater than that of the North light sensor, the Arduino microcontroller converts the data into an analogue signal and then orders pin 8 of servomotor 2 to turn the solar array from North to South, and inversely. If servomotor 2 remains in the stop position, we find that there is no appreciable change in illumination. The proposed algorithm was able to monitor the sun's rays perpendicular to the solar panel at an angle of 3° every 12 minutes, according to the simulation findings.

3.3.2 The solar tracker's mechanical design and modelling

In this part, we used SolidWorks2023 software to perform the mechanical design and modelling of the smart solar tracker. The mechanical design consists of: The primary structure consists of a vertical support column that permits the solar panel to rotate in azimuth and a square frame that is anchored to the ground. The azimuth axis, the solar panel, and two servomotors with internal gears that enable the solar panel to rotate either vertically or horizontally to the appropriate angle. To determine the mechanical design, we measured each component of the experimental prototype using a ruler. Figure 3.20 shows the results of the computer-aided design and modelling of the three-dimensional design of the two-axis solar tracker structure was created using SolidWorks software.



(a) (b)

Figure3.20: (a) View from above of the three-dimensional design of the two-axis solar tracker structure et (b) The basic design of a dual-axis solar tracker.

A 3D view of a solar panel, a 3D view of two servomotors, one for azimuth rotation and the other for elevation rotation ,a 3D view of a solid base fixed to the ground with a hole above it

that permits the passage of free wheels to achieve resistance-free rotation of the solar panel in azimuth, and a 3D view of an appropriate solar panel support make up the overall structure of the solar tracker. The MG996R servomotor was disassembled. All of the servomotor's measured internal components were designed and simulated by us. Lastly, we simulated the full servomotor. Figure 2.21 shows the results of the design and modelling of the 3D model of the servomotor arrangement.

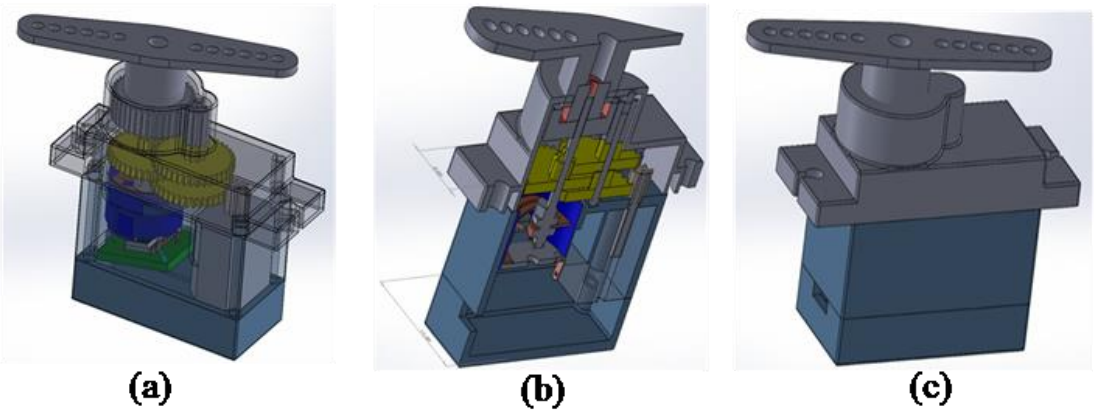
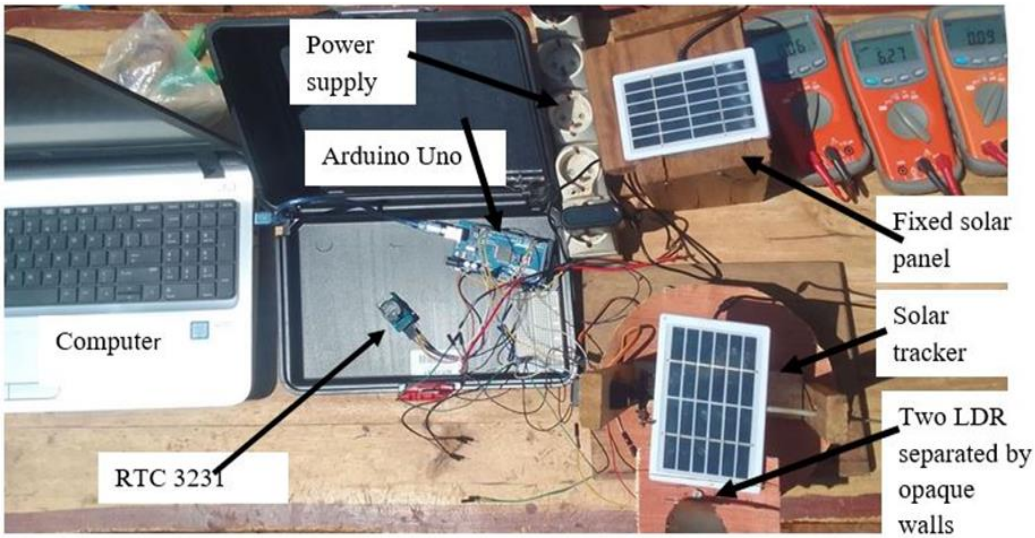


Figure3.21: (a): (a) Internal diagram of the servomotor design; (b): Sectional representation of the internal design of the servomotor, (c) Schematic diagram of the general design of the servomotor.

By influencing the gears' rotation, this simulation allowed us to turn the servomotor that will move the solar panel to the required angle. This validates the other simulation results and demonstrates the effectiveness of the system being studied.

3.3.3 Experimental results

The experimental results for a fixed solar panel, a single solar tracker, and a dual-axis solar tracker on the solar energy captured are shown in this section. This experimental investigation was carried out in the provincial capital of Gitega. Gitega province’s center is located in latitude 3° 25' 42.583 and longitude 29° 55' 29.898. We discovered that 15° is the ideal yearly degree of Inclination for the fixed solar panel using the model created by [1]. As a result, the fixed solar panel in-this work is slanted at the ideal 15° angle. Regarding the prototype dual-axis solar tracker, we employed two 1.2 Wp solar panels that were polycrystalline, had dimensions of 84*130*10 mm, a maximum power of 1.2 W, a voltage at Pmax (Camp) of 6 V, and a current at Pmax (Imp) of 0.2 A. We used a single servomotor and no LDR light sensors for the single-axis solar tracker prototype. The dual-axis solar tracker experimental prototype is shown in Figure 3.22 with various components that were utilized.



.

Figure3.22: Experimental prototype of the dual-axis solar tracker

Using the serial monitor, let us analyze how the developed algorithm works. Figure 3.23 shows the messages from the Arduino IDE serial monitor that describe how the developed algorithm for the two-axis solar tracker system and the single-axis solar tracker work.

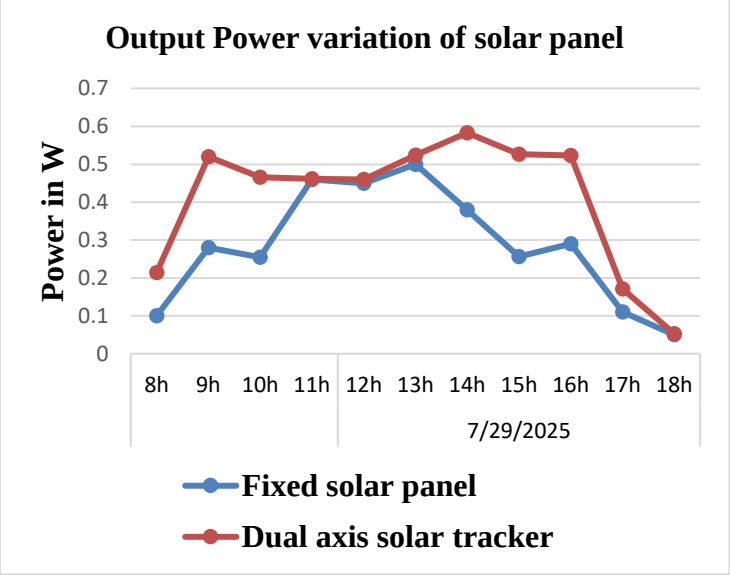
```
->  Date and hour : 2025/7/22 12:11:59
->  Lux1: 326
-> Lux2: 311
->
-> servo2 in stop position
-> angle servo2 is:0
->  Date and hour : 2025/7/22 12:12:0
->   servo1 move in East to Oueast
-> angle servo1 is:93   Lux1: 307
-> Lux2: 294
->
-> servo2 in stop position
-> angle servo2 is:0
->  Date and hour : 2025/7/22 12:12:1
->  Lux1: 331
-> Lux2: 314
->
-> servo2 in stop position
-> angle servo2 is:0
->  Date and hour : 2025/7/22 12:12:2
->  Lux1: 319
-> Lux2: 305
->
-> servo2 in stop position
-> angle servo2 is:0
->  Date and hour : 2025/7/22 12:12:3
->  Lux1: 306
-> Lux2: 293
->
-> servo2 in stop position
-> angle servo2 is:0
```

```
->  Date and hour : 2025/7/22 13:0:0
->   servo1 move in East to Oueast
-> degre:105
->    Lux1: 314
-> Lux2: 300
->
-> servo2 in stop position
-> angle servo2 is:0
->  Date and hour : 2025/7/22 13:0:1
->  Lux1: 304
-> Lux2: 289
->
-> servo2 in stop position
-> angle servo2 is:0
->  Date and hour : 2025/7/22 13:0:2
->  Lux1: 305
-> Lux2: 291
->
-> servo2 in stop position
-> angle servo2 is:0
->  Date and hour : 2025/7/22 13:0:3
->  Lux1: 332
-> Lux2: 314
->
-> servo2 in stop position
-> angle servo2 is:0
->  Date and hour : 2025/7/22 13:0:4
->  Lux1: 336
-> Lux2: 318
```

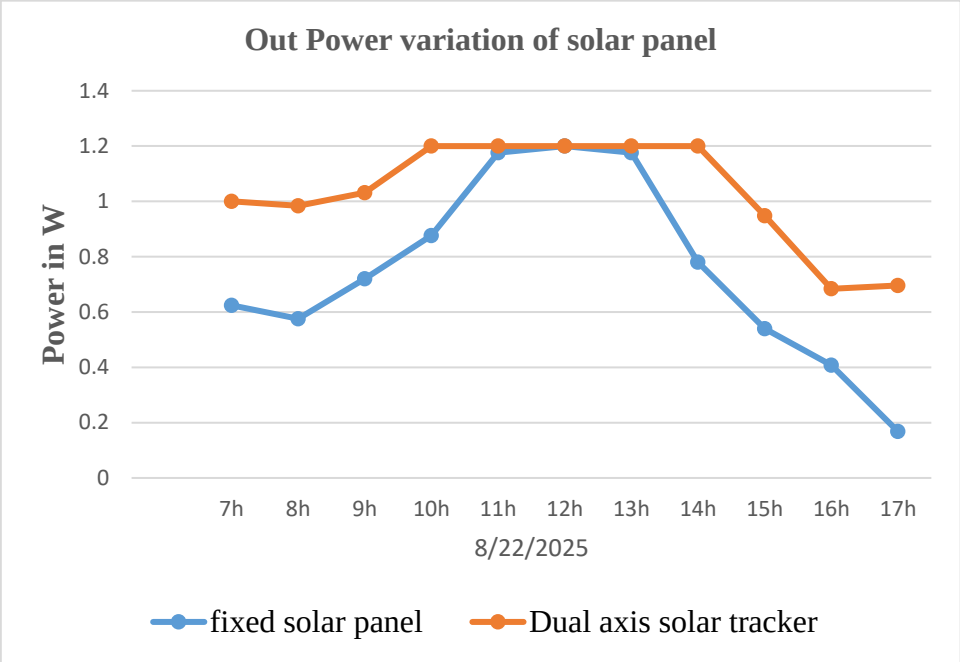
Figure3.23: Diagram displaying the results on the serial monitor.

The solar tracking system begins at 6:00 AM, and the solar panel returns to its starting position of 3° by 6:30 PM, according to an analysis of the trial results shown in the serial monitor. We observe that the Arduino UNO microprocessor instructs servomotor 1 to spin at a 3° angle

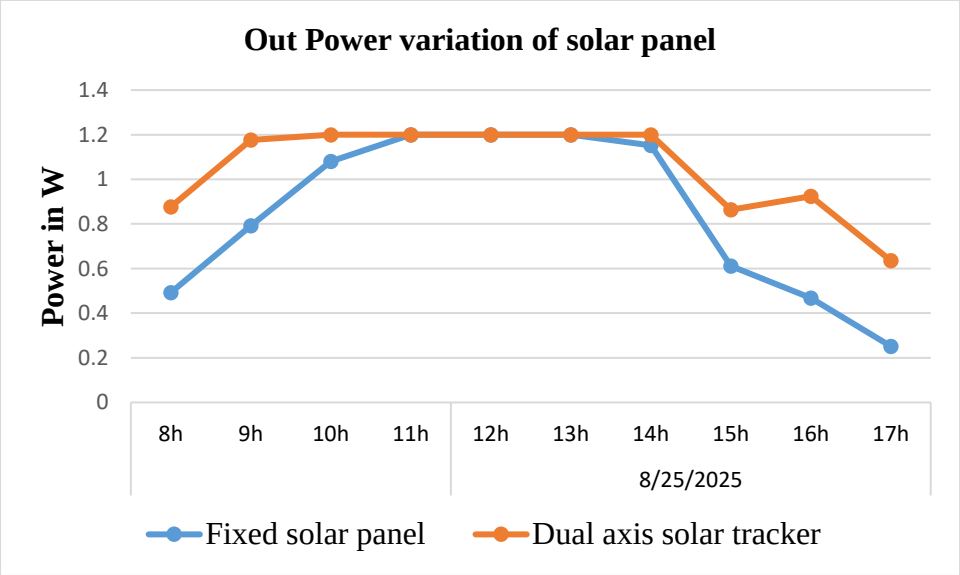
every 12 minutes, moving the solar panel from east to west (in elevation). We note that a message to move the solar panel from east to west at a 93° angle was detected at midnight. Additionally, we observe that around 1:00 PM, the solar panel's repositioning angle is 105°, and the serial monitor shows that it has been turned from east to west. The serial monitor shows that the solar panel is moving from west to east at 6:30 p.m., returning to its morning position. Analysis of the data also reveals that servomotor 2 stays in the stop position when there is no discernible variation in the light flux of the two LDR sensors. We observe that there is a correspondence between the experimental and model simulation outcomes. Figures 3.24(a), 24(b) and 24(c) illustrate the curves of the experimental results obtained for a fixed solar panel and a two-axis solar tracker. Figure 3.25 (a) and Figure 3.25 (b) show the experimental results on a graph for a fixed solar panel and a one-axis solar tracker.



(a)



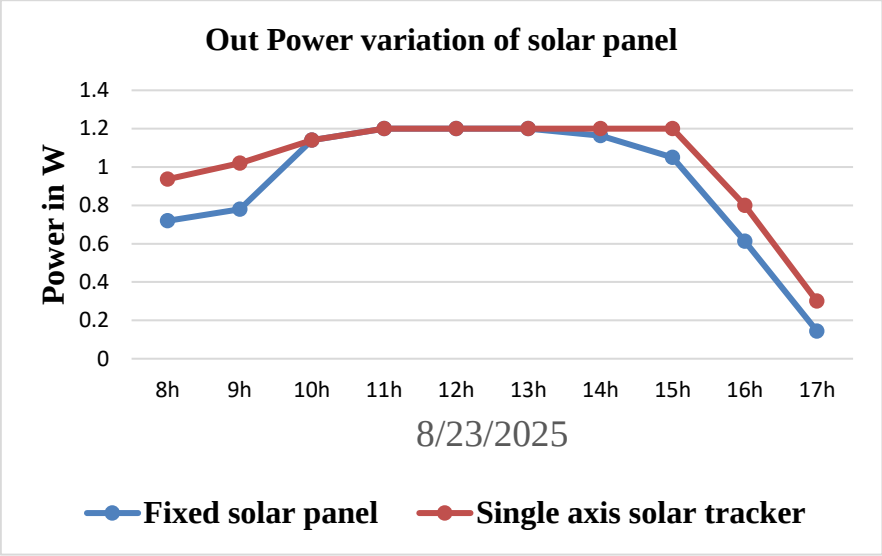
(b)



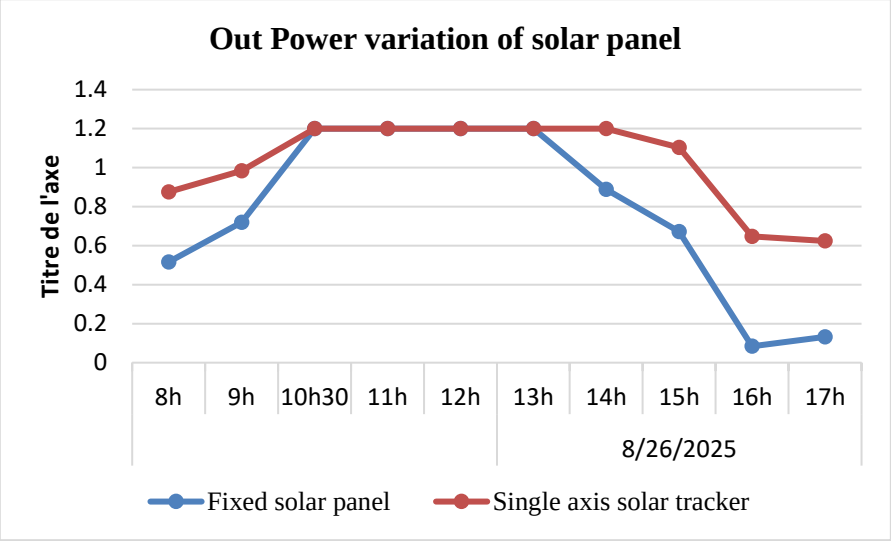
(c)

Figure3.24: Diagram of experimental results of dual axis tracker solar (a) for 7/29/2025, (b) for date 8/22/2025 and (c) for date 8/25/2025.

.



(a)



(b)

Figure3.25: Diagram of experimental results of dual axis tracker solar (a) for 8/23/2025, (b) for date 8/26/2025

The two-axis solar tracker and the fixed solar panel produced significantly different amounts of solar energy in the morning, with the difference diminishing by 11:00 A.M., according to an analysis of the trial results. We find that the dual-axis solar tracker's energy production is comparable to that of the fixed solar panel between 11:00 a.m. and 1:00 p.m. Analysis of the data reveals an Increase in energy gain between the fixed solar panel and the dual-axis solar tracker starting at 2:00 PM. We make the conclusion that the dual-axis solar tracker has an energy gain of between 42% and 50% when compared to the fixed solar panel based on the experimental data. We observe that July 29, 2025, had little sun radiation from a climatic perspective

In order to assess the energy gain of the single-axis solar tracker in comparison to a fixed solar panel installation, we recorded experimental findings on August 23 and 26, 2025. The single-

axis solar tracker and the fixed solar panel had significantly different energy gains between 8:00 A.M. and 10:30 P.M., according to an analysis of the experimental results. The variation graph indicates that as 11:00 P.M. draws near, the energy differential decreases. Additionally, we see that the production of the solar panel achieves its greatest value between 12:00 and 1:00 PM, and that the solar energy acquired by the single-axis solar tracker is comparable to the solar energy captured by a stationary solar panel. We conclude that the single-axis solar tracker achieves an energy gain of between 29% and 41% in comparison to the fixed solar panel based on an examination of the experimental findings obtained. We note that on 25/08/2025 and 26/08/2025, the sun's rays were oriented in an East-West trajectory, whereas on other days, the sun was in an East-north trajectory in the morning and a West-north trajectory in the afternoon.

3.4. Outcomes for the creation of a battery charge and discharge control system to maximize energy storage batteries

In this section, we present the results of designing the battery charge and discharge management system and the results obtained through design, programming and simulation using MATLAB, Arduino IDE and Proteus software. We showed the analysis of the simulation results of the effect of temperature on different battery parameters. Finally, we evaluated the results of the battery ageing prediction model.

3.4.1. Design and simulation of the battery charge and discharge management mechanism

Using equations (2.40), (2.41), (2.42), (2.43), (2.44) and (2.45), Figure 3.26 illustrates the design and modelling scheme for the lead-acid battery management of charges and discharges monitoring using MATLAB software. The SOC is calculated using the Coulomb method.

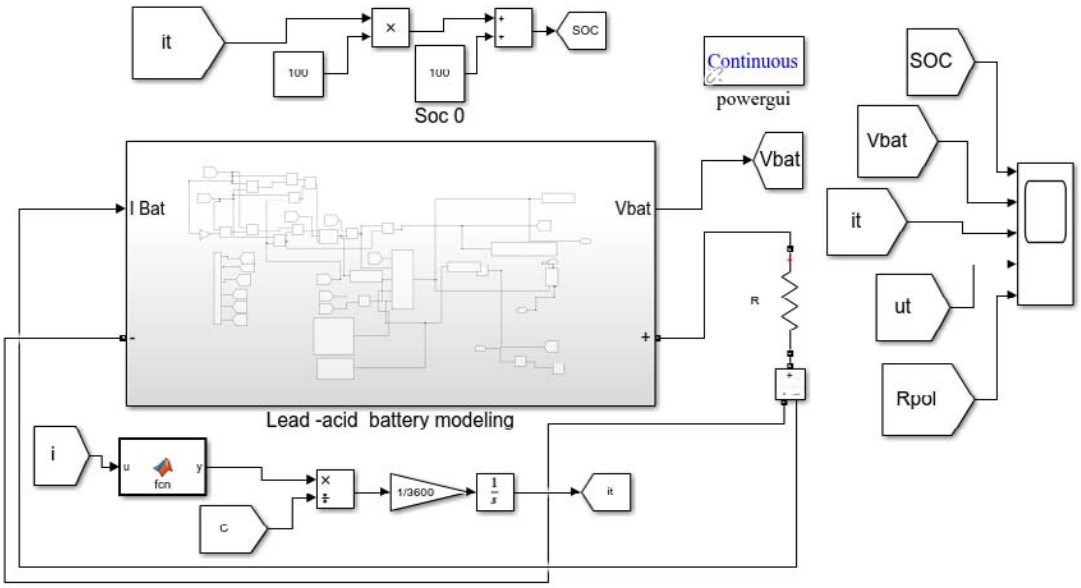


Figure3.26: MATLAB block diagram for modelling a lead-acid battery.

For K=0.0058935; A=1.0154; V0=12; V=2.0354; C=30; R=0.073 and SOC0=100. Simulation results in discharge mode are shown in **Figure 3.27**and Figure 3.28 in charge mode with K=0.0058935; A=1.0154; V0=12; V=2.0354; C=30; R=0.073 and SOC0=90.32.

.

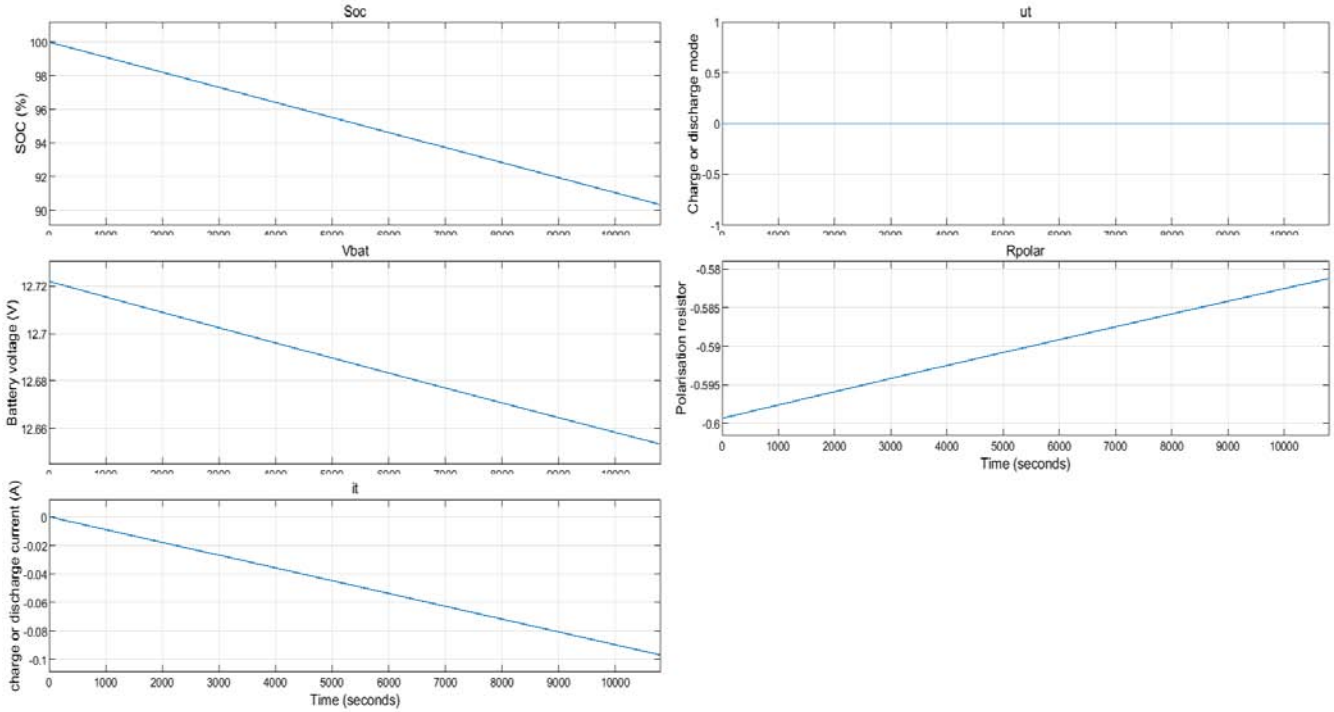


Figure3.27: Battery discharge

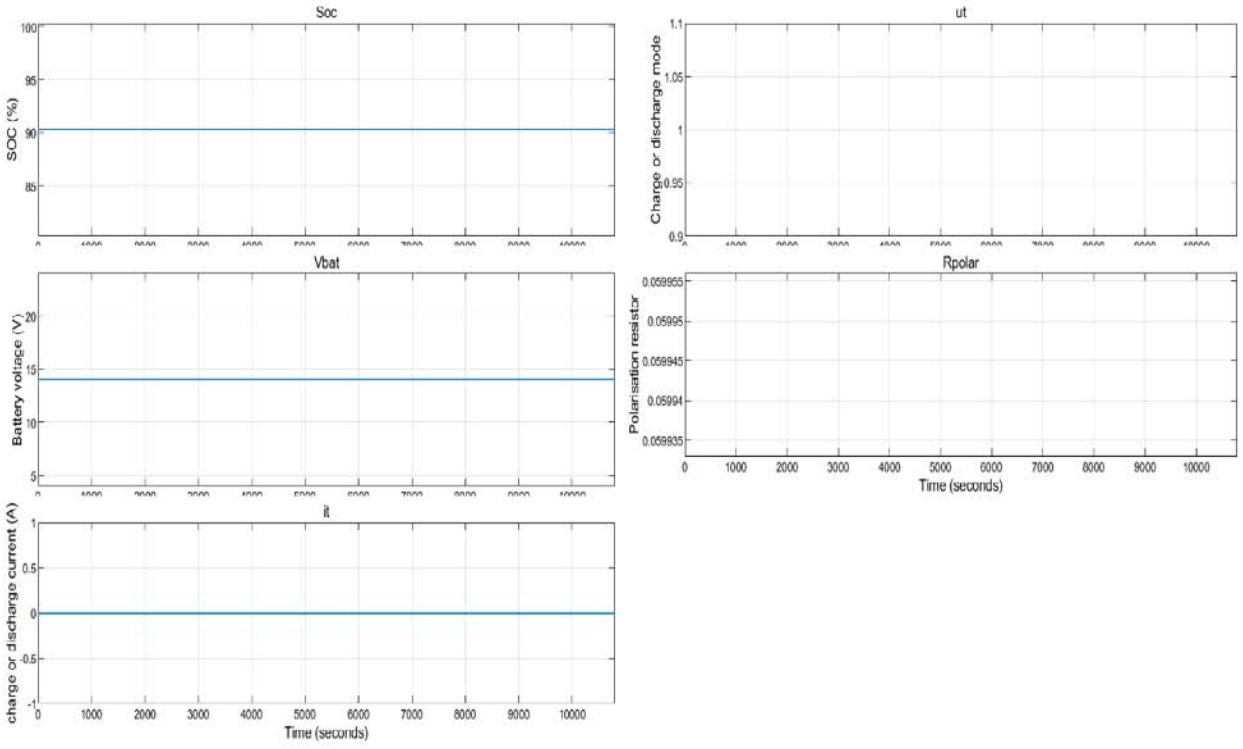


Figure3.28: Battery completely charged indicator

For results in Figure3.27, he battery is discharged at a SOC of 90.32%, which translates to a discharge voltage of 12.65 V as depicted in the figure, according to analysis of the SOC and Vbat fluctuation curves. In this instance, the findings demonstrate that the battery is in discharge mode (ut=0) since the discharge current is likewise negative. Based on results in Figure 3.28, because ut is at a high level (ut=1), an analysis of the simulation results indicates that the battery is in charging mode. The battery is fully charged (VAB=14V) with a state of charge of 100% and it=0, according to the variation curves. As predicted by theory, we can also observe that the polarization resistance has an unlimited value. Using MATLAB software, we can assess the algorithm created (see the algorithm in Figure2.20) for the battery charging and discharging mechanism after simulating the battery with a DHT1, two batteries of SOC_Max=100 and SOC_min=80. Figure 3.29 demonstrates the design of the battery storage system with temperature regulator in MATLAB.

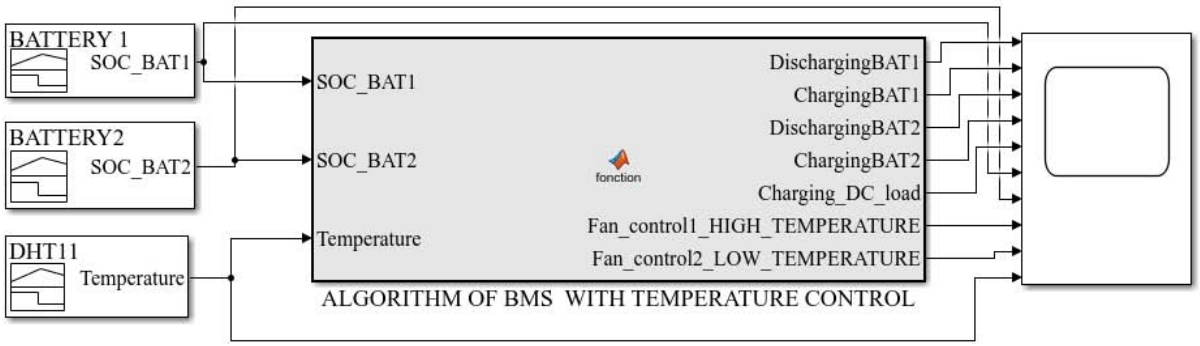


Figure3.29: Design of the battery storage management system with temperature regulator

Let's examine the design outcomes of the algorithm created with MATLAB Simulink for a minimum discharge voltage of 11.2 V and a state of charge (SOC) of 80%. The results of the MATLAB program simulation are shown in Figure 3.30.

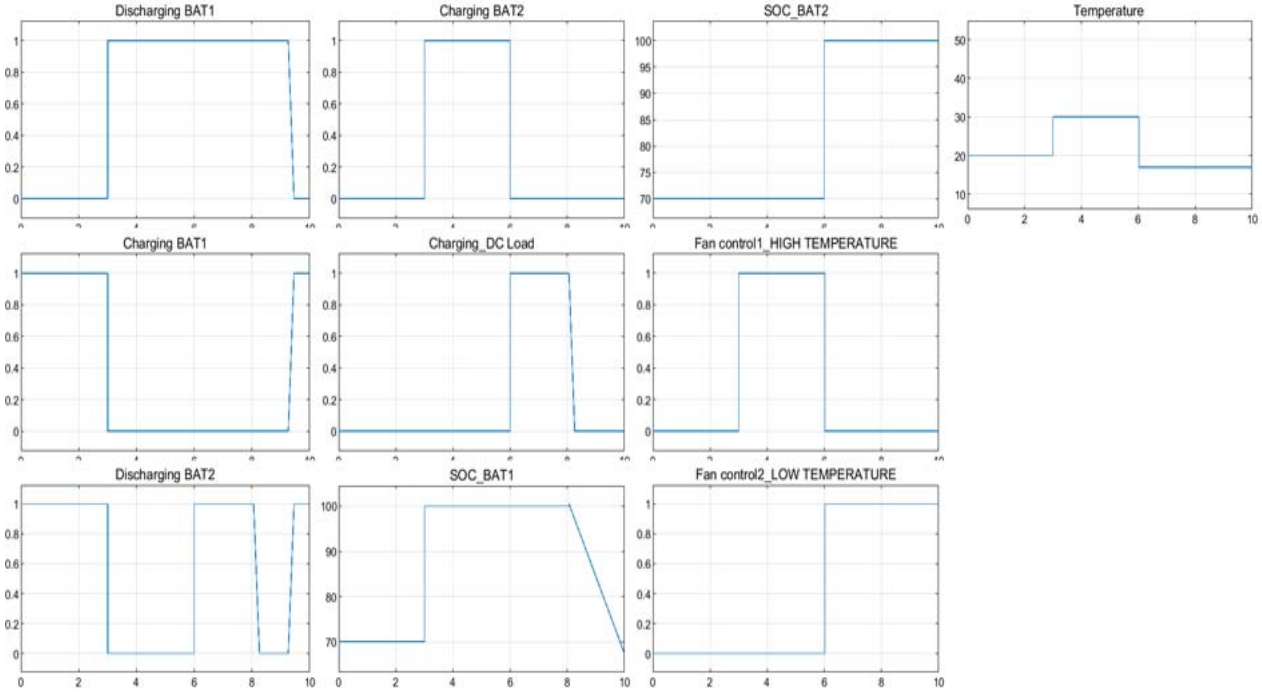


Figure3.30: Curves showing the state of charge and discharge of batteries with temperature monitoring.

Based on the variation curves, we note that in the range [0, 3], SOC_BAT1=SOC_BAT2=70%, which shows that all batteries are discharged .Battery 1 has priority at the HIGH level, indicating that it is in charge mode, according to an analysis of the variation curve for the battery charge and discharge mode. In this instance, battery 2's charge and discharge mode is at the LOW level, indicating that the battery is not a charging priority. We have SOC_BAT1 = 100% and SOC_BAT2 = 70% in the interval [3,6]. While battery 2 is at the HIGH

level, indicating that the battery charge and discharge system is in charge mode, battery 1 is at the LOW level, indicating that the battery charge and discharge system is in discharge mode. When SOC_BAT1=SOC_BAT2 = 100% occurs in the period [6,8.5], batteries 1 and 2 are at the LOW level, signifying that they are in discharge mode. In this instance, charge mode is engaged since the DC charge curve is at the HIGH level.

We see a SOCBAT1 below 80% and SOC_BAT2 = 100% in the interval [8.5, 10], while battery 1 is in charging mode. Now let's examine the temperature control fluctuation curves. We observe that the temperature is higher than 25 °C in the interval [3,6] and that a HIGH level is identified, signifying the activation of ventilation mode, we have a temperature below 20 °C in the interval [6,10], which indicates the requirement for air conditioning. Let's use Proteus professional design software and the Arduino IDE programming software to further assess the established algorithm for the battery charge and discharge management mechanism after examining the simulation results using MATLAB software.

The design and simulation diagram using Proteus software Includes: an Arduino UNO microcontroller, which is the control and command element, a solar panel, two 12V batteries, two relays to activate battery charging, two relays to activate battery conditioning based on room temperature, LEDs to indicate battery charge and discharge status, polarization resistors, and two potentiometers to vary the battery voltage.

From a configuration point of view, analogue ports A0 and A1 of the Arduino UNO microcontroller receive analogue signals from the battery voltage via the voltage divider bridge and are configured as inputs. Port 2 of the Arduino UNO microcontroller receives the room temperature signal and is configured as an input. Ports 1, 2, 3, 4, 9, 10, 11, and 12 send control signals and are configured as outputs. Figure 3.31 illustrates the design diagram of the developed algorithm for the battery charging and discharging mechanism with temperature control. We installed LEDs to indicate the operating status of the developed algorithm for the battery charging or discharging system in four cases:

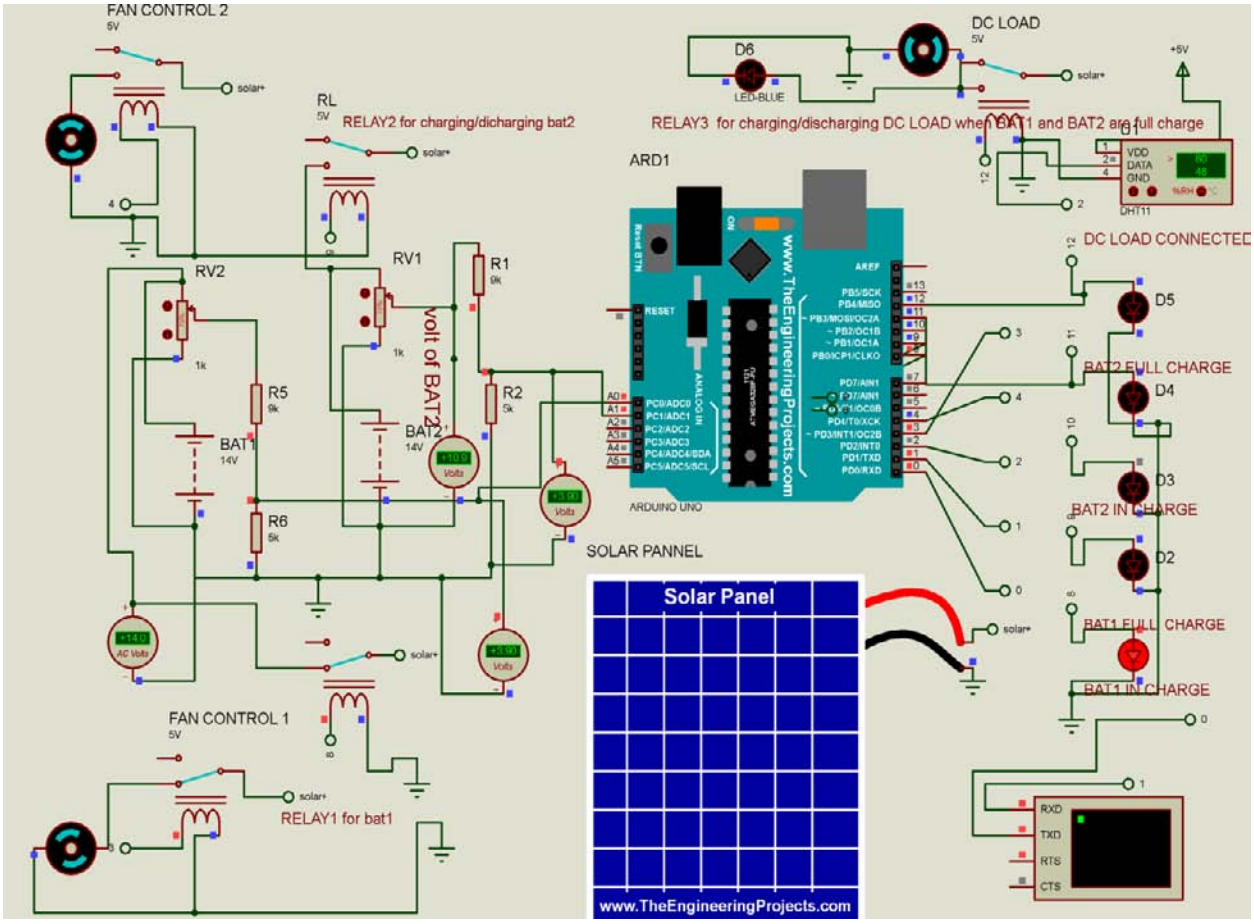


Figure3.31: Built algorithm's design schematic for the battery charging and discharging system with temperature control.

Let us evaluate the developed algorithm when all batteries are discharged. We programmed the developed algorithm using ARDUINO IDE software, and then transferred the hexadecimal file code with the .hex extension to the diagram designed with Proteus professional software. After simulation, Figure 3.32 illustrates the simulation results obtained when the batteries are discharged.

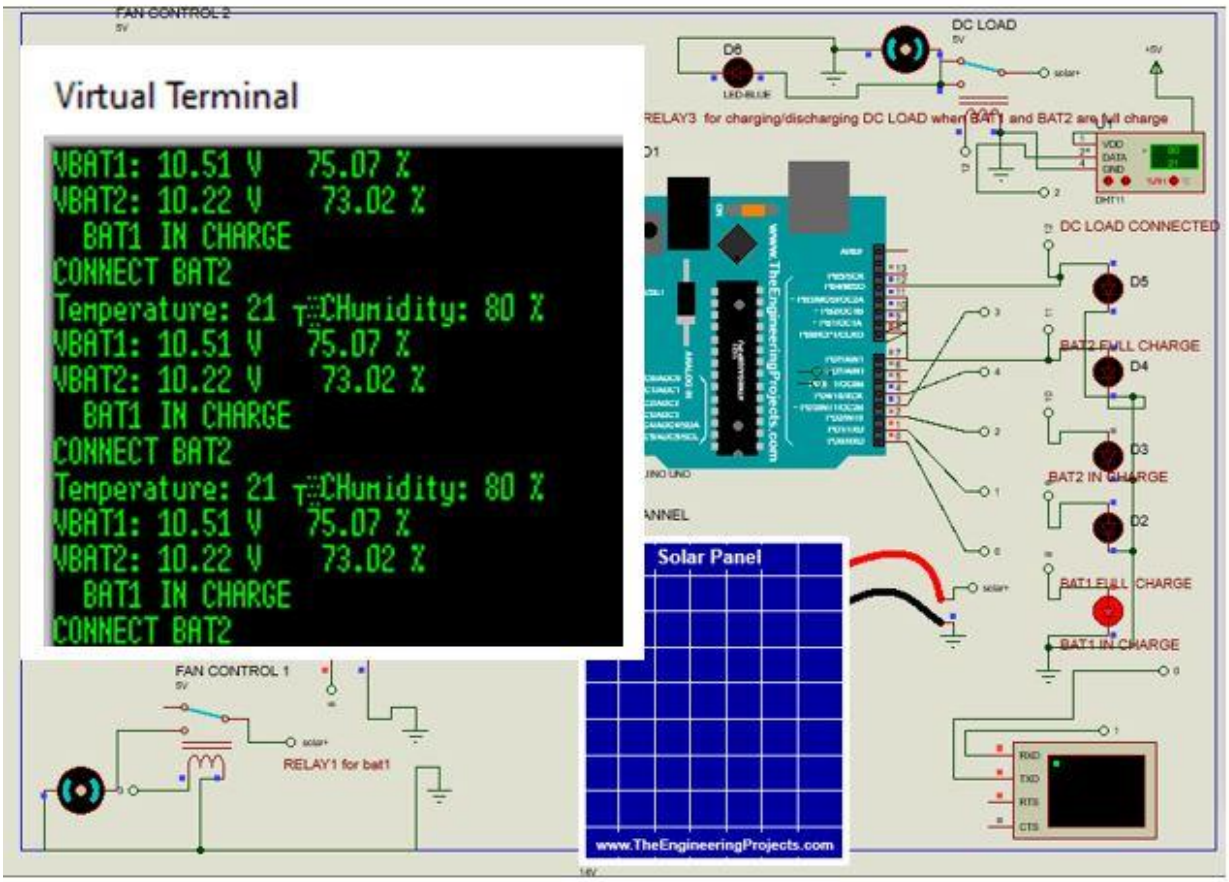


Figure3.32: Battery 1 charging diagram when all batteries are discharged

Based on the results obtained, we have an SOC of less than 80% for all batteries and a temperature of 21°C. Analysis of these results shows that relay1 received a command via port 8 of the Arduino UNO to activate charging of battery 1 as a priority. In this case, the LED is lit, indicating that battery 1 is in charging mode. We also note that conditioning has not been activated since the room temperature is within the normal operating temperature range.

Let us test the behavior of the developed algorithm when battery 2 is discharged, battery 1 is charged, and the temperature is low. Figure 3.33 shows how the battery charge and discharge management mechanism works when battery 2 is discharged and battery 1 is charged. We evaluated the operation of the developed algorithm when battery 1 is discharged, bat
charged, and the temperature is below 20°C. The simulation results are shown in Figure

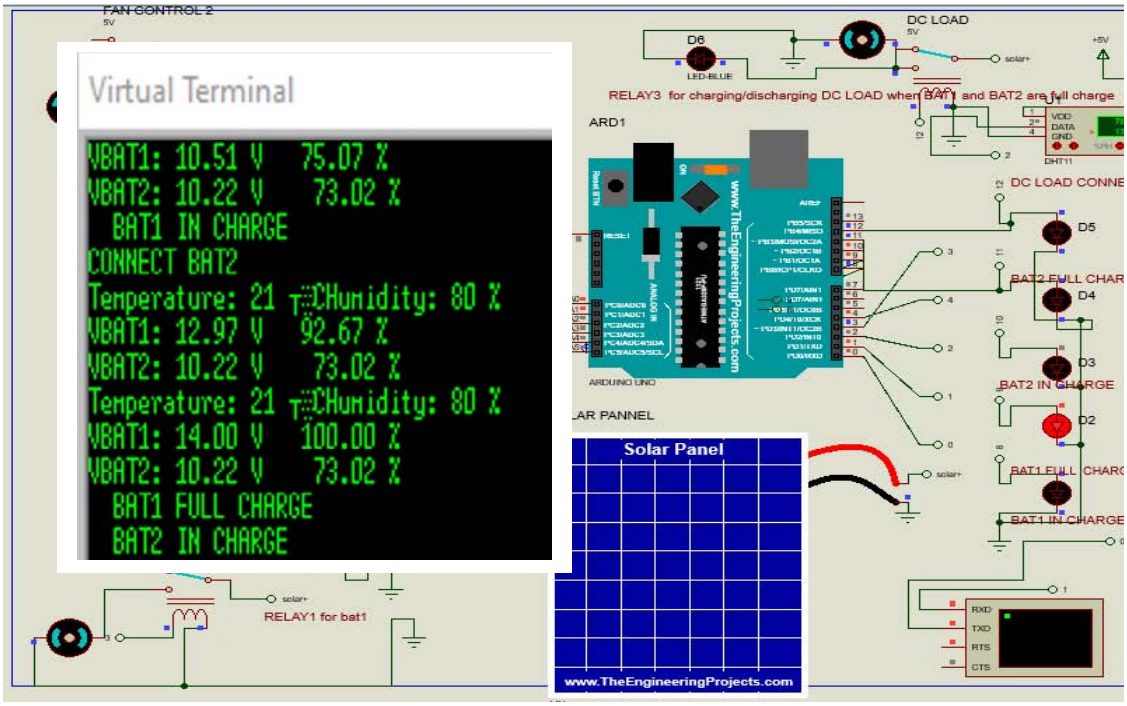


Figure3.33: Battery 2 charging diagram when battery 1 is charged

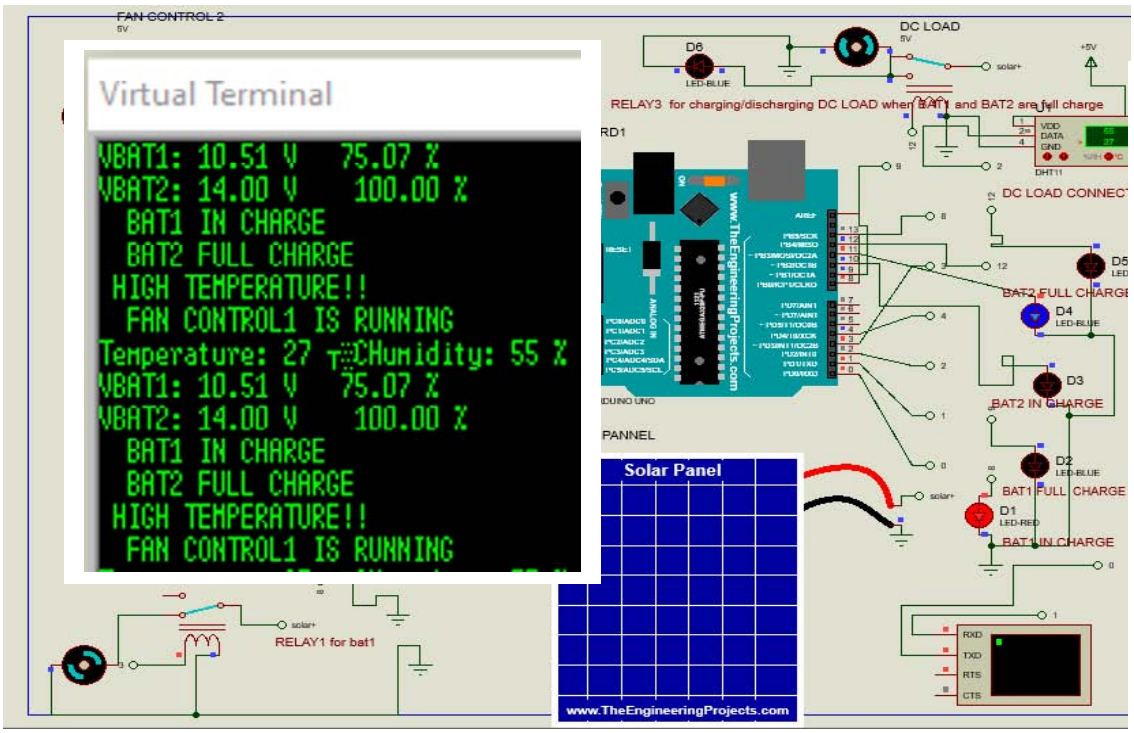


Figure3.34: Case where battery 1 is discharged and battery 2 is fully charged.

Analysis of the simulation results in Figure 3.33 shows a SOC of 78% for battery 2 and a SOC of 100% for battery1. We note that the Arduino UNO microcontroller activates relay 2 to charge battery 2 through port 9 of the Arduino UNO. We see that the LED is lit, indicating that battery 2 is in charging mode. At the same time, the LED is lit via a command on the Arduino

UNO port, indicating that battery 1 is fully charged. We also have a temperature of 17°C and we notice that a low temperature has been detected and the Arduino UNO microcontroller sends a command to relay 3 to activate the room conditioning.

Analysis of the simulation results in Figure 3.34 shows a SOC of 78% for battery 1 and a SOC of 100% for battery 2. We note that the Arduino UNO microcontroller activates relay 1 to charge battery 1 through port 9 of the Arduino UNO. The LED is lit, indicating that battery 2 is fully charged. We also have a temperature of 27°C and we note that a high temperature has been detected and the Arduino UNO microcontroller sends a command to relay 4 to activate the room conditioning.

We evaluated the developed algorithm for the battery charge and discharge management system in the case where the SOC is 85% and in the case where battery 2 is charged. The simulation results obtained are shown in Figure 3.35.

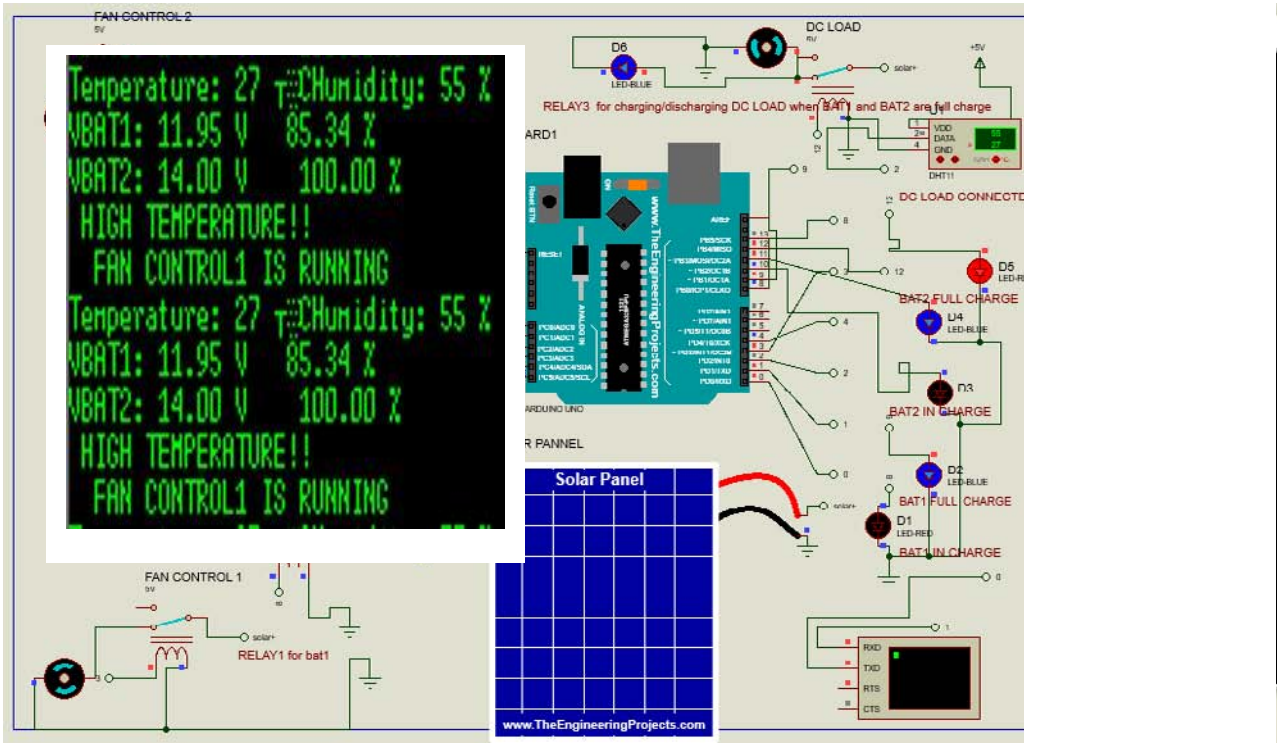


Figure3.35: Battery 1 with SOC of 85% and battery 2 fully charg

Based on the analysis of the simulation results obtained, we have a SOC of 85% for battery 1 and a SOC of 100% for battery 2. We note that no action has been taken to charge the battery with a low SOC compared to battery 2. This indicates that the battery has not been activated for charging because its SOC is not below 80%. Finally, let us test the case where all batteries are charged. Figure 3.36 illustrates the simulation results.

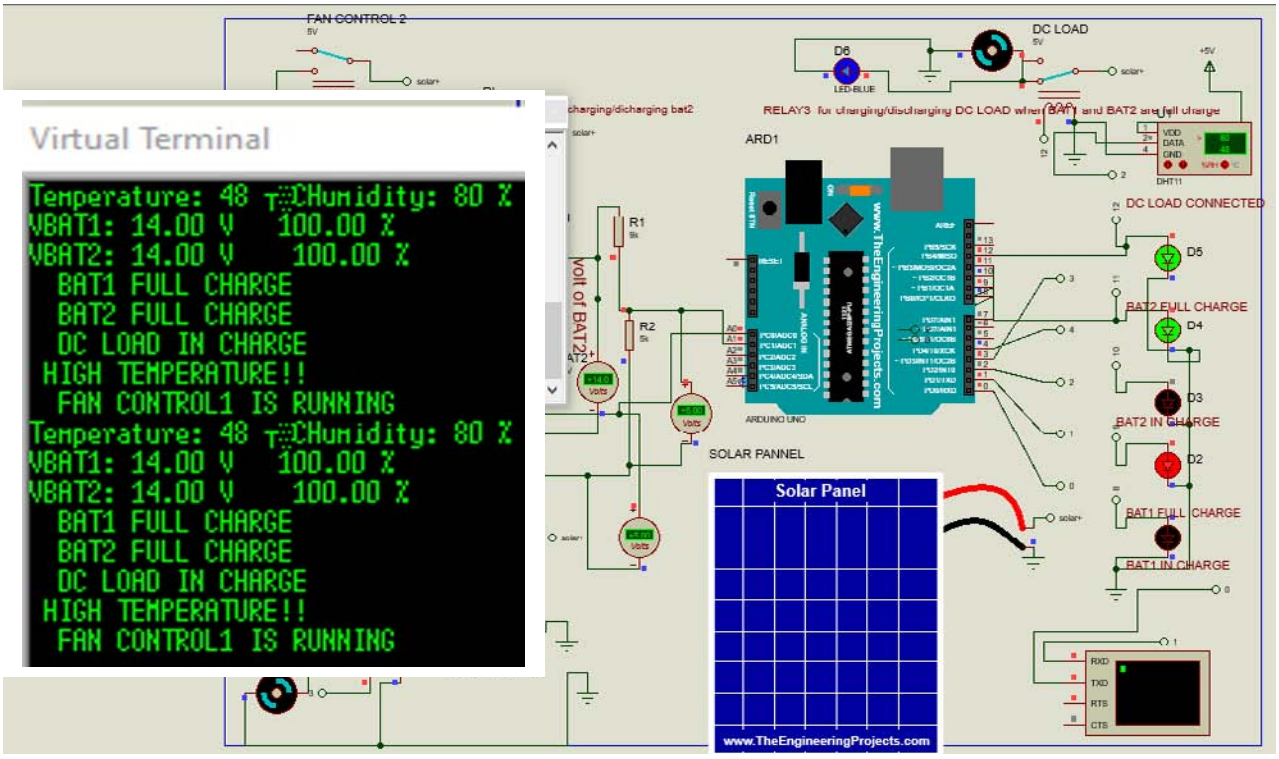


Figure3.36 : Battery 1 fully charged, Battery 2 fully charged, DC LOAD Activate charging and FAN_CONTROL1 when the temperature is over 25°C.

The simulation results show that both batteries have a SOC of 100%, which indicates that they are fully charged. As we can see, the Arduino UNO microcontroller sends an instruction via pin 12 to engage relay 3 in order to charge further DC electrical loads after detecting that all batteries are fully charged. Additionally, the microprocessor sends a signal to close relays 4 or 5 for air cooling if the local temperature rises above the battery's operational range. It is evident that the computational findings produced by MATLAB Simulink and Proteus software are consistent.

3.4.2. Analysis of the effect of temperature on various battery parameters

Let us evaluate the effect of temperature on the internal resistance of the battery, which is an important parameter in battery optimization. Figure 3.37 indicates the impact of temperature on resistance. And now let's assess how temperature affects battery voltage. Figure 3.38 indicate the impact of varying temperatures on battery voltage in this case.

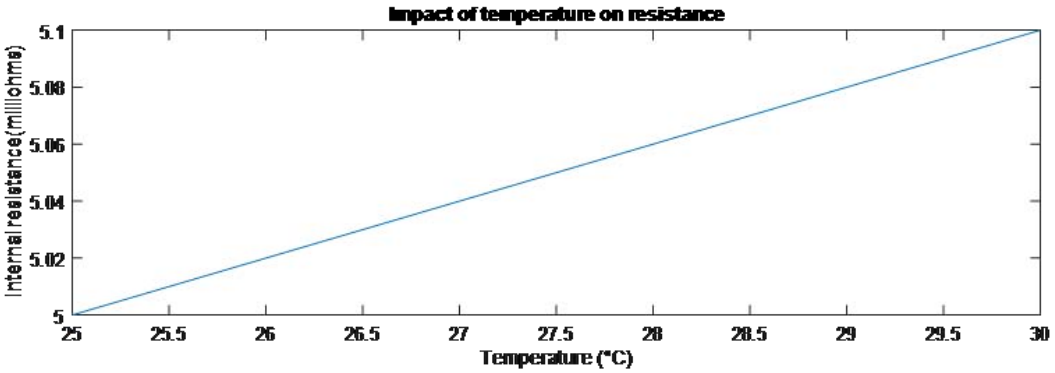


Figure3.37: Impact of temperature on resistance

Internal resistance increases with temperature, according to an analysis of the variation curve. This supports the literature's assertion that heating the internal resistance raises the material's internal resistance.

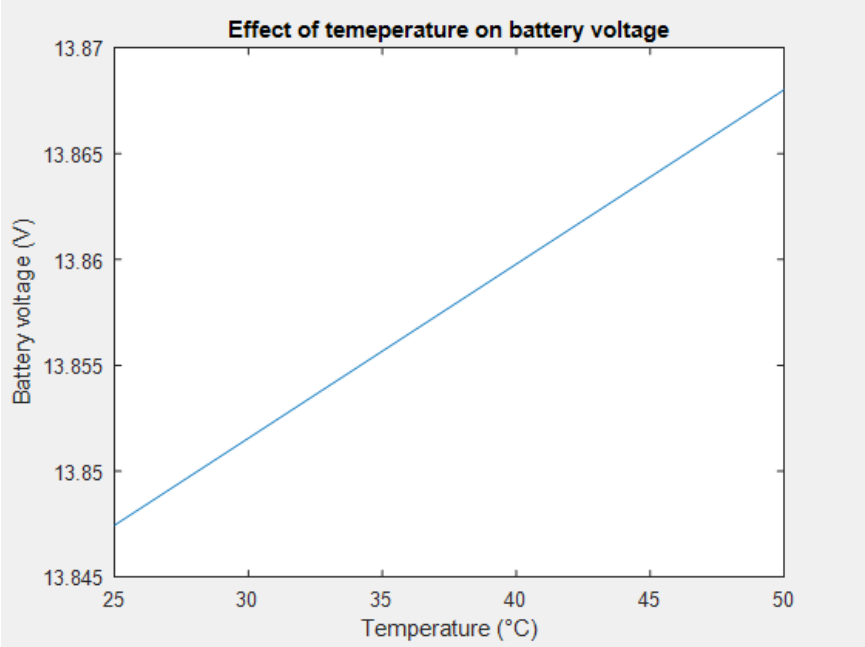


Figure3.38: Impact of varying temperatures on battery voltage

We can see from the variation graph that the voltage dropped as the temperature dropped below 25 °C. An examination of the derived variation curve demonstrates that rising temperatures cause voltage to rise. This phenomenon also affects the SOC, which Increases or decreases depending on the variation in voltage. Figure 3.37 shows the influence of temperature on battery capacity.

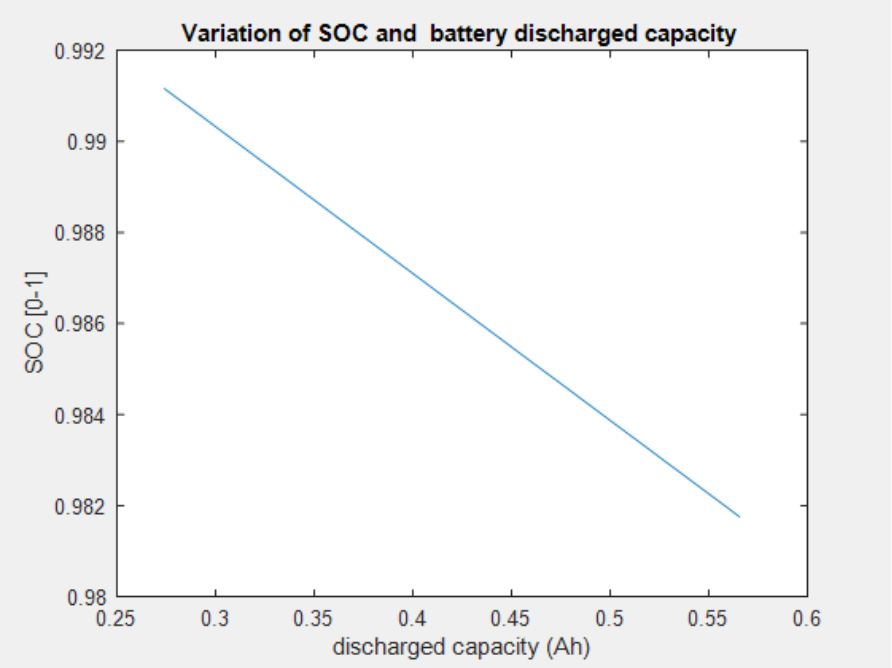


Figure3.39: Impact of varying temperatures on the battery capacity

The fluctuation graph shows that when the discharge capacity rises, SOC decreases and vice versa. However, the battery's capacity will decrease if the discharge capacity rises. According to these investigations, the resistance of the sulphuric acid solution keeps rising as the battery drops below 0 °C, which results in a polarization effect and lowers the battery capacity. As a result, as the battery's level of charge drops, its depth increases and it ages. For K = 0.00004308; A = 1.889; V0 = 12.16; B = 0.3053; C = 30; R = 0.0006, Figure 3.40 shows the impact of battery discharging current on battery voltage.

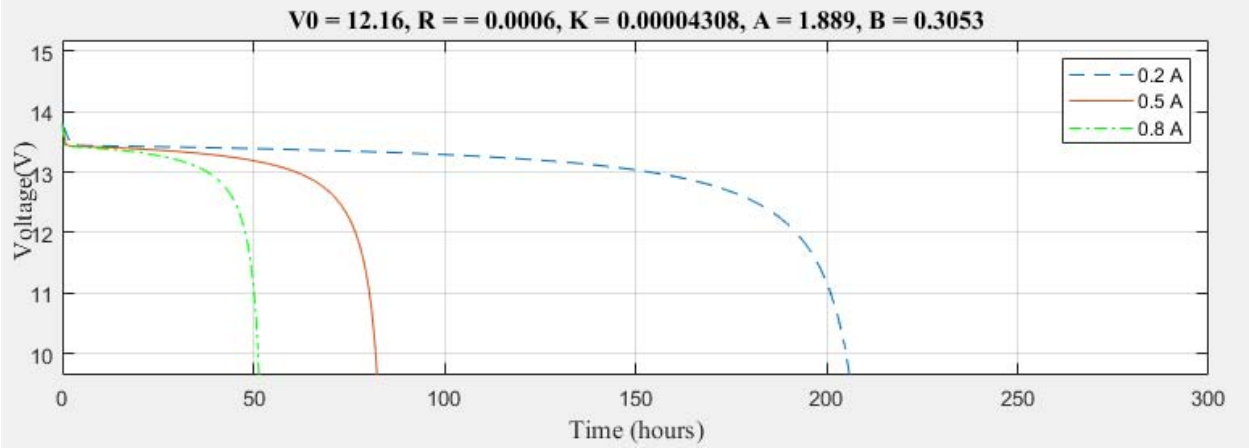


Figure3.40: Impact of battery discharging current on battery voltage.

According to the simulation results, analysis of the variation curves shows that the voltage decreases rapidly as the current increases.

3.4.3 Predictive battery life cycle management

Using equations (2.55), (2.56), (2.57), (2.58), (2.59) and (2.60), we have developed a predictive model of the battery life cycle. Figure 3.41 illustrates the results obtained from the predictive battery management model.

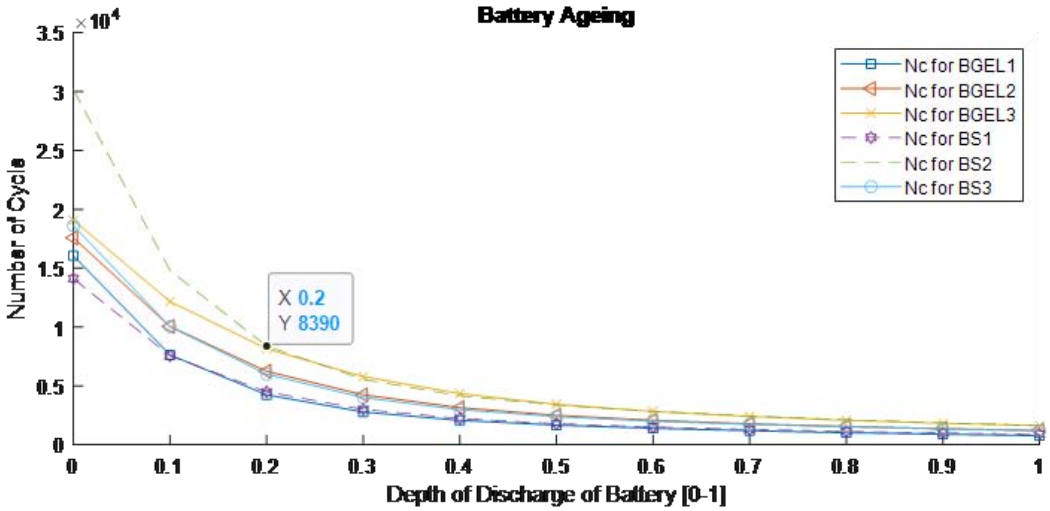


Figure3.41 : Diagram showing variation in the number of cycles of a lead-acid battery as a function of DoD

Based on the variation curves, we can see that the BS2 battery type has a battery life cycle of 8,390 for a DoD of 0.2.

3.4.4. Experimental Results

The actual use of a battery charge/discharge control mechanism connected to a temperature control system for the created algorithm is the main topic of this section. We used an experimental prototype comprising two batteries with the following characteristics: (6FM-7AH (12V7AH/20HR)), sealed lead-acid rechargeable battery, operating cycle: 14.5-14.9 V (25 °C); initial current: less than 2.1 A; Standby use: 13.6-13.8 V (25 °C). The control element is an Arduino UNO microcontroller and we used a soldering iron to raise the temperature. The other components used are two potentiometers, four resistors, two voltage divider bridges, connection cables, four relays, four LEDs, a DHT11 temperature sensor, a test plate, a fan, and LEDs for signaling. The voltage is varied using the potentiometer. Figures 3.42 and 3.43 illustrate the experimental prototype for evaluating the algorithm developed using the Arduino IDE software.

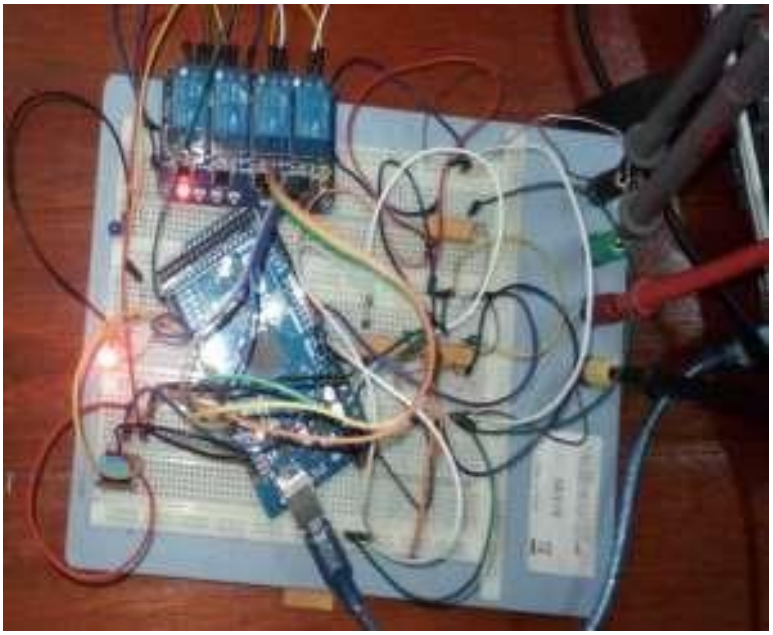


Figure3.42: Indicator for charging of battery 1

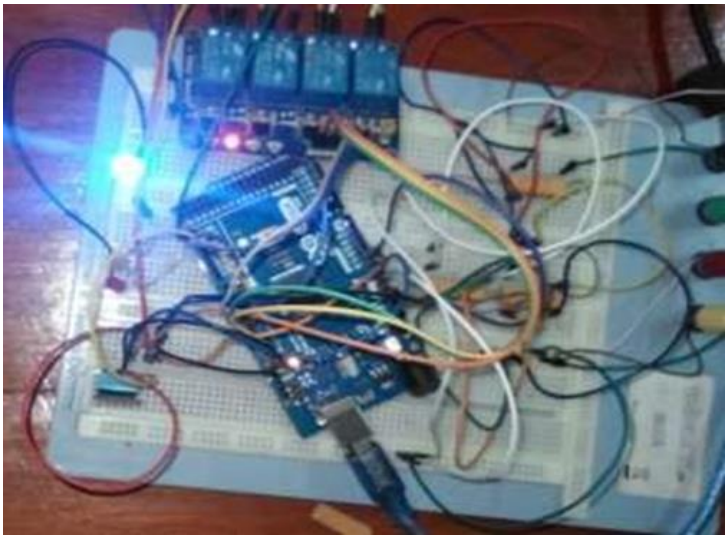


Figure3.43: Indicator for charging of battery 2

According to the experimental findings, relay 1 is triggered by an Arduino UNO microcontroller command to charge battery 1 (VBAT1) as a priority if the battery reaches a state of charge (SOC) of 80% of its nominal capacity. The Arduino UNO microprocessor activates relay 2 to charge battery 2 if battery 1 is fully charged. Furthermore, we discovered that the Arduino UNO microprocessor triggers relay 3 to charge additional DC electrical loads when all batteries are fully charged. The Arduino UNO microcontroller engages relay 3 to power the fan if it detects a temperature higher than 25°C, according to an analysis of the data. The experimental results of the investigated technique utilizing the serial monitor are displayed in Figure 3.44.

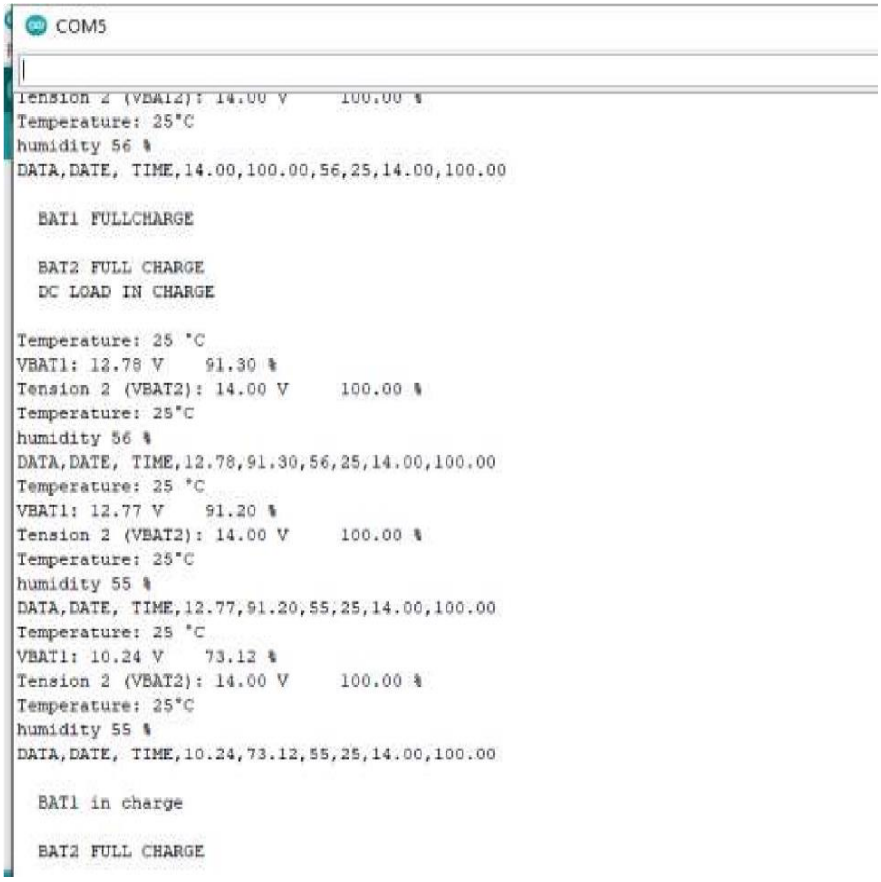


Figure3.44 : Displays results via the serial monitor.

Using the Plx_DAQ program, we imported the experimental data into Excel. The temperature and humidity variation curves that Plx_DAQ collected on July 11, 2024, are recorded in Excel and shown in Figure 3.45.

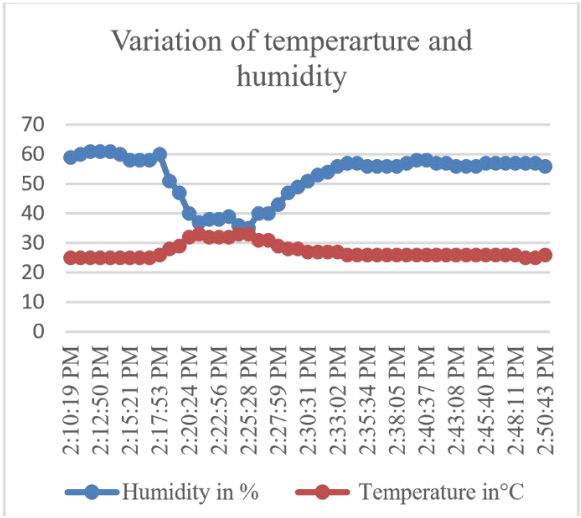


Figure3.45: Plx_DAQ system recorded the following temperature and humidity variation curves on 11/07/2024.

An increase in temperature causes a reduction in humidity, and vice versa, according to an analysis of the temperature and humidity variation curves. The DHT11 measures temperatures between 23 and 27 degrees Celsius. We can observe that the temperature was high based on the measurements taken on July 11, 2024. Based on the lead-acid battery's functioning range, we observe that air cooling is necessary because the lowest temperature found during experimentation is higher than 25 °C.

3.5. The solar tracker's design with a battery charge and discharge control system.

We used MATLAB software to construct, model, and simulate a solar tracker with a battery charge and discharge management system based on the equations of the proposed method. The design diagram of the solar tracker with a battery charge and discharge control system using MATLAB software is displayed in Figure 3.46.

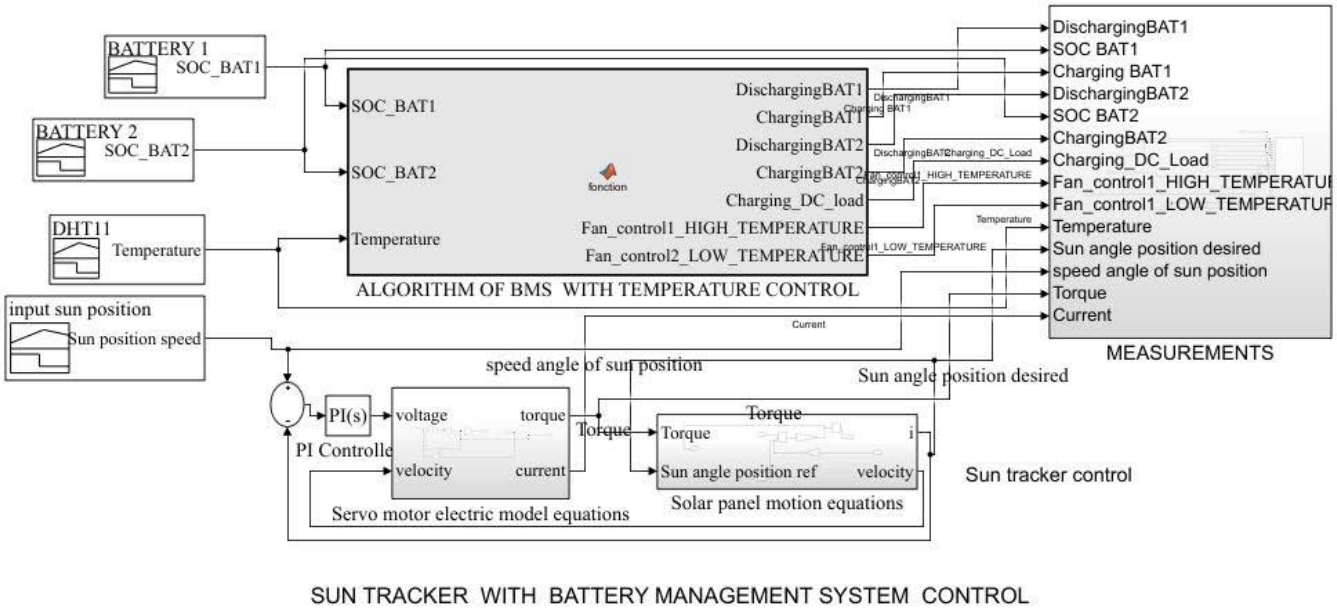
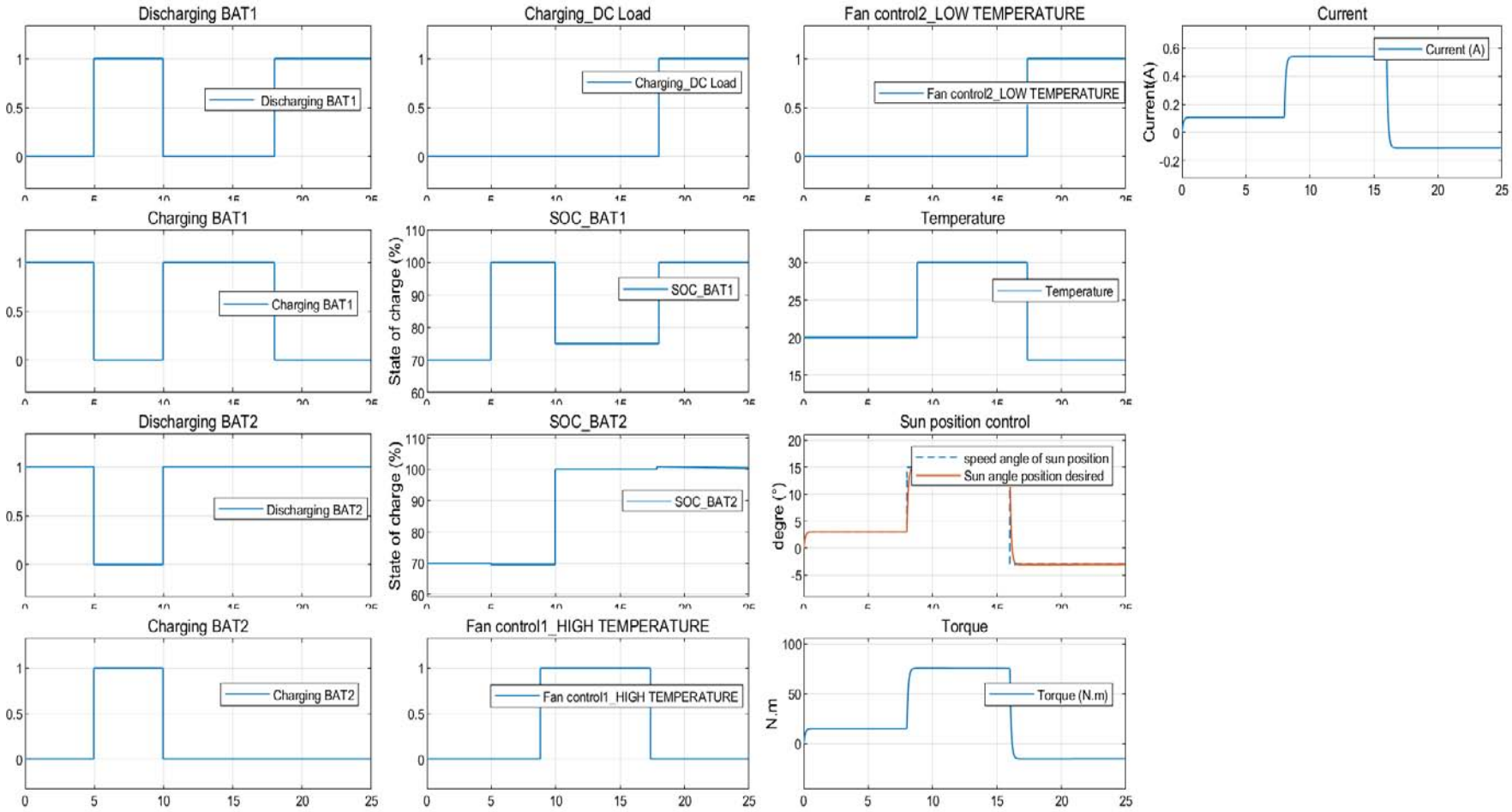
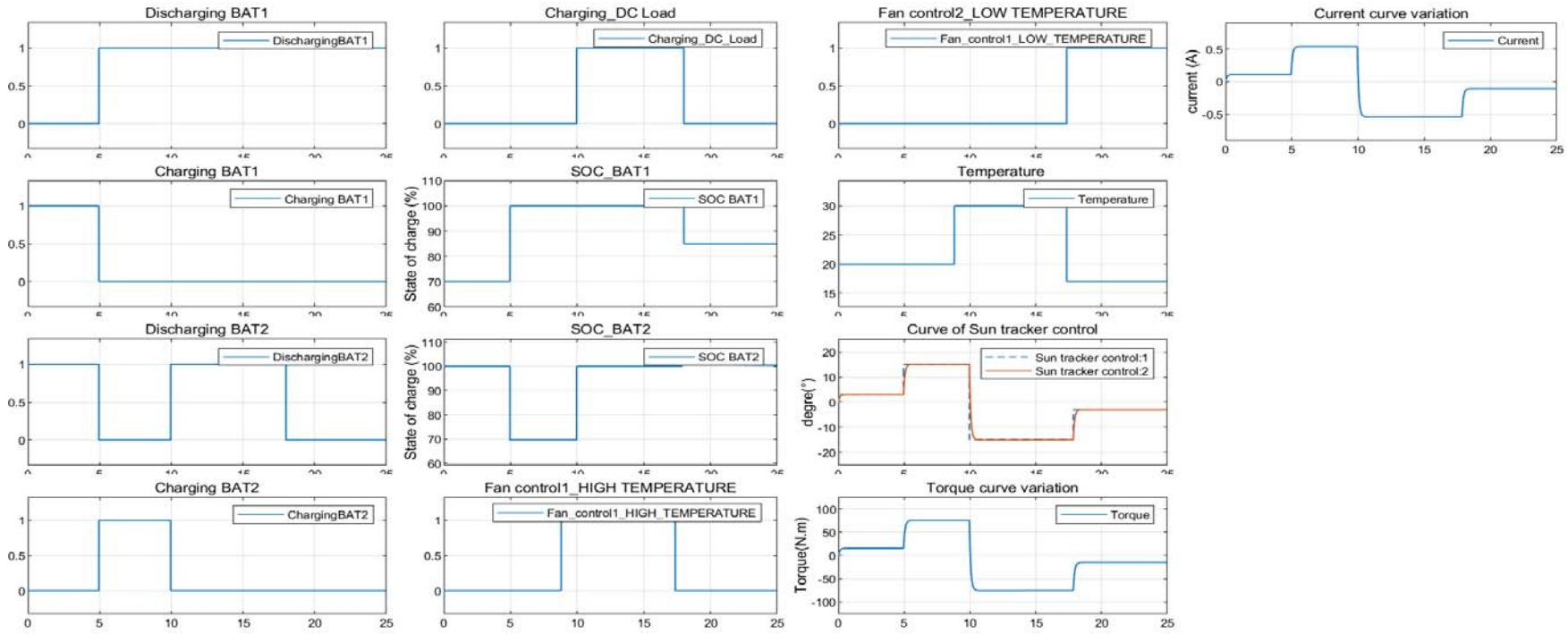


Figure3.46: Design diagram of a solar tracker system equipped with a battery charge and discharge management system

We performed simulations for different input values of the servomotor rotation angle, different input values of the battery charge status, and different input values of the room temperature. Figure3.47 (a) and (b) provide the simulation results for the solar tracker's system design schematic that includes a battery charge and discharge control system.


Discharging BAT1
Discharging BAT1
Charging_DC Load
Charging_DC Load
Fan control2_LOW TEMPERATURE
Fan control2_LOW TEMPERATURE
Current
Current (A)
Current(A)
Charging BAT1
Charging BAT1
SOC_BAT1
SOC_BAT1
State of charge (%)
Temperature
Temperature
Discharging BAT2
Discharging BAT2
SOC_BAT2
SOC_BAT2
State of charge (%)
Sun position control
speed angle of sun position
Sun angle position desired
degre (°)
Charging BAT2
Charging BAT2
Fan control1_HIGH TEMPERATURE
Fan control1_HIGH TEMPERATURE
Torque
Torque (N.m)
N.m

(a)



(b)

Figure3.47: (a) and (b): Variation curve of the solar tracker for different desired angles with variation curve of the battery state of charge for different SOC values and temperatures

Based on the simulation results obtained in Figure 4.2 (a), in the interval [0,8], we have an input value of a rotation angle of 3°, in the interval [8,16], we have an input value of a rotation angle of 15°, and in the interval [16,25], we have an input value of an angle of -3°. We note that for all these reference angle input values, the variation curve of the output angle of the solar tracker's sun position control follows the reference value (input value). For a negative or positive input value of the servomotor rotation angle, we obtained the same sun position control angle value.

Let us analyze the battery charge status results. In the interval [0,5], we have a SOC BAT1=70% and SOC BAT2=50%. We note that in this interval, battery 1 is primarily in charging mode because all batteries are discharged. battery 1 is primarily in charging mode because all batteries are discharged.

In the interval [5,10], we have a SOC BAT1=100% and a SOC BAT2=70%. We note that battery 2 is in charging mode since it has a SOC of less than 80%. In the interval [10, 18], we have SOC BAT1=77% and SOC BAT2=100%. In the interval [18, 25], we have SOC BAT1 and SOC BAT2 =100%. In the interval [0,9], we have a temperature of 20°C. We note that the room air conditioning has not been activated since the temperature is normal. In the interval [9,18], we have a temperature of 30°C and we note that Fan control1 has been activated to allow the room to be air conditioned since a high temperature has been detected. In the interval [18,25], we have a room temperature of 18°C and we see that Fan control2 has been activated to allow the room to be cooled since a low temperature has been detected. Based on the simulation results obtained in Figure 4.2 b, in the interval [0,25] we have input values of 3°, 15°, -15°, 0° and -3°. We also note that, according to the variation curve of the sun position control, the output values follow the input values (reference value). Interpreting the torque and electric current variation curves, we see that the electric current and electric torque values Increase as the angle Increases, decrease as the angle of rotation decreases, and become zero when there is no rotation (angle = 0°). Let us interpret the simulation results for the battery charge status.

In the interval [0,5], SOCBAT1 = 70% and SOCBAT2 = 100%, which triggers the activation of battery 1 charging. In the interval [5,10], we have a SOC BAT1 of 100% and a SOC BAT2 of 78%. We note that no battery charging action takes place since battery 2 has a SOC greater than 80%. In the interval [10,18], we have a SOC BAT1 of 77% and a SOC BAT2 of 100%. In the interval [18,25], we have a SOC BAT1 of 82% and a SOC BAT2 of 100%. We have a SOC BAT1 of 100% and a SOC BAT2 of 78%. We see that no battery charging action is taking place sInce battery 1 has a SOC greater than 80%.

Let us evaluate the design and simulation results of an intelligent tracker equipped with a battery charge and discharge management system using Proteus design software and Arduino IDE programming software. The design and simulation diagram Includes the following components: Arduino UNO microcontroller, a solar panel, five relays, voltmeters for measuring voltages, signal LEDs, a display, a DHT11 temperature sensor, two LDR sensors, two potentiometers, DC power supply, and a Real Clock Time 3231. The design diagram of the solar tracker with a Proteus software-based battery charge and discharge control system is displayed in Figure 3.48. When the batteries are discharged and at room temperature, let's assess the algorithm created for the dual-axis solar tracker system with a battery charge and discharge management system. Figure 3.49 shows the simulation results obtained.

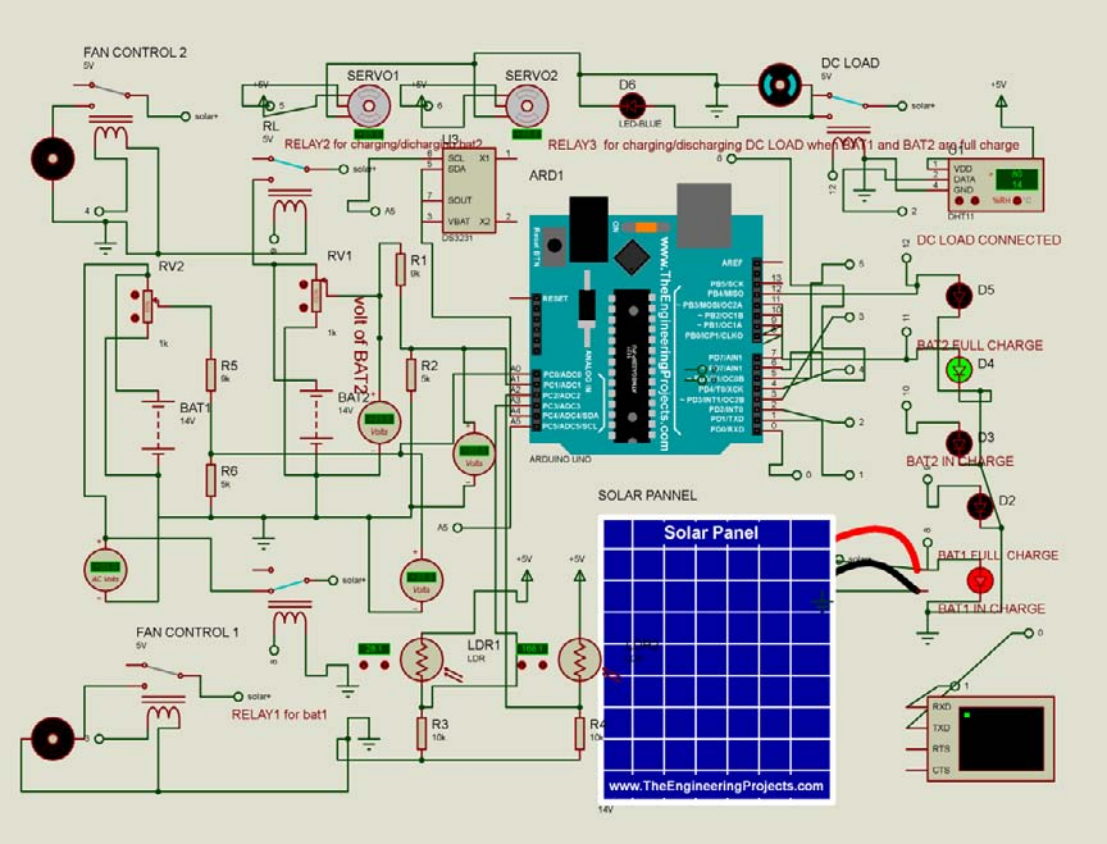


Figure3.48: Design Schematic diagram of a two-axis solar tracker with a battery charging and discharging management system.

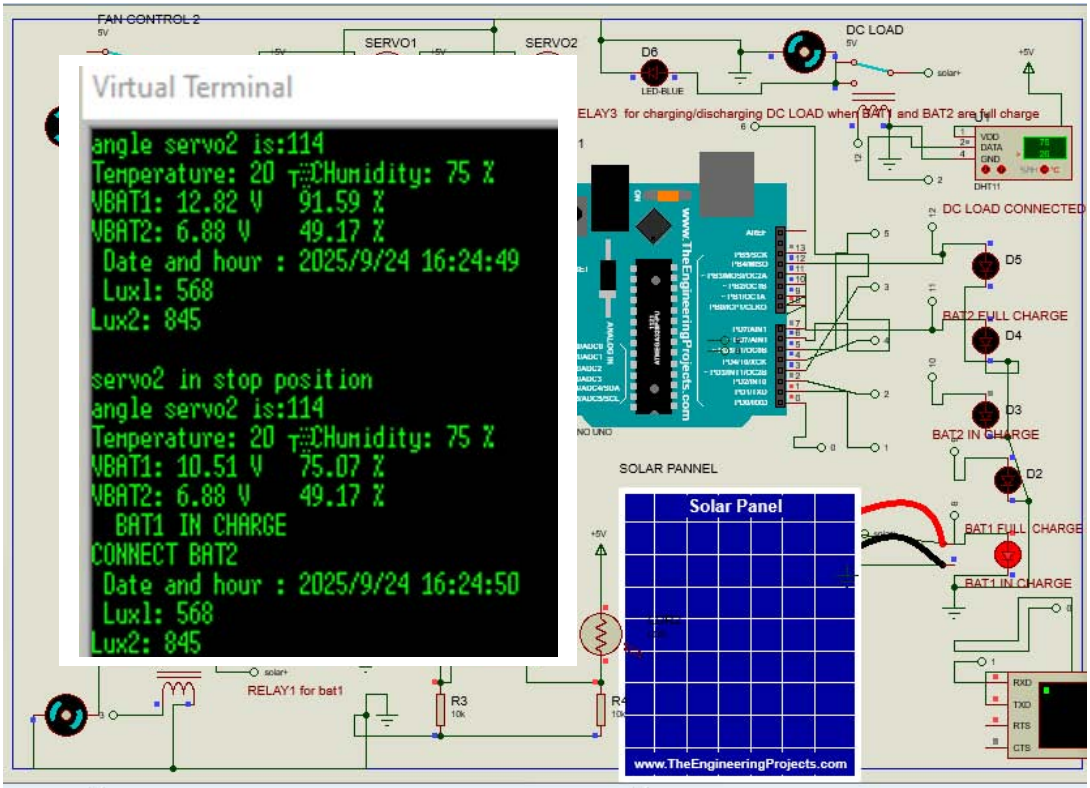


Figure3.49: Diagram showing battery1 charging and dual-axis solar tracker control with display

Based on the simulation results obtained, we have a SOC for battery 1 of 50.15%, a SOC for battery 2 of 49.17%, luminous flux of LDR1=568lux, luminous flux of LDR2=845 and a temperature of 20 °C. Analysis of these simulation results shows that the SOCs of the batteries are below 80% (batteries discharged), which triggers a priority battery charging command, as indicated by the LED signal in the figure. We note that the room is not being conditioned as the temperature is normal. We also note that the servomotors that operate the solar panel are in stop mode as the repositioning time has not yet arrived and the difference in illumination between the LDR sensors is low (below tolerance).

Let us evaluate the case where Battery 1 is charged and Battery 2 is discharged with a temperature below 20°C. The results obtained after simulation are shown in Figure 3.50.

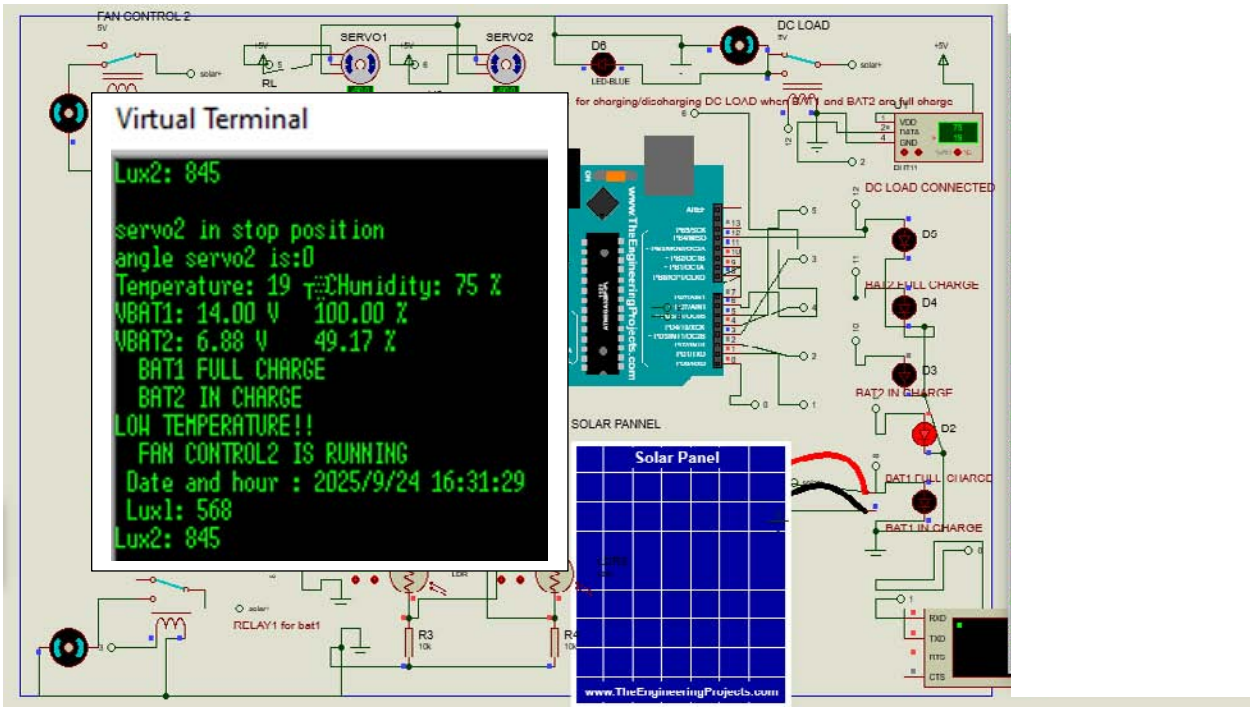


Figure3.50: Case of charging battery 2 if battery 1 is charged and servomotor 2 is in the stop position.

According to the simulation results obtained, we have a SOC for battery 1 of 100% and a SOC for battery 2 of 49.17%, luminous flux of LDR1=568lux, luminous flux of LDR2=845 and a temperature of 19°C. We note that relay 2 has been activated to charge battery 2, with an LED indicating that charging mode has been detected since the SOC is below 80%. Analysis of the simulation results also shows that a low temperature has been detected and relay 4 of fan control 2 has been activated to allow the room to be conditioned. The solar tracker servomotors remain in stop mode, indicating that the pivot detection conditions have not yet been met.

Let us analyze the case where all batteries are charged, with a difference in LDR sensor illumination and a normal temperature. Figure3.51 shows the diagram for charging DC loads and repositioning the solar panel.

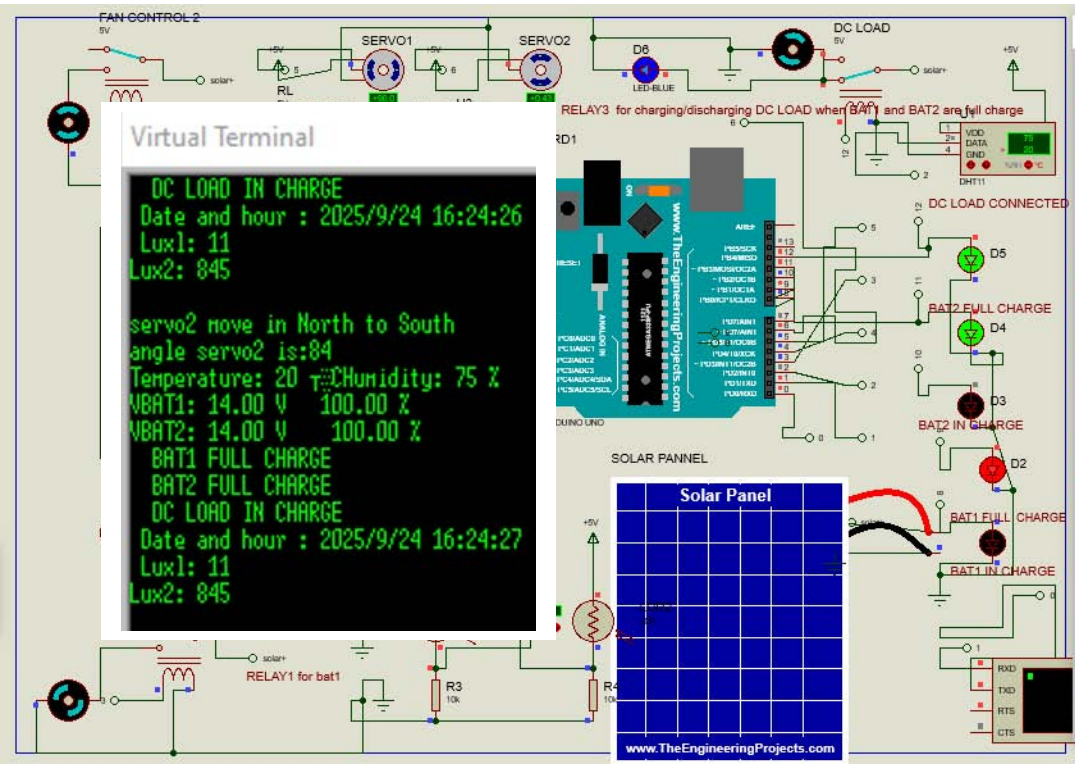


Figure3.51: Situation where all batteries are fully charged and the North LDR sensor's voltage is greater than the South LDR sensor's voltage

The display messages and indicator LEDs show the system's operation at all times. According to the simulation results obtained, we have a SOC of 100% for battery 1 and battery 2, which shows that all batteries are charged. This can also be seen from the LEDs that are lit. We can see that relay 3 has been activated to power the other DC loads. We can also see that relay 2 has been activated to pivot the solar panel from North to South, as a large difference in the illumination of the LDR sensors has been detected. We have a normal temperature of 20°C and we see that the fan control relays are not activated.

Let us now analyze the case where the battery has an SOC of 82%, battery 2 is charged, there is a difference in illumination between the LDR sensors and the temperature is above 25°C. The simulation results for the servomotor rotating in the indirect direction and the room conditioning are shown in Figure 3.52. The display messages and indicator LEDs show the system's operation at all times.

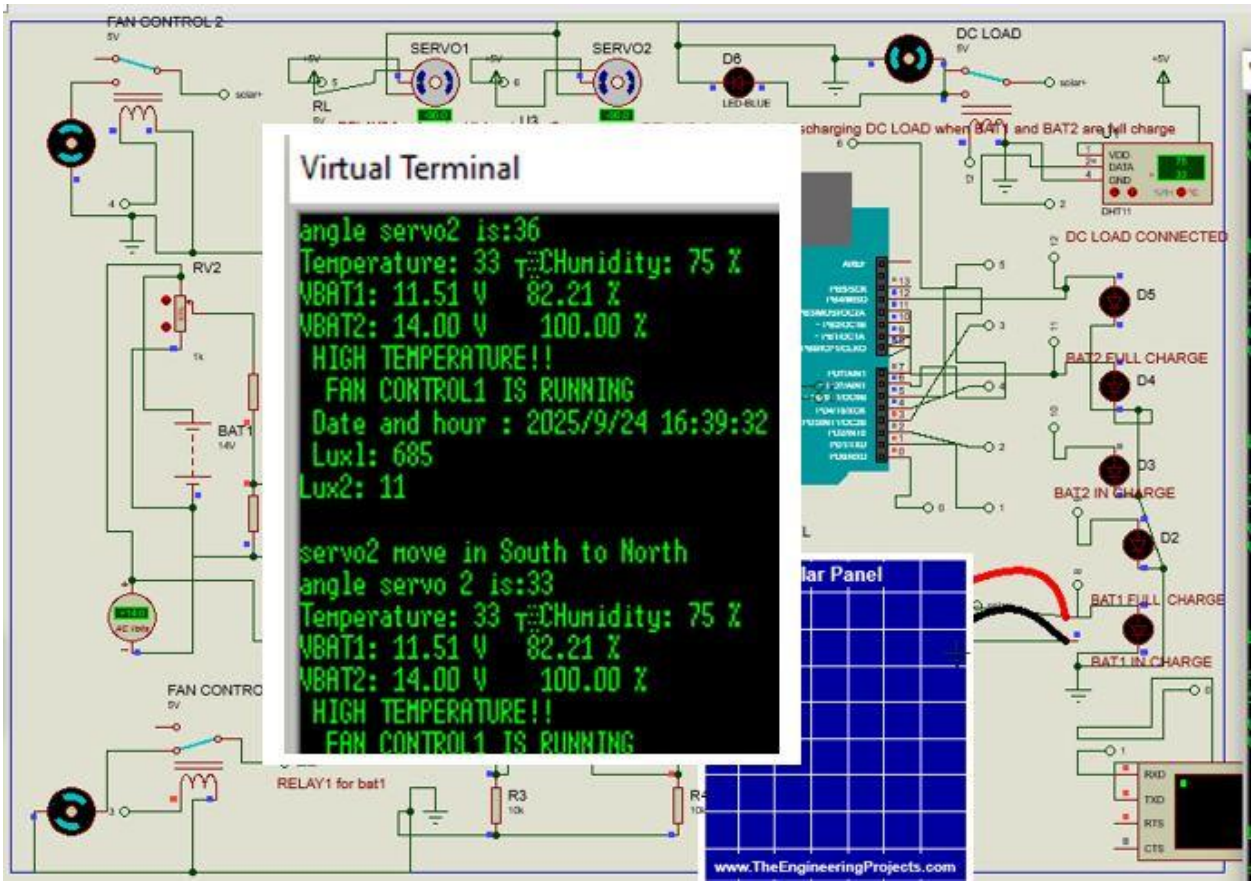


Figure3.52: Servomotor rotation in the indirect direction and detection of high temperature

We have a SOC battery1 of 82.21% and a SOC battery2 of 100%. Based on the analysis of the results, we note that relay 1 was not activated to allow battery 1 to charge because even though battery 1 is discharged, the SOC is not below 80%. We also have a temperature of 33°C, which triggered the activation of the relay for room conditioning. We also note that the illumination of the LDR1 sensor is much higher than that of the LDR2 sensor, which caused the servomotor to rotate from South to north. Let's run a test when battery 1 is discharged and battery 2 is fully charged. Figure 3.53 shows the simulation results obtained, the messages on the display and the indicator LEDs that show the operation of the system at each stage. And Let us evaluate the algorithm developed in the case of controlling the pivoting of the solar panel from East to West and if all batteries are charged. The simulation results obtained are shown in Figure 3.53.

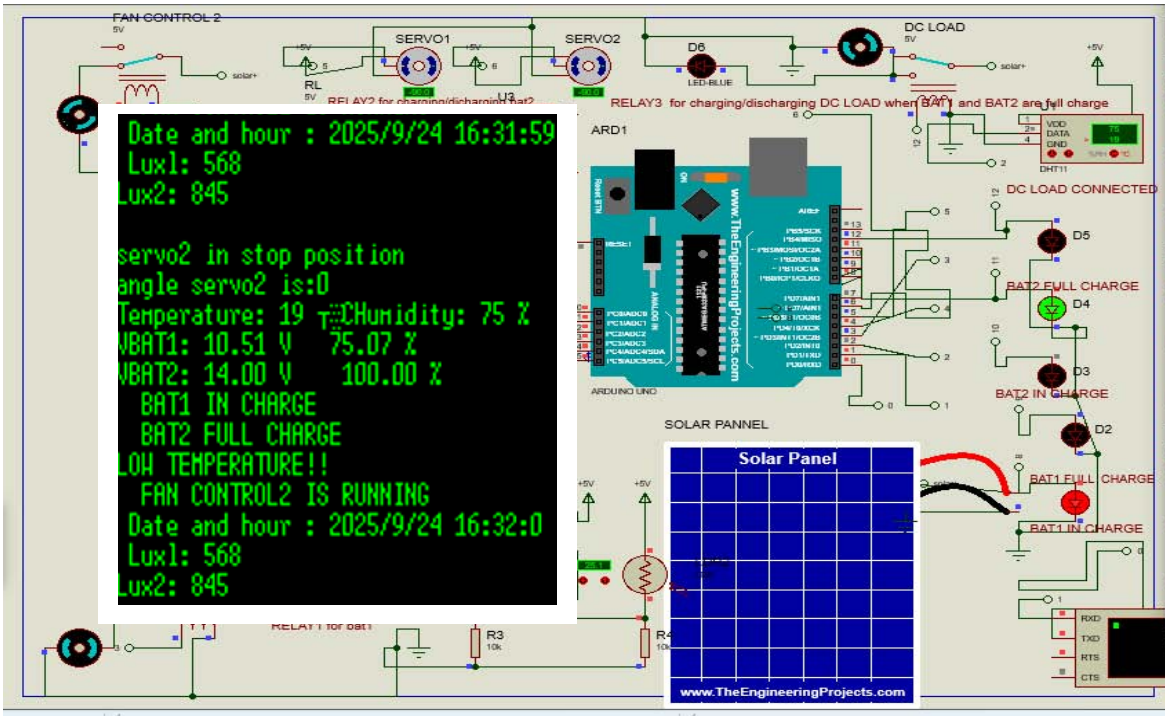


Figure3.53: Battery 1 charging scenario when battery 2 is charged and the servomotors are stop position

Analysis of the simulation results in Figure 3.53 shows that battery 1 charging is activated when

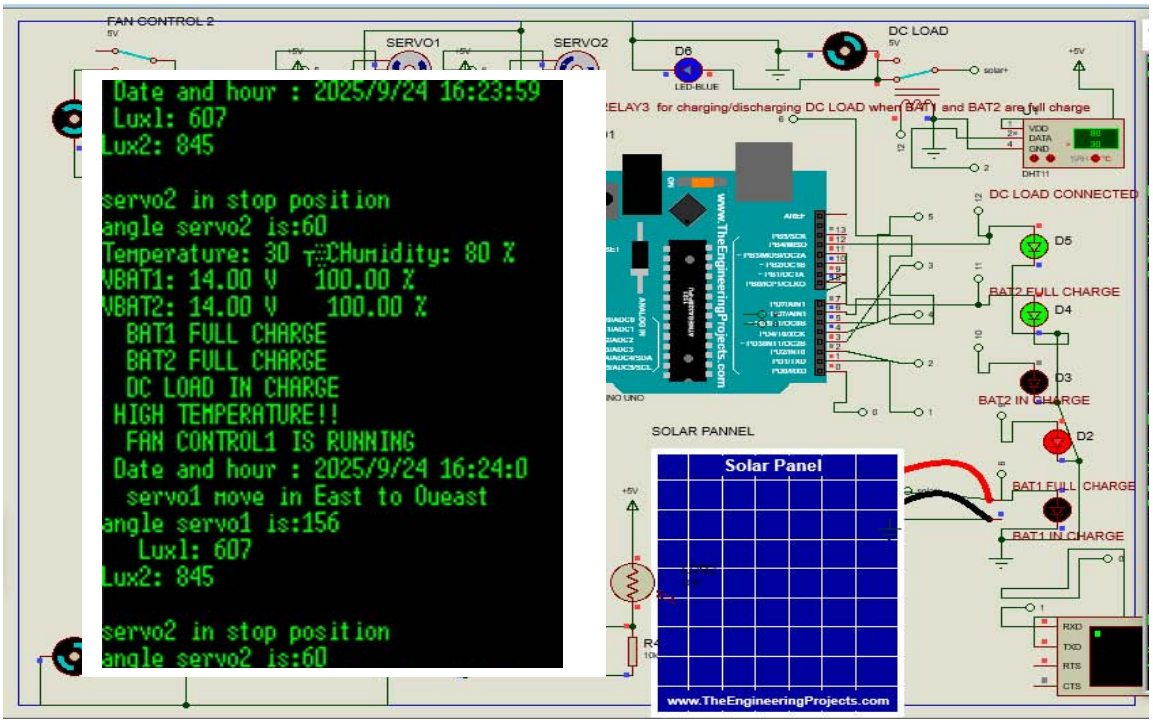


Figure3.54: Case where all batteries are charged with a time detection of 4:24 PM

For the results simulation in Figure 3.54, the Arduino UNO microcontroller signals servomotor 1 to rotate the solar panel from east to west at 4:24 PM, according to the display results. This time corresponds to the solar panel repositioning time of the developed algorithm, which detects the time every 12 minutes. We note that servomotor 2 remains in the stop position because there is no significant difference in illumination between the LDR sensors. Additionally, we see that all of the batteries are fully charged, and the Arduino UNO microprocessor instructs relay 3 to supply power to the remaining DC loads. Let's assess how the algorithm created at 6:30 PM behaves. The created algorithm's simulation results are displayed in Figure 3.55.

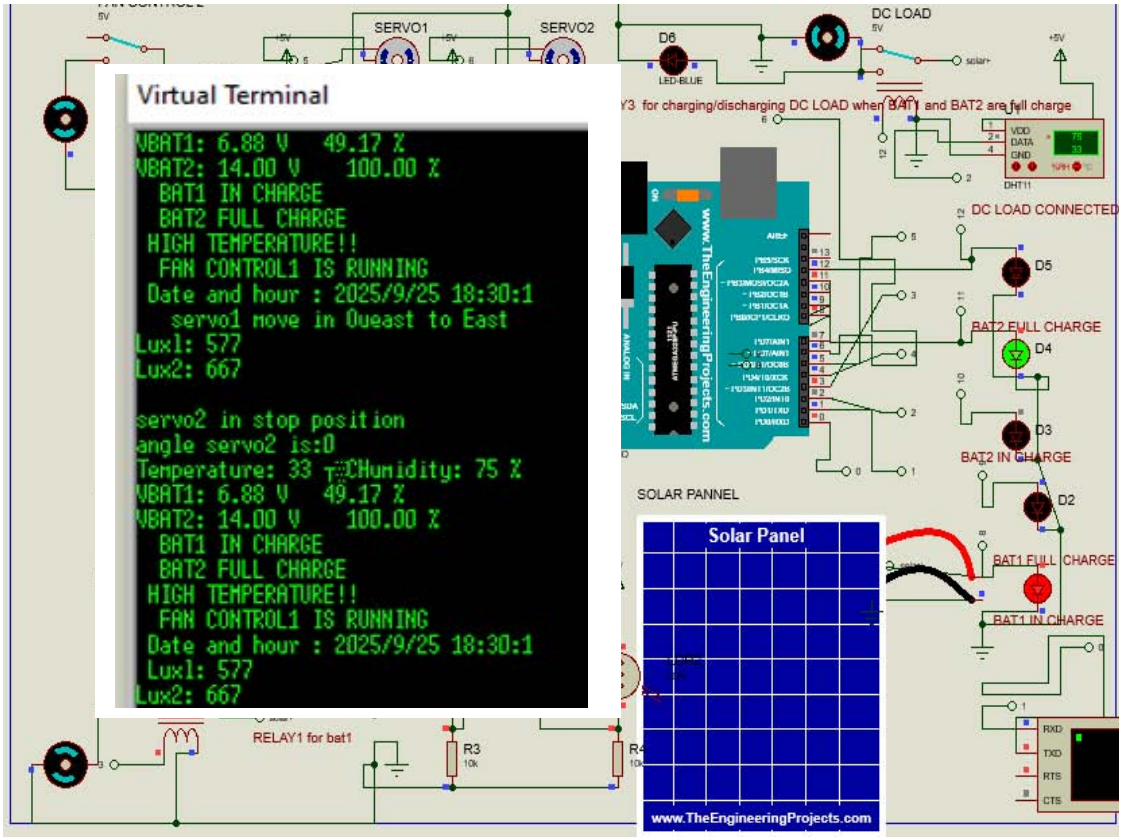


Figure3.55: Behavior of the algorithm developed at 6:30 PM

According to the simulation results shown on the screen, the solar panel returns to its starting position at 6:30 PM. This demonstrates that the microprocessor instructed servomotor 1 to rotate the solar panel from west to east at 6:30 PM.

We note that the simulation results obtained by MATLAB software validate the simulation results obtained by Proteus Professional and Arduino IDE software, which demonstrates the effectiveness of the developed algorithm. Also, the simulation results we obtained for each method

are similar to the main results of the solar tracker equipped with a battery charge and discharge management mechanism.

3.6. Experimental prototype

In this section, using the same materials as for the other prototypes, Figure 3.56 illustrates the experimental prototype of diagram of the solar tracker with a battery charge and discharge management system



Figure3.56: Experimental assembly of a solar tracker with a battery charging and discharging management system

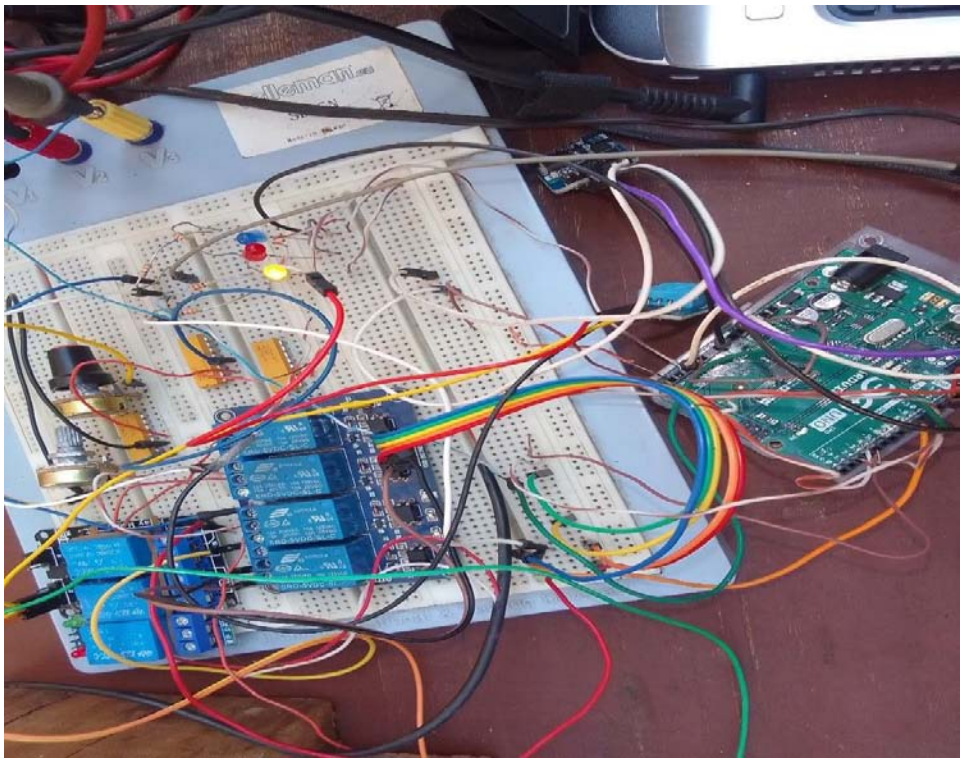


Figure3.57: Battery 1 charging indicator

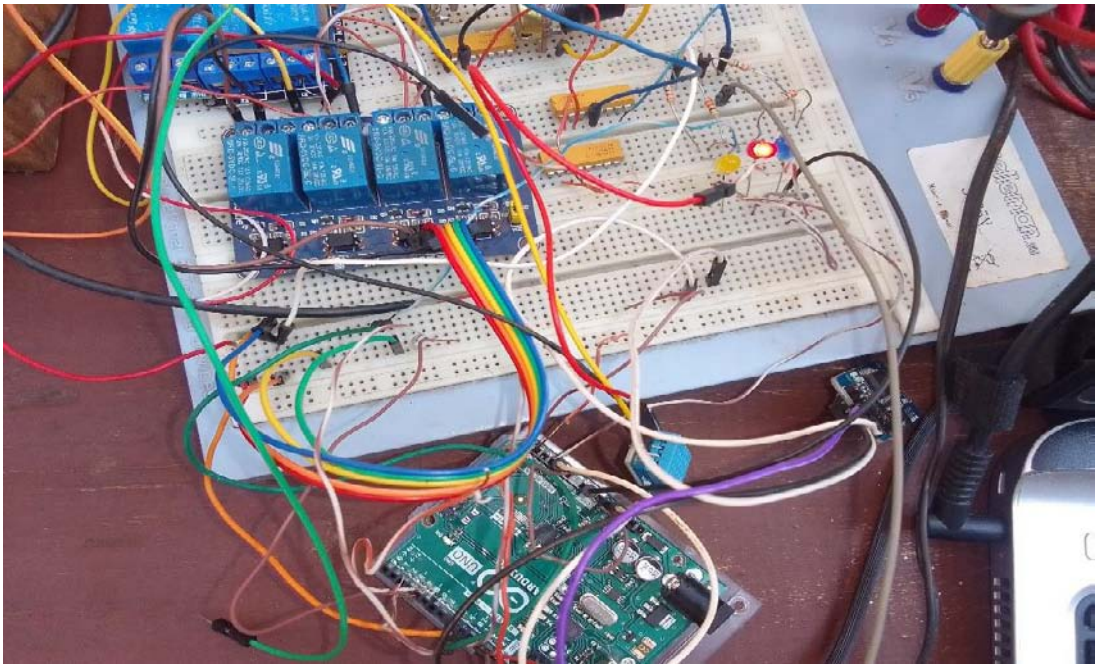


Figure3.58: Battery 2 charging indicator

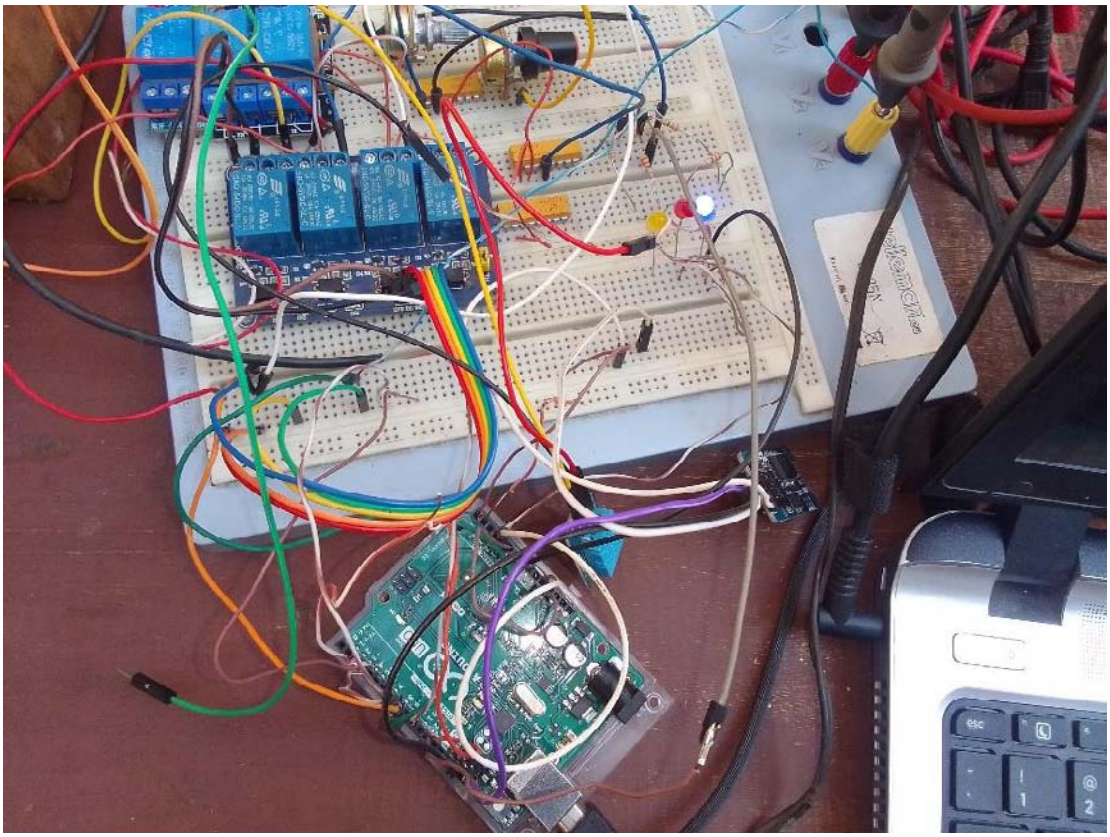


Figure3.59: DC Load charging indicator



Figure3.60 :Using the serial monitor to display the results at 9:00 AM

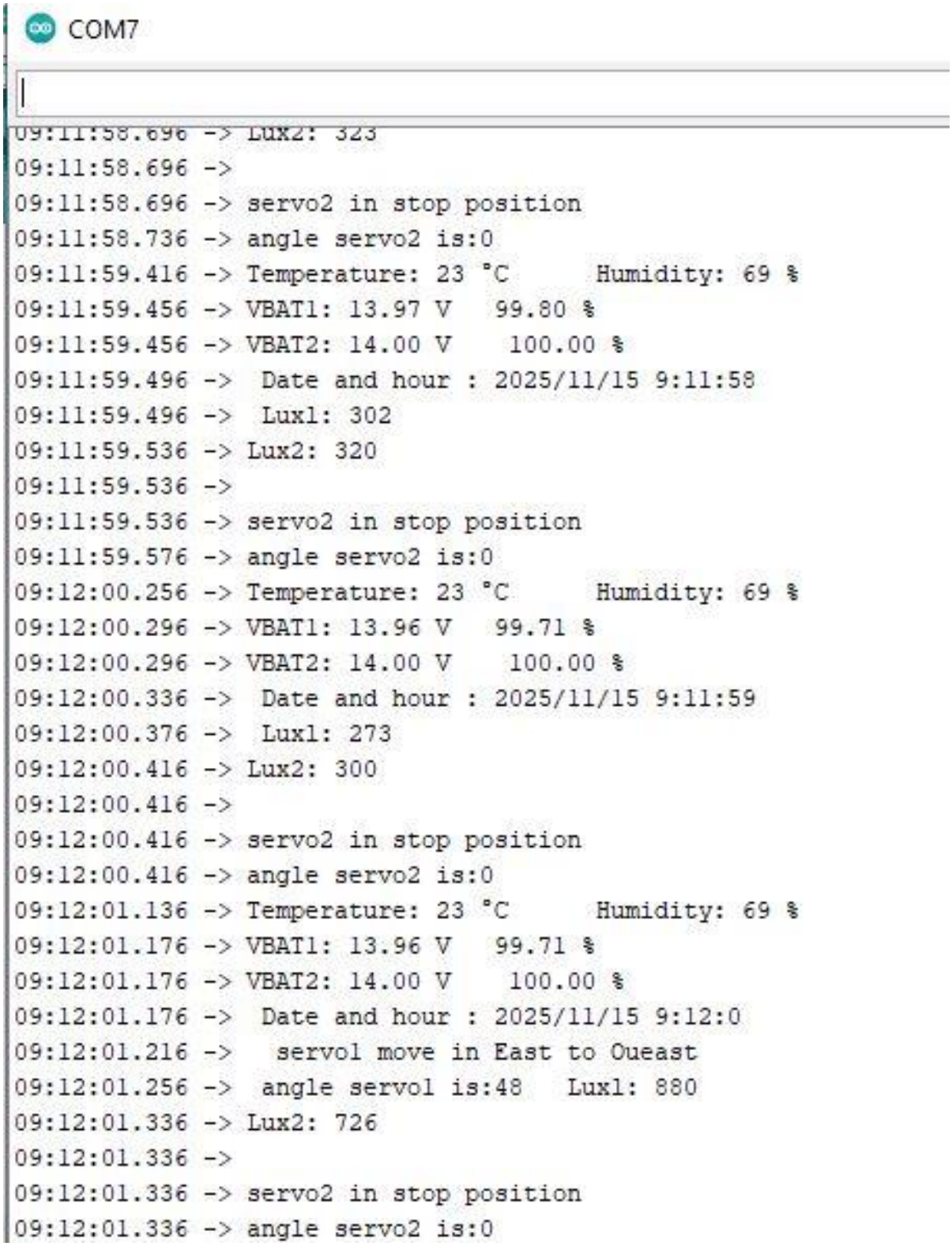


Figure3. 61: Using the serial monitor to display the results at 9:12:00 AM

The experimental results verify the developed algorithm. In Figure 3.57, Figure 3.58 and Figure 3.59, we see that the first battery was activated first to be charged, then battery 2, and finally the DC loads if all batteries are charged. In Figure 3.60 and Figure 3.61, we also note that after

every 12 minutes, a repositioning of the solar panel from East to West was detected (at 9:00:00 and 9:12:00 AM).

Conclusion

The third chapter presented and critically analyzed the results obtained from the various optimization methods implemented. The experiments and simulations proved the applicability of the models created and validated the methods selected for solar tracker control, hybrid MPPT regulation, and optimal tilt. With an average percentage of 68.1%, we discovered that the ideal yearly tilt of the fixed solar panel in Burundi ranges from 13˚ to 15.8˚, depending on the site's latitude. The correctness of the generated models was confirmed by the energy gain of 20% for the experimental results and 20.2% for the model simulation results. The results showed that the solar tracking system provides significant energy gains compared to fixed panels, while the combined MPPT algorithm significantly improves the stability of the maximum power point. In addition, tests on battery charge and discharge management revealed a notable improvement in the service life and energy efficiency of the storage system. The results as a whole confirmed the consistency and overall efficiency of the proposed system. We used MATLAB software to build and simulate the solar tracker algorithm with a battery charge and discharge management system, followed by Proteus and Arduino IDE software. The outcomes attest to the system's efficacy.
In summary, this chapter experimentally confirms the validity of the models presented in Chapter 2 and sets the stage for critical discussions of the overall performance of the system.

Chapter 4 Discussion of results obtained

4.1. Introduction

This chapter is devoted to discussing the results obtained by method and the main findings, and provides an interpretative summary of the research. It compares the results obtained with previous work presented in the literature review in order to assess the real contribution of this work to advancing knowledge in the field of photovoltaic energy production. This chapter highlights the contribution of the developed system, which combines an intelligent solar tracker, a hybrid MPPT regulator (P&O and fuzzy logic) and a predictive storage battery management mechanism in an integrated manner. A critical analysis of energy performance, system stability and storage sustainability demonstrates the relevance of the proposed approach to the energy challenges facing Burundi. Beyond the technical results, this chapter also discusses the socio-economic and environmental implications of the system, including its potential contribution to rural electrification, energy cost reduction and the promotion of sustainable development based on renewable energies.

4.2. Discussion of results on the impact of a fixed solar panel tilted at an optimal angle regulated by an MPPT controller

Numerous studies on maximizing photovoltaic efficiency have demonstrated that the ideal angle of Inclination for solar panels varies with the site's latitude and, according to some authors, is near the latitude ([10] - [13]). Based on the results of our work, we also observe that the ideal annual angle of Inclination of the solar panel varies according to the site's latitude at an average dependency percentage of 68.1%. For sites with a latitude of less than 10 degree, we find that this angle is not close to the site's latitude. According to [11]–[14], the ideal tilt angle is near to the latitude. We find that this assumption depends on the latitude of the site. Burundi has a latitude of -3°, and we have found that tilting a solar panel at an angle of -3° causes dust to settle on the solar panel, which has a negative impact on the lifespan of photovoltaic cells and photovoltaic efficiency.

Analyzing the simulation results from the mathematical models created to ascertain the ideal angle of Inclination of the fixed solar panel and to calculate the solar energy captured reveals that the results of the mathematical models confirm the results obtained using the pvsyst software, validating the efficacy of the mathematical models developed. Based on the simulation results

obtained, we note that for the optimal annual tilt, the values of annual solar irradiation on the collector plane coincide with the values of global horizontal solar irradiation for the site obtained using the PVGIS software shown in Table 2.1, which proves the effectiveness of the pvsyst software, whose results correspond to the results of the mathematical models developed. In [18], an angle of 10° is found for a site with a latitude of less than 10. We see that in this instance, the worldwide horizontal irradiation value determined by the PVGIS5.2 software for the ideal site tilt is less than the annual solar irradiation value on the collection plane. We observe high losses compared to the annual optimum in winter.

Furthermore, as not all locations in Burundi have the same latitude, this indicates a contradictory view that the angle of Inclination of the solar panel does not change based on the site's latitude. In our work based on photovoltaic yield optimization, this factor of variation in solar irradiation has been addressed and we have made a significant contribution by integrating a P&O MPPT controller associated with a fuzzy logic controller. Among conventional algorithms, we noticed that the Increment and conductance MPPT algorithm has a problem with delay in tracking the reference compared to the P&O MPPT algorithm, and we chose the P&O MPPT algorithm. Thanks to this developed algorithm, which combines a conventional algorithm (traditional methods: direct methods and indirect methods) and an unconventional algorithm (techniques include both bio-inspired and artificial intelligence-based techniques); we have succeeded in eliminating this reference tracking delay. Although the developed MPPT approach is cost-effective because it improves the efficiency and tracking stability of the conventional P&O algorithm, it has several drawbacks, such as lower peak convergence speed, high oscillation around a maximum MPPT power point, the previously mentioned drift problem associated with irradiance variation, and complex implementation compared to conventional MPPT methods. Further research is needed to improve energy efficiency in response to climate change.

The research in [31,32] reports a contribution to reducing these problems. Nevertheless, putting all of these strategies into practice is more difficult than using traditional MPPT procedures. The simulation results obtained from the developed algorithm verify the effectiveness of the developed algorithm, which shows good tracking of the reference power. A comparison of the energy gain from the effect of the optimal tilt angle of the solar panel with a solar panel fixed on a horizontal surface is reported in [11]. In our work, we compared the energy gain from the effect of the optimal tilt angle of the solar panel with a fixed solar panel mounted on a residential roof with an average roof angle of 30°. This made it possible for us to calculate the energy lost during the installation of a fixed solar panel on a home's roof. We were able to evaluate and validate

the suggested mathematical models by analyzing the experimental findings obtained in Nyakabiga, where the ideal yearly tilt is 14˚. By adapting it to the results in Table 3.9 and the model in Equation 3.2, for a 10Wp solar panel tilted at an optimal annual tilt angle of 14˚, we obtained a daily available energy of 40.5 kWh/day. In this instance, the projected daily energy available for a fixed solar panel slanted at a 30° angle is 38.47 kWh/day. We observed an energy gain of 20.2% for the results of the simulation of the mathematical model developed. The experimental results indicate a 20% energy gain for a fixed 10Wp solar panel assessed at angles of 30° and 14°. Using the R approach of the SPSS program, which is based on the linear regression model, we developed a model to estimate the optimal annual tilt of solar panels and a model to determine the available energy matched to each site across the country. The optimal annual tilt of fixed solar panels in Burundi is between 13˚ and 15.8˚, depending on the latitude of the site, with an average percentage of 68.1%.

The energy increase of 20% for the experimental results and 20.2% for the model simulation results verified the accuracy of the created models. We note that the model simulation findings are consistent with the results obtained by the pvsyst software and the experimental data. In terms of innovation, this project uses models created for each location with a latitude of less than 10˚ to make it easier to find the ideal tilt angle of the solar panel and the available energy. We generate the conclusion that the model simulation results and the experimental findings are comparable, proving the efficacy and reliability of the models created. For the next project of integrating the solar tracker with battery management, the outcomes of this approach will be a useful reference for examining the gain of the solar tracker in comparison to the fixed solar panel.

4.3. Discussion of results obtained for the intelligent solar tracker

In this section, we will present the results of the solar tracker designed in relation to the literature in Chapter 1. Several research projects on solar tracking systems have been conducted on optimizing photovoltaic efficiency. In the research projects in [37] - [52], solar tracking technologies make it possible to track the sun's rays at all times. In our research, to prevent the solar tracker system from consuming a lot of the energy produced, we have created a solar tracker control algorithm that enables the solar panel to be moved at a 3° angle every 12 minutes using a microcontroller since the panel is constantly shifting. This method reduces the amount of energy used by the servomotors and maximizes the amount of solar energy gathered. Next, we determined the ideal angle of Inclination for the fixed solar panel and examined its impact on the energy gathered in order to accurately compare the energy gains between the tracker and the fixed solar panel .

Following this study, we designed, modelled and simulated the intelligent solar tracker using MATLAB software and Proteus professional software.

We noticed that the simulation results and experimental results are similar. This verified the effectiveness of the developed intelligent solar tracker algorithm. In the equatorial zone, the energy gain of a dual-axis solar tracker over a stationary solar panel system ranges from 31.8% to 37.0%, according to the findings of [54]. Comparing the single-axis solar tracker to the fixed solar panel, an analysis of the testing data for our study shows a gain of 29% to 41%. Based on the same experimental results, we also discovered that the dual-axis solar tracker had an energy gain of between 42% and 50% when compared to the fixed solar panel. We found that between 12:00 and 13:00, the fixed solar panel assembly and the solar tracker assembly produce almost equal amounts of electrical energy. Considering the daily energy saved by the servomotors, we know that the Earth spins 360 degrees on its axis in 24 hours (the normal solar day). As a result, the Sun's hour angle, which is the angle formed by the Sun's location and the local meridian, varies by 15 degrees every hour. If the solar panel is moved by 1° each time, there will be fifteen repositioning in an hour, or 15°.

In our study, we will adjust the solar panel five times in an hour at a 3° angle. In this instance, we observe 100% servomotor consumption for a one-degree actuator repositioning for a solar tracking system that shifts by 1° each time there is a variation in sensor illumination. In our instance, the servomotor uses 0.333 electrical energy for five solar panel repositioning in an hour. We find that for our solar tracking system, the servomotor consumes 33.33% of the electrical energy compared to a solar tracking system that tracks the sun's rays at all times. We deduce an electrical energy saving of approximately 66.67% in servomotor consumption compared to a system that tracks the sun's rays at all times. Further research is needed on strategies for saving the electrical energy consumed by servomotors. From a financial standpoint, we find that, considering the sun's path in tropical nations, a single-axis monitoring system works well in Burundi.

We observed that the solar energy recorded by the dual-axis solar tracker was comparable to that recorded by a single-axis solar tracker on days when the sun's journey was from east to west. Figure 3.12, which depicts the sun's path across Burundi in April, August, March, September, February, and October, further illustrates this. The single-axis solar tracker features a more straightforward design, less motorization, and cheaper installation and maintenance expenses. In contrast, the structure of the two-axis solar tracker is more intricate (dual motorization, accurate sensors, more sophisticated control electronics). It is expected that the dual-

axis solar tracker will cost between thirty and fifty percent more to install and maintain than the single-axis solar tracker.

The single-axis solar tracker requires fewer moving parts, is more reliable, and has a lower failure rate than the single-axis solar tracker in terms of technical complexity and dependability. The solar tracker needs more motors, sensors, and components than the single-axis solar tracker system. Compared to a single-axis sun tracker, the dual-axis solar tracker has a higher chance of mechanical or electronic failure. Regular maintenance is done to prevent any loss of. Maintenance is carried out regularly to avoid any loss of efficiency. Research into optimization technologies to overcome these problems is needed.

The integration of smart solar trackers into Burundi's energy landscape offers significant potential for improving the efficiency of photovoltaic systems compared to fixed installations. These devices enable more efficient capture of solar radiation, resulting in a notable Increase in the amount of energy produced. Local industrialization of this technology would be an important lever for strengthening energy independence, particularly in rural areas with limited access to electricity. Furthermore, the development of a value chain around solar trackers, Including design, manufacturing and maintenance, is likely to generate skilled employment opportunities and stimulate the local economy. However, the success of this technological transition depends on several key factors: adequate institutional support, the implementation of specialized technical training, and sustained investment in research, development and innovation. The results of this method will serve as a useful reference for the project to integrate the solar tracker with a battery charge and discharge management system.

4.4. Discussion of results obtained for a mechanism for managing the charging and discharging of energy storage batteries.

The outcomes of an algorithm based on a battery charge and discharge management system created in connection with the literature review is shown in this section. Several authors have conducted various studies on battery charge and discharge management technologies to significantly improve the overall efficiency of photovoltaic systems, the useful life of batteries, and the safety and stability of storage. In research papers [61], [63], [64], [69] and [70], programs for controlling a single battery's charging and discharging were created to highlight the significance of each technique and its effectiveness. Taking into account the problem of the impossibility of not charging all the batteries during the rainy season and the loss of unused energy when the batteries are fully charged while the sun is shining, as shown in Table 3.4, using an Arduino microcontroller, we have created an algorithm based on a cascade charging and

discharging mechanism for batteries in a solar system to maximize the energy generated. Based on the results in Table 3.4, we note that if we used the developed algorithm its allows for the recovery of unused annual energy of around 34.47kWh/year (EUnused) which corresponds to 2.98% of annual production when the batteries are fully charged.

Based on the examination of the developed algorithm's results, we see that, in comparison to the current solar kit, this automatic switching mechanism enhances the effectiveness of battery charge and discharge management and helps to optimize the management of the solar energy produced. When compared to the current solar installation kit, the created algorithm also performs well on the battery's charge and discharge status and helps to optimize the management of the solar energy produced. The developed algorithm allows the battery charge status to be managed at a minimum threshold of 80%, which corresponds to a DOD of 20%. According to [15], a battery depth of depletion of 20% translates into a maximum of 8,500 battery cycles. It also indicates that increasing the depth of discharge causes a decrease in the number of battery cycles, which has an impact on reducing the life of a battery. For our work, we find that battery management maximizes the battery life cycle to a BS2 battery life cycle number of 8,390. The algorithm developed also manages the temperature of the room, which negatively affects battery capacity and internal resistance. High temperatures cause an Increase in operating current, which in turn leads to overload accumulation, increased grid corrosion, gas generation and precipitation, thereby shortening the battery's lifespan. In [14], the state of health (SOH) of lead-acid batteries was estimated using impedance measurements and fuzzy logic data analysis. When the voltage surpasses the minimal value, our algorithm for the charge and discharge mechanism disconnects the battery from the charge.

The energy lost as a result of defective batteries' charging and discharging issues in Burundi's varied solar fields can be recovered using the algorithm we created. We used MATLAB software to construct and run the algorithm we created, followed by the Arduino IDE and Proteus software for comparative analysis. We noticed that the simulation outcomes from MATLAB Simulink and Proteus are consistent. A single battery bank with a direct power supply to other DC loads can be charged and discharged using the developed battery charge and discharge management system's algorithm. In this instance, charging the second battery bank requires that the DC loads be connected directly to the solar generator. We observe that the outcomes of the simulation using Proteus and MATLAB Simulink software match the outcomes of the experiments, proving the efficiency of the provided algorithm. The combination of these technologies has led to a significant improvement in the overall energy efficiency of the

photovoltaic system compared to conventional fixed-tilt installations without active storage management. This performance reinforces the relevance of deploying such solutions in rural areas of Burundi, where access to electricity remains limited. The literature review concludes with the need to design an integrated system combining solar tracking, MPPT regulation and intelligent battery management, which has not been addressed. As part of a synthetic analysis of the results of a solar tracker system equipped with a battery charge and discharge management system, we combined the solar tracker algorithm with the battery charge and discharge management mechanism algorithm. This allowed us to have a single solar tracker system equipped with a battery charge and discharge management system.

We used MATLAB software to build and simulate the solar tracker algorithm with a battery charge and discharge management system, followed by Proteus and Arduino IDE software. The results obtained validate the effectiveness of the system studied. Based on our research, we have technical suggestions for improving the solar tracker, such as using light sensors such as pyro-metric sensors to analyze their effects on reducing reading errors caused by clouds or shadows, and gradually replacing lead-acid batteries with longer-life lithium batteries, when the budget allows. Experimentally, we suggest testing the number of battery cycles to measure the real impact of the management algorithm on battery life. From an economic point of view, we suggest studying cost reduction strategies using locally available materials and evaluating the financial gains associated with Increasing the photovoltaic efficiency of the solar tracker compared to a fixed panel. From an environmental and social perspective, we suggest promoting the adoption of smart photovoltaic systems in rural areas without electricity to improve access to energy.

Conclusion

The final chapter discussed and contextualized the results obtained in light of scientific literature and the Burundian energy context. The performance of the integrated system combining an intelligent solar tracker, a hybrid MPPT regulator and predictive battery management demonstrated a significant improvement in the overall efficiency of the photovoltaic system. Simulations and experimental validations confirmed that the proposed solution offers better adaptation to climatic variations, optimal exploitation of solar radiation, and extended energy storage life. The discussion also highlighted the scientific and technological contributions of the research, showing that the coherent integration of these subsystems contributes not only to optimizing efficiency, but also to the reliability and sustainability of photovoltaic installations in resource-constrained contexts.

In conclusion, this chapter confirms the relevance and applied value of the research work, while opening up suggestions and perspectives for future research. This work carried out has been shown to follow an integrated logic linking the why, how, what and ultimate why.

General conclusion

This work focused on integrating a solar tracking system combined with a battery management system (BMS) for storage, with the aim of optimizing photovoltaic efficiency in Burundi. In a context marked by high solar potential but low exploitation of renewable energies, this work is part of an innovative approach aimed at improving the energy efficiency and sustainability of autonomous solar installations. The first chapter was devoted to a literature review presenting the factors that influence the optimization of fixed solar panel photovoltaic systems: irradiation, Inclination and optimal angle. We showed the various recent research studies on the effect of the optimal tilt angle of fixed solar panels on energy capture. The various recent research studies on optimizing photovoltaic efficiency through the integration of MPPT controllers were examined. We also presented recent research on trackers and battery charge and discharge management systems. We also described the situation regarding access to energy in the world and in Burundi.

In Chapter 2, we described the methods and materials to be used to optimize photovoltaic efficiency. We described methods for determining the optimal angle of Inclination for fixed solar panels and for determining the amount of solar energy captured using pvsyst and SPSS software. Taking climate change into account, we discussed a method for optimizing a fixed-panel PV system by integrating an MPPT controller. We demonstrated our approach by developing methods for optimizing photovoltaic efficiency using an intelligent solar tracker and an algorithm based on a battery charge and discharge management mechanism. Predictive modelling of the number of battery life cycles was studied. This chapter allowed us to put into practice the approaches inspired by the first chapter1 of the literature review and helped us to prepare the synthetic analysis of the simulation and experimental results by method.

In Chapter 3, a presentation of the analysis of the summary results by method was carried out. The first method of optimizing photovoltaic efficiency focused on optimizing the photovoltaic efficiency of a fixed solar panel tilted at an optimal angle and connected to an MPTT regulator. First, we demonstrated that the majority of Burundians install solar panels on their homes' roofs without a model to determine the solar panels' degree of Inclination. We started using pvsyst software to determine the ideal annual tilt of the panels as part of this research. We created a model to determine the ideal annual tilt of solar panels and a model to determine the available energy tailored to each location across the nation using the R method of SPSS software, which is based on the linear regression model. We confirmed the correctness of the generated models by finding an energy gain of 20.2% for the model simulation results and an energy gain of 20% for the experimental data. We observe that the results obtained by

the pvsyst software and the experimental results align with the model simulation results. In terms of innovation, this project uses models created for each location with a latitude of less than 10˚ to make it simple to identify the ideal tilt angle of the solar panel and the available energy.

In this work, our contribution to the MPPT technology used in relation to existing work is based on the introduction of an MPPT regulator based on the P&O MPPT algorithm combined with a fuzzy logic controller in order to dynamically improve the efficiency of electricity production. The MPPT controller technology developed offers many advantages over the PWM controller generally used in Burundi. The research hypotheses, constraints and complexities were demonstrated in our research project. We found that the MPPT algorithm developed has the advantage of being robust. Its design is very simple as it does not require knowledge of the exact model. It also does not require any training data, which means that all types of photovoltaic modules can work with the regulator developed. Any site in the world can use the MPPT algorithm that was created as part of this study. Additionally, we have highlighted the several Burundian locations with adequate potential. The study shows that a solar panel tilted at an optimal angle has 20% more energy output than a panel tilted at 30°, which corresponds to the slope of a house roof.

The approach improves reliability and accuracy in energy production as part of the energy transition policy towards renewable energy. For the upcoming project of integrating the solar tracker with battery management in Burundi, the results of this approach have been a useful reference for examining the gain of the solar tracker in comparison to the fixed solar panel. We then carried out a second study on the integration of the solar tracker. In our work, this method aims to develop an intelligent solar tracker designed to improve the efficiency of photovoltaic systems in Burundi. Burundi is a country located in the equatorial zone, with variable solar radiation due to cloud cover, atmospheric humidity and low seasonal variations. However, during the day, the apparent position of the Sun changes continuously due to the Earth's rotation. As the majority of photovoltaic installations are fixed, a significant proportion of the potential solar energy is not captured because the Sun's rays do not always strike the surface of the panels at an optimal angle. In a context marked by low electrification rates and high dependence on fossil fuels, which represent both an economic and environmental challenge, the integration of a solar tracking system is an innovative and sustainable solution.

However, existing tracking systems have the disadvantage of consuming a significant amount of stored energy due to the continuous tracking of the Sun's position. To remedy this, we took an original approach based on the development of an intelligent algorithm that repositions the solar panel at an angle of 3° every 12 minutes from 6:00 A.M. to 6:00 P.M. and

finally returns it to its initial position at 6:30 P.M., thereby reducing the system's energy consumption while maximizing solar exposure. The implementation was based on modelling, simulation and programming tools such as MATLAB 2020a, Proteus 8, Arduino IDE and SolidWorks. The simulation results obtained were consistent with the experimental results, confirming the reliability and effectiveness of the intelligent algorithm developed. The application of a two-axis solar tracker in the Burundian context resulted in estimated net energy gains of between 42% and 50%, confirming the value of such technology for optimizing photovoltaic efficiency.

The implementation of a single-axis solar tracker in the Burundian climate context achieves net gains in solar energy capture ranging from 29% to 41% compared to fixed photovoltaic systems. We have noted that, based on the results found between the dual-axis solar tracker and the single-axis solar tracker, and compared to the results of the sun's trajectory in Burundi, the single-axis solar tracker is a good choice for installation in the region.

From an economic standpoint, we have also demonstrated the advantage of single-axis solar trackers over dual-axis solar trackers. The major contribution in our case lies in the design and implementation of an intelligent solar tracker mechanism using a real-time clock (RTC3231) and photo resistive sensors, ensuring that the solar panel is oriented almost perpendicular to the sun's rays every 12 minutes. This study contributes significantly to the optimization of available solar energy, while reducing the energy consumption associated with actuators (servomotors) and extending their service life through more rational control of servomotor movements. We also conducted a study to optimize photovoltaic efficiency by integrating a battery charging and discharging mechanism. An algorithm based on an intelligent battery charge and discharge control mechanism was created, simulated, and experimentally verified as part of a synthetic analysis of the outcomes of an algorithm based on a battery charge and discharge management mechanism to maximize solar energy.

The algorithm design phase was carried out using MATLAB 2020a, with dynamic modelling via Simulink. We then designed and simulated the developed algorithm using Proteus software by transferring a hexadecimal file compiled via Arduino IDE programming software to Proteus. These design and programming tools enabled us to evaluate the efficiency of the battery charge and discharge management system. The predictive battery management modelling showed the battery life cycle performance using the algorithm developed for battery management at a minimum SOC of 80%. We obtained a battery life cycle number of 8,839 cycles. However, it was observed that the battery operating temperature exceeded 25°C, highlighting the need for a thermal regulation system (passive or active air conditioning) to ensure the longevity of the storage system.

Experimental validation was conducted using a prototype. The results obtained during numerical simulations showed a significant correlation with the experimental results, confirming the robustness and effectiveness of the algorithm developed. In Chapter 4, as part of a synthetic analysis of the results of a solar tracker system equipped with a battery charge and discharge management system, we combined the solar tracker algorithm with the battery charge and discharge management mechanism algorithm. This allowed us to have a single solar tracker system equipped with a battery charge and discharge management system. We worked with MATLAB software to design and simulate the solar tracker algorithm with a battery charge and discharge management system, followed by Proteus and Arduino IDE software.

The devised algorithm enables the panel to be rotated at a 3° angle every 12 minutes in an east-west direction from 6:00 AM to 6:00 PM, according to the simulation and testing results. Additionally, we demonstrated how the proposed algorithm rotates the solar panel from North to South or South to North when there is a significant variation in the lighting of the LDR sensors. In terms of battery discharge and charge control, we observed that the created algorithm can be verified, tested, and validated based on simulation and experimental findings. The results obtained from the numerical simulations showed significant correspondence with the experimental results, confirming the robustness and effectiveness of the developed algorithm. These results correspond with the results found in Chapter 3 for each method.

Discussions of the results for the different approaches were presented to demonstrate our contribution. It was noted that the design of a solar tracker equipped with a battery charge and discharge management system to optimize photovoltaic efficiency is new. The combination of these two technologies has led to a significant improvement in the overall energy efficiency of the photovoltaic system compared to existing solar installations. This performance reinforces the relevance of deploying such solutions in rural areas of Burundi, where access to electricity remains limited. By providing a model for determining the ideal solar electricity generation, this initiative also benefits the national, regional, and global communities regarding the social impact of rural lighting in Burundi. The importance of this project lies in raising public awareness of solar energy exploitation with optimal solar panel tilt at these sites, which is in the interests of the environment, public health, the country's economy, family finances, as well as entrepreneurship and the social economy.

The development of a smart solar tracker equipped with a battery charge and discharge management mechanism, specifically adapted to equatorial climate conditions, is a high-potential solution for improving the profitability and energy efficiency of photovoltaic systems in this area. At the local level, widespread adoption of this type of technology could promote energy transition, strengthen communities' energy independence, and support sustainable

development policies. This project is particularly important because of its ability to maximize energy recovery in a resource-constrained environment. Furthermore, the proposed system stands out for its integration of smart technologies, partially replacing human intervention and illustrating the growing interest in artificial intelligence applied to autonomous energy systems. It thus sets a benchmark for technological innovation in Africa, demonstrating the feasibility and effectiveness of high value-added local solutions.

This project is particularly important because of its ability to maximize energy recovery in an environment with limited resources. Furthermore, the proposed system stands out for its integration of smart technologies, partially replacing human intervention and illustrating the growing interest in artificial intelligence applied to autonomous energy systems. It thus sets a benchmark for technological innovation in Africa, demonstrating the feasibility and effectiveness of local solutions with high added value. The project to integrate a smart solar tracker with a battery management system (BMS) in Burundi has a strategic impact in energy, economic, technological and social terms. From an energy perspective, in a country where access to electricity remains limited, particularly in rural areas, this project contributes to significantly improving the efficiency of photovoltaic installations (42% and 50% gain in production). By tracking the sun's trajectory and optimizing storage, it allows for better use of available solar radiation, which is particularly variable in equatorial climates.

From an economic perspective, improved energy efficiency translates into a reduction in the cost of producing solar kWh, making photovoltaic systems more profitable in the long term. In addition, the extended battery life achieved through the battery charge and discharge management mechanism reduces maintenance and replacement costs, further enhancing the economic viability of the installations. On the technological side, the development of local solutions integrating intelligent algorithms, microcontrollers and solar sensors is stimulating technological innovation in Burundi. This project can serve as a basis for training, applied research and industrialization programs in the renewable energy sector. In terms of social impact, access to reliable solar energy promotes energy Inclusion and empowers households, schools and health centers. Environmentally, reducing dependence on generators and fossil fuels helps to reduce CO_2 emissions, thereby contributing to the fight against climate change. Academically, the project makes a scientific contribution to the university community as a model of multidisciplinary integration between electronics, energy, automation and embedded computing. It can inspire further research and strengthen local and regional research capacity on smart photovoltaic systems.

There are a number of ways to enhance the system under study's sustainability and performance: developing the impact of integrating a three-axis solar tracker (tilt, azimuth,

elevation) adapted to equatorial conditions, integrating an automatic solar panel cleaning system, studying the integration of super capacitors coupled with batteries to absorb power peaks, and developing an Internet of Things (IoT) platform for real-time monitoring of system performance.

The project has certain limitations. In terms of hardware limitations, the system was implemented using low-cost components (Arduino, standard servo motors, simple sensors, a small 1.2Wp solar panel), which may have limited the use of an MPPT controller for the solar tracker and its long-term robustness. More powerful actuators or more sensitive sensors could improve performance but are more expensive for larger-scale systems. Arduino microcontrollers cannot withstand high temperatures.

In relation to the system's energy requirements, although the system aims to improve production, the continuous operation of the motors (even when optimized by an algorithm) and the control system requires energy consumption, which reduces part of the net gain obtained from solar energy. This becomes critical in areas with low production. Due to the high cost of imported components, we did not include a wind control system in the project to analyze its effectiveness, even though wind speeds can exceed the recommended limits, affecting the system's operation. Although the system is functional on a small scale, extending it to a large-scale photovoltaic installation would require a complete re-engineering, both in terms of hardware, communication between modules and centralized management via IoT.

From an economic and social perspective, the vulnerability of local energy infrastructure, the cost of importing certain components, and the level of local technical expertise may hinder widespread adoption of the system. Specialized maintenance also remains a challenge in many rural areas.

References

[1] Neill, W. O. (2024). Seeing the light: important innovations that shed light on the world. Journal of Physics: Conference Series 2887, 1-19. https://doi.org/10.1088/1742-6596/2877/1/012068

[2] Benhamida M. T., Sahraoui T. (2022). "Estimation de l ' état de charge d ' une batterie Li-ion utilisé dans un véhicule électrique Dédicace :" universite kasdi merbah ouargla. https://dspace.univ-ouargla.dz/jspui/handle/123456789/30197

[3] Max F., Margret W.M., Markus H., Thomas W.(2024). Temperature-driven path dependence in Li-ion battery cyclic aging .Journal of Power Sources, Volume 594, 28. https://doi.org/10.1016/j.jpowsour.2023.233948

[4] https://www.astrojem.net/translation-of-the-earth-around-the-sun-at-106-000-km-hour/

[5] BELKEBIR, Armel,R., ABDERRAHIM, K., MOHAMMED,Y.(2024).Prédiction du rayonnement solaire par la méthode de réseaux de neurones (application pour le site de Ouargla) https://dspace.univ-ouargla.dz/jspui/handle/123456789/38307

[6] Green, M. A., Dunlop, E. D., Hohl-Ebinger, J., Yoshita, M., Kopidakis, N., & Hao, X. (2022). Solar cell efficiency tables (version 59). Progress in Photovoltaics, 30(1), 3–12. https://doi.org/10.1002/pip.3506

[7] IEA. (2023). Renewables 2023. International Energy Agency. https://www.iea.org

[8] Olivier, I., Singh, P., Denis, B., Bosco, N.J., and Noel, N. (2025). Détermination de l'angle d'Inclinaison optimal des panneaux solaires et de l'énergie produite dans les différentes provInces du Burundi.. JOURNAL OF POWER AND ENERGY ENGINEERING, 13, 11-35. HTTPS://DOI.ORG/10.4236/JPEE.2025.135002

[9] Reindl, D. T., Beckman, W. A., & Duffie, J. A. (1990). *Diffuse fraction correlations*. Solar Energy, 45(1), 1-7. https://doi.org/10.1016/0038-092X(90)90060-P

[10] Radziemska, E. (2003). The effect of temperature on the power drop in crystalline silicon solar cells. Renewable Energy, 28(1), 1–12. *https://doi.org/10.1016/S0960-1481(02)00015-0*

[11] GUESSOUMI,F. and SAADI,A. « Commande de panneau solaire à l'aide d'une carte a PIC » Université Mohamed Khider Biskra d'Algérie. http://dspace.univbiskra.dz:8080/jspui/bitstream/123456789/6619/1/COMMANDE%20DE%20PANNEAU%20SOLAIRE%20A%20L%27AIDE%20D%27UNE%20CARTE%20A%20PIC.pdf

[12] Kılcı, O. and Koklu, M. (2019) .Analysis of Solar Power Plants: The Significance of

Fixed and Variable Angle. International Journal of Applied Mathematics Electronics and Computers, 7, 75-83. https://doi.org/10.18100/ijamec.653371

[13] Zang, H., Guo, M., Wei, Z., and Sun, G. (2016) .Determining the Ideal Solar Collector Tilt Angle for Various Chinese Climates. Sustainability, 8, Article 654. https://doi.org/10.3390/su8070654

[14 Benghanem, M. (2011) .Solar Panel Tilt Angle Optimisation: Madinah, Saudi Arabia Case Study. Applied Energy, 88, 1427-1433. https://doi.org/10.1016/j.apenergy.2010.10.001

[15] Shaker Al-Sayyab, A.K., Al Tmari, Z.Y., and Taher, M.K. (2019). Optimal Tilted Angle Photovoltaic Cell Performance: A Theoretical and Experimental Study of Basra City. Case Studies in Thermal Engineering, 14, Article ID: 100421. https://doi.org/10.1016/j.csite.2019.100421

[16] Abdallah, R., Juaidi, A., Abdel-Fattah, S., and Manzano-Agugliaro, F. (2020). Estimated the ideal tilt angles for Palestine's south-facing surfaces. Energies, 13, Article 623. https://doi.org/10.3390/en13030623

[17] Wessley, G.J.J., Sandhya, S., and Narciss Starbell, R. (2017) Modelling the Ideal Tilt Angle for Solar Collectors in Eight Indian Cities. International Journal of Renewable Energy Research, 7, 353-358.

[18] Al-Sayyab Shaker, A.K., Abdulwahid, M.A., and Ali Morad, A.M. (2018). Optimisation des angles Inclinés d'une cellule photovoltaïque pour déterminer la puissance électrique maximale générée : étude de cas de certaines villes irakiennes. Case Studies in Thermal Engineering, 12, 484-488. https://doi.org/10.1016/j.csite.2018.07.001

[19] Memon, Q.A., Rahimoon, A.Q., Ali, K., Shaikh, M.F., and Shaikh, S.A. (2021). Determining the Best Tilting Angle for a 1 MW Solar Energy System in Sukkur, Pakistan. In ternational Journal of Photoenergy, 2021, Article ID: 5552637. https://doi.org/10.1155/2021/5552637

[20] Ayara, W.A., Akinboro, F.G., Usikalu, M.R., Oyeyemi, K.D., and Orovwode, H. (2019) Optimal Angle of Inclination for a Fixed Stand-Alone Photovoltaic: A Review.Journal of Physics: Conference Series, 1299, Article 012021. https://doi.org/10.1088/1742-6596/1299/1/012021

[21] Abed, S. et Ibrahim, L. (2022). Dimensionnement d'une installation solaire afin d'améliorer l'efficacité énergétique du décanat de l'université de MOSTA-GANEM. http://e-biblio.univ-mosta.dz/handle/123456789/21043

[22] Mustapa, M. S., Winoko, Y. A., Faizal, E., and Kozin, M. (2023). An analysis of the efficiency of solar charger controllers using maximum power point tracking (MPPT) and

pulse width modulation (PWM). Asian Journal Science and Engineering, 1(2), 90-102. https://doi.org/10.51278/ajse.v1i2.546

[23] Hossam, H.H.M., Abdel-Rah,Y., Essam, E.M. M.(2021). State of the art perturb and observe MPPT algorithms based wind energy conversion systems: a technology review. Int. J. Electr. Power & Energy Syst., vol 126, 2021, 106598. https://doi.org/10.1016/j.ijepes.2020.106598

[24] Mohammed ,H.A., Mohammad,Z., Sally , E.T.(2025). A comprehensive study of recent maximum power point tracking techniques for photovoltaic systems. Scientific Reports, 15 (1), 2025, 14269. https://doi.org/10.1038/s41598-025-96247-5

[25] Chun-Liang, L., Chung-Wen, H., Yi-Feng,L., Guan-Jhu,C., Cheng-Sin, H. (2025).A Study on Maximum Power Point Tracking Technology for Solar Power Systems Using Power Variation to Adjust Step Response. The 2025 International Conference on Artificial Life and Robotics (ICAROB2025). https://alife-robotics.co.jp/members2025/icarob/data/html/data/OS/OS8/OS8-4.pdf

[26] Deghfel, N., Badoud, A.E., Merahi, F. *et al.(2024).* A new intelligently optimized model reference adaptive controller using GA and WOA-based MPPT techniques for photovoltaic systems. *Sci Rep* **14**, 6827 (2024). https://doi.org/10.1038/s41598-024-57610-0

[27] Yali,L., Ming L., Xu,J., Xi,L., Meidi,W., Ying, Z.(2014). A comparative study of maximum power point tracking methods for PV systems. Energy Conversion & Management, vol 85, pp 809-816, 2014. https://doi.org/10.1016/j.enconman.2014.01.049

[28] Premkumar,M., Umashankar,S., Thanikanti, S.B., Sanjeevikumar P., Jens B. H.-N., Massimo,M, Sowmya R.(2020). Improved perturb and observe MPPT technique for solar PV power generation systems. IEEE Systems Journal, 15(2), 3024-3035, 2020. https://doi.org/10.1109/JSYST.2020.3003255

[29] Khadidja S., Mountassar M., M'hamed B.(2019). A new high-performance variable step size P&O MPPT algorithm for PV systems. IJPEDS (International Journal of Power Electronics & Drive Systems) 10(3), pp 1662-1674, 2019 http://doi.org/10.11591/ijpeds.v10.i3.pp1662-1674

[30] Abdel-Salam, M., El-Mohandes, M.T. & El-Ghazaly, M.(2020) . An Efficient Tracking of MPP in PV Systems Using a Newly-Formulated P&O-MPPT Method Under Varying Irradiation Levels. *J. Electr. Eng. Technol.* **15**, 501–513 (2020).

https://doi.org/10.1007/s42835-019-00283-x

[31] Feriel, G. and Rim, M. (2024) Maximum Power Point Trackers (MPPT) for a photovoltaic system using both traditional and intelligent methods. Digital Repos itory-Abdel Hafid Boussouf University Center of Mila.
http://dspace.centre-univ-mila.dz/jspui/handle/123456789/3672

[32] Katche, M.L., Makokha, A.B., Zachary, S.O. and Adaramola, M.S. (2023) .A Comprehensive Review of Maximum Power Point Tracking (MPPT) Techniques Used in So lar PV Systems. Energies, 16, Article 2206.
https://doi.org/10.3390/en16052206

[33] McFee R.H.(1975). Power collection reduction by mirror surface non flatness and tracking error for a central receiver solar powersystem. (Appl. Opt. 1975); 14:1493

[34] Naima F.M., Yaghobian N.A. (1990).Design and construction of a solar tracking system. Solar Wind Technol. 1990;7:611–7:6.
https://doi.org/10.1016/0741-983X(90)90072-A

[35] Riedel-Lyngskaer, N., Berrian, D., Alvarez Mira, D., Aguilar Protti, A., Poulsen, P.B., Libal, J. et al. (2020) Validation du logiciel de simulation photovoltaïque bifacial basé sur des données de surveillance provenant de suiveurs à axe unique à grande échelle et de systèmes à Inclinaison fixe au Danemark. Applied Sciences, 10, Article 8487.
https://doi.org/10.3390/app10238487

[36] Huilin S., Wei S..(2023) Conception et mise en œuvre d'un système de suivi solaire à deux axes. Énergies 16 (17), 6330, 2023.
https://DOI : 10.3390/en16176330

[37]Awasthi, A., Shukla, AK, Manohar, SRM, Dondariya, C., Shukla, K., Porwal, D., and Richhariya, G. (2020). Analysis of solar monitoring technology in solar photovoltaic systems. Energy Relations, 6, 392-405. https://doi.org/10.1016/J.EGYR.2020.02.004

[38] Hafez A.Z.,., Soliman A., Ismail I.M.(2018).Un examen complet de la conception des systèmes de suivi solaire dans les applications de cellules, modules, panneaux, réseaux et systèmes photovoltaïques. *7e Conférence mondiale IEEE 2018 sur la conversion de l'énergie photovoltaïque (WCPEC) (conférence conjointe des 45e IEEE PVSC*, 28e PVSEC et 34e EU PVSEC), 1188-1193, 2018
DOI : 10.1109/PVSC.2018.8547901

[39] Yousef A.M, Harag N.M., Hafez A.Z. (2018). Systèmes de suivi solaire : technologies et kinds de suivi – Un aperçu. *Review of Durable and Renewable Energy* 91, 754-782.
DOI : 10.1016/j.rser.2018.03.094

[40] Moradi, H., Abtahi, A., and Messenger, R. (2016) .Comparing Tracking and Fixed Photovoltaic Arrays for Annual Performance. *2016 IEEE 43rd Photovoltaic Spe cialists Conference (PVSC)*, Portland, 5-10 June 2016, 3179-3183. https://doi.org/10.1109/pvsc.2016.7750252

[41] Nsengiyumva, W., Chen, S.G., Hu, L. et Chen, X. (2018) Progrès récents et défis dans les systèmes de suivi solaire (STS) :A Review. Renewable and Sustainable Energy Reviews, 81, 250-279. https://doi.org/10.1016/j.rser.2017.06.085

[42] Khadidja, B., Dris, K., Boubeker, A. et Noureddine, S. (2014) Optimisation d'un système de suivi solaire pour les centrales photovoltaïques dans la région saharienne, cas d'Ouargla. *Energy Procedia*, 50, 610-618. https://doi.org/10.1016/j.egypro.2014.06.075

[43] Nguyen, X., Nguyen, V., Nguyen, D., Nguyen, L. et Nguyen, D. (2017). Étude comparative de la performance entre le système photovoltaïque suivi et fixe : étude de cas du parc technologique avancé Hoa Lac à Hanoi. *International Seminar on Intelligent Technology and Its Applications (ISITIA*), Surabaya, 28-29 August 2017, 128-133. https://doi.org/10.1109/isitia.2017.8124067

[44] González,A, Muñoz-Maldonado, H.Y., Ospino-Castro, A., Serrano, J., Atencio, A.and Saavedra, C.J. (2021) Conception et évaluation de la performance d'un panneau solaire à suivi uniaxe en Colombie. International Journal of Electrical and Computer Engineering (IJECE), 11, 2889-2898. https://doi.org/10.11591/ijece.v11i4.pp2889-2898

[45] Ihab, M.N., Ahmed, M.M. et Mustafa, R.H. (2020). Amélioration des performances des panneaux photovoltaïques grâce à un suiveur solaire à double axe. Journal of University of Babylon for Engineering Sciences, 28, 119-126. https://www.journalofbabylon.com/index.php/JUBES/article/view/3229

[46] Doğukan, P., and Ilhan, V.O. (2021). A Comparative Analysis of Two-Axis Solar Tracking Systems and Fixed Solar Panels in Menderes District. International Journal of Innovative Re-search and Reviews, 5, 32-38. http://www.injirr.com/article/view/80

[47] Er, Z. and Balci, E. (2018) Dual Axis Solar Angle Tracking System without Any Sensor. Journal of Energy Systems, 2, 127-136. https://doi.org/10.30521/jes.456606

[48] Baouche, F.Z., Abderezzak, B., Ladmi, A., Arbaoui, K., Suciu, G., Mihaltan, T.C. et al. (2022) Conception et Simulation d'un Système de Suivi Solaire pour Photovoltaïques.

Applied Sciences, 12, Article 9682.
https://doi.org/10.3390/app12199682

[49] Mollahasanoglu, M., and Okumus, H.İ. (2021) Evaluation of Efficiency of the Two-Axis Solar Tracking System Designed for Trabzon. IETE Journal of Research, 69, 5338-5350. https://doi.org/10.1080/03772063.2021.1973592

[50] Sakina, A. et al. (2023). Optimisation des performances d'un générateur photovoltaïque via un mécanisme de suivi solaire à double axe utilisant des capteurs en Algérie. *Telkomnika 23(6).*
http://doi.org/10.12928/telkomnika.v23i6.26872

[51] Salem, A., Abido, M.A., and Hamanah, W.M. (2024) a Heliostat Two-Axis Sun Tracking System: A Study of the Case in Saudi Arabia. RE&PQJ, 18, 488-493. https://doi.org/10.24084/repqj18.406

[52] Algarín, C.R., Castro, A.O., Naranjo, J.C., Magdalena, U. et Ingeniería, F.D. (2017). Système de suivi solaire à double axe destiné aux systèmes photovoltaïques. *International Journal of Renewable Energy Research*, 7, 138-145.
https://hdl.handle.net/11323/4606

[53] Zarei Zohdi, H. and Sarvi, M. (2023) Optimal and Economic Evaluation of Using a Two-Axis Solar Tracking System in Photovoltaic Power Plants, a Case Study of "Tehran", Iran. Journal of Solar Energy Research, 8, 1211-1221.

[54] Tchakounté, H., Bertin, C., Fapi, N. et Kamta, M. (2022) Prépublication Easy Chair : Optimisation de la performance d'un module photovoltaïque par un traqueur solaire intelligent. *1st International Conference on Engineering Sciences and Development (ICESD2022),* Monastir, 27-29 December 2022, 1-8.
https://easychair.org/publications/preprint/mrwbR/download

[55] Alexandru, C. (2024) Optimisation et Simulation d'un Mécanisme de Suivi Solaire à Double Axe. *Mathematics*, 12, 1034.
https://doi.org/10.3390/math12071034

[56] Ponce-Jara, M.A., Pazmino, I., Moreira-Espinoza, Á., Gunsha-Morales, A., and Rus Casas, C.(2024). Evaluated the effectiveness of a single-axis solar tracking system in equatorial regions using Manta as a case study., *Ecuador. Energies*, 17, Article 3946. https://doi.org/10.3390/en17163946

[57] Tarek,C.,Omar,G.,Imad,Q.,Youcef,.B.(2022).“Réalisation d ’ un Suiveur Solaire à deux axes Commandé par une Carte Arduino”.University of Echahid Hamma Lakhdar - El Oued, Algérie,pp1-59.
https://archives.univ-eloued.dz/handle/123456789/12091

[58] Sadeghi R., Parenti M., Memme S., Fossa M., Morchio S.(2025). « A Review and Comparative Analysis of Solar Tracking Systems ». Energies, vol. 18, no 10, 2553, 2025. https://www.mdpi.com/1996-1073/18/10/2553.

[59] Liu, B., Zong, C., & Huang, W. (2023). Evaluation and Characterization of the Influence of Solar Position Algorithm on the Performance of Parabolic Trough Solar System.Applied Sciences, 13(3), 1821
https://doi.org/10.3390/app13031821

[60] Rodolfo D-L,Tomás C.-A. ,Jesús S. A.-S. and José L. B.-A..(2021). Comparison of Lead-Acid and Li-Ion Batteries Lifetime Prediction Models in Stand-Alone Photovoltaic Systems. Appl. Sciences, 11(3);
https://doi.org/10.3390/app11031099

[61] Benhamida, M.T., and Sahraoui, T. (2022) Calculating the charge capacity of a Li-Ion battery in an electrical vehicle. Kasdi Merbah Ouargla University.
HTTPS://DSPACE.UNIV-OUARGLA.DZ/JSPUI/HANDLE/123456789/30197

[62] Singh, P., Vinjamuri, R., Wang, X. and Reisner, D. (2006).Design and Implementation of a Fuzzy Logic-Based State-Of-Charge Meter for Li-Ion Batteries Used in Port able Defibrillators. Journal of Power Sources, 162, 829-836.
https://doi.org/10.1016/j.jpowsour.2005.04.039

[63] Singh, P., Damodar, Y.S., Fennie, C. and Reisner, D.E. (2002) Fuzzy Logic-Based De termination of Lead Acid Battery State-of-Charge by Impedance Interrogation Meth ods. Proceedings. EVS-17, Montreal, 15-18 October 2000, 1-19

[64] Singh, P., Fennie, C. and Reisner, D.E. (1999) Fuzzy Logic Enhanced Electrochemical Impedance Spectroscopy (FLEEIS) to Determine Battery State-of-Charge. Proceedings 15th Annual Battery Conference on Applications and Advances, 1-5 Aug 1999, Vancouver, page.
doi : 10.1109/BCAA.2000.838404.

[65] Han, W., Wik, T., Kersten, A., Dong, G. and Zou, C. (2023) Reconfiguration Next Generation Battery Management Systems: Dynamic Reconfiguration. IEEE Indus trial Electronics Magazine, 14, 20-31.
doi : 10.1109/MIE.2020.3002486

[66] Belazi, N. (2012) Estimation of the state of charge (SOC) and state of health (SOH) of a lithium-ion battery used in electric vehicles. Mémoire de maîtrise électronique, Montréal, École de technologie supérieure.
https://espace.etsmtl.ca/id/eprint/967

[67] Qudah, A. et Mokheimer, E.M.A. (2024) Optimisation de l'intégration du photovoltaïque

et des batteries pour la désalinisation RO en utilisant l'algorithme d'évolution différentielle. Energy Proceedings, 43, 1-7.

[68] Louahlia, H., Gualous, H., Schaetzel, P., and Ziat, K. (2020). Charge and Discharge Current Effect on Lithium Ion Battery Temperature Elevation. Energy Storage. 28è conférence Française de thermique, 1-8. https://www.energyproceedings.org/wpcontent/uploads/icae2023/1704027976.pdf

[69] Balasingam, B., Ahmed, M. and Pattipati, K. (2020) Battery Management Systems—Challenges and Some Solutions. Energies, 13, Article 2825. https://doi.org/10.3390/en13112825

[70] Abdelhamid, B. (2023) Design and implementation of a base battery storage system in a photovoltaic conversion chain. Ghardaïa University, Algérie, 1-101. https://dspace.univ-ghardaia.edu.dz/xmlui/handle/123456789/6666

[71] Draia, U.A. (2021) Contribution à la réalisation d'un système de suivi et de gestion des batteries d'accumulateurs.

[72] Aymen, B.M. and Islam, S.(2023). " Investigation and Realisation of a Ni-MH Battery Charger ". *Mohamed El-Bachir El-Ibrahimi - Bordj Bou Arreridj University* http://10.10.1.6:4000/handle/123456789/3795

[73] https://www.victronenergy.fr/upload/documents/Optimiser-la-vie-des-batteries plomb-Leçon-V02-Bis.pdf

[74] Singh, P., and Reisner, D. (2002) Fuzzy Logic-Based Lead Acid Battery State-of-Health Assessment. *24th Annual International Telecommunications Energy Con ference , Montreal,* 29 September-3 October 2002, 583-590 https://doi.org/10.1109/intlec.2002.1048716

[75] Sérgio F. C., Elisson da S.R., Bruna C., Ermeson C. de A., Danilo R. B. A.(2021). A Mapping Study of Machine Learning Methods for Remaining Useful Life Estimation of Lead-Acid Batteries. arXiv:2307.05163v1 DOI : 10.48550/arXiv.2307.05163

[76] Olarte, J., Martínez de Ilarduya, J., Zulueta, E., Ferret, R., Fernández-Gámiz, U. et Lopez-Guede, JM. (2021). Un système de gestion de batterie avec surveillance EIS de l'espérance de vie des batteries au plomb. Électronique , 10 (11), 1228. https://doi.org/10.3390/electronics10111228

[77] Wang, Z., Xiao, Y. Research on energy management strategy of photovoltaic–battery energy storage system. International Journal of Low-Carbon Technologies, Volume 17, 2022. https://doi.org/10.1093/ijlct/ctac024

[78] Paramasivama, M., Issac, A., Rakesh, N., Subramaniam, S. (2023). Integrated battery

management system employing multi-port DC/DC converter for standalone solar photovoltaic system. Energy Sources, Part A, 45(3), 8239–8256. https://doi.org/10.1080/15567036.2023.2227157

[79] Qays, M. O., Buswig, Y., Basri, H., Hossain, M. L., Abu-Siada, A., Rahman, M. M., & Muyeen, S. M. (2020). An Intelligent Controlling Method for Battery Lifetime Increment Using State of Charge Estimation in PV-Battery Hybrid System. Applied Sciences, 10(24), 8799. https://doi.org/10.3390/app10248799

[80] Magsumbol, J.-A. V., Rosales, M. A., Palconit, M. G. B., Concepcion II, R. S., Bandala, A. A., Vicerra, R. R. P., Culaba, A., & Dadios, E. P. (2022). A Review of Smart Battery Management Systems for $LiFePO_4$: Key Issues and Estimation Techniques for Microgrids. JACIII, 26(5), 824-833.

[81] Ma, Y., & Li, B. (2020). Hybridized Intelligent Home Renewable Energy Management System for Smart Grids. *Sustainability,* 12(5), 2117. https://doi.org/10.3390/su12052117 https://doi.org/10.20965/jaciii.2022.p0824

[82] Puati Zau, A. T., Lencwe, M. J., Chowdhury, S. P. D., & Olwal, T. O. (2022). A Battery Management Strategy in a Lead-Acid and Lithium-Ion Hybrid Battery Energy Storage System for Conventional Transport Vehicles. Energies, 15(7). DOI : 10.3390/en15072577

[83] Jan-Philipp M., Julian P. and Florian H. .(2024). Les panneaux solaires comme source de silicium : opportunités et défis. Actes du colloque « Le silicium pour l'industrie chimique et solaire XVII » - ISBN 978-82-692919-3-3 https://dx.doi.org/10.2139/ssrn.4943266

[84] Anatoli C0, Georgia K., Sandor S., Arnulf J.-W.(2024). « Aperçu et perspectives du photovoltaïque intégré, en particulier dans l'Union européenne », Sciences appliquées 14 (22). Applied Sciences , 14 (22), 10628 ; https://doi.org/10.3390/app142210628

[85] Michael H. and Cordula W..(2024). «État de la reprise et du recyclage des modules photovoltaïques en Allemagne », Agence internationale de l'énergie (AIE). https://doi.org/10.69766/UMNT5335

[86] Martin S, Sara W., Paul S., Frank L.(2022). "Équilibrer les coûts et les revenus du recyclage des panneaux photovoltaïques en fin de vie aux Pays-Bas », Rapport TNO 2022 R10860. https://resolver.tno.nl/uuid:821b6338-95d6-4980-b9bc-4224fca9af32

[87] CHATZIPANAGI, A., JAEGER-WALDAU, A., LETOUT, S., MOUNTRAKI, A., GEA BERMUDEZ, J., GEORGAKAKI, A., INCE, E. et SCHMITZ, A.(2024). Observatoire des technologies de l'énergie propre : Le photovoltaïque dans l'Union européenne - Rapport d'étape 2024 sur le développement technologique, les tendances, les chaînes de valeur et les marchés. *Publications Office of the European Union*. https://publications.jrc.ec.europa.eu/repository/handle/JRC139297 Doi:10.2760/1812909

[88] Fenni Fadila. (2022). « Potentiels et perspectives des énergies renouvelables en Algérie) Expériences de certains pays », *Revue Organisation&Travail* 11 (1)

[89] Henri B., Joël A., (2019). « Les énergies renouvelables, le cas du solaire en Afrique, et plus particulièrement au Bénin », Annales des Mines-Réalités industrielles 2019 (3), 38-42 DOI : 10.3917/rindu1.193.003

[90]https://www.ecofinagency.com/news-industry/3006-47478-burundi-access-to-electricity-remains-low-despite-sharp-Increase-in-energy-production

[91] https://www.ecofinagency.com/news-industry/2909-49077-burundi-unveils-3-5b-energy-plan-calls-for-private-investment-to-boost-electrification

[92] https://re.jrc.ec.europa.eu/pvg_tools/en/

[93] 10.18100-ijamec.653371-907453

[94] Claude, J.N. (2013) National Climate Change Policy. Burundi's Ministry of Water, Environment, Land Management, and Urbanization. https://bi.chm-cbd.net/sites/bi/files/2020-12/politique-cc-bi.pdf

[95] Bélanger M., El-Jabi N., Caissie D., F. Ashkar and J. M. Rib. (2025). Water temperature prediction using neural networks and multiple linear regression .Journal of Water Science (18),3. https://doi.org/10.7202/705565ar

[96]Simon, A. and Alejandro,O.(2005). Power-Switching Converters, Second. Boca Raton, FL: CRC Press, 2005. https://books.google.co.uk/books?id=YTC9D5YRvqcC&lpg=PP1&hl=fr&pg=PR13#v=onepage&q&f=false

[97] Habitouche,M. S. and Sahli,I. (2021). “Etude et conception d’une commande non linéaire appliquée au convertisseur statique DC-DC,” Université Mohamed El Bachir El Ibrahimi - Bordj Bou Arréridj, http://10.10.1.6:4000/handle/123456789/1224

[98] Katche, M.L., Makokha, A.B., Zachary, S.O. and Adaramola, M.S. (2023) A Compre hensive Review of Maximum Power Point Tracking (MPPT) Techniques Used in So lar PV Systems. Energies, 16,
https://doi.org/10.3390/en16052206

[99] Chaieb, H. and Sakly, A.(2015).Une comparaison entre les algorithmes MPPT basés sur les méthodes P&O et P.S.O pour les systèmes photovoltaïques. National Engineering School of Monastir, University of Monastir, Tunisia.
DOI : 10.1109/STA.2015.7505205

[100] Femia, N., Petrone, G., Spagnuolo, G., et Vitelli, M. (2005). Optimisation de la méthode de suivi du point de puissance maximale perturbé et observé. IEEE Transactions on Power Electronics, 20(4), 963–973.
https://doi.org/10.1109/TPEL.2005.850975

[101] T. Selmi, M. Abdul-Niby, L. Devis and A. Davis (2014), P&O MPPT implementation using MATLAB/Simulink. Ninth International Conference on Ecological Vehicles and Renewable Energies (EVER), 1-4.
Doi:10.1109/EVER.2014.6844065.

[102] Kuznetsov, O., Poluyanenko, N., Kuznetsova, K., Frontoni, E., & Arnesano, M. (2024). Hybrid Population-Based Hill Climbing Algorithm for Generating Highly Nonlinear S-boxes. Computers, 13, 320.
DOI: 10.3390/computers13120320.

[103] Baimel, D.; Tapuchi, S.; Levron, Y.; Belikov, J.(2019). Improved Fractional Open Circuit Voltage MPPT Methods for PV Systems Electronics, Vol 8, Issue 3, Article 321. DOI : 10.3390/electronics8030321.

[104] Esram, T., & Chapman, P. L. (2007). Comparaison des techniques de suivi du point de puissance maximale pour les panneaux photovoltaïques. *Transactions de l'IEEE sur la conversion d'énergie, 22(2), 439–449.*
https://doi.org/10.1109/TEC.2006.874230

[105] Femia, N., Petrone, G., Spagnuolo, G., et Vitelli, M. (2005). Optimisation de la méthode de suivi du point de puissance maximale Perturb and Observe. *IEEE Transactions on Power Electronics, 20(4), 963–973.*
https://doi.org/10.1109/TPEL.2005.850975

[106] Geoffroy B., Philippe D., Golam G., Mohammed F. E., Alexis P. Y., Emmanuel T. K., Noel D. (2024). A modified fractional short circuit current MPPT and multicellular converter for improving power quality and efficiency in PV chain. Plos one 19 (9), e0309460, 2024

DOI 10.1371/journal.pone.0309460

[107] Villalva, M. G., Gazoli, J. R., & Filho, E. R. (2009). Comprehensive Approach to Modeling and Simulation of Photovoltaic Arrays. IEEE Transactions on Power Electronics, 24(5), 1198–1208. https://doi.org/10.1109/TPEL.2009.2013862

[108] Almufti, S.M., Ahmad, H.B., Marqas, R.B. et Asaad, R.R. 2021.Optimiseur de loup gris : Aperçu, modifications et applications. Revue internationale de recherche en science, Technologie, Education et gestion,vol 1. no 1.p 44-56. DOI : 10.5281/zenodo.5195644

[109] Fathy, A., Mekhilef, S., & Abido, M. A. (2020). Grey Wolf Optimizer-based MPPT for photovoltaic systems under partial shading conditions. IEEE Access, 8, 121258–121271. https://doi.org/10.1109/ACCESS.2020.3006627

[110] Tripathi, R. K., & Ghosh, A. (2022). Grey Wolf Optimization Based MPPT Algorithm for PV System Under Partial Shading Conditions. Solar Energy, 233, 1042–1054. https://doi.org/10.1016/j.solener.2022.01.047

[111] Dernoncourt, F., Baratgin, S.J. and Sander, P.E. (2011) La Logique Floue: Entre raisonnement humain et intelligence artificielle Table des matières. https://www.academia.edu/download/6439910/fcs2-report_ _la_logique_floue_20110204a.pdf

[112] Ishaque, K., Salam, Z., & Amjad, M. (2012). Fuzzy logic based MPPT for photovoltaic modules under partial shading conditions. *Energy and Buildings*, 49, 317–325. https://doi.org/10.1016/j.enbuild.2012.02.007

[113] Tarek,C.,Omar,G.,Imad,Q.,Youcef,.B.(2022).“Réalisation d’un Suiveur Solaire à deux axes Commandé par une Carte Arduino”.University of Echahid Hamma Lakhdar - El Oued, Algérie,pp1-59. https://archives.univ-eloued.dz/handle/123456789/12091

[114] FARID, G., AMEL. S. (2010)." Commande de panneau solaire à l'aide d'une carte a PIC, *". Faculté des Sciences et de la technologie (FST).* http://archives.univ-biskra.dz/handle/123456789/6619

[115] Olivier, I., Noel, N., Denis, B., Singh, P., and Bosco, N.J. (2025). Intelligent Solar Tracker Developed to Increase Burundi's Photovoltaic Production. Journal of Power and Energy Engineering, 13, 41-60. HTTPS://DOI.ORG/10.4236/JPEE.2025.1310004

[116] Achaibou, N., Haddadi, M., & Malek, A. (2012). Modeling of lead acid batteries in PV systems. Energy Procedia, 18, 538–544. https://doi.org/10.1016/j.egypro.2012.05.065

[117] Tremblay, Olivier, and Louis-a Dessaint. (2009). “Experimental Validation of a Battery Dy namic Model for EV Applications.”*World electric vehicle journal,* 3, 289–98. https://doi.org/10.3390/wej3020289.

[118] Chang, W.Y. (2013)." The State of Charge Estimating Methods for Battery: A Review".*International Scholarly Research Notices.* https://doi.org/10.1155/2013/953792

[119] Dufo, R. (2021). " Comparison of Lead-Acid and Li-Ion Batteries Lifetime Prediction Models in Stand-Alone Photovoltaic Systems". Applied sciences https://doi.org/10.3390/app11031099

[120] Achaibou, N., Malek, A. and Bacha,N. et al.(2015). “Modèle de Vieillissement Des Batteries Plomb-Acide Dans Les Systèmes PV.”*Rev.Des Ener.Renouvelables*,61-66. https://www.researchgate.net/profile/Nadia-Achaibou/publication/242132515_Modele_de_Vieillissement_des_Batteries_Plomb-Acide_dans_les_Systemes_PV/links/55e46c9e08ae2fac4722e0a2/Modele-de-Vieillissement-des-Batteries Plomb-Acide-dans-les-Systemes-PV.pdf

[121] Toufik M. L., Gérard C. (2023).Etude du vieillissement d’un banc de stockage plomb-acide dans un système hybride multi-sources . *Conférence : SYMPOSIUM DE GENIE ELECTRIQUE (SGE'14) : EF-EPF-MGE.À : ENS CACHAN, France.* https://www.researchgate.net/publication/265296693_Etude_du_vieillissement_d'un_banc_de_stockage_plomb-acide_dans_un_systeme_hybride_multi-sources

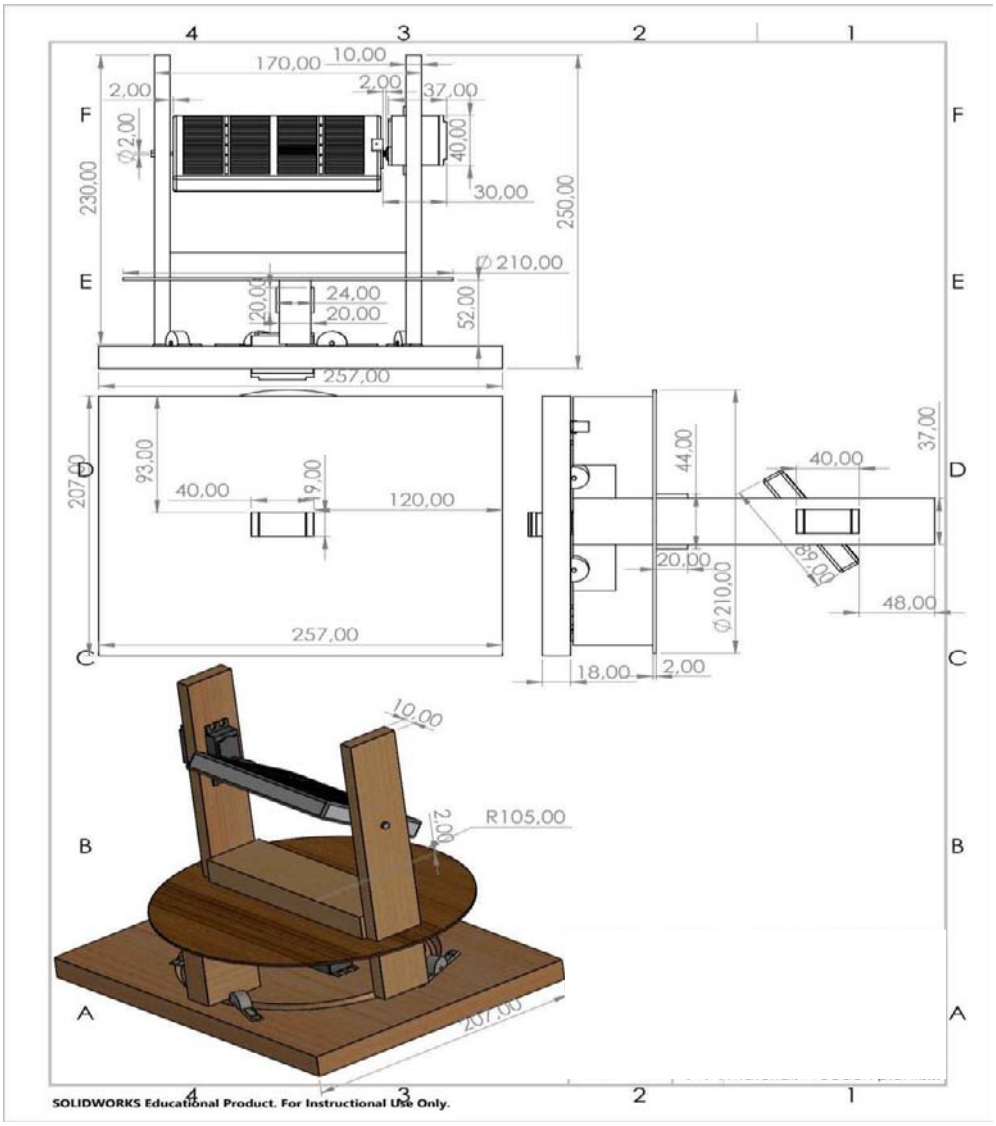
[122] Wang, X. , Wang, J. , Weng, Z. , Wei, Y. , Han, D. et Gong, C. (2022) Exploration de la réforme de l'enseignement pratique de la simulation virtuelle Proteus en électronique. Advances in Applied Sociology, 12, 93-101. doi: 10.4236/aasoci.2022.124009

[123] Prabowo, N. K., & Irwanto, I. (2025). The Implementation of Arduino Microcontroller Boards in Science: A Bibliometric Analysis from 2008 to 2022. *Journal of Engineering Education Transformations*, 37(2), 106–123. https://doi.org/10.16920/jeet/2023/v37i2/23154

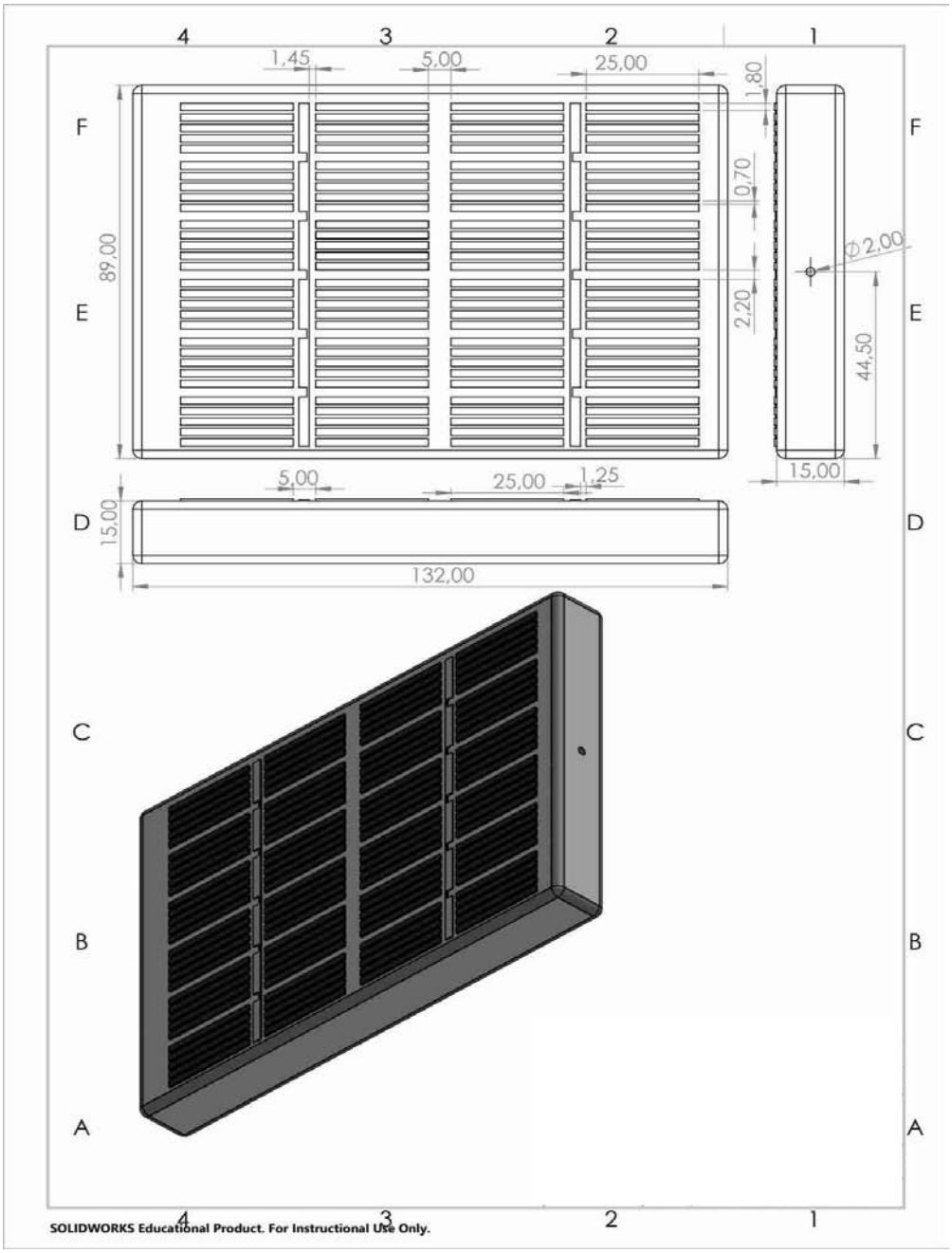
[124] Geng, J. P., Cui, H. B., Liu, X. Y., et al. (2013). Parametric Design and Automatic Adjustment Technique of Engineering Drawing Based on SolidWorks. *Advanced Materials Research, Vols. 706-708, pp. 1958-1962.* DOI :10.4028/www.scientific.net/AMR.706-708.1

APPENDICES

APPENDICE 1: View 2D of all assembly of the solar tracker



APPENDICE 2: View 2D of solar array dimension



APPENDIC3: View 2D of solar tracking system support dimension

